

Half-sandwich Ruthenium(II)-Arene Complexes as Anticancer Agent

Ph.D. Thesis

By
POULAMI MANDAL



DISCIPLINE OF CHEMISTRY
INDIAN INSTITUTE OF TECHNOLOGY INDORE
MAY 2018

Half-sandwich Ruthenium(II)-Arene Complexes as Anticancer Agent

A THESIS

*Submitted in partial fulfillment of the
requirements for the award of the degree
of*

DOCTOR OF PHILOSOPHY

by

POULAMI MANDAL



**DISCIPLINE OF CHEMISTRY
INDIAN INSTITUTE OF TECHNOLOGY INDORE
MAY 2018**



INDIAN INSTITUTE OF TECHNOLOGY INDORE

CANDIDATE'S DECLARATION

I hereby certify that the work which is being presented in the thesis entitled **Half-sandwich Ruthenium(II)-Arene Complexes as Anticancer Agent** in the partial fulfillment of the requirements for the award of the degree of **DOCTOR OF PHILOSOPHY** and submitted in the **Discipline of Chemistry, Indian Institute of Technology Indore**, is an authentic record of my own work carried out during the time period from **January 2014** to **May 2018** under the supervision of **Dr. Suman Mukhopadhyay**, Professor, Discipline of Chemistry, Indian Institute of Technology Indore.

The matter presented in this thesis has not been submitted by me for the award of any other degree of this or any other institute.

Signature of the student with date
(**POULAMI MANDAL**)

This is to certify that the above statement made by the candidate is correct to the best of my/our knowledge.

Signature of Thesis Supervisor with date
(**DR. SUMAN MUKHOPADHYAY**)

MS. POULAMI MANDAL has successfully given his/her Ph.D. Oral Examination held on

Signature of Chairperson
Date:

Signature of External Examiner
Date:

Signature(s) of Thesis Supervisor(s)
Date:

Signature of PSPC Member #1
Date:

Signature of PSPC Member #2
Date:

Signature of Convener, DPGC
Date:

Signature of Head of Discipline
Date:

ACKNOWLEDGEMENTS

After a long journey of five years, today is the day: writing this note of thanks is the finishing touch on my thesis. It has been a period of intense learning for me, not only in the scientific arena, but also on a personal level. Writing this thesis has had a big impact on me. I would like to reflect on the people who have supported and helped me so much throughout this period.

Foremost, I would like to express my sincere gratitude to my supervisor Prof. Suman Mukhopadhyay for encouragement, guidance and support of my PhD study and research, for his motivation, patience and enthusiasm. His guidance helped me in all the time of research and writing of this thesis. I have been very privileged to have the most hard working and supportive advisor anyone could ask for. I grew as a person during my PhD days learning not only Chemistry but also various aspects of life. At a personal level, I will always cherish the valuable lessons and suggestions I received from him.

I am thankful to my PSPC members, Dr. Sanjay Kumar Singh and Dr. Somaditya Sen for their valuable suggestions and guidance. I wish to express my gratitude to all faculty members of Discipline of Chemistry, IIT Indore for continuous support in every aspect.

I would like to thank Dr. C. M. Nagaraja for solid state characterisation study, Dr. A. Helen for enzyme activity study and Dr. K. Bhabak for computational studies. A special thanks to Mr. Sandeep Singh Dhankar for single crystal XRD analysis.

I thank Department of Science and Technology (DST) for financial support. I would like to thank the Department of Chemistry, IIT Indore for providing me financial support for conferences. I am grateful to Sophisticated Instrument centre (SIC) for instrumentation facility and the office members of the Chemistry Department for facilitating various official processes.

I am thankful to my former and present group members Dr. Rajender Nasani, Dr. Manideepa Saha, Dr. Mriganka Das, Dr.

Komal Vyas, Dr. Rinky Singh, Ms. Novina Malviya, Mr. Bidyut Kumar Kundu, Ms. Chanchal Sonkar, Mr. Rishi Ranjan for creating an enjoyable atmosphere to work. I owe a lot to Dr. Komal and Bidyut for their invaluable suggestions. I would like to thank all my co-researchers at IIT Indore. I would like to acknowledge all the technical and non-technical staffs of IIT Indore for their assistance and service. It has been a wonderful experience to work with many friends during my Ph.D. who really helped me in many aspects.

I thank my parents for their wise counsel and sympathetic ear. They are always there for me. I don't have enough word to describe all the sacrifices they continue to make to see me through this milestone. Without your constant support and unconditional love it would not have been possible. I want to say thanks to my sister Pallabi. It would take up too much space to list even the biggest things, but know that I couldn't have done it without you too!

Last but not the least, I thank Sayandip for being there when I needed it most. Thank you very much!!!

May 2018

Poulami Mandal

Dedicated to
Baba, Ma and
Phool

ABSTRACT

Metals are rarely considered as promising candidate for pharmaceutical components and it is a common perception that metal compounds are toxic, unstable and generally not well suited for pharmaceutical applications. However, over the past few decades certain particular chemical reactivity of metals, their magnetic and nuclear properties and the structural variety of their compounds, have become important for a possible medical applications. The organ specific uptake of technetium radio-pharmaceuticals and the highly specific nature of the binding of *cis*-platin to DNA demonstrate the potential of this class of compounds in specific medicinal applications. Although platinum drugs, particularly *cis*-platin, carboplatin and oxaliplatin, are used worldwide for number of neoplasms and are essential constituents of many anticancer therapies, they have consistent side effects and often become extra sensitive towards resistance mechanisms. These drugs and their associated problems have guided the search for new transition metal based chemical entities to overcome such limitations and among many others, ruthenium based compounds have shown remarkable activities and promising development. Two of the ruthenium complexes, KP1019 and NAMI-A are currently undergoing chemical trials and have shown some success in preliminary results. After more than 25 years of discovery of these compounds, during which a number of chemical possibilities have been explored, a series of Ru(II) complexes were developed, named as RAPTA, which represent a new important class of compound to treat cancer. RAPTA complexes of the general formula $[\text{Ru}(\eta^6\text{-arene})(\text{PTA})\text{X}_2]$ show relatively low toxicity *in vitro*, but *in vivo* studies revealed excellent inhibition of metastasis growth, in addition to high selectivity and extremely low general toxicity. Although reaction mechanism of RAPTA complexes is still unclear and there is uncertainty on the main molecular target responsible for its anti-tumour and anti-metastatic activity, investigations on the anticancer activity of organometallic Ru(II)-arene compounds have emerged a new era for the last few decades. Therefore, design of new Ru(II)-arene complexes with

potential targets and analysis of the mode of action within the cell becomes most vital part in the arena of ruthenium based anti-cancer drugs.

The primary objectives of the research work reported in this thesis are:

- To design and synthesize new ruthenium based anticancer compounds based on a flexible scaffold (RAPTA) onto which various groups of known biological function can get attached.
- To develop target specific anticancer drug by attaching biologically active groups with known therapeutic function to the ruthenium centre.
- To explore antiproliferative activity of the prepared compounds.
- To investigate interaction of the compounds with different biomolecules *e.g.* DNA, BSA, HSA, amino acids etc.
- To investigate possible mechanistic pathway to determine the mode of action of synthesized compounds.

Summary of research work

The contents of each chapter included in the thesis are discussed briefly as follows:

Chapter 1: General Introduction and Background

A brief overview of the basic concepts and recent scientific developments towards the generation of metal based anticancer drugs has been reported. Moreover, importance of introducing ruthenium metal as potential candidate in cancer therapy has also been discussed. Finally, a brief summary of the research reported in this thesis and the relevance in the prospects of recent developments have been put forward.

Chapter 2: Fine Tuning Through Valence Bond Tautomerization of Ancillary Ligands in Ruthenium(II) Arene Complexes for Better Anticancer Activity and Enzyme Inhibition Properties

In this chapter, four new ruthenium arene complexes of general formula $[\text{Ru}(\text{L})(\eta^6\text{-arene})\text{Cl}]$ have been synthesized using substituted picolinamide derivatives as ancillary ligands ($\text{HL}^1 = \text{pyridine-2-carboxylic acid(4-nitrophenyl)-amide}$, $\eta^6\text{-arene} = p\text{-cymene}$ **1** and $\text{HL}^1 = \text{pyridine-2-carboxylic acid(4-nitrophenyl)-amide}$, $\eta^6\text{-arene} = \text{benzene}$ **3**, $\text{HL}^2 = 4\text{-(N-(2-pyridyl)carbamoyl)pyridine}$, $\eta^6\text{-arene} = p\text{-cymene}$, **5** $\text{HL}^3 = 3\text{-(N-(2-pyridyl)carbamoyl)pyridine}$, $\eta^6\text{-arene} = p\text{-cymene}$ **7**). These chloro-complexes have been substituted with 1,3,5-triaza-7-phosphoadamantane (PTA) which in turn yielded water soluble complexes $[\text{Ru}(\text{L})(\eta^6\text{-arene})(\text{PTA})]^+$ [**2**, **4**, **8**] and $[\text{Ru}(\text{HL}^2)(\eta^6\text{-arene})(\text{PTA})]^{++}$ [**6**]. All the complexes have been characterized by spectroscopic methods. In one of the complexes, the ancillary ligand has shown an unprecedented valence-bond tautomerization in the presence of an ammonium salt to act as a polar neutral donor ligand making the ligand more prone towards substitution. The same compound has shown remarkable antiproliferative activity against three cancer cell lines with GI_{50} values comparable to adriamycin, a known therapeutic drug. Along with this it also strongly inhibits the action of thioredoxin reductase, which might be a probable reason for the enhanced proliferative action of the valence-bond tautomerized compound.

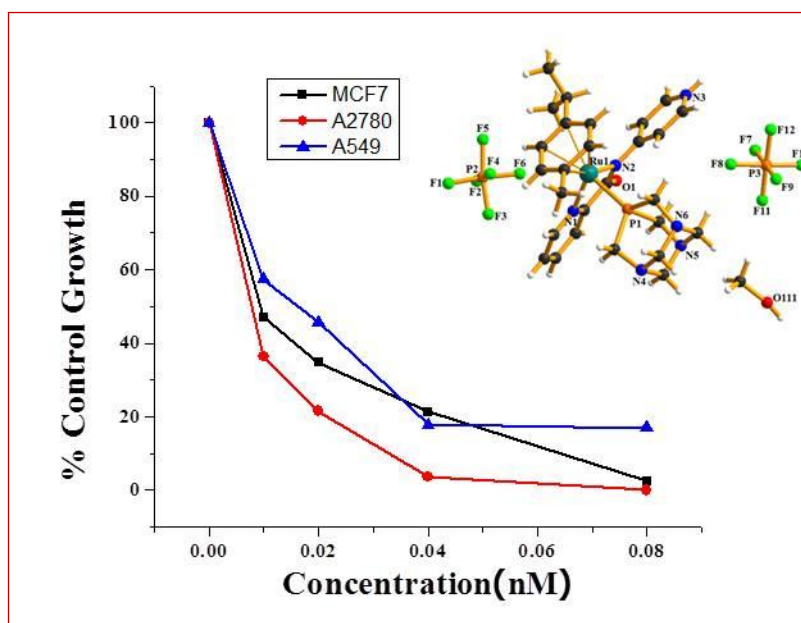


Fig.1: Analysis of the GI_{50} value of compound **6** against different cell lines using adriamycin as a positive control.

Chapter 3: Ruthenium(II) Arene NSAID Complexes : Inhibition of Cyclooxygenase and Antiproliferative Activity Against Cancer Cell Lines

Chapter 3 describes synthesis of four novel ruthenium(II)-arene complexes viz. $[\text{Ru}(\eta^6\text{-}p\text{-cymene})(\text{nap})\text{Cl}]$ **9** [Hnap = naproxen or (*S*)-2-(6-methoxy-2-naphthyl)propionic acid], $[\text{Ru}(\eta^6\text{-}p\text{-cymene})(\text{diclo})\text{Cl}]$ **10** [Hdiclo = diclofenac or 2-[(2,6-dichlorophenyl)amino] benzeneacetic acid, $[\text{Ru}(\eta^6\text{-}p\text{-cymene})(\text{ibu})\text{Cl}]$ **11** [Hibu = ibuprofen or 2-(4-isobutylphenyl)propanoic acid] and $[\text{Ru}(\eta^6\text{-}p\text{-cymene})(\text{asp})\text{Cl}]$ **12** [Hasp = aspirin or 2-acetoxy benzoic acid] using different NSAID drugs as chelating ligands. Complexes **9-11** have shown promising antiproliferative activity against three different cell lines with GI_{50} (concentration of drug causing 50% inhibition of cell growth) values comparable to adriamycin. At the concentration of 50 μM , complex **11** is more effective in inhibition of cyclooxygenase and lipooxygenase enzyme, followed by complex **10** and complex **9** with comparison to their respective free NSAID ligands indicating a possible correlation between inhibition of COX and/or LOX and anticancer property. Molecular docking studies with COX-2 reveal that complexes **9** and **10** having naproxen and diclofenac ligands exhibit stronger interactions with COX-2 than their respective free NSAIDs and these results are in well agreement with their relative experimentally observed COX inhibition as well as anti-proliferative activities.

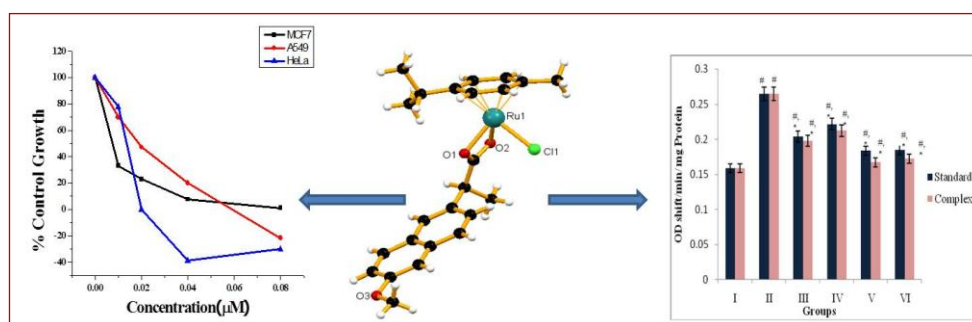


Fig.2: Schematic diagram of Ru(II)-arene complexes with NSAIDs as co-ligand, which have shown marked antiproliferative activity against cancer cell lines along with cyclooxygenase inhibition property.

3.4. Chapter 4: RAPTA Complexes Containing N-substituted Tetrazole Scaffolds: Synthesis, Characterization and Antiproliferative Activity

Chapter 4 illustrates the synthesis of a series of Ru(II)-arene complexes of general formula $[\text{Ru}(\text{L})(\eta^6\text{-arene})\text{Cl}_2]$ using different *N*-substituted tetrazole ligands (L = 1-(4-methoxy-phenyl)-1*H*-tetrazole, $\eta^6\text{-arene} = p\text{-cymene}$ **13**, L = 1-(4-methoxy-phenyl)-1*H*-tetrazole, $\eta^6\text{-arene} = \text{benzene}$ **15**, L = 1-(3,4,5-trimethoxy-phenyl)-1*H*-tetrazole, $\eta^6\text{-arene} = p\text{-cymene}$ **17**, L = 1-(3,4,5-trimethoxy-phenyl)-1*H*-tetrazole, $\eta^6\text{-arene} = \text{benzene}$ **19** and their PTA analogues (**14**, **16**, **18** and **20**). All the complexes have been characterized thoroughly using different analytical techniques. Antiproliferative activity of the synthesized complexes against different cancer cell lines indicates remarkable activity of certain complexes upto nanomolar level. In few cases introduction of water soluble PTA (PTA = 1,3,5- triaza-7-phospha-tricyclo-[3.3.1.1]decane) ligand induces significant cytotoxic activity in the ruthenium complex with respect to their chloro-analogue, particularly against Jurkat and MCF-7 cell lines. Interaction with different biomolecules for all the complexes have been investigated as well as stability of the RAPTA complexes have been explored in pseudo-pharmacological conditions.

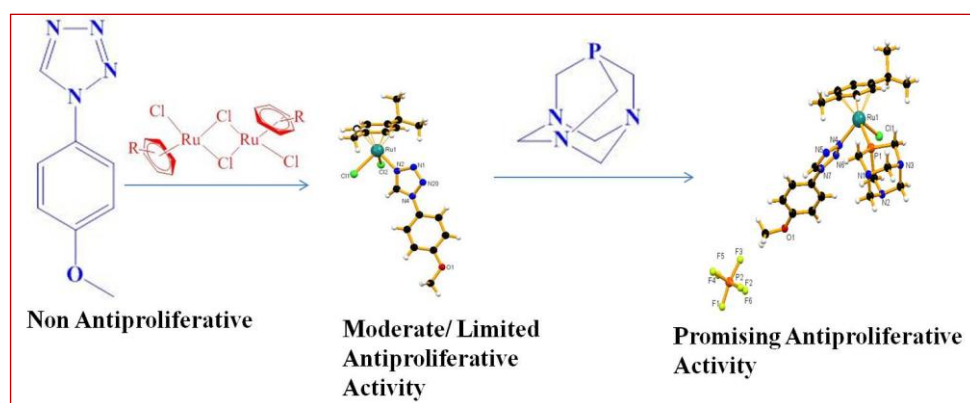


Fig.3: Synthesis of RAPTA compounds using different tetrazole scaffold to tune their antiproliferative activity.

Chapter 5: RAPTA Complexes Containing Ferrocenamide Ligands : Synthesis, Characterization and Antiproliferative Activity Against Cancer Cell Lines.

This chapter deals with synthesis of new ferrocenamide ligands *i.e.* pyridine-2-carboxylic acid(4-ferrocenyl aniline)- amide, **HL**⁷ and quinoline-1-carboxylic acid(4-ferrocenyl aniline)- amide, **HL**⁸ and two new heterobimetallic Ru(II)-arene complexes of general formula [Ru(L)(η^6 -arene)Cl] using synthesized ferrocenamide ligands (**L**⁷ = pyridine-2-carboxylic acid(4-ferrocenyl aniline)-amide, η^6 -arene = *p*-cymene **21**, and **L**⁸ = quinoline-1-carboxylic acid(4-ferrocenyl aniline)-amide, η^6 -arene = *p*-cymene **23**). These chloro-complexes have been substituted with 1,3,5-triaza-7-phosphoadamantane (PTA) which produced water soluble complexes of general formula [Ru(L)(η^6 -arene)(PTA)]⁺ [**22**, **24**]. All the complexes have been characterized thoroughly with different analytical tools and their antiproliferative activity has been evaluated against different cancerous cell lines. Among them, Compound **23** has shown promising antiproliferative activity against all the cell lines, owing to its lower stability than the other complexes in solution as well as ability to interact with different biomolecules, which makes it a potential candidate as anticancer drug to investigate further.

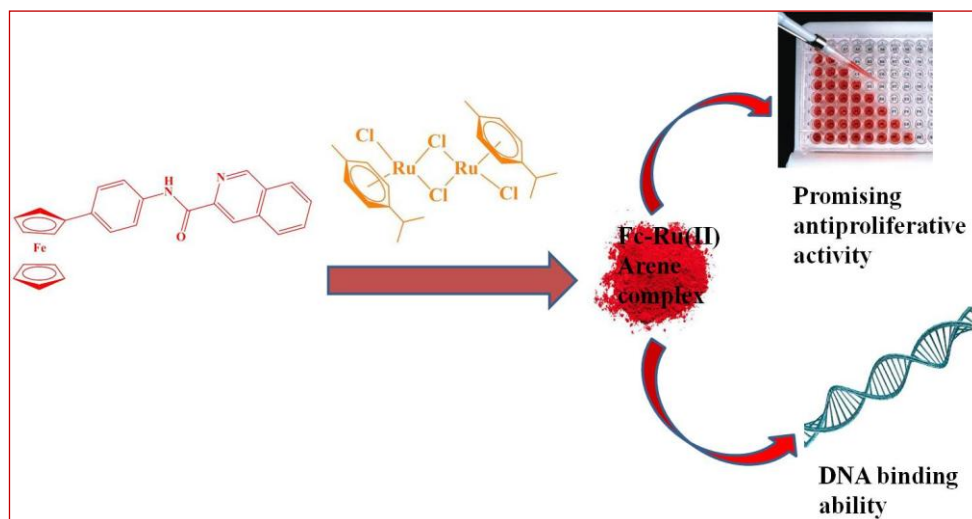


Fig.4: Synthesis of Fc-Ru(II) arene complexes and their antiproliferative activity.

Chapter 6: RAPTA Type of Complexes Containing Different Phosphine Ligands: Synthesis, Characterisation and Antiproliferative Activity

In chapter 6, RAPTA type of complexes has been prepared using different phosphine ligands $[\text{Ru}(\eta^6\text{-}p\text{-cymene})(\text{TFP})\text{Cl}_2]$ **25**, $[\text{Ru}(\eta^6\text{-}p\text{-cymene})(\text{TFP})_2\text{Cl}]\text{BF}_4$ **26**, $[\text{Ru}(\eta^6\text{-}p\text{-cymene})(\text{TFP})(\text{PPh}_3)\text{Cl}]\text{Cl}$ **27** and $[\text{Ru}(\eta^6\text{-}p\text{-cymene})(\text{TFP})(\text{PTA})\text{Cl}]\text{BF}_4$ **28**. All complexes have been characterized with different analytical techniques, whereas three complexes have been characterized by single crystal X-ray diffraction. Antiproliferative activity, stability study as well as interactions with biomolecules have been explored for the prepared complexes.

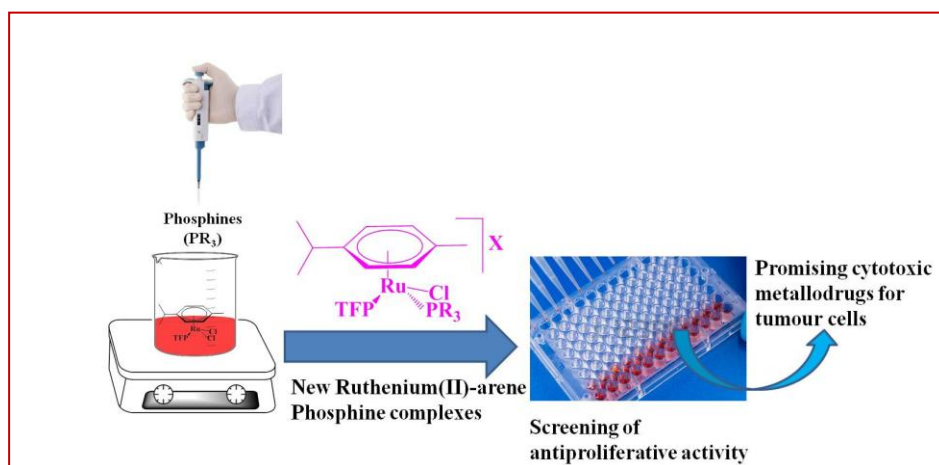


Fig.5: Schematic diagram of Ru(II)-arene phosphine complexes and their antiproliferative activity.

Chapter 7: General Conclusions and Future Scope

- In this thesis work, it has been observed that ruthenium(II)-arene complexes with different ancillary ligands show promising cytotoxic activity, whereas the free ligands are non cytotoxic in the same condition. Thus it could be the stepping stone for further tuning of the ligands to design new ruthenium metallodrugs with lower side effects as well as lesser cell resistance mechanism than Pt-anticancer drugs.
- As ruthenium(II) complexes, coordinated to biologically active ligands, have shown promising antiproliferative activity and enzyme inhibition property, idea of attaching this type of ligands to Ru(II) centre can be explored further in order to develop potential metallodrug for cancer therapy.

LIST OF PUBLICATIONS

[1] **Fine tuning through valence bond tautomerization of ancillary ligand in ruthenium(II) arene complex for better anticancer activity and enzyme inhibition property.**

Poulami Mandal, Novina Malviya, M. Fátima C. Guedes da Silva, Sandeep Singh Dhankhar, C. M. Nagaraja, Shaikh M Mobin, Suman Mukhopadhyay, Dalton Trans, 2016, 45, 19277-19289.(DOI: 10.1039/c6dt02969h)

[2] **Ruthenium(II) arene NSAID complexes : inhibition of cyclooxygenase and antiproliferative activity against cancer cell lines.**

Poulami Mandal, Bidyut Kumar Kundu, Komal Vyas, Vidya Sabu, A. Helen, Sandeep Singh Dhankhar, C. M. Nagaraja, Debojit Bhattacharjee, Krishna Pada Bhabak, Suman Mukhopadhyay, Dalton Trans., 2018, 47(2), 517–527. (DOI: 10.1039/c7dt03637j)

[3] **RAPTA complexes containing N-substituted tetrazole scaffolds: synthesis, characterization and antiproliferative activity.**

Poulami Mandal, Novina Malviya, Bidyut Kumar Kundu, Sandeep Singh Dhankhar, C. M. Nagaraja, Suman Mukhopadhyay, Appl. Organomet. Chem., 2017, 32(3), e4179.(DOI: 10.1002/aoc.4179)

[4] **Investigation on chemical protease, nuclease and catecholase activity of two copper complexes with flexidentate Schiff base ligands.**

Mriganka Das, Bidyut Kumar Kundu, Ritudhwaj Tiwari, Poulami Mandal, Debasis Nayak, Rakesh Ganguly, Suman Mukhopadhyay, Inorg. Chim. Acta, 2018, 469, 111-122.(DOI:10.1016/j.ica.2017.09.013)

[5] **A smart organic gel template as metal cation and inorganic anions sensor.**

Novina Malviya, Mriganka Das, Poulami Mandal, Suman Mukhopadhyay, Soft Matter, 2017, 13, 6243-6249. (DOI: 10.1039/C7SM01199G)

[6] **Nickel tetrazolato complexes synthesized by microwave irradiation : catecholase like activity and interaction with biomolecules.**

Novina Malviya, Poulami Mandal, Mriganka Das, Rakesh Ganguly, Suman Mukhopadhyay, *J Coord Chem*, 2017, 70, 261-278. (DOI: 10.1080/00958972.2016.1260121)

[7] **Copper complexes with flexible piperazinyl arm: nuclearity driven catecholase activity and interactions with biomolecules.**

Mriganka Das, Poulami Mandal, Novina Malviya, Indrani Choudhuri, Maria Adilia Januário Charmier, Susana Morgado, Shaikh M Mobin, Biswarup Pathak, Suman Mukhopadhyay, *J Coord. Chem.* 2016, 69, 3619-3637. (DOI: 10.1080/00958972.2016.1236193)

LIST OF CONFERENCES

1. **P. Mandal, N. Malviya, S. Mukhopadhyay; *Ruthenium(II) Arene NSAID Complexes : Synthesis, Antiproliferative Activity Against Cancer Cell Lines and Inhibition of Cyclooxygenase; 6th International Symposium on Metallomics; August 14-17, 2017, Vienna, Austria (Poster presented).***
2. **P. Mandal, N. Malviya, S. Mukhopadhyay; *Ruthenium(II) Arene NSAID Complexes : Synthesis, Antiproliferative Activity Against Cancer Cell Lines and Inhibition of Cyclooxygenase; Frontiers of Organometallic Chemistry; December 3-6, 2016, Thiruvanthapuram, India (Poster presented).***
3. **Frontiers in Inorganic and Organometallics, April 14-15, 2016, Indore, India.**
4. **P.Mandal, M. Das, F. da Silva, S. Mukhopadhyay; *Water Soluble Arene Ruthenium(II) Complexes: Interactions With Biomolecules; Modern Trends in Inorganic Chemistry; December 3-5, 2015, Kolkata, India (Poster presented).***
5. **Frontier Lecture Series in Chemistry, January 30-31, 2014, IIT Indore.**

6. Laboratory Health & Safety Workshop, April 4, 2014

TABLE OF CONTENTS

List of Nomenclature	xxiii
List of Acronyms	xxv
List of Figures	xxviii
List of Schemes	xxxiv
List of Tables	xxxv
Chapter 1	
General introduction and background	1
1.1 Introduction.....	2
1.2 Metals in medicinal Chemistry.....	3
1.3 Definition of cancer.....	3
1.4 Classification.....	4
1.4.1 Carcinoma.....	4
1.4.2 Sarcoma.....	4
1.4.3 Lymphoma and Leukemia.....	4
1.4.4 Brain and spinal cord cancer.....	4
1.5 Statistics.....	5
1.6 Different modes of cancer treatment.....	7
1.6.1 Surgery.....	7
1.6.2 Radiation therapy.....	7
1.6.3 Hormonal therapy.....	8
1.6.4 Immunotherapy.....	8
1.6.5 Stem cell transplantation therapy.....	8
1.6.6 Chemotherapy.....	8
1.6.6.1 Intercalating agents.....	8
1.6.6.2 Alkylating agents.....	9
1.6.6.3 Antimetabolites.....	10
1.6.6.4 Topoisomerase inhibitors.....	10
1.6.6.5 Metal based chemotherapeutic drug.....	11
1.7 Platinum based anticancer drug.....	11
1.8 Mechanism of <i>cis</i> -platin.....	12
1.9 Non-platinum metal complexes as anticancer agents.....	13
1.10 Ruthenium anticancer drug.....	14

1.10.1 NAMI-A.....	15
1.10.2 KP1019.....	16
1.11 Metal-arene compound as anticancer drugs.....	17
1.11.1 Piano stool complexes.....	18
1.11.2 Piano stool complexes.....	18
1.11.3 Cycloruthenated complexes.....	19
1.12 Structural features of ru(II)-arene complexes for anticanceractivity.....	19
1.12.1 The arene.....	19
1.12.2 The XY chelating ligand.....	20
1.12.3 The Z leaving group.....	21
1.13 Investigation on recent work.....	21
1.14 Purpose and span of present investigation.....	25
1.15 References.....	26

Chapter 2.....

Fine Tuning Through Valence Bond Tautomerization of Ancillary Ligands in Ruthenium(II) Arene Complexes for Better Anticancer Activity and Enzyme Inhibition Properties.....

2.1 Introduction.....	43
2.2 Experimental section.....	44
2.2.1 Materials and methods.....	44
2.2.1.1 Synthesis of $[\text{Ru}(\eta^6\text{-}p\text{-cymene})(\text{L}^1)(\text{PTA})][\text{BF}_4] [\mathbf{2}] \cdot 2\text{H}_2\text{O}$	45
2.2.1.2 Synthesis of $[\text{Ru}(\eta^6\text{-benzene})(\text{L}^1)(\text{PTA})][\text{PF}_6] [\mathbf{4}] \cdot \text{CH}_3\text{OH}$	46
2.2.1.3 Synthesis of $[\text{Ru}(\eta^6\text{-}p\text{-cymene})(\text{L}^2)\text{Cl}] [\mathbf{5}]$	47
2.2.1.4 Synthesis of $[\text{Ru}(\eta^6\text{-}p\text{-cymene})(\text{HL}^2)(\text{PTA})](\text{PF}_6)_2 [\mathbf{6}] \cdot \text{CH}_3\text{OH}$	47
2.2.1.5 Synthesis of $[\text{Ru}(\eta^6\text{-}p\text{-cymene})(\text{L}^3)\text{Cl}] [\mathbf{7}]$	48
2.2.1.6 Synthesis of $[\text{Ru}(\eta^6\text{-}p\text{-cymene})(\text{L}^3)(\text{PTA})][\text{BF}_4] [\mathbf{8}]$	49
2.2.2 X-ray crystallography.....	50
2.2.2.1 X-ray crystallography of Compound 2	50
2.2.2.2 X-ray crystallography of Compound 4	50
2.2.2.3 X-ray crystallography Compound 6 and 8	51
2.2.3 Protein binding experiments.....	51

2.2.4 Inhibition of the Trx-R enzyme.....	52
2.2.5 Supplementary materials.....	53
2.3 Results and discussion.....	53
2.3.1 Syntheses of complexes.....	53
2.3.2 Conductivity measurements.....	68
2.3.3 Protein binding studies.....	68
2.3.4 Growth inhibition of ruthenium–arene complexes.....	70
2.3.5 Stability study of compounds 6 and 8	72
2.3.6 Mammalian Trx-R inhibition.....	75
2.4 Conclusion.....	75
2.5 References.....	76

Chapter 3	
Ruthenium(II) Arene NSAID Complexes: Inhibition of Cyclooxygenase and Antiproliferative Activity Against Cancer Cell Lines	84
3.1 Introduction.....	85
3.2 Experimental section.....	86
3.2.1 Materials and methods.....	86
3.2.1.1 Synthesis of [Ru(η^6 - <i>p</i> -cymene)(nap)Cl] [9].....	87
3.2.1.2 Synthesis of [Ru(η^6 - <i>p</i> -cymene)(diclo)Cl] [10].....	87
3.2.1.3 Synthesis of [Ru(η^6 - <i>p</i> -cymene)(ibu)Cl] [11].....	88
3.2.1.4 Synthesis of [Ru(η^6 - <i>p</i> -cymene)(asp)Cl] [12].....	89
3.2.2 X-ray crystallography.....	90
3.2.2.1 X-ray crystallography of complex 9 and 10	90
3.2.3 Growth inhibition study.....	90
3.2.4 Stability studies in DMSO.....	90
3.2.5 Assay of Cyclooxygenase (COX).....	90
3.2.6 Assay of Lipoxygenase (LOX).....	90
3.2.7 DNA binding experiments.....	91
3.2.8 Protein binding experiments.....	91
3.2.9 Interaction with Amino acids.....	91
3.2.10 Docking Studies.....	91
3.2.10.1 AutoDock simulation method.....	91
3.2.10.2. Gold simulation method.....	92

3.2.11 Supplementary materials.....	92
3.3 Results and discussion.....	93
3.3.1 Synthesis of complexes.....	93
3.3.2 Growth inhibition study of Ru(II)–NSAID complexes.....	100
3.3.3 Stability study in DMSO.....	102
3.3.4 COX inhibition studies.....	105
3.3.5 LOX inhibition studies.....	107
3.3.6 DNA binding study.....	108
3.3.7 Protein binding studies.....	109
3.3.8 Interaction with amino acids.....	110
3.3.9 Docking analysis.....	112
3.4 Conclusion.....	116
3.5 References.....	117

Chapter 4.....	
RAPTA Type Complexes Containing N-substituted Tetrazole Scaffolds: Synthesis, Characterization and Antiproliferative Activity.....	129
4.1 Introduction.....	130
4.2 Experimental section.....	132
4.2.1 Materials and methods.....	132
4.2.1.1 Synthesis of [Ru(η^6 - <i>p</i> -cymene)(L ⁴)Cl ₂] [13].....	133
4.2.1.2 Synthesis of [Ru(η^6 - <i>p</i> -cymene)(L ⁴)(PTA)Cl]PF ₆ [14].....	133
4.2.1.3 Synthesis of [Ru(η^6 -benzene)(L ⁴)Cl ₂] [15].....	134
4.2.1.4 Synthesis of [Ru(η^6 -benzene)(L ⁴)(PTA)Cl]Cl [16].....	134
4.2.1.5 Synthesis of [Ru(η^6 - <i>p</i> -cymene)(L ⁵)Cl ₂] [17].....	135
4.2.1.6 Synthesis of [Ru(η^6 - <i>p</i> -cymene)(L ⁵)(PTA)Cl]Cl [18].....	136
4.2.1.7 Synthesis of [Ru(η^6 -benzene)(L ⁵)Cl ₂] [19].....	136
4.2.1.8 Synthesis of [Ru(η^6 -benzene)(L ⁵)(PTA)Cl]Cl [20].....	137
4.2.2 X-ray crystallography.....	137
4.2.3 Protein binding experiments.....	138
4.2.4 Supplementary materials.....	138
4.3 Results and discussions.....	139
4.3.1 Synthesis and characterization of Complexes.....	139

RAPTA Type of Complexes Containing Different Phosphine Ligands: Synthesis, Characterisation and Antiproliferative Activity	198
6.1 Introduction.....	199
6.2 Experimental section.....	201
6.2.1 Materials and methods.....	201
6.2.1.1 Synthesis of [Ru(η^6 - <i>p</i> -cymene)(TFP)Cl ₂] [25].....	201
6.2.1.2 Synthesis of [Ru(η^6 - <i>p</i> -cymene)(TFP) ₂ Cl]BF ₄ [26].....	202
6.2.1.3 Synthesis of [Ru(η^6 - <i>p</i> -cymene)(TFP)(PPh ₃)Cl]Cl [27].....	202
6.2.1.4 Synthesis of [Ru(η^6 - <i>p</i> -cymene)(TFP)(PTA)Cl]BF ₄ [28].....	203
6.2.2 X-ray crystallography.....	203
6.2.2.1 X-ray crystallography of complex 25 , 26 and 28	203
6.2.3 Growth inhibition study.....	204
6.2.4 Stability studies in DMSO.....	204
6.2.5 Supplementary materials.....	204
6.3 Result and discussions.....	204
6.3.1 Synthesis of complexes.....	204
6.3.2 Growth inhibition study of prepared complexes.....	214
6.3.3 Solution stability study.....	215
6.4 Conclusion.....	216
6.5 References.....	216
 Chapter 7	
General Conclusion and Future Scope	223

List of Nomenclature

α	Alpha
β	Beta
γ	Gama
T	Fluorescence Lifetime
Å	Angstrom
X	Chi
Λ	Wavelength
M	Micro
Π	Pi
nm	Nanometer
ns	Nanosecond
mM	Milli Molar
μ M	Micro Molar
K _{sv}	Stern Volmer Quenching Constant
ϵ	Molar Extinction coefficient
cm	Centimeter
°	Degree
K _{nt}	Kelvin
mL	Milliliter
μ L	Microliter
a. u.	Arbitrary Unit
Λ_{ex}	Excitation Wavelength
λ_{em}	Emission Wavelength
pH	The negative logarithm of hydronium-ion concentration
H	Eta (Efficiency)
K _a	Binding Constant
Ω	Mho

List of Acronyms

ACTREC	Advanced Centre for Treatment, Research and Education in Cancer
BMOV	Bis(Maltato) OxoVanadium
BSA	Bovine Serum Albumin
CAP	1,4,7-triaza-9-phosphatricyclo [5.3.2.1] tridecane
CCDC	Cambridge Crystallographic Data Centre
COX	Cyclo Oxygenase
CV	Cyclic Voltammetry
CDCl ₃	Chloroform - <i>d</i>
DCM	Dichloromethane
DMEM	Dulbecco's Modified Eagle's Medium
DMF	Dimethylformamide
DMSO- <i>d</i> ₆	Dimethyl sulfoxide- <i>d</i> ₆
DNA	Deoxyribo Nucleic Acid
DTNB	Di Thio Nitro Benzoicacid
EB	Ethidium Bromide
EDTA	Ethelene Diammine Tetraacetic Acid
EGFR	Epidermal Growth Factor Receptors
ESI-MS	Electron Spin Ionization Mass Spectroscopy
5-FU	5-Fluorodeoxyuridine
Fc	Ferrocene
GOF	Goodness of Factor
GI ₅₀	Concentration of drug that produces 50% growth inhibition of cells
GST	Glutathione Transferase
HETE	Hydroxy Eicosa Tetraenoicacid
HPV	Human Papilloma Virus
HSA	Human Serum Albumin
HSAB	Hard Soft Acid Base
Ind	Indazole
IR	Infrared
KP1019	Trans-[tetrachlorobisruthenate(III)]

LC ₅₀	Concentration of the drug that kills 50% of the cells
LOX	Lipo Oxygenase
MeOH	Methanol
NaDPH	Nicotinamide Adenine Dinucleotide Phosphate
NAMI-A	Imidazolium trans-imidazoledimethylsulfoxide tetrachlororuthenate (III)
NMR	Nuclear Magnetic Resonance
NSAID	Non Steroidal Anti Inflammatory Drug
<i>p</i> -cymene	<i>Para</i> -cymene
PBS	Phosphate-buffered saline
PDB	Protein Data Bank
SCXRD	Single Crystal X-Ray Diffraction
SRB	Sulforhodamine B
TFP	Tris-(2-furyl) phosphine
TGI	Concentration of the drug that produces total inhibition of the cells
TrxR	Thioredoxin Reductase
TRIS	Tris(Hydroxymethyl)aminomethane
UV-Vis	Ultra Violet-Visible
XRD	X-ray Diffraction

List of Figures

Chapter 1

Fig.1.1: Structure of metal based drugs	3
Fig.1.2: Rate of occurrence of different types of cancer in 2015.....	5
Fig.1.3: Incidence of cancer around the world in 2017.....	6
Fig.1.4: Study on cancer patients in different states of India.....	7
Fig.1.5: Molecular structure of intercalating agent.....	9
Fig.1.6: Molecular structure of alkylating agent.....	9
Fig.1.7: Molecular structure of antimetabolites.....	10
Fig.1.8: Molecular structure of topoisomerase inhibitor.....	11
Fig.1.9: Molecular structure of <i>cis</i> -platin.....	12
Fig.1.10: Molecular structure of Oxaliplatin and Carboplatin.....	12
Fig.1.11: DNA adduct formation with <i>cis</i> -platin.....	13
Fig.1.12: Molecular structure of metal based anticancer drugs.....	14
Fig.1.13: Molecular structure of NAMI-A.....	15
Fig.1.14: Molecular structure of KP1019.....	17
Fig.1.15: Structure of piano stool complex.....	18
Fig.1.16: Structure of RAPTA complexes.....	19
Fig.1.17: Structure of cycloruthenated complex.....	19
Fig.1.18: Schematic representation of a RuII extended arene complex intercalating between DNA bases.....	20

Chapter 2

Fig.2.1: ¹ H NMR spectra of complex 2	55
Fig.2.2: ¹ H NMR spectra of complex 4	55
Fig.2.3: ¹ H NMR spectra of complex 5	56
Fig.2.4: ¹ H NMR spectra of complex 6	56
Fig.2.5: ¹ H NMR spectra of complex 7	57
Fig.2.6: ¹ H NMR spectra of complex 8	57
Fig.2.7: ¹³ C NMR spectra of complex 2	58
Fig.2.8: ¹³ C NMR spectra of complex 4	58
Fig.2.9: ¹³ C NMR spectra of complex 6	59
Fig.2.10: ¹³ C NMR spectra of complex 8	59

Fig.2.11: ^{31}P NMR spectra of complex 2	60
Fig.2.12: ^{31}P NMR spectra of complex 4	60
Fig.2.13: ^{31}P NMR spectra of complex 6	61
Fig.2.14: ^{31}P NMR spectra of complex 8	61
Fig.2.15: ESI-MS of complex 2	62
Fig.2.16: ESI-MS of complex 4	62
Fig.2.17: ESI-MS of complex 6	62
Fig.2.18: ESI-MS of complex 8	62
Fig.2.19: ESI-MS of complex 5	63
Fig.2.20: ESI-MS of complex 7	63
Fig.2.21: The solid state crystal structure of compound 2	64
Fig.2.22: The solid state crystal structure of compound 4	65
Fig.2.23: The solid state crystal structure of compound 6	66
Fig.2.24: The solid state crystal structure of compound 8	67
Fig.2.25: Fluorescence quenching of HSA by Complex 2, 4, 6 and 8	69
Fig.2.26: Analysis of GI_{50} value of Compound 6 against different cell lines using adriamycin as positive control.....	71
Fig.2.27: ^{31}P NMR of compound 6 in 100mM NaCl solution after 7 days. ^{31}P NMR of compound 6 in 10% DMSO- d_6 [inset].....	73
Fig.2.28: ^{31}P NMR of compound 8 in 5 mM NaCl solution after 7 days. ^{31}P NMR of compound 8 in 10% DMSO- d_6 [inset].....	73
Fig.2.29: ^{31}P NMR of compound 8 in 100mM NaCl solution after 7 days. ^{31}P NMR of compound 8 in 10% DMSO- d_6 [inset].....	74
 Chapter 3	
Fig.3.1: ^1H NMR spectra of complex 9	95
Fig.3.2: ^1H NMR spectra of complex 10	95
Fig.3.3: ^1H NMR spectra of complex 11	96
Fig.3.4: ^1H NMR spectra of complex 12	96
Fig.3.5: ^{13}C NMR spectra of complex 9	97
Fig.3.6: ^{13}C NMR spectra of complex 10	97
Fig.3.7: ^{13}C NMR spectra of complex 11	98
Fig.3.8: ^{13}C NMR spectra of complex 12	98
Fig.3.9: ESI-MS of complex 9	99
Fig.3.10: ESI-MS of complex 10	99

Fig.3.11: ESI-MS of complex 11	99
Fig.3.12: ESI-MS of complex 12	99
Fig.3.13: The solid state crystal structure of compound 9 and 10	100
Fig.3.14: Analysis of the GI ₅₀ value of complexes 9 , 10 , 11 and 12 against different cancer cell lines.....	101
Fig.3.15: ESI-MS spectra of compound 9 , 10 , 11 and 12 in DMSO–MeOH.....	103
Fig.3.16: ESI-MS of Compound 9 , 10 , 11 and 12 in 1% DMSO-media..	103
Fig.3.17: ¹ H NMR spectra of compound 9 , 10 , 11 and 12 in DMSO- <i>d</i> ₆ ...	104
Fig.3.18: ¹³ C NMR spectra of complex 9 , 10 , 11 and 12 in DMSO- <i>d</i> ₆ ...	105
Fig.3.19: Effect of complexes on total COX activity at 50µM concentration.....	106
Fig.3.20: Effect of complexes on 15-LOX at 50 µM concentration.....	107
Fig.3.21: Fluorescence quenching of ct-DNA by compound 11	108
Fig.3.22: Fluorescence quenching of HSA by..... Complex 9 , 10 , 11 and 12	109
Fig.3.23: ESI-MS of Histidine Adduct by Compound 9 , 10 , 11 and 12 ...	110
Fig.3.24: ESI-MS of Cysteine adduct by Compound 9 , 10 , 11 and 12	111
Fig.3.25: ESI-MS of Methionine adduct by..... Compound 9 , 10 , 11 and 12	111
Fig.3.26: ESI-MS of mixture of [histidine+cysteine+methionine] adduct by compound 9 , 10 , 11 and 12	112
Fig.3.27: Docking interaction illustration of the selected ligands as well as complexes with COX-2.....	115
Fig.3.28: Overlay diagrams for the binding of complex 10 and free diclofenac at the binding site of COX-2.....	116

Chapter 4

Fig.4.1: Structure of combretastatin.....	131
Fig.4.2: ¹ H NMR spectra of complex 13	142
Fig.4.3: ¹ H NMR spectra of complex 14	142
Fig.4.4: ¹ H NMR spectra of complex 17	143
Fig.4.5: ¹ H NMR spectra of complex 18	143
Fig.4.6: ¹ H NMR spectra of complex 15	144

Fig.4.7: ^1H NMR spectra complex 16	144
Fig.4.8: ^1H NMR spectra of complex 19	145
Fig.4.9: ^1H NMR spectra of complex 20	145
Fig.4.10: ^{13}C NMR spectra of complex 13	146
Fig.4.11: ^{13}C NMR spectra of complex 14	146
Fig.4.12: ^{13}C NMR spectra of complex 15	147
Fig.4.13: ^{13}C NMR spectra of complex 16	147
Fig.4.14: ^{13}C NMR spectra of complex 17	148
Fig.4.15: ^{13}C NMR spectra of complex 18	148
Fig.4.16: ^{13}C NMR spectra of complex 19	149
Fig.4.17: ^{13}C NMR spectra of complex 20	149
Fig.4.18: ^{31}P NMR spectra of complex 14	150
Fig.4.19: ^{31}P NMR spectra of complex 16	150
Fig.4.20: ^{31}P NMR spectra of complex 18	151
Fig.4.21: ^{31}P NMR spectra of complex 20	151
Fig.4.22: ESI-MS spectra of complex 13	152
Fig.4.23: ESI-MS spectra of complex 15	152
Fig.4.24: ESI-MS spectra of complex 17	152
Fig.4.25: ESI-MS spectra of complex 19	152
Fig.4.26: ESI-MS spectra of complex 14	153
Fig.4.27: ESI-MS spectra of complex 16	153
Fig.4.28: ESI-MS spectra of complex 18	153
Fig.4.29: ESI-MS spectra of complex 20	153
Fig.4.30: The solid state crystal structure of compound 13	154
Fig.4.31: The solid state crystal structure of compound 15	154
Fig.4.32: The solid state crystal structure of compound 19	155
Fig.4.33: The solid state crystal structure of compound 14	155

Chapter 5

Fig.5.1: ^1H NMR spectra of ligand HL ⁷	174
Fig.5.2: ^1H NMR spectra of ligand HL ⁸	175
Fig.5.3: ^{13}C NMR spectra of ligand HL ⁷	175
Fig.5.4: ^{13}C NMR spectra of ligand HL ⁸	176

Fig.5.5: ESI-MS of ligand HL ⁷	176
Fig.5.6: ESI-MS of ligand HL ⁸	176
Fig.5.7: The solid state crystal structure of compound HL ⁷	177
Fig.5.8: The solid state crystal structure of compound HL ⁸	177
Fig.5.9: ¹ H NMR spectra of complex 21	179
Fig.5.10: ¹ H NMR spectra of complex 22	179
Fig.5.11: ¹ H NMR spectra of complex 23	180
Fig.5.12: ¹ H NMR spectra of complex 24	180
Fig.5.13: ¹³ C NMR spectra of complex 21	181
Fig.5.14: ¹³ C NMR spectra of complex 22	181
Fig.5.15: ¹³ C NMR spectra of complex 23	182
Fig.5.16: ¹³ C NMR spectra of complex 24	182
Fig.5.17: ³¹ P NMR spectra of complex 22	183
Fig.5.18: ³¹ P NMR spectra of complex 24	183
Fig.5.19: ESI-MS spectra of complex 21	184
Fig.5.20: ESI-MS spectra of complex 23	184
Fig.5.21: ESI-MS spectra of complex 22	184
Fig.5.22: ESI-MS spectra of complex 24	184
Fig.5.23: Absorption spectral titration of HL ⁸ (A) and 23 (B) with DNA in PBS buffer	187
Fig.5.24: Cyclic voltammogram of HL ⁷ and HL ⁸	188
Fig.5.25: Cyclic voltammogram of 21-24	189

Chapter 6

Fig.6.1: Piano-stool and model of RAPTA complex	200
Fig.6.2: ¹ H NMR spectra of complex 25	206
Fig.6.3: ¹ H NMR spectra of complex 26	206
Fig.6.4: ¹ H NMR spectra of complex 27	207
Fig.6.5: ¹ H NMR spectra of complex 28	207
Fig.6.6: ¹³ C NMR spectra of complex 25	208
Fig.6.7: ¹³ C NMR spectra of complex 26	208
Fig.6.8: ¹³ C NMR spectra of complex 27	209
Fig.6.9: ¹³ C NMR spectra of complex 28	209

Fig.6.10: ^{31}P NMR spectra of complex 25	210
Fig.6.11: ^{31}P NMR spectra of complex 26	210
Fig.6.12: ^{31}P NMR spectra of complex 27	211
Fig.6.13: ^{31}P NMR spectra of complex 28	211
Fig.6.14: ESI-MS of complex 25	212
Fig.6.15: ESI-MS of complex 26	212
Fig.6.16: ESI-MS of complex 27	212
Fig.6.17: ESI-MS of complex 28	212
Fig.6.18: The solid state crystal structure of compound 25	213
Fig.6.19: The solid state crystal structure of compound 26	213
Fig.6.20: The solid state crystal structure of compound 28	214
Fig.6.21: Electronic absorption spectra of 25-28 in 1% DMSO-PBS medium.....	216

List of Schemes

Chapter 2

- Scheme 2.1:** Synthesis of compounds $[\text{Ru}(\eta^6\text{-}p\text{-cymene})(\text{L}^1)(\text{PTA})][\text{BF}_4]$ **2**, $[\text{Ru}(\eta^6\text{-benzene})(\text{L}^1)(\text{PTA})][\text{PF}_6]$ **4**, $[\text{Ru}(\text{HL}^2)(\eta^6\text{-}p\text{-cymene})(\text{PTA})][\text{PF}_6]_2$ **6**, and $[\text{Ru}(\eta^6\text{-}p\text{-cymene})(\text{L}^3)(\text{PTA})][\text{BF}_4]$ **8**.....54
- Scheme 2.2:** Valence bond tautomerism of compound **6**.....66

Chapter 3

- Scheme 3.1:** *Synthesis of compounds* $[\text{Ru}(\eta^6\text{-}p\text{-cymene})(\text{nap})\text{Cl}]$ **9**, $[\text{Ru}(\eta^6\text{-}p\text{-cymene})(\text{diclo})\text{Cl}]$ **10**, $[\text{Ru}(\eta^6\text{-}p\text{-cymene})(\text{ibu})\text{Cl}]$ **11**, and $[\text{Ru}(\eta^6\text{-}p\text{-cymene})(\text{asp})\text{Cl}]$ **12**.....94

Chapter 4

- Scheme 4.1:** Structures of ligand L^4 and L^5132
- Scheme 4.2:** Synthesis of complex **13-20**.....140

Chapter 5

- Scheme 5.1:** Synthesis of Ferrocenyl ligands HL^7 and HL^8174
- Scheme 5.2:** Synthesis of Complexes **21-24**.....178

Chapter 6

- Scheme 6.1:** Synthesis of compound $[\text{Ru}(\eta^6\text{-}p\text{-cymene})(\text{TFP})\text{Cl}_2]$ **25**..204
- Scheme 6.2:** *Synthesis of compounds* $[\text{Ru}(\eta^6\text{-}p\text{-cymene})(\text{TFP})_2\text{Cl}]\text{BF}_4$ **26**, $[\text{Ru}(\eta^6\text{-}p\text{-cymene})(\text{TFP})(\text{PPh}_3)\text{Cl}]\text{Cl}$ **27** and $[\text{Ru}(\eta^6\text{-}p\text{-cymene})(\text{TFP})(\text{PTA})\text{Cl}]\text{BF}_4$ **28**.....205

List of Tables

Chapter 2

Table 2.1: Various parameters obtained from HSA interaction with the prepared complexes.....70

Table 2.2: GI₅₀ value (nM) of the prepared complexes in human cancer cells.....71

Chapter 3

Table 3.1: GI₅₀ value (nM/mL) of the prepared complexes in human cancer cell lines.....101

Table 3.2: Various parameters obtained from BSA interaction with the prepared complexes.....110

Table 3.3: Summary of molecular interactions of complex **9**, complex **10** and their corresponding ligands with COX-2.....113

Chapter 4

Table 4.1: GI₅₀ value (nM/mL) of the prepared complexes in human cancer cell lines.....157

Table 4.2: Various parameters obtained from BSA interaction with the prepared complexes.....158

Chapter 5

Table 5.1: GI₅₀ value (nM/mL) of the prepared complexes in human cancer cell lines.....185

Table 5.2: Redox potential of prepared complexes.....189

Chapter 6

Table 6.1: GI₅₀ value (nM/mL) of the prepared complexes in human cancer cell lines.....215

Chapter 1

General Introduction and Background

1.1 Introduction

Transition metal based coordination complexes are widely available in mineral, plant and animal world and play various significant roles in the area of metallurgy, biological systems, analytical chemistry, and industry. Versatile applications of these complexes in catalysis^[1] (*Ziegler natta* catalyst for polymerization of ethylene and propylene), dye industry^[2] (iron containing dye *Prussian blue* for fabrics), naturally occurring enzymes in bioinorganic chemistry^[3] (haemoglobin contains Fe, Co-containing vitamin-B₁₂) *etc.* have made them an integral part of our daily life. However, application of transition metal complexes in medicinal chemistry has not received much attention owing to its toxic nature. Biological activity of a metal complex depends very much on speciation and it has now been proved that, ‘toxic’ metals can exhibit novel therapeutic properties, if coordination chemistry around the metal centre is designed carefully.^[4] Therefore, investigation and understanding of the effects upon variation in oxidation state, numbers and geometries of coordinated ligands on the biological properties of metal complexes is necessary in order to design metal-based drugs with therapeutic applications.

Pt-based drug *cis-platin* is used extensively for the treatment of cancer.^[5] But *cis-platin* is associated with several undesirable side effects and they are extra sensitive towards resistance mechanism.^[6] To overcome limitations of Pt-based drugs, research is going on to develop new anticancer drug using other transition metal atoms.^[7] Among them, ruthenium based compound NAMI-A has shown remarkable activities.^[8] Two other complexes *viz.* indazolium trans-[tetrachloridobis(1*H*-indazole)ruthenate(III)] (KP1019) and (Him)[trans-RuCl₄(im)₂] have also shown considerable activity against various primary tumors. (Him)[trans-RuCl₄(im)₂] complex has shown promising antitumor activity against human colon carcinoma cell lines *i.e.* SW707 and SW948 *in vitro* comparable to that of KP1019.^[9]

1.2 Metals in medicinal chemistry

Although research on metal based medicinal chemistry started in early 1900s, metal complexes have been used for medicinal purpose from ancient time. The Egyptians used copper to sterilise water, zinc was used for healing of wounds and many more.^[10] However, discovery of Pt-based drug, *cis*-platin has stimulated the research for metal based drugs in a great way^[11] in recent years the study and progression of metal-based pharmaceutical agents has increased and lead to a more varied approach to the use of metals in biological and medicinal systems. For example; gold complex auranofin is used for arthritis treatment^[12], sodium nitroprusside is an iron containing cardiovascular drug^[13], bis(maltato) oxovanadium (BMOV) is an orally active insulin mimetic drug useful for diabetes treatment^[14], whereas silvadene (silver sulfadiazine) has antibacterial and antifungal properties^[15] and is used in the treatment of burns, and Ceretec is a ^{99m}Tc(V) complex used as an imaging agent (Fig.1.1).^[16] However, till date the number of metal based approved drugs are only handful and the use of metal complexes in treatment of cancer is limited to platinum based drug only.^[17]

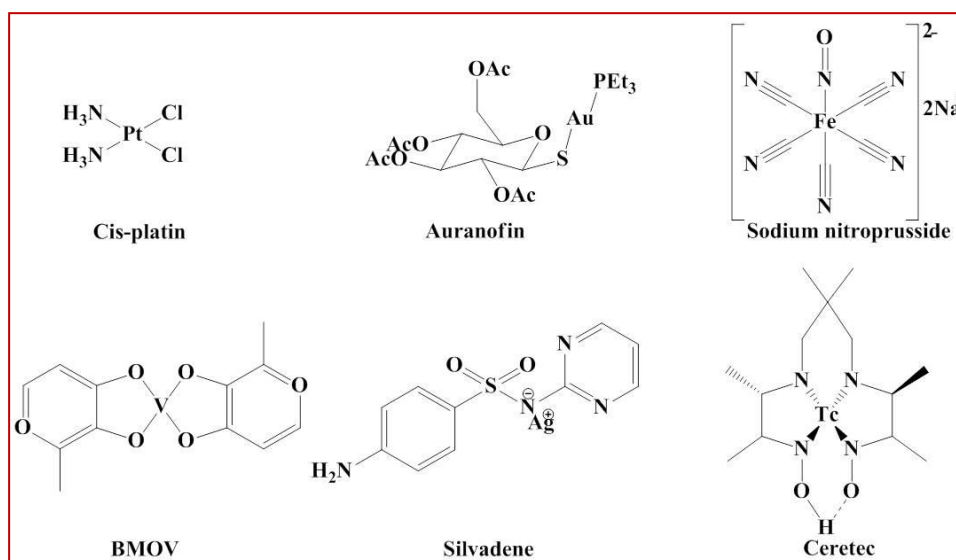


Fig.1.1: Structure of metal based drugs.

1.3 Definition of cancer

Cancer is a group of diseases characterized by uncontrolled growth and spread of abnormal cells. The word “Cancer” originates from the greek

word *Karkinos*, which actually means *crab*.^[18] The name was given by Hippocrates (460-370 B.C.), considered as “Father of medicine”, because malignant tumour is usually surrounded by swollen blood vessels which reminded him of a crab with a central body (the tumour or lump) from which several rays-the legs, spread into the surrounding tissues.^[19] The uncontrollably divided premature cells accumulate to form lumps or masses of tissues, which is known as tumour. There are two types of tumours that can be formed because of uncontrolled cell growth; non cancerous tumour and cancerous tumour. Non cancerous tumours (often known as benign tumour) stay in one place and do not spread to other parts of the body, whereas a tumour is cancerous when the cells invade adjacent tissues and spread to other parts of the body *via* blood or lymph. Cancer that develops from the first place it originated (called the primary tumour) to a new part of the body is called metastatic cancer. When cancer cells spread and develop into new tumours, the new tumours are called metastases.

1.4 Classification

Different types of cancers are classified according to the origin of the abnormal cells.^[20]

1.4.1 Carcinoma:

The tumour cells arise from the epithelial cells and this type of cancer is the most common one. This category comprises of lung, prostate, breast and colon cancer.

1.4.2. Sarcoma:

This type of cancer originates from connective tissues e.g. muscle, fat, cartilage and bone.

1.4.3. Lymphoma and Leukemia:

In this case, cancer does not form solid tumours as it originates from lymphatic system (lymphoma) or bone marrow (leukemia). Lymphoma or leukemia develops because of the abnormal growth of white blood cells in the blood stream.

1.4.4. Brain and spinal cord cancer:

As the name suggests, this type of cancer occurs at central nervous system. The brain is made up of nerve cells (neurones) as well as special connective tissue cells (glial), that support the nerve cells. The most common type of brain tumour originates from glial cells and is called glioma.

To differentiate among the different forms of cancer, latin prefixes are added to the name. Each prefix is derived from the location where the tumorous growth originates, *e.g.*, myosarcoma is the term for cancer of the muscle.^[21]

1.5 Statistics

Cancer is the second leading cause of death globally and was responsible for 8.8 million deaths in 2015. The most common causes of cancer death are blood cancer, followed by non hodgkin's lymphoma and breast cancer. Oral cancer and lung cancer in males and cervix as well as breast cancer in females account for over 50% of all cancer deaths in India. Around one third of deaths from cancer are due to the 5 leading behavioral and dietary risks: high body mass index, deficiency in fruit and vegetable intake, lack of physical activity, consumption of alcohol and tobacco. In first world countries, overweight and obesity is one of the main reasons for cancer occurrence, whereas, in second and third world countries cancer results from low fruit and vegetable intake and chronic infections from Hepatitis B, C and Human Papilloma Virus (HPV), the latter leading to many cases of cervical cancer (Fig.1.2).

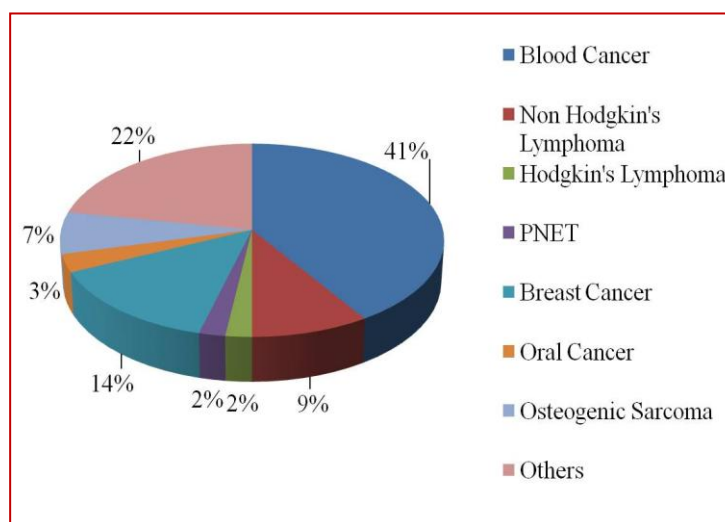


Fig.1.2: Rate of occurrence of different types of cancer in 2015.

Although rate of cancer incidence in India is lower than other developed countries, the death rate is worrisome (Fig.1.3). World Health Organisation's Globocan 2012 reported that only 1 out of every 5 or 6 women newly diagnosed with breast cancer died in the US, whereas corresponding figures in India stood at 1 out of every 2 patients. Around 1,500 people die of cancer in India every day, making it the second most common cause of death in India after cardiovascular disease. According to National Institute of Cancer Prevention and Research, 2,000 new cancer cases are detected in the country daily. The number of new cases of cancer is expected to be 17.3 lakh by 2020.

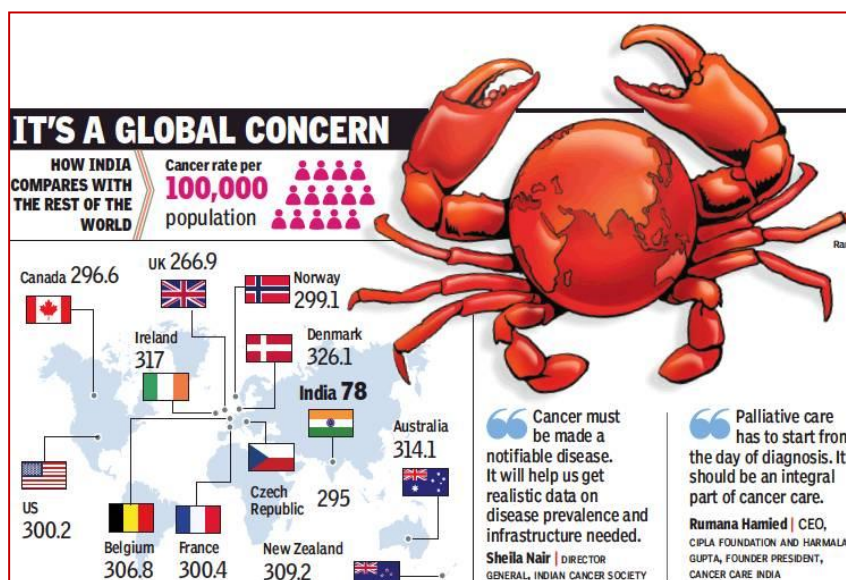


Fig.1.3: Incidence of cancer around the world in 2017.^[22]

Apart from lifestyle, geography also follows an important role in mapping of cancer cases in India (Fig.1.4). In metro cities, lung cancer is the most common one, whereas for women, breast cancer is more likely in urban areas than the rural localities. The Indian government's Million Death Study released in 2012 showed that the area an Indian lives in, his economic and educational status and religion are also responsible for the outcome of cancer. Rise in tobacco use has increased the occurrence of lung cancer in men, whereas women are suffering from breast cancer in northeast India more than any other parts of India.

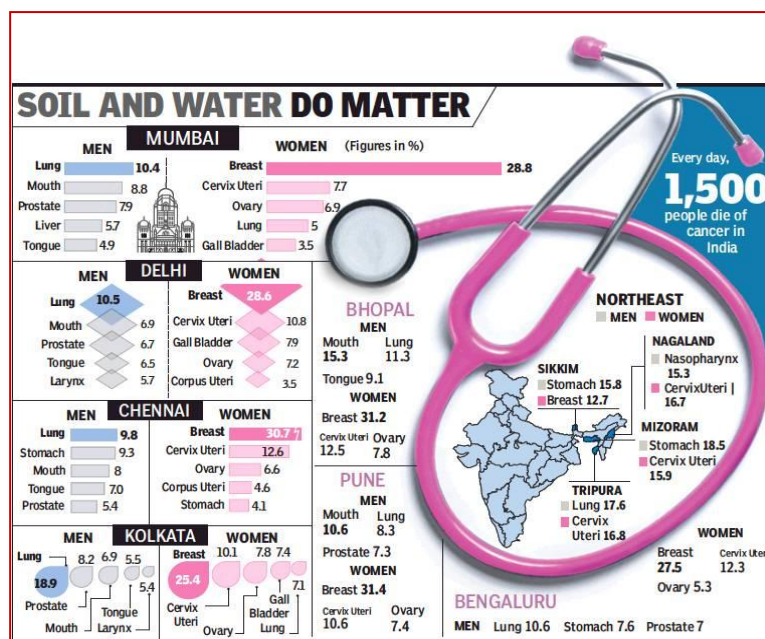


Fig.1.4: Study on cancer patients in different states of India. ^[23]

1.6 Different modes of cancer treatment

As cancer is a collection of different diseases, cancer treatment is also comprised of various techniques.^[24] The method of treatment depends on the class, the state, location of the tumour as well as health and age of the patient. The most common approaches for cancer treatment are

1.6.1 Surgery:

The aim of surgical treatment is to remove the cancer affected body part completely and applicable for primary tumours and localized metastases e.g. breast cancer, cancers of the gastro-intestinal tract, renal cancer, bladder cancer etc. Unfortunately, this treatment option is not applicable for difficult accessible body sites, metastasized and late stage tumours, and hematological malignancies.

1.6.2 Radiation therapy:

Here, tumour mass is destroyed by targeting cancerous DNA by ionizing radiation e.g. gamma rays, X-rays, neutrons and proton beams. In radiation therapy, the energy and dose can be applied extremely accurately due to the physical properties of the protons. Therefore the side effects are less severe because the protons release almost all of their energy when they get in

contact with the cancerous tissue, thus not releasing any side effects to the surrounding healthy tissues. This method is very much effective in the treatment of children as keeping the surrounding tissue intact is of utmost importance because the body is still in the developing phase.^[25]

1.6.3 Hormonal therapy:

The aim of hormonal therapy is to block the activity of the hormones which take part in the expansion of tumours. Tamoxifen is used in hormonal therapy to limit the activity of estrogen hormone, which is involved in progression of breast cancer.^[26]

1.6.4 Immunotherapy:

This technique is used to activate the immune system of the patient to destroy the tumour. Various techniques of immunotherapy are applied to diagnose cancer, which include monoclonal antibodies (drugs that are designed to bind to specific targets in the body, causing immune response to cancer cells), cytokines (biologically active substances which regulate processes in the body like cell division or the activity of the immune system) etc.^[27]

1.6.5 Stem cell transplantation therapy:

Stem cell transplantations are techniques that restore blood-forming stem cells in patients whose blood forming cells have been destroyed by the very high doses of chemotherapy or radiation therapy during cancer treatment. This technique is used mostly for the leukemia patients.^[28]

1.6.6. Chemotherapy:

Chemotherapy is defined as the treatment of cancer cells with pharmaceutical compounds. These compounds can kill cancer cells by targeting DNA or enzymes which are involved in cell replication or by inhibiting the pathway of mitosis. Chemotherapeutic reagents have been classified in various categories depending upon their mode of actions.

1.6.6.1 Intercalating agents:

Intercalating reagents get inserted between the layers of nucleic acid pairs and rupture the shape of the helix, thus preventing replication and transcription of DNA. Doxorubicin is used as intercalating agent extensively for several malignancies, including breast, hepatic and lymphatic cancer despite of its cardiotoxic side effects (Fig.1.5).^[29]

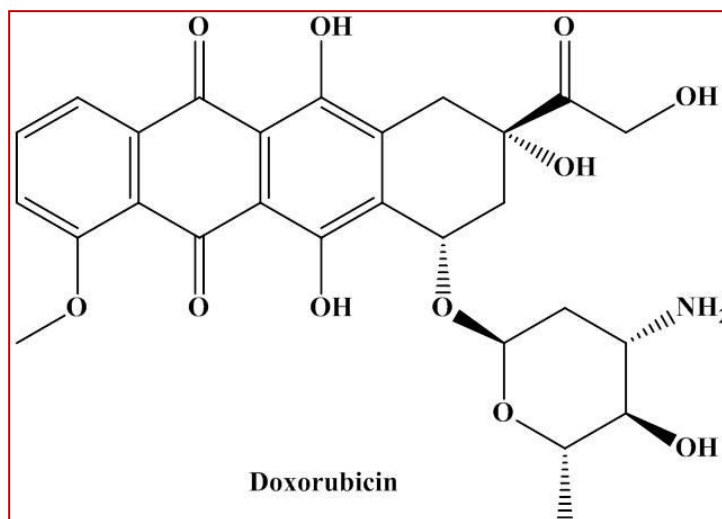


Fig.1.5: Molecular structure of intercalating agent.

1.6.6.2 Alkylating agents:

Alkylating agents contain highly electrophilic groups which covalently bind to nucleophilic groups in DNA. Most of the alkylating agents are bipolar in nature and therefore capable of forming bridges between a single strand or two separate strands of DNA, disturbing the activity of the enzymes involved in DNA replication. As a result, either cell death occurs or cell becomes unable to divide further. Cyclophosphamide is a versatile alkylating agent which is used for treatment of lymphomas, breast cancer and acute lymphoblastic leukemia (Fig.1.6).^[30]

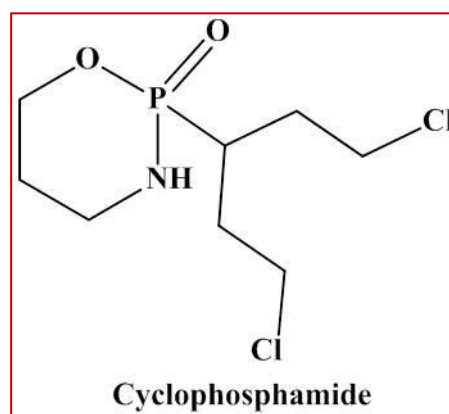


Fig.1.6: Molecular structure of alkylating agent.

1.6.6.3 Antimetabolites:

Compounds which are structurally similar to naturally occurring substances such as vitamins, nucleosides or amino acids, are known as antimetabolites. These can interrupt metabolic processes by interaction with enzymes inducing cell cycle arrest. Methotrexate was one of the first developed antimetabolites used for cancer treatment. Methotrexate inhibits dihydrofolate reductase and therefore the synthesis of thymidine. Another example of antimetabolites is 5-fluorouracil (Fig.1.7), which is converted into 5-fluorodeoxyuridine monophosphate leading to inhibition of the synthetic pathway of the DNA. 5-FU is used in combination therapy against several malignancies including colorectal, mammary and bladder carcinoma.^[31]

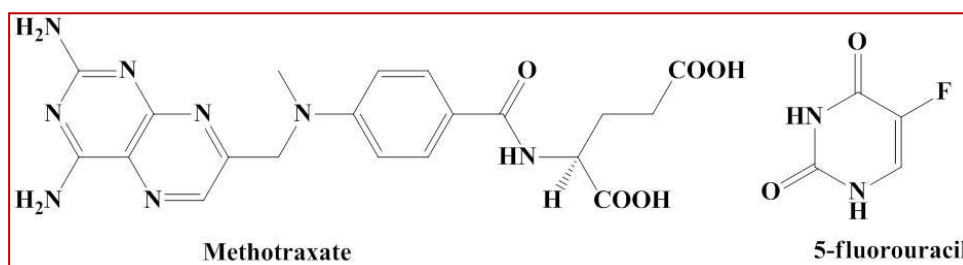


Fig.1.7: Molecular structure of antimetabolites.

1.6.6.4 Topoisomerase inhibitors:

Topoisomerase is one of the enzymes that is involved in DNA replication and transcription process. During replication or transcription, topoisomerases catalyze the unwinding of DNA regions by transient cleavage of the phosphodiester bonds of the DNA backbone. Once unwinding and the relevant DNA process is completed, topoisomerases catalyze the religation of the DNA nick. Irinotecan, which acts as topoisomerase inhibitor, is used with 5-Fluorouracil for the treatment of metastatic colorectal carcinoma (Fig.1.8).^[32]

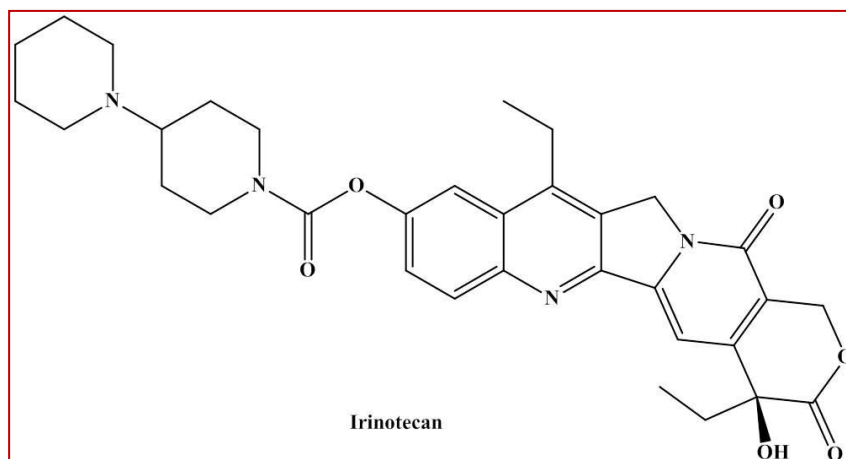


Fig.1.8: Molecular structure of topoisomerase inhibitor.

1.6.6.5. Metal based chemotherapeutic drug: Although organic molecules have been used for cancer treatment predominantly, there are few metal based drugs as well which have been applied in cancer diagnosis. Surgery and radiotherapy were the dominating cancer therapies till 1960, after the discovery of different chemotherapeutic drugs, treatment of cancers combining surgery, radiation and drugs maximized the anti-tumor effect and as a consequence became standard in clinical practice.^[33]

1.7 Platinum based anticancer drug

Although *cis*-platin was first reported by Michel peyrone in 1844, its antiproliferative property was discovered accidentally by Barnett Rosenberg about hundred years later, while investigating the influence of an electric field on the growth of *Escherichia coli* bacteria.^[34] *Cis*-platin is the first chemotherapeutic drug which got approval from FDA in 1978 for worldwide clinical practice. *Cis*-platin, also known as *cis*-diamminedichloroplatinum(II), is a square planar platinum(II) coordination compound(Fig.1.9). It is air stable light yellow crystalline compound, slightly soluble in water, and soluble in DMF.



Fig.1.9: Molecular structure of *cis-platin*.

Presently *cis-platin* is the most widely prescribed anticancer drug with promising curative ability in cancer treatment. It is used for the treatment of various types of cancer including lung cancer, cervical cancer, metastatic testicular tumours, ovarian cancer and many more. It is used in combination therapy with surgery and radiation therapy of many other solid tumours e.g. Bladder, head, neck and lung cancers. There are two other platinum based drugs which are used for cancer treatment as well are carboplatin^[35] and oxaliplatin^[36], with improved effectiveness and broader spectrum of activity (Fig.1.10).

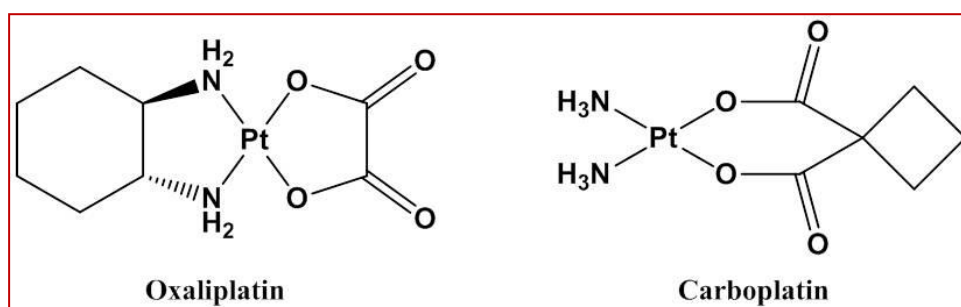


Fig.1.10: Molecular structure of *Oxaliplatin* and *Carboplatin*.

Carboplatin exhibits tumour inhibiting property similar as *cis-platin*, whereas, oxaliplatin is useful in a combination therapy against metastatic colorectal cancer.^[37]

1.8 Mechanism of *cis-platin*

Cis-platin is administered by intravenous injection as an aqueous saline solution in blood stream.^[38] Approximately 50-70% of the platinum binds to the serum proteins and gets excreted within 24 h and the remaining part is spread among various tissues.^[39] As the chloride ion concentration in the

blood stream is higher (100 mM), hydrolysis of *cis*-platin does not occur spontaneously in that concentration and it remains in neutral state as *cis*-Pt(NH₃)₂Cl₂.^[40] But when the *cis*-platin diffuses passively across the cell membranes into the cytoplasm, hydrolysis gets facilitated owing to its lower chloride ion concentration (5mM) inside the cell. The drug, *cis*-platin undergoes hydrolysis with substitution of one chloride ligand, forming cationic species *cis*-[Pt(NH₃)₂(Cl)(H₂O)]⁺ which can aim cellular targets readily.^[41] This active cationic species then binds to N7 of two intrastand adjacent guanine bases of DNA forming initially monofunctional DNA adducts and later on bifunctional intrastrand cross-links of the type 1,2-d(GpG) and 1,2-d(ApG) (Fig.1.11).^[42] These adducts induce a conformational changes in the DNA, resulting in the inhibition of DNA replication and transcription which leads towards the programmed cell death in cancerous tissue.

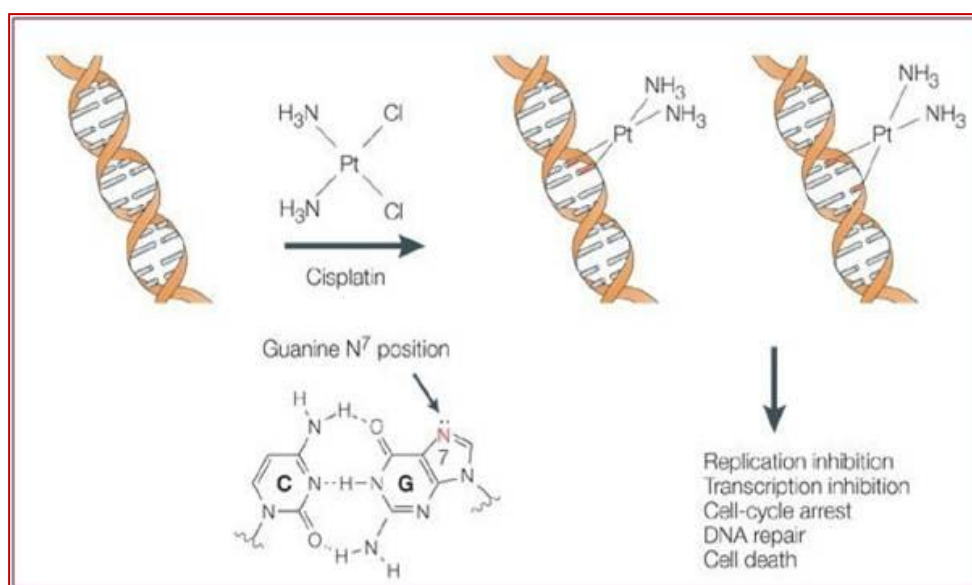


Fig.1.11: DNA adduct formation with *cis*-platin.^[43]

1.9 Non-platinum metal complexes as anticancer agents

Though the clinical success of *cis*-platin and other platinum-based anticancer drugs showed the viability of this approach, but the limitations associated with the platinum drugs (mainly required or inherent drug resistance and severe dose-limiting side effects) provided the impetus for the search of alternative chemotherapeutic strategies based on different complexes with other metals. As a result, scientists around the globe are

searching for new anticancer drug with better activity, higher selectivity towards tumour cells and a broader spectrum of activity than *cis-platin*.^[44] Various complexes incorporating different metal ions other than platinum *e.g.* gold, titanium, iron, ruthenium, and osmium are under investigation for the development of new chemotherapeutic drug. Among them, metal-based drugs which have entered clinical trials contain titanium^[45], gold^[46] and gallium atom (Fig.1.12).^[47]

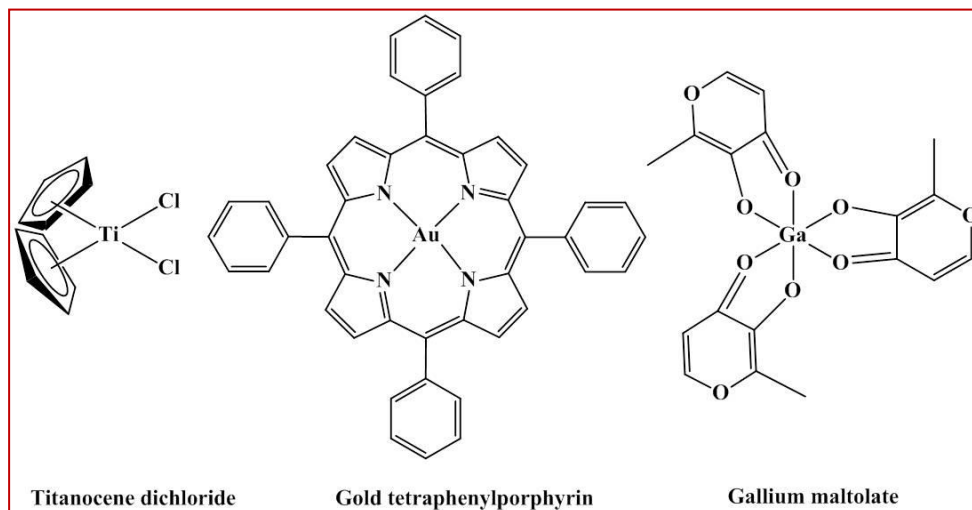


Fig.1.12: Molecular structure of metal based anticancer drugs.

Non platinum metal atoms have different chemical property (flexibility in oxidation number, versatile coordination geometry, binding preferences to different biomolecules according to HSAB theory), which may lead to death of cancer cells *via* mechanism different from platinum drugs.^[48]

1.10 Ruthenium Anticancer Drug

Among several other transition metals, ruthenium is considered as an promising alternative to platinum. The availability of ruthenium in several oxidation states (+II, +III and +IV) at physiological condition has an extra advantage along with its rich and well-established synthetic and coordination chemistry.^[49] The other key advantages of ruthenium complexes are the ability to tune the metal–ligand exchange kinetics by ligand variation and considerable lower toxicity than the platinum complexes *in vivo*.^[50]

There are various features that have made ruthenium as a potential candidate for cancer treatment. Cancer cells are overexpressed with transferrin receptors due to their high demand for iron. As ruthenium species has high affinity to bind with serum transferrin, there is a high possibility that transferrin-bound metal ions can be easily released in the relatively low pH of tumor cells. Again cancerous cells have relatively low electrochemical potential as well as low pH because of their hypoxic nature. In hypoxic environment, reduction of Ru(III) to Ru(II) becomes favourable, which has the ability to bind with different biomolecules.^[51]

Therefore, scientists have developed a number of ruthenium complexes for the last few years, which can show enhanced activity than the Pt-based drugs. Among them, NAMI-A and KP1019 have shown significant activity till now and have entered clinical trials.^[52]

1.10.1 NAMI-A

NAMI-A [ImH][*trans*-RuCl₄(dms_o-S)(Im)] (dms_o-S = sulfur-bonded dimethyl sulfoxide, Im = imidazole) is a novel ruthenium compound with outstanding antimetastatic property which has entered phase-II clinical studies (Fig.1.13).^[53] Till date, NAMI-A is the only ruthenium compound that has entered phase-II clinical studies and has been studied on human beings.^[54]

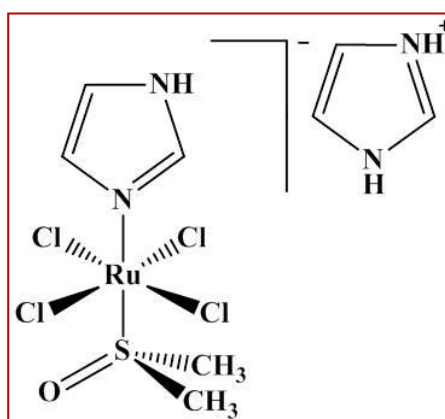


Fig.1.13: Molecular structure of NAMI-A.

NAMI-A breaks the “platinum paradigm” which says that metal based drugs show anticancer property through interaction with DNA.^[55] (NAMI-A can reduce metastases weight as well as it has the ability of terminating the spread of secondary tumours, especially in case of solid metastases and lung cancers.^[56] But NAMI-A is not capable either of showing direct cytotoxicity to adherent cancer cells or any effect on primary tumour growth.^[57] The complex has pseudo-octahedral geometry at the Ru(III) centre, where four equatorial axes are occupied by four chloride ligands, and DMSO and imidazole occupy the two axial positions. Although NAMI-A is stable in solid state, in presence of biological reducing agents such as cysteine, ascorbic acid or glutathione, Ru(III) centre of the drug is reduced to Ru(II), which then undergoes stepwise hydrolysis of equatorial chloride ligands. This process further initiates the substitution of DMSO ligand, which leads to the formation of uncharacterized dark-green polyoxo species.^[58] The aqua complex of NAMI-A can bind to different protein molecules, which could be the plausible reason for this drug to show antimetastatic property.^[59] Although the detailed mechanism of NAMI-A is still unknown, the fact that this poly-oxo compound is taken up more effectively than freshly dissolved NAMI-A by the metastatic tumour cells *in vitro*, has prompted the scientists to give more emphasis on NAMI-A hydrolysis products.

1.10.2 KP1019

KP1019 HInd[*trans*-RuCl₄(Ind)₂] (Ind = indazole)] is another ruthenium anticancer drug which has entered clinical trials (Fig.1.14).^[60] To increase the aqueous solubility of the complex, its Na-salt has been prepared Na[*trans*-[RuCl₄(Ind)₂], which has shown remarkable antiproliferative activity both *in vitro* and *in vivo* against human colon carcinoma cell lines and a variety of primary tumour models.^[61]

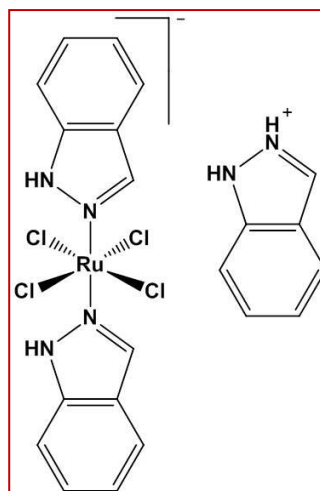


Fig.1.14: Molecular structure of KP1019.

A comparison of DNA binding studies of KP1019 and *cis*-platin reveals that KP1019 is capable of binding to DNA irreversibly by affecting its conformation in a different mechanism than that of *cis*-platin.^[62] Protein binding studies show that it interacts with serum proteins especially with albumin and transferrin.

Both KP1019 and NAMI-A are prodrugs which are converted to active species *in situ*.^[63] In the physiological environment, the equatorial chlorido ligands of KP1019 and NAMI-A, and the axial dimethylsulfoxide (DMSO) ligand of NAMI-A, become labile and as a consequence, Ru(III) centre is reduced to Ru(II) by biological reductants present in the system *e.g.* ascorbate, glutathione etc. *via* “Activation by Reduction” hypothesis proposed by Clarke.^[64] In biological buffers, Ru-drugs bind to different serum proteins *via* non-covalent hydrophobic interactions initially followed by covalent coordination bonding.^[65] NAMI-A derivatives coordinates to HSA *via* histidine imidazoles^[66], whereas KP1019 interacts with apoTf to form covalent adducts.^[67]

1.11 Metal-Arene Compound as Anticancer Drugs

There are mainly three families of organometallic ruthenium complexes which have been extensively studied for their biological activity.

1.11.1 Piano stool complexes

Literature studies reveal that, Ru(II) aminophosphanes was the first Ru(II) complex which was studied for cytotoxicity and had shown positive results. But to overcome the solubility and stability issues associated with this type of complex, η^6 -arene ligands were introduced to these complexes as they can stabilise Ru(II) to prevent oxidation to Ru(III) species as well as the formation of Ru(II) complexes with a positive charge allows for an increased solubility in water.^[68] This type of complex is known as half-sandwich “piano stool” complex. Half-sandwich "piano stool" complexes $[(\eta^6\text{-arene})\text{Ru}(\text{X})(\text{Y})(\text{Z})]$ produced by Sadler group have been studied extensively (where X–Y is a neutral chelating ligand, and Z is monoanionic) (Fig.1.15) recently.^[69] In general Ru–arene complexes show promising antiproliferative activity against human ovarian cancer cell lines. The structure-activity relationship show that cytotoxicity increases with increase in size of arene rings.

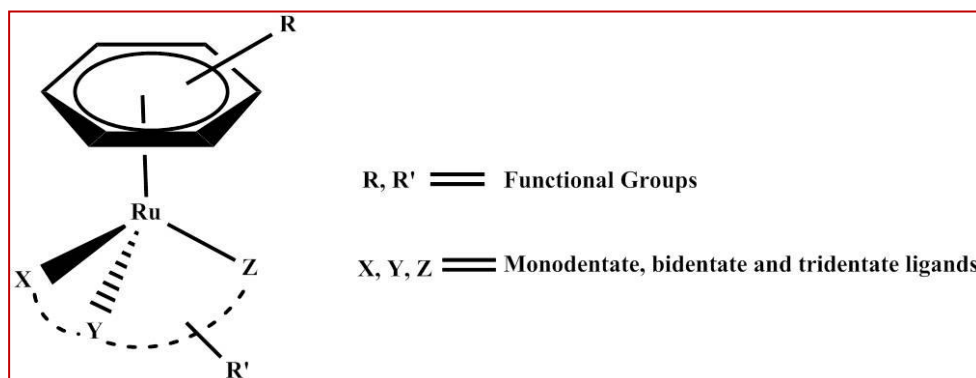


Fig.1.15: Structure of piano stool complex.

1.11.2 RAPTA complexes

A group of compounds which is structurally similar to piano stool complexes has been reported by Dyson group which is based on RAPTA scaffold (Fig.1.16). As the name suggests, RAPTA compounds are characterized by a η^6 -arene ligand bound facially to the metal center and the presence of a monodentate 1,3,5-triaza-7-phosphatricyclo-[3.3.1.1]decane (PTA) ligand, leaving the other two coordination sites by labile chloride ligands.^[70] These RAPTA compounds interact strongly with proteins and have the ability to discriminate binding to different proteins,

but show a relatively low propensity to bind DNA, which is considered to be the main target of many Pt-based drugs.^[71]

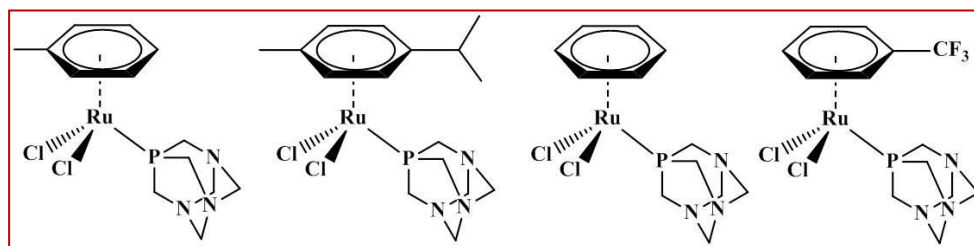


Fig.1.16: Structure of RAPTA complexes.

1.11.3 Cycloruthenated complexes

The third group of compounds are cycloruthenated derivatives which are prepared by making use of the well-known cyclometalation reaction involving C-H bond activation at an early stage of the procedure (Fig. 1.17).^[72] A number of these compounds induce cytostatic and cytotoxic effects on mammalian tumour cells as effectively as *cis*-platin.

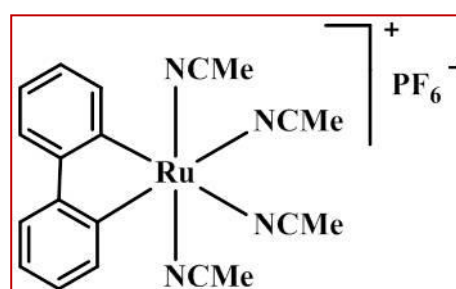


Fig.1.17: Structure of cycloruthenated complex.

1.12 Structural Features of Ru(II)-arene complexes for anticancer activity

There are various structural features through which anticancer activity of this type of complexes can be tuned. This provides considerable scope for the optimisation of their design in terms of mechanisms of action, selection of target sites, and modulation of possible side effects.

1.12.1 The Arene

Arene ring present in the complexes of general formula $[(\eta^6\text{-arene})\text{Ru}(\text{X})(\text{Y})(\text{Z})]^{n+}$ stabilises the ruthenium centre in +2 state. The nature of the arene ring can influence cell uptake and interactions with

potential targets.^[73] It has been observed that the cytotoxic activity of Ru(II) arene complexes used to increase with the size of the coordinated arene. When a series of Ru(II) arene ethylenediamine (en) was tested against the human ovarian cancer cell line (A2780), IC₅₀ values were found to decrease in the order as : benzene (bz, 17 μ M) > *para*-cymene (*p*-cym, 10 μ M) > biphenyl (bip, 5 μ M) > dihydroanthracene (dha, 2 μ M) > tetrahydroanthracene (tha, 0.5 μ M).^[74] The increased cytotoxic potency in these complexes is assumed to arise from the ability of such hydrophobic arenes to intercalate into DNA, thus generating medium-to-strong π -stacking interactions that cause a significant distortion of the structure of DNA.^[75]

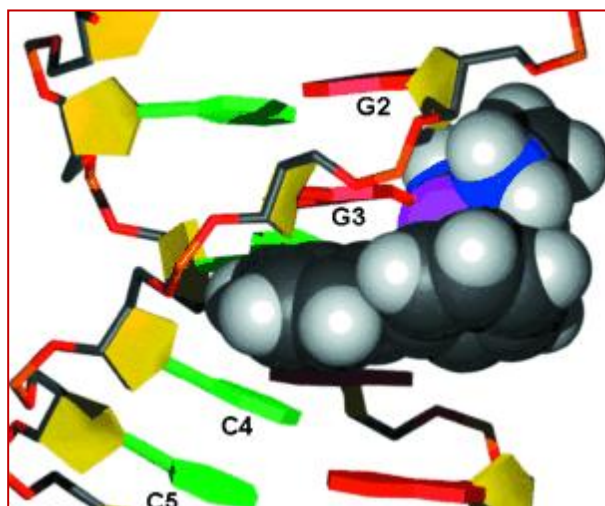


Fig.1.18: Schematic representation of a Ru(II) extended arene complex intercalating between DNA bases. Ru(II) atom shown as a purple sphere, bip arene shown as grey and white spheres, chelating ligand shown as blue and white spheres, and guanine bases in red.^[76]

1.12.2 The XY Chelating Ligand

XY ligand may be nitrogen or oxygen donor ligands (*NN*-, *NO*-, *OO*-) or it may be two monodentate ligands. In order to design tumour specific metallodrug, some biologically active molecules are also used as chelating ligands. A series of novel ruthenium half sandwich complexes have been prepared using picolinamide ligands for use as anticancer drug. One ruthenium complex was found to be more cytotoxic than cisplatin on HT-29 and MCF-7 cells, and it remains active with MCF-7 cells even under hypoxic conditions, making it a promising candidate for in vivo studies.^[77]

1.12.3 The Z leaving group

The leaving group, Z, which is used to be a halogen atom in most of the “piano-stool” complexes, plays an important role as removal of the leaving group from the metal centre makes a vacant site available for the coordination of potent biomolecules to the same metal centre. A number of new ruthenium compounds have been synthesised, which exhibit excellent cytotoxicity against a number of different human tumour cell lines including a defined cisplatin resistant cell line and colon cancer cell lines. Addition of hydrophobic groups to the ruthenium molecules has a positive effect on the cytotoxicity values. After incubation of a ruthenium compound with a 46 mer oligonucleotide duplex and subsequent nuclease treatment, ruthenium is bound to a guanine residue.^[78]

1.13 Investigation on recent work

In order to develop advanced chemotherapeutic molecules, scientists are looking to introduce various functionalities in ruthenium centre to better target cancer cells. Ruthenium derivatives have included various functionalities of biological significance in different ways to generate multifunctional chemotherapeutic, often with enhanced activities.^[79] One of the examples of this effort was reported where ethacrynic acid, tethered to the arene ligand was used to overcome the glutathione transferase drug resistance mechanism.^[80] Again, Ru(II)-arene complexes were coupled to human serum albumin (HSA) using the benzaldehyde function of the arene ligand *via* a hydrazone bond.^[81] It has been observed that cellular internalization for this albumin-arene-ruthenium conjugate was increased compared to non-functionalized arene ruthenium analogues, thereby improving the selectivity *in vitro*.

Introduction of additional functionality through X, Y and/or Z ligand of half-sandwich arene ruthenium unit is another strategy to improve the efficacy of Ru-based metallodrugs. Kinase inhibitor staurosporine has been used as a bidentate chelating ligand, attached to Ru(II) centre to enhance nanomolar activity against melanoma cell lines.^[82] Again, a series of arene ruthenium derivatives containing

inhibitors of tyrosine kinase activity of the epidermal growth factor receptors (EGFR) has been also synthesized.^[83] Similarly, a series of arene ruthenium derivatives containing inhibitors of cyclooxygenase activity has been also synthesized. Enhanced selectivity and cytotoxicity in cancer cells was observed for the neutral ruthenium(II) chloro complexes.^[84]

To utilize biologically active molecule with known therapeutic values, as chelating agent for the synthesis of Ru(II)-arene anticancer drug, different organic moieties have been tethered to the motif. Avobenzone, which is extensively used in the formulation of sunscreens and cosmetic products, has been used as chelating agent, to prepare RAPTA complexes.^[85] The cytotoxicity of the complexes has been evaluated in vitro against human ovarian carcinoma cells, A2780 and A2780cisR, as well as against nontumorous Human Embryonic Kidney (HEK293) cells. The ionic complexes with hydrophilic PTA and PTA-Me ligands are considerably more active than the neutral chloro complexes. Again, curcumin, which has a number of relevant medicinal properties, has been attached to Ru(II)-arene moiety and their antiproliferative activity have been investigated against different cancer cell lines.^[86-91]

A report was published where an acridine ruthenocycle was shown to be more active than *cis*-platin against *cis*-platin-sensitive and *cis*-platin resistant breast and ovarian cell lines.^[92] As acridine ligand is polyaromatic as well as azaaromatic in nature, it facilitates intercalation between DNA base pairs. Arene ruthenium complexes introducing phosphitecarbohydrate ligands to modulate the lipophilicity of the complexes have also been reported.^[93-94] The compounds were found to possess moderate cytotoxic activity against various cancer cells, with however, the lowest activity being observed on non-tumour alendothelial cells, suggesting a degree of selectivity for cancer cells.

The approach to design heteronuclear bimetallic complexes are additional strategies used to modify the mode of action of metal-based drugs.^[95-98] These strategies have been utilised in the synthesis of ruthenium(II) arene complexes using ferrocene derivatives.

Among the most promising Fc-Ru dinuclear complexes, first and second-generation heterometallic ferrocenyl-derived metal–arene metallodendrimers, have been prepared and cytotoxicity studies have been evaluated against A2780 cisplatin-sensitive and A2780cisR cisplatin-resistant human ovarian cancer cell lines and against a non-tumorigenic HEK-293 human embryonic kidney cell lines.^[99] Moreover, RAPTA compounds have been prepared taking ferrocenyl derived metallodendrimers.^[100] *In vitro* antiproliferation activity of the dendritic ligands and their complexes were evaluated against A2780 and A2780cisR human ovarian cancer lines, the SISO human cervix cancer line, the LCLC-103H human lung cancer line, and the 5637 human bladder cancer line. Few of the reported compounds slowed the growth of the ovarian cancer cell lines by more than 50% at equi-iron concentrations of 5 μM . Lu *et al* reported two new Ru(II)-arene complexes containing carborane unit and ferrocene unit.^[101] Observation illustrates that a structural change from a ferrocene unit to a carboxyl group could lead to high selectivity toward cancer cells and facilitate the efficient inhibition of the proliferation of target cells. Thus tuning of the overall properties of the ruthenium(II) arene complex by appropriate ligand tagging is critical to create a selective antineoplastic agent.

Trinuclear complexes have been also investigated as anticancer agents. Studies suggest that excellent biological activity observed for cationic triruthenium clusters such as $[(p^i\text{PrC}_6\text{H}_4\text{Me})(\text{C}_6\text{Me}_6)_2\text{Ru}_3(\mu_2\text{H})_3(\mu_3\text{O})]^+$ involves a supramolecular process within cancer cells.^[102] These clusters contain a hydrophobic pocket where planar aromatic moieties can be well accommodated and a μ_3 -oxo ligand, present in the system can interact with hydroxyl groups^[103], which allows supramolecular interactions to take place with proteins or other biological targets.

Teranuclear rectangular shaped metalla-cycles of the general formula $[(\text{arene})_4\text{Ru}_4(\text{OO}\cap\text{OO})_2(\text{N}\cap\text{N})_2]^{4+}$ (arene = hexamethylbenzene, *p*-cymene; $\text{OO}\cap\text{OO}$ = oxamido, oxalato 1,4-benzoquinonato-2,5-diolato, 3,6-dichlorido-1,4-benzoquinonato; $\text{N}\cap\text{N}$ =

pyrazine, 4-4'-bipyridine, 1,2-bis(4-pyridyl)ethylene, 1,2-bis(4-pyridyl)ethane) have been tested against cancer cells.^[104] The activity of these metalla-cycles against human ovarian cancer cell lines (A2780 and A2780cisR) was found to be moderate to excellent, depending on the nature of the arene ligand as well as the size of the linker, with IC₅₀ values as low as 4 mM.

Larger metalla-assemblies have been synthesized using tetra(pyridyl)porphyrin panels giving rise to octacationic Ru(II)-arene complexes. These systems show slight preference to interact with quadruplex DNA.^[105] They have also shown high cytotoxicity against A2780 and A2780cisR cancer cells. The porphyrin panels can be metallated, thus affording even more cytotoxic agents.^[106] The authors postulated that the EPR effect plays an important role in the activity of these systems.

The first Ru-arene compound which was tested for anticancer activity was [Ru(η^6 -C₆H₆)Cl₂(metronidazole)] (metronidazole = 1- β -hydroxyethyl-2-methyl-5-nitroimidazole). Metronidazole, which is marketed under the tradename of Flagyl, is used for the treatment of infection. When Metroimidazole was coordinated with Ru(II) centre, it showed more selected cytotoxicity than the free ligand.^[107] In recent years, various approaches have been explored to enhance antiproliferative activity of by attaching *P*- or *N*- donor ligands or *N,N*-, *N,O*- or *O,O* chelating ligands, dinuclear complexes, oxo capped trinuclear clusters, photoactive tetranuclear porphyrin derivatives, hexanuclear cages^[108-112] or attaching bioactive molecules such as letrozole to the arene ruthenium unit.^[113]

Although there are a number of reports on Ru-arene compounds with significant anticancer activity, till date, no compound has entered successfully for the use of anticancer drug. Several questions associated with Ru(II)-arene complex *e.g.* solubility problem, stability issues, ambiguity on target specificity, active species of the drug complexes have focussed for further investigation on this field.

1.14 Purpose and span of present investigation

The purpose of present work is to design and synthesis of different Ru-arene metallodrugs taking different ancillary ligands as well as various biologically active molecules and evaluation of their anticancer activities.

Chapter 2 illustrates synthesis of four water soluble RAPTA type of compounds involving picolinamide ligands and their antiproliferative activities against three different cancer cell lines alongwith thioredoxin enzyme property (**2**, **4**, **6** and **8**).

Chapter 3 describes synthesis of four arene Ru(II)-NSAID complexes and their antiproliferative activities against three different cancer cell lines (**9-12**). To investigate the possible mechanistic pathway for those compounds for their promising growth inhibition properties, protein binding studies, hydrolysis studies, amino acid interaction studies and cyclooxygenase and lipooxygenase enzyme inhibition studies have also been investigated.

Chapter 4 demonstrates synthesis of a series of Ru(II)-arene (arene=*p*-cymene, benzene) complexes (**13-20**) using different *N*-substituted tetrazole ligands and their PTA analogues and their antiproliferative activity against different cell lines.

Chapter 5 deals with synthesis of new ferrocenamide ligands *i.e.* pyridine-2-carboxylic acid(4-ferrocenyl aniline)- amide, **HL**⁷ and quinoline-1-carboxylic acid(4-ferrocenyl aniline)- amide, **HL**⁸ and two new heterobimetallic Ru(II)-arene complexes (**21** and **23**) of general formula [Ru(L)(η^6 -arene)Cl] using synthesized ferrocenamide ligands as well as their PTA analogue (**22** and **24**). All the complexes have been characterized thoroughly with different analytical tools and their antiproliferative activity has been evaluated against different cancerous cell lines.

In chapter 6, RAPTA type of complexes has been prepared using different phosphine ligands (**25-28**). Antiproliferative activity against different cell lines as well as stability study of the complexes have been explored for the prepared complexes.

1.15 References

- [1] Natta, G., Pasquon, I., Zambelli, A. (1962), Stereospecific catalysts for the head-to-tail polymerization of propylene to a crystalline syndiotactic polymer, *J. Am. Chem. Soc.*, 84(8), 1488-1490. (DOI: 10.1021/ja00867a029)
- [2] Gervais, C., Languille, M. A., Reguer, S., Garnier, C., Gillet, M. (2014), Light and anoxia fading of Prussian blue dyed textiles, *Heritage Sci.*, 2(26), 1-8. (DOI: 10.1186/s40494-014-0026-x)
- [3] Brill, A. S. (1977), *Transition metals in biochemistry*, Springer-Verlag, Berlin, ISBN 978-3-642-81148-7.
- [4] Ronconi, L., Sadler, P. J. (2007), Using coordination chemistry to design new medicines, *Coord. Chem., Rev.*, 251, 1633-1648. (DOI:10.1016/j.ccr.2006.11.017)
- [5] Wilson, J. J., Lippard, S. J. (2014), Synthetic methods for the preparation of platinum anticancer complexes, *Chem. Rev.*, 114(8), 4470-4495. (DOI: 10.1021/cr4004314)
- [6] Hazlitt, R. A., Min, J., Zuo, J. (2018), Progress in the development of preventative drugs for *cis*-platin induced hearing loss, *J. Med. Chem.*, XXX, XXXX. (DOI: 10.1021/acs.jmedchem.7b01653).
- [7] Hartinger, C. G., Metzler-Nolte, N., Dyson, P. J. (2012), Challenges and opportunities in the development of organometallic anticancer drugs, *Organometallics*, 31(16), 5677-5685. (DOI: 10.1021/om300373t)
- [8] (a) Sava, G., Zorzet, S., Turrin, C., Vita, F., Soranzo, M., Zabucchi, G., Cocchietto, M., Bergamo, A., DiGiovine, S., Pezzoni, G., Sartor, L., Garbisa, S. (2003), Dual action of NAMI-A in inhibition of solid tumor metastasis: selective targeting of metastatic cells and binding to collagen, *Clin. Cancer Res.*, 9, 1898-1905. (DOI: clincancerres.aacrjournals.org/content/9/5/1898), (b) Rademaker-Lakhai, J. M., van den Bongard, D., Pluim, D., Beijnen, J. H., Schellens, J. H. M. (2004), A Phase I and pharmacological study with imidazolium-*trans*-DMSO-imidazole-tetrachlororuthenate, a

- novel ruthenium anticancer agent, *Clin. Cancer Res.*, 10, 3717-3727. (DOI: 10.1158/1078-0432.CCR-03-0746).
- [9] (a) Bijelic, A., Theiner, S., Keppler, B. K., Rompel, A. (2016), X-ray structure analysis of indazolium trans-[tetrachlorobis (1*H*-indazole) ruthenate (III)] (KP 1019) bound to human serum albumin reveals two ruthenium binding sites and provides insights into the drug binding mechanism, *J. Med. Chem.*, 59(12), 5894-5903. (DOI: 10.1021/acs.jmedchem.6b00600) (b) Hartinger, C. G., Jakupec, M. A., Zorbas-Seifried, S., Groessl, M., Egger, A., Berger, W., Zorbas, H., Dyson, P. J., Keppler, B. K. (2008), KP1019, A new redox-active anticancer agent-preclinical development and results of a clinical phase I study in tumor patients, *Chem. Biodiversity*, 5, 2140-2155. (DOI: 10.1002/cbdv.200890195)
- [10] Fricker, S. P. (2007), Metal based drugs: from serendipity to design, *Dalton Trans.*, 4903-4917. (DOI: 10.1039/B705551J)
- [11] Rosenberg, B., Camp, L. V., Trosko, J. E., Mansour, V. H. (1969), Platinum compounds: a new class of potent antitumour agents, *Nature*, 222, 385-386. (DOI: 10.1038/222385a0)
- [12] (a) Pope, J. E., Hong, O., Koehler, B. E. (2002), Prescribing trends in disease modifying antirheumatic drugs for rheumatoid arthritis: a survey of practicing canadian rheumatologists, *J. Rheumatol.*, 29(2), 255-260. (ISSN:1499-2752) (b) Williams, H. J., Ward, J. R., Reading, J. C., Brooks, R. H., Clegg, D. O., Skosey, J. L., Weisman, M. H., Willkens, R. F., Singer, J. Z., Alarcon, G. S., Field, E. H., Clements, P. J., Russell, I. J., Hochman, R. F., Boumpas, D. T., Marble, D. A. (1992), Comparison of auranofin, methotrexate, and the combination of both in the treatment of rheumatoid arthritis. a controlled clinical trial, *Arthritis Rheum.*, 35, 259-269 (DOI: 10.1002/art.1780350304)
- [13] Tuzel, I. H. (1974), Sodium nitroprusside: a review of its clinical effectiveness as a hypotensive agent, *Clin. Pharmacol.*, 14, 494-503. (DOI: 10.1002/j.1552-4604.1974.tb01363.x)

- [14] Sheela, A., Roopan, S. M., Vijayaraghavan, R. (2008), New diketone based vanadium complexes as insulin mimetics, *Eur. J. Med. Chem.*, 43, 2206-2210. (DOI: 10.1016/j.ejmech.2008.01.002)
- [15] Fox, C. L., Modak, S. M. (1974), Mechanism of silver sulfadiazine action on burn wound infections, *Antimicrob. Agents Chemother.*, 5(6), 582-588. (DOI: 10.1128/AAC.5.6.582)
- [16] Sharp, P. F., Smith, F. W., Gemmell, H. G., Lyall, D., Evans, N. T. S., Gvozdanovic, D., Davidson, J., Tyrrell, D. A., Pickett, R. D., Neirinckx, R. D. (1986), Technetium-99m HM-PAO stereoisomers as potential agents for imaging regional cerebral blood flow: human volunteer studies, *J. Nucl. Med.*, 27(2), 171-177. (ISSN: 2159-662X)
- [17] (a) Guo, Z., Sadler, P. J. (1999), Metals in medicine, *Angew. Chem. Int. Ed.*, 38, 1512-1531. (DOI:10.1002/(SICI)15213773(19990601)38:11<1512::AID-ANIE1512>3.0.CO;2-Y) (b) Barry, N. P. E., Sadler, P. J. (2013), Exploration of the medical periodic table: towards new targets, *Chem. Commun.*, 49, 5106-5131. (DOI: 10.1039/c3cc41143e), (c) Gaynor, D., Griffith, G. M. (2012), The prevalence of metal-based drugs as therapeutic or diagnostic agents: beyond platinum, *Dalton Trans.*, 41, 13239-13257 (DOI: 10.1039/c2dt31601c)
- [18] Hajdu, S. I. (2011), A note from history: landmarks in history of cancer, part 1, *Cancer*, 117, 1097-1102. (DOI: 10.1002/cncr.25553)
- [19] (a) Sudhakar, A. (2009), History of Cancer, Ancient and Modern Treatment Methods. *J Cancer Sci. Ther.*, 1(2), i-iv. (DOI:10.4172/1948-5956.100000e2). (b) Faguet, B. G. (2015), A brief history of cancer: Age-old milestones underlying our current knowledge database, *Int. J. Cancer*, 136, 2022-2036. (DOI: 10.1002/ijc.29134)
- [20] Cancer research UK (2017), <http://www.cancerresearchuk.org/what-is-cancer/how-cancer-starts/types-of-cancer>.
- [21] US National Institute of Health (2011), <http://cancer.gov/cancertopics/understandingcancer>.

- [22] TNN (2018), India's cancer cases far lower than those in west, yet death rate higher, Times of India, <https://articleshow/62550136.cms>, accessed Jan 18, 2018.
- [23] Narayan, P., Mitra, P. TNN. (2018), Not lifestyle alone, geography too plays vital role in mapping of cancer cases, Times of India, <https://articleshow/62502688.cms>, accessed Jan 15, 2018.
- [24] Cancer Management (2003), International agency for research on cancer, www.iarc.fr/en/publications/pdfs-online/wcr/2003/wcr-6.pdf.
- [25] Levin, W. P., Kooy, H., Loeffler, J. S., DeLaney, T. F. (2005), Proton beam therapy, *Br. J. Cancer.*, 93, 849-854. (DOI: 10.1038/sj.bjc.6602754)
- [26] Chan, K., Yeung., Rebecca. (2006), Hormonal therapy for cancer treatment, Palliative medicine doctors' meeting, HKSPM Newsletter, 2, 8.
- [27] Pisconti, S., Scarpati, G. D. V., Facchini, G., Cavaliere, C., D'aniello, C., Friscinni, A., Mellissano, A., Bellini, E., Perri, F. (2018), The evolving landscape of immunotherapy against cancer, *World Can. Res. J.*, 5(1), e1042.
- [28] Sagar, J., Chaib, B., Sales, K., Winslet, M., Seifalian, A. (2007), Role of stem cells in cancer therapy and cancer stem cells: a review, *Cancer Cell Int*, 7(9), 1-11. (DOI: 10.1186/1475-2867-7-9)
- [29] Pérez-Arnaiz, C., Busto, N., Leal, J. M., Garcia, B. (2014), New Insights into the Mechanism of the DNA/Doxorubicin Interaction, *J. Phys. Chem., B.*, 118(5), 1288-1295. (DOI: 10.1021/jp411429g)
- [30] Borch, R. F., Canute, G. W. (1991), Synthesis and antitumor properties of activated cyclophosphamide analogs, *J. Med. Chem.*, 34(10), 3044-3052. (DOI: 10.1021/jm00114a013)
- [31] Grem, J. L., (2000), 5-Fluorouracil: forty-plus and still ticking. A review of its preclinical and clinical development. *Invest. new drugs.* 18, 299-313. (DOI: 10.1023/A:1006416410198)
- [32] Lan, H., Li, Y., Lin, C-Y. (2014), Irinotecan as a palliative therapy for metastatic breast cancer patients after previous chemotherapy,

- Asian Pac. J Cancer Prev., 15(24), 10745-10748. (DOI: 10.7314/APJCP.2014.15.24.10745)
- [33] DeVita, Jr. V.T., Chu, E. (2008), Cancer Res, 68 (21), 8643-53. (DOI: 10.1158/0008-5472.CAN-07-6611)
- [34] Rosenberg, B., Camp, L. V., Krigas, T. (1965), Inhibition of cell division in *Escherichia coli* by electrolysis products from a platinum electrode, Nature, 205, 698-699. (DOI: 10.1038/205698a0)
- [35] Di Pasqua, A. J., Goodisman, J., Kerwood, D. J., Toms, B. B., Dubowy, R. L., Dabrowiak, J. C. (2006), Activation of carboplatin by carbonate, Chem. Res. Toxicol., 19(1), 139-149. (DOI: 10.1021/tx050261s)
- [36] Graham, J., Muhsin, M., Kirkpatrick, P. (2004), Oxaliplatin, Nat. Rev. Drug Discov., 3, 11-12. (DOI: 10.1038/nrd1287),
- [37] Cheff, D. M., Hall, M. D. (2017), A drug of such damned nature.1 challenges and opportunities in translational platinum drug research, J. Med. Chem., 60(11), 4517-4532. (DOI: 10.1021/acs.jmedchem.6b01351)
- [38] Kelland, L. (2007), The resurgence of platinum-based cancer chemotherapy, Nat Rev Cancer, 7(8), 573-584. (DOI: 10.1038/nrc2167)
- [39] Gately, D. P., Howell, S. B. (1993), Cellular accumulation of the anticancer agent cisplatin: a review, Br. J. Cancer, 67(6), 1171-1176.
- [40] Jamieson, E. R., Lippard, S. J. (1999), Structure, recognition, and processing of cisplatin-DNA adducts, Chem. Rev., 99(9), 2467-2498. (DOI: 10.1021/cr980421n)
- [41] Appleton, T. G., Hall, J. R., Ralph, S. F., Thompson, C. S. M. (1989), NMR study of acid-base equilibria and other reactions of ammineplatinum complexes with aqua and hydroxo ligands, Inorg. Chem., 28(10), 1989-1993. (DOI: 10.1021/ic00309a044)
- [42] Fichtinger-Schepman, A. M. J., van der Veer, J. L. , den Hartog, J. H., Lohman, P. H., Reedijk, J. (1985), Adducts of the antitumor drug cis-diamminedichloroplatinum(II) with DNA: formation,

- identification, and quantitation, *Biochemistry*, 24(3), 707-713 (DOI: 10.1021/bi00324a025)
- [43] Wang, D., Lippard, S. J. (2005), Cellular processing of platinum anticancer drugs, *Nat. Rev. Drug Discov.*, 4, 307-320. (DOI: 10.1038/nrd1691)
- [44] Gasser, G., Metzler-Nolte, N. (2011), Organometallic anticancer drug, *J. Med. Chem.*, 54(1), 3-25. (DOI: 10.1021/jm100020w).
- [45] Guo, M., Sun, H., McArdle, H. J., Gambling, L., Sadler, P. J. (2000), Ti^{IV} uptake and release by human serum transferrin and recognition of Ti^{IV} -transferrin by cancer cells: understanding the mechanism of action of the anticancer drug titanocene dichloride, *Biochemistry*, 39(33), 10023-10033. (DOI: 10.1021/bi000798z)
- [46] Zou, T., Lum, C. T., Lok, C-N., Zhang, J-J., Che, C-M. (2015), Chemical biology of anticancer gold(III) and gold(I) complexes, *Chem. Soc. Rev.*, 44, 8786-8801. (DOI: 10.1039/C5CS00132C)
- [47] Timerbaev, A. R. (2009), Advances in developing tris(8-quinolinolato)gallium(III) as an anticancer drug: critical appraisal and prospects, *Metallomics*, 1, 193-198. (DOI: 10.1039/B902861G)
- [48] Bergamo, A., Dyson, P J., Sava, G. (2018), The mechanism of tumour cell death by metal-based anticancer drugs is not only a matter of DNA interactions, *Coord. Chem. Rev.*, 360, 17-33. (DOI: 10.1016/j.ccr.2018.01.009)
- [49] Yan, Y. K., Melchart, M., Habtemariam, A., Sadler, P J. (2005), *Chem. Commun.*, 4764-4776. (DOI: 10.1039/B508531B)
- [50] Levina, A., Mitra, A., Lay, P. A. (2009), Recent developments in ruthenium anticancer drugs, *Metallomics*, 1, 458-470. (DOI: 10.1039/B904071D)
- [51] Bergamo, A., Sava, G. (2011), Ruthenium anticancer compounds: myths and realities of the emerging metal-based drugs, *Dalton Trans.*, 40, 7817-7823. (DOI:10.1039/C0DT01816C).
- [52] Dyson, P. J., Sava, G. (2006), Metal-based antitumour drugs in the post genomic era, *Dalton Trans.*, 1929-1933. (DOI: 10.1039/b601840h)

- [53] Alessio, E., (2017), Thirty years of the drug candidate NAMI-A and the myths in the field of ruthenium anticancer compounds: a personal perspective, *Eur. J. Inorg. Chem.*, 1549-1560. (DOI: 10.1002/ejic.201600986).
- [54] Bergamo, A., Sava, G. (2007), Ruthenium complexes can target determinants of tumour malignancy, *Dalton Trans.*, 1267-1272 (DOI: 10.1039/b617769g)
- [55] Pelillo, C., Mollica, H., Eble, J. A., Grosche, J., Herzog, L., Codan, B., Sava, G., Bergamo, A. (2016), Inhibition of adhesion, migration and of $\alpha 5\beta 1$ integrin in the HCT-116 colorectal cancer cells treated with the ruthenium drug NAMI-A, *J. Inorg. Biochem.*, 160, 225-235. (DOI: 10.1016/j.jinorgbio.2016.02.025).
- [56] Bergamo, A., Messori, L., Piccioli, F., Cocchietto, M., Sava, G. (2003), Biological role of adduct formation of the ruthenium(III) complex NAMI-A with serum albumin and serum transferrin, *Invest. New Drug.*, 21, 401-411. (DOI: 10.1023/A:1026243000320).
- [57] Gava, B, Zorzet, S., Spessotto, P., Cocchietto, M., Sava, G. (2006), Inhibition of B16 melanoma metastases with the ruthenium complex Imidazolium *trans*-imidazoledimethylsulfoxide-tetrachlororuthenate and down-regulation of tumour cell invasion, *J. Pharmacol Exp Ther.*, 317(1), 284-291. (DOI: 10.1124/jpet.105.095141),
- [58] Alessio, E., Mestroni, G., Bergamo, B., Sava, G. (2004), Ruthenium antimetastatic agents, *Curr. Top. Med. Chem.* 4, 1525-1535 (DOI: 10.2174/1568026043387421)
- [59] Messori, L., Orioli, P., Vullo, D., Alessio, E., Iengo, E. (2000), A spectroscopic study of the reaction of NAMI, a novel ruthenium(III) anti-neoplastic complex, with bovine serum albumin, *Eur. J. Biochem.*, 267, 1206-1213. (DOI: 10.1046/j.1432-1327.2000.01121).
- [60] (a) Hartinger, C. J., Jakupec, M. A., Zorbas-Seifried, S., Groessl, M., Egger, A., Berger, W., Zorbas, H., Dyson, P. J., Keppler, B. K. (2008), KP1019, A new redox-active anticancer agent-preclinical

- development and results of a clinical phase I study in tumor patients, *Chem Divers.*, 5, 2140-2155. (DOI: 10.1002/cbdv.200890195) (b) Hartinger, C. G., Zorbas-Seifried, S., Jakupec, M. A., Kynast, M., Zorbas, H., Keppler, B. K. (2006), From bench to bedside-preclinical and early clinical development of the anticancer agent indazolium *trans*-[tetrachlorobis(1*H*-indazole)ruthenate(III)] (KP1019 or FFC14A), *J. Inorg. Biochem.*, 100, 891-904. (DOI: 10.1016/j.jinorgbio.2006.02.013)
- [61] (a) Heffeter, P., Pongratz, M., Steiner, E., Chiba, P., Jakupec, M. A., Elbling, L., Marian, B., Körner, M., Sevelda, M., Micksche, M., Keppler, B. K., Berger, W. (2004), Intrinsic and acquired forms of resistance against the anticancer ruthenium compound KP1019 [Indazolium *trans*- [tetrachlorobis(1*H*-indazole)ruthenate (III)] (FFC14A), *J. Pharmacol Exp Ther.*, 312(1), 281-289. (DOI: 10.1124/jpet.104.073395), (b) Bijelic, A., Theiner, S., Keppler, B. K., Rompel, A. (2016), X-ray structure analysis of indazolium *trans*-[tetrachlorobis(1*H*-indazole)ruthenate(III)] (KP1019) bound to human serum albumin reveals two ruthenium binding sites and provides insights into the drug binding mechanism, *J. Med. Chem.*, 59(12), 5894-5903.(DOI: 10.1021/acs.jmedchem.6b00600)
- [62] Malina, J., Novakova, O., Keppler, B. K., Alessio, E., Brabec, V. (2001), Biophysical analysis of natural, double-helical DNA modified by anticancer heterocyclic complexes of ruthenium(III) in cell free media, *J. Biol. Inorg. Chem.*, 6(4), 435-445. (DOI: 10.1007/s007750100223)
- [63] Gransbury, G. K., Kappen, P., Glover, C. J., Hughes, J. N., Levina, A., Lay, P. A., Musgrave, I. F., Harris, H. H. (2016), Comparison of KP1019 and NAMI-A in tumour-mimetic environments, *Metallomics*, 8, 762-773. (DOI: 10.1039/c6mt00145a)
- [64] Clarke, M. J. (1980), Oncological implications of the chemistry of ruthenium, *Met. Ions Biol. Syst.*, 11, 231-283.
- [65] Webb, M. I., Walsby, C. J. (2011), Control of ligand-exchange processes and the oxidation state of the antimetastatic Ru(III)

- complex NAMI-A by interactions with human serum albumin, Dalton Trans., 40, 1322–1331 (DOI: 10.1039/C0DT01168A).
- [66] Webb, M. I., Walsby, C. J. (2015), Albumin binding and ligand-exchange processes of the Ru(III) anticancer agent NAMI-A and its bis-DMSO analogue determined by ENDOR spectroscopy, Dalton Trans., 44, 17482–17493 (DOI: 10.1039/C5DT02021B)
- [67] Cetinbas, N., Webb, M. I., Dubland, J. A., Walsby, C. J. (2010), Serum-protein interactions with anticancer Ru(III) complexes KP1019 and KP418 characterized by EPR, J. Biol. Inorg. Chem., 15, 131-145. (DOI: 10.1007/s00775-009-0578-5)
- [68] Scolaro, C., Hartinger, C. G., Allardyce, C. S., Keppler, B. K., Dyson, P. J. (2008), Hydrolysis study of the bifunctional antitumour compound RAPTA-C, $[\text{Ru}(\eta^6\text{-}p\text{-cymene})\text{Cl}_2(\text{pta})]$, J. Inorg., Biochem., 102, 1743-1748. (DOI: 10.1016/j.jinorgbio.2008.05.004)
- [69] Pizzaro, A. M., Sadler, P. J. (2009), Biochimie, 91, 1198-1211. (DOI: 10.1016/j.biochi.2009.03.017).
- [70] Ang, W. H., Casini, A., Sava, G., Dyson, P. J. (2011), Organometallic ruthenium-based antitumor compounds with novel modes of action, J. Organomet Chem., 696, 989-998. (DOI:10.1016/j.jorganchem.2010.11.009)
- [71] (a) Babak, M. V., Meier, S. M., Huber, K. V. M., Reynisson, J., Legin, A. A., Jakupec, M. A., Roller, A., Stukalov, A., Gridling, M., Bernett, K. L., Colinge, J., Berger, W., Dyson, P. J., Superti-Furga, G., Keppler, B. K., Hartinger, C. G. (2015), Target profiling of an antimetastatic RAPTA agent by chemical proteomics: relevance to the mode of action, Chem. Sci., 6, 2449-2456. (DOI: 10.1039/C4SC03905J), (b) Weiss, A., Berndsen, R. H., Dubois, M., Müller, C., Schibli, R., Griffioen, A. W., Dyson, P. J., Nowak-Sliwinski, P. (2014), *In vivo* anti-tumor activity of the organometallic ruthenium(II)-arene complex $[\text{Ru}(\eta^6\text{-}p\text{-cymene})\text{Cl}_2(\text{pta})]$ (RAPTA-C) in human ovarian and colorectal carcinomas, Chem. Sci., 5, 4742-4748. (DOI: 10.1039/c4sc01255k)
- [72] Leyva, L., Sirlin, C., Rubio, L., Franco, C, Le Lagadec, R., Spencer, J., Bischoff, P., Gaidon, C., Loeffler, J. P., Pfeffer, M. (2007),

- Synthesis of cycloruthenated compounds as potential anticancer agents, *Eur. J. Inorg. Chem.*, 19, 3055-3066. (DOI: 10.1002/ejic.200601149)
- [73] Meier-Menches, S.M., Gerner, C, Berger, W., Hartinger, C. G., Keppler, B. K. (2018), Structure-activity relationships for ruthenium and osmium anticancer agents-towards clinical development, *Chem. Soc. Rev.*, 47, 909-928. (DOI: 10.1039/C7CS00332C)
- [74] Aird, R.E., Cummings, J., Ritchie, A. A., Muir, M., Morris, R.E., Chen, H., Murdoch, P. S., Sadler, P. J., Jodrell, D. I. (2002), In vitro and in vivo activity and cross resistance profiles of novel ruthenium (II) organometallic arene complexes in human ovarian cancer, *Br. J. Cancer*, 86, 1652–1657. (DOI: 10.1038/sj.bjc.6600290)
- [75] (a) Nováková, O., Malina, J., Suchankova, T., Kasparkova, J., Bugarcic, T., Sadler, P. J., Brabec, V. (2010), Energetics, conformation, and recognition of DNA duplexes modified by monodentate Ru^{II} complexes containing terphenyl arenes, *Chem. Eur. J.*, 16, 5744-5754 (DOI: 10.1002/chem.200903078) (b) Nováková, O., Nazarov, A. A., Hartinger, C. G., Keppler, B. K., Brabec, V. (2009), DNA interactions of dinuclear RuII arene antitumor complexes in cell-free media, *Biochem. Pharmacol.*, 77, 364-374. (DOI: 10.1016/j. bcp.2008.10.021)
- [76] Liu, H. K., Wang, F. Y., Parkinson, J. A., Bella, J., Sadler, P. J. (2006), Ruthenation of duplex and single-stranded d(CG GCCG) by organometallic anticancer complexes, *Chem. Eur. J.*, 12, 6151–6165). (DOI: 10.1002/chem.200600110)
- [77] (a) Almodares, Z., Lucas, S. J., Crossley, B. D., Basri, A. M., Pask, C. M., Hebden, A. J., Phillips, R. M., McGowan, P. C. (2014), Rhodium, iridium, and ruthenium half-sandwich picolinamide complexes as anticancer agents, *Inorg. Chem.*, 53, 727–736. (DOI: 10.1021/ic401529u). (b) Süß-Fink, G.(2010), Arene ruthenium complexes as anticancer agents, 1673-1688. (DOI: 10.1039/B916860P)

- [78] Camm, K. D., El-Sokkary, A., Gott, A. L., Stockley, P. G., Belyaeva, T., McGowan, P. C. (2009), *Dalton Trans.*, 10914-10925. (DOI: 10.1039/B918902E)
- [79] Thota, S., Rodrigues, D. A., Crans, D. C., Barreiro, E. J. (2018), Ru(II) compounds: next-generation anticancer metallotherapeutics?, *J. Med. Chem.*, XXX, XXX-XXX. (DOI: 10.1021/acs.jmedchem.7b01689).
- [80] Ang, W. H., Parker, L. J., De Luca, A., Juillerat-Jeanneret, L., Morton, C. J., Lo Bello, M., Parker, M. W., Dyson, P. J. (2009), Rational design of an organometallic glutathione transferase inhibitor, *Angew. Chem. Int. Ed.*, 48(21), 3854-3957. (DOI: 10.1002/anie.200900185).
- [81] Ang, W. H., Daldini, E., Juillerat-Jeanneret, L., Dyson, P. J. (2007), Strategy to tether organometallic ruthenium-arene anticancer compounds to recombinant human serum albumin, *Inorg. Chem.*, 2007, 46, 9048-9050. (DOI: 10.1021/ic701474m)
- [82] Williams, D. S., Atilla, G. E., Bregman, H., Arzoumanian, A., Klein, P. S., Meggers, E. (2005), Switching on a signaling pathway with an organoruthenium complex, *Angew. Chem. Int. Edn.*, 44, 1984-1987. (DOI: 10.1002/anie.200462501)
- [83] Biersack, B., Zoldakova, M., Effenberger, K., Schobert, R. (2010), (Arene)Ru(II) complexes of epidermal growth factor receptor inhibiting tyrophostins with enhanced selectivity and cytotoxicity in cancer cells, *Eur. J. Med. Chem.*, 45, 1972-1975. (DOI: 10.1016/j.ejmech.2010.01.040).
- [84] Aman, F., Hanif, M., Siddiqui, W. A., Ashraf, A., Filak, L. K., Reynisson, J., Söhnel, T., Jamieson, S. M. F., Hartinger, C. G. (2014), Anticancer ruthenium(η^6 -*p*-cymene) complexes of nonsteroidal anti-inflammatory drug derivatives, *Organometallics*, 33 (19), 5546-5553. (DOI: 10.1021/om500825h)
- [85] Pettinari, R., Marchetti, F., Petrini, A., Pettinari, C., Lupidi, G., Smoleński, P., Scopelliti, R., Riedel, T., Dyson, P. J. (2016), From sunscreen to anticancer agent: ruthenium(II) arene avobenzon

- complexes display potent anticancer activity, *Organometallics*, 35, 3734-3742. (DOI: 10.1021/acs.organomet.6b00694)
- [86] Pettinari, R., Marchetti, F., Condello, F., Pettinari, C., Lupidi, G., Scopelliti, R., Mukhopadhyay, S., Riedel, T., Dyson, P. J. (2014), Ruthenium(II)-arene RAPTA type complexes containing curcumin and bisdemethoxycurcumin display potent and selective anticancer activity, 33(14), 3709-3715. (DOI: 10.1021/om500317b)
- [87] Shanmugaraju, S., la Cour Poulsen, B., Arisa, T., Umadevi, D., Dalton, H. L., Hawes, C. S., Estalayo-Adrián, S., Savyasachi, A. J., Watson, G. W. Williams, D. C., Gunnlaugsson, T. (2018), Synthesis, structural characterisation and antiproliferative activity of a new fluorescent 4-amino-1,8-naphthalimide Tröger's base-Ru(II)-curcumin organometallic conjugate, *Chem. Commun.*, 54, 4120-4123. (DOI: 10.1039/C8CC01584H)
- [88] Pettinari, R., Condello, F., Marchetti, F., Pettinari, C., Smolénski, P., Riedel, T., Scopelliti, R., Dyson, P. J. (2017), Dicationic ruthenium(II)-arene-curcumin complexes containing methylated 1,3,5-Triaza-7-phosphaadamantane: synthesis, structure, and cytotoxicity, *Eur. J. Inorg. Chem.*, 2017(22), 2905-2910. (DOI: 10.1002/ejic.201700183)
- [89] Li, P., Lei, X., Xiao, Q., Huang, S. (2017), Synthesis, characterization and anticancer activity of a series of curcuminoids and their half-sandwich ruthenium(II) complexes, *Appl. Organomet.Chem.*, 31(9), e3685. (DOI: 10.1002/aoc.3685)
- [90] Caruso, F., Rossi, M., Benson, A., Opazo, C., Freedman, D., Monti, E., Gariboldi, M. B., Shaulky, J., Marchetti, F., Pettinari, R., Pettinari, C. (2012), Ruthenium-arene complexes of curcumin: X-Ray and density functional theory structure, synthesis, and spectroscopic characterization, in vitro antitumor activity, and DNA docking studies of (*p*-cymene)Ru(curcuminato)chloro, *J. Med. Chem.*, 55 (3), 1072-1081. (DOI: 10.1021/jm200912j)
- [91] Bonfili, L., Pettinari, R., Cuccioloni, M., Cekarini, M., Mozzicafreddo, M., Angeletti, M., Lupidi, G., Marchetti, F., Pettinari, C., Eleuteri, A. M. (2012), Arene-Ru^{II} complexes of

- curcumin exert antitumor activity via proteasome inhibition and apoptosis induction, *Chem. Med. Chem.*, 7(11), 2010-2020. (DOI: 10.1002/cmdc.201200341)
- [92] Ruiz, J., Vicente, C., de Haro, C., Bautista, D. (2009), A novel ruthenium(II) arene based intercalator with potent anticancer activity, *Dalton Trans.*, 5071-5073. (DOI: 10.1039/B907296A)
- [93] Berger, I., Hanif, M., Nazarov, A. A., Hartinger, C. G., John, R. O., Kuznetsov, M. L., Groessl, M., Schmitt, F., Zava, O., Biba, F., Arion, V. B., Galanski, M., Jakupec, M. A., Juillerat-Jeanneret, L., Dyson, P. J., Keppler, B. K. (2008), In vitro anticancer activity and biologically relevant metabolism of organometallic ruthenium complexes with carbohydrate-based ligands, *Chem. Eur. J.*, 14, 9046-9057. (DOI: 10.1002/chem.200801032)
- [94] Hartinger, C. G., Nazarov, A. A., Ashraf, S. M., Dyson, P. J., Keppler, B. K. (2008), Carbohydrate-metal complexes and their potential as anticancer agents, *Curr. Med. Chem.*, 15, 2574-2591. (DOI: 10.2174/092986708785908978)
- [95] Luengo, A., Fernández-Moreira, V., Marzo, I., Gimeno, M. C. (2017), Trackable metallodrugs combining luminescent Re(I) and bioactive Au(I) fragments, *Inorg. Chem.*, 56, 15159-15170. (DOI: 10.1021/acs.inorgchem.7b02470)
- [96] Mui, Y. F., Fernández-Gallardo, J., Elie, B. T., Gubran, A., Maluenda, I., Sanaú, M., Navarro, O., Contel, M. (2016), Titanocene-gold complexes containing N-heterocyclic carbene ligands inhibit growth of prostate, renal, and colon cancers in vitro, *Organometallics*, 35, 1218-1227. (DOI: 10.1021/acs.organomet.6b00051)
- [97] Fernández-Gallardo, J., Elie, B. T., Sanaú, M., Contel, M. (2016), Versatile synthesis of cationic N-heterocyclic carbene-gold(I) complexes containing a second ancillary ligand. Design of heterobimetallic ruthenium-gold anticancer agents, *Chem. Commun.*, 52, 3155-3158. (DOI: 10.1039/c5cc09718e)
- [98] Massai, L., Fernández-Gallardo, J., Guerri, A., Arcangeli, A., Pillozzi, S., Contel, M., Messori, L. (2015), Design, synthesis and

- characterisation of new chimeric ruthenium(II)-gold(I) complexes as improved cytotoxic agents, *Dalton Trans.*, 44, 11067-11076. (DOI: 10.1039/c5dt01614b)
- [99] Govender, P., Riedel, T., dyson, P. J., Smith, G. S. (2016), Regulating the anticancer properties of organometallic dendrimers using pyridylferrocene entities: synthesis, cytotoxicity and DNA binding studies, *Dalton Trans.*, 45, 9529-9539. (DOI: 10.1039/C6DT00849F)
- [100] Govender, P., Lemmerhirt, H., Hutton, A. T., Therrien, B., Bednarski, Smith, G. S. (2014), First- and second-generation heterometallic dendrimers containing ferrocenyl-ruthenium(II)-arene motifs: synthesis, structure, electrochemistry, and preliminary cell proliferation studies, *Organometallics*, 33(19), 5535-5545. (DOI: 10.1021/om500809g)
- [101] Wu, C-H., Wu, D-H., Liu, X., Guoyiqibayi, G., Guo, D-D., Lv, G., Wang, X-M., Yan, H., Jiang, H., Lu, Z-H, (2009), Ligand-based neutral ruthenium(II) arene complex: selective anticancer action, *Inorg. Chem.*, 48(6), 2352–2354. (DOI: 10.1021/ic900009j)
- [102] Therrien, B., Ang, W. H., Chérioux, F., Vieille-Petit, L., Juillerat-Jeanneret, L., Süß-Fink, G., Dyson, P. J. (2007), Remarkable anticancer activity of triruthenium-arene clusters compared to tetraruthenium-arene clusters, *J. Cluster Sci.*, 18(3),741-752. (DOI: 10.1007/s10876-007-0140-y)
- [103] Vieille-Petit, L., Therrien, B., Süß-Fink, G., Ward, T. R. (2003), Isolation and single-crystal X-ray structure analysis of the catalyst-substrate host-guest complexes $[\text{C}_6\text{H}_6\text{C}\text{H}_3\text{Ru}_3\{\text{C}_6\text{H}_5(\text{CH}_2)_n\text{OH}\}(\text{C}_6\text{Me}_6)_2(\text{O})]^+$ ($n=2, 3$), *J. Organomet. Chem.*, 684, 117-123. (DOI: 10.1016/S0022-328X(03)00519-9)
- [104] Mattsson, J., Govindaswamy, P., Renfrew, A. K., Dyson, P. J., Štěpnička, P., Süß-Fink, G., Therrien, B. (2009), Synthesis, molecular structure, and anticancer activity of cationic arene ruthenium metallarectangles, *Organometallics*, 28, 4350-4357. (DOI: 10.1021/om900359j)

- [105] Barry, N. P. E., Abd Karim, N. H., Vilar R., Therrien, B. (2009), Interactions of ruthenium coordination cubes with DNA, *Dalton Trans.*, 10717-10719. (DOI: 10.1039/B913642H)
- [106] Barry, N. P. E., Zava, O., Dyson P. J., Therrien, B. (2010), Synthesis, characterization and anticancer activity of porphyrin-containing organometallic cubes, *Aust. J. Chem.*, 63(11), 1529-1537)
- [107] Dale, L. D., Tocher, J. H., Dyson, T. M., Edwards, D. I., Tocher, D. A. (1992), Studies on DNA damage and induction of SOS repair by novel multifunctional bio-reducible compounds. II. A metronidazole adduct of a ruthenium-arene compound, *Anticancer Drug Des.*, 7(1), 3-14.
- [108] Peacock, Anna F. A., Sadler, P. J. (2008), Medicinal organometallic chemistry: designing metal arene complexes as anticancer agents, *Chem. Asian J.*, 3(11), 1890-1899. (DOI: 10.1002/asia.200800149)
- [109] Süss-Fink, G. (2010), Arene ruthenium complexes as anticancer drugs, *Dalton Trans.* 39(7), 1673-1688. (DOI: 10.1039/B916860P)
- [110] Prior, T. J., Savoie, H., Boyle, R. W., Murray, B. S. (2018), pH-Dependent modulation of reactivity in ruthenium(II) organometallics, *Organometallics*, 37, 294-297. (DOI: 10.1021/acs.organomet.7b00868)
- [111] Zhao, J., Zhang, D., Hua, W., Li, W., Xu, G., Gou, S. (2018), Anticancer activity of bifunctional organometallic Ru(II) arene complexes containing a 7-hydroxycoumarin group, *Organometallics*, 37, 441-447. (DOI: 10.1021/acs.organomet.7b00842)
- [112] Li, J., Tian, M., Tian, Z., Zhang, S., Yan, C., Shao, C., Liu, Z. (2018), Half-sandwich iridium(III) and ruthenium(II) complexes containing P⁴-chelating ligands: a new class of potent anticancer agents with unusual redox features, *Inorg. Chem.*, 57, 1705-1716. (DOI: 10.1021/acs.inorgchem.7b01959)
- [113] Castonguay, A., Doucet, C., Juhas, M., Maysinger, D. (2012), New ruthenium(II)-letrozole complexes as anticancer therapeutics, *J. Med. Chem.*, 55 (20), 8799–8806, (DOI: 10.1021/jm301103y)

Chapter 2
Fine Tuning Through Valence Bond
Tautomerization of Ancillary Ligands in
Ruthenium(II) Arene Complexes for
Better Anticancer Activity and Enzyme
Inhibition Properties

2.1 Introduction

Arene-ruthenium(II) complexes with a pseudo-octahedral coordination environment also named as piano-stool compounds have been studied in the recent past widely for their potential application in catalysis, crystal engineering and metallopharmaceuticals.^[1-5] However because of their lower toxicity, amphiphilic properties generated from a hydrophobic arene ring and a hydrophilic metal centre, improved selectivity and possibility to play around with the ligands to improve target (DNA, enzyme and proteins) specific chemotherapy, could be an important tool for next generation of metallodrug. Ruthenium arene complexes have shown significant antimetastatic and anticancer properties which can be modulated by factors like hydrophobicity of arene ligands, hydrogen bond forming ability and other properties of the ancillary ligands.^[6-8] One of the biggest advantages of ruthenium complexes is that they are transported inside cancer cells by transferrin enzyme, an iron transporter in the human body which promotes the selective accumulation of ruthenium compounds in cancer cells that overexpress the transferrin receptor.^[9] The problem of water solubility of ruthenium–arene complexes has been largely tackled by the introduction of an amphiphilic ligand called PTA (PTA=1,3,5-triaza-7-phospha-tricyclo-[3.3.1.1]decane) to generate a ruthenium–arene–PTA combination, known as RAPTA compounds.^[10-13] With fixation of the arene ring and the PTA ligand coordinated to the ruthenium centre, scientists around the world have tried different ancillary ligands with various characteristics to evaluate their possible effects on cytotoxicity and target specificity.^[14-17] Recently some reports have been published where picolinamide or carboxamide complexes have shown interesting anticancer properties due to their dynamic coordinating nature to the metal centre.^[18-21] To explore the reactivity of ruthenium-arene complexes further with picolinamide based ligands, nitro-substituted aniline and 3-pyridyl and 4-pyridyl amines have been used in this particular work to generate picolinamide derivatives to monitor the effect of ancillary ligands on anticancer activity. To the best of my knowledge, there is no report where the N-substituted picolinamide part as an ancillary ligand is modulated in the RAPTA scaffold to explore the

anticancer properties of the ruthenium-arene based complexes. Interestingly, one of the synthesized complexes has shown marked antiproliferative activity against different cancer cell lines. As it is evident that RAPTA compounds work upon molecular targets other than DNA,^[22] the interaction of the synthesized complexes with thioredoxin reductase (TrxR) has been explored, which is one of the key targets identified so far^[23] because of the presence of a selenolate group that prefers to bind with a softer metal ion after reduction making it suitable as a pharmacological target for metallodrugs.

2.2 Experimental section

2.2.1 Materials and methods

All the chemical reagents required were purchased from Sigma and used without further purification. NMR spectra were recorded on an AVANCE III 400 Ascend Bruker BioSpin machine at ambient temperature. Mass spectrometric analyses were performed on a Bruker-Daltonics microTOF-Q II mass spectrometer and elemental analyses were carried out with a ThermoFlash 2000 elemental analyzer. Spectrophotometric measurements were performed on a Varian UV-Vis spectrophotometer (Model: Cary 100) (for absorption) and a Fluoromax-4p spectrofluorometer from Horiba JobinYvon (Model: FM-100) (for emission) using a quartz cuvette with a path length of 1 cm. Far-ultraviolet (UV) (190 to 260 nm) spectra were recorded in a 0.1 cm path length cell (Hellma, Muellheim/Baden, Germany) using a step size of 0.5 nm, a bandwidth of 1 nm and a scan rate of 20 nm min⁻¹. Conductivity measurements were performed using a Digital Conductivity Meter Model 611 instrument. The conductivities of the complexes were obtained with 1 mM solutions in acetonitrile. [Ru(η^6 -*p*-cymene)(L¹)Cl] **1** and [Ru(η^6 -benzene)(L¹)Cl] **3** [**HL**¹ = pyridine-2-carboxylic acid (4-nitro-phenyl)amide] were prepared using a literature method.^[24] Ligand **HL**² [**HL**² = 4-(N-(2-pyridyl)carbamoyl)pyridine] and **HL**³ [**HL**³ = 3-(N-(2-pyridyl) carbamoyl)pyridine] were also prepared using the method reported earlier.^[25] Sulforhodamine B (SRB) growth inhibition (GI₅₀) assays were carried out by the Advanced Centre for

Treatment, Research and Education in Cancer (ACTREC), Mumbai, by following the literature procedure.^[26]

2.2.1.1 Synthesis of $[\text{Ru}(\eta^6\text{-}p\text{-cymene})(\text{L}^1)(\text{PTA})][\text{BF}_4][2]\cdot 2\text{H}_2\text{O}$

0.05 g (0.09 mmol) of complex $[\text{Ru}(\eta^6\text{-}p\text{-cymene})(\text{L}^1)\text{Cl}]$ **1** was dissolved in 20 mL of methanol. A methanolic solution (10 mL) of 1,3,5-triaza-7-phosphoadamantane (PTA) (0.01 g, 0.09 mmol) was added dropwise to the solution of compound **1**. The reaction mixture was stirred for 2 h at room temperature and then filtered. The filtrate was reduced *in vacuo* to a volume of *ca.* 5 mL. An excess of diethyl ether was added to accomplish precipitation. The precipitate was filtered, washed with diethyl ether and dried *in vacuo* to afford a yellow coloured crystalline solid as the product. Yield: 76%. The yellow coloured complex was dissolved in methanol. A methanolic solution of NaBF_4 (0.1 g, 0.08 mmol) was added to it and stirred for 2 h. The resulting solution was then filtered and the filtrate was then concentrated *in vacuo* to a volume of *ca.* 5 mL. The filtrate was kept in a refrigerator overnight, from which crystals suitable for X-ray analysis were obtained. Yield: 62%. ^1H NMR (400.13 MHz, 298 K, $\text{DMSO-}d_6$): 8.98 [d, 1H, CH of $\text{C}_5\text{H}_4\text{N}$], 8.29 [m, 3H, 1×CH of $\text{C}_5\text{H}_4\text{N}$ and 2×CH of $\text{C}_6\text{H}_4\text{NO}_2$], 8.11 [d, 1H, CH of $\text{C}_5\text{H}_4\text{N}$], 7.84 [t, 1H, CH of $\text{C}_5\text{H}_4\text{N}$], 7.57 [d, 2H, CH of $\text{C}_6\text{H}_4\text{NO}_2$], 6.26 [d, 1H, CH of C_6H_4], 5.92 [d, 1H, CH of C_6H_4], 5.75 [d, 1H, CH of C_6H_4], 5.43 [d, 1H, CH of C_6H_4], 4.40 [m, 6H, 3× NCH_2N], 4.00 [m, 6H, 3× PCH_2N], 2.84 [m, 1H, $\text{CH}(\text{CH}_3)_2$], 2.28 [s, 3H, $\text{C}_6\text{H}_4\text{CH}_3$], 0.98 [d, 3H, $\text{CH}(\text{CH}_3)_2$], 0.74 [d, 3H, $\text{CH}(\text{CH}_3)_2$]. ^{13}C NMR (100.61 MHz, $\text{DMSO-}d_6$): δ 167.0 [C of CON], 157.7 [C of $\text{C}_6\text{H}_4\text{NO}_2$], 156.3 [C of $\text{C}_5\text{H}_4\text{N}$], 154.1 [CH of $\text{C}_5\text{H}_4\text{N}$], 142.3 [CH of $\text{C}_5\text{H}_4\text{N}$], 140.7 [C of $\text{C}_6\text{H}_4\text{NO}_2$], 128.9 [CH of $\text{C}_5\text{H}_4\text{N}$], 127.1 [2×CH of $\text{C}_6\text{H}_4\text{NO}_2$], 126.7 [CH of $\text{C}_5\text{H}_4\text{N}$], 124.1 [2×CH of $\text{C}_6\text{H}_4\text{NO}_2$], 119.1 [C of C_6H_4], 101.1 [C of C_6H_4], 91.4 [CH of C_6H_4], 90.1 [CH of C_6H_4], 88.0 [CH of C_6H_4], 87.4 [CH of C_6H_4], 71.4 [3× NCH_2N of PTA], 50.0–48.5 [3× PCH_2N of PTA], 30.4 [$\text{C}_6\text{H}_4\text{CH}_3$], 21.9 [$\text{CH}(\text{CH}_3)_2$], 20.9 [$\text{CH}(\text{CH}_3)_2$], 18.1 [CH of $\text{CH}(\text{CH}_3)_2$]. ^{31}P NMR ($\text{DMSO-}d_6$, 126 MHz): δ -34.4. ESI-MS (+ve

mode): $[\text{Ru}(\eta^6\text{-}p\text{-cymene})(\text{L}^1)(\text{PTA})]^+$: 635.1 (m/z). Anal. Calcd for $\text{C}_{28}\text{H}_{38}\text{BF}_4\text{N}_6\text{O}_5\text{PRu}$: C, 44.40; H, 5.06; N, 11.09. Found: C, 44.53; H, 5.11; N, 10.89.

2.2.1.2 Synthesis of $[\text{Ru}(\eta^6\text{-benzene})(\text{L}^1)(\text{PTA})][\text{PF}_6][4]\cdot\text{CH}_3\text{OH}$

Complex $[\text{Ru}(\eta^6\text{-benzene})(\text{L}^1)\text{Cl}]$ **3** (0.08 g, 0.1 mmol) was dissolved in a mixture of methanol (15 mL) and dichloromethane (15 mL). A methanolic solution (10 mL) of 1,3,5-triaza-7-phosphoadamantane (PTA) (0.02 g, 0.1 mmol) was added dropwise to the solution of compound **3**. The reaction mixture was stirred for 2 h at room temperature and then filtered. The filtrate was reduced *in vacuo* to a volume of *ca.* 5 mL. An excess of diethyl ether was added to accomplish precipitation. The precipitate was filtered, washed with diethyl ether and dried *in vacuo*, affording a yellow solid. Yield: 62%. The yellow coloured compound was dissolved in methanol. A methanolic solution of NH_4PF_6 (0.12 g, 0.1 mmol) was added to it and stirred for 2 h. The resulting solution was then filtered and concentrated *in vacuo* to a volume of *ca.* 5 mL. The filtrate was kept for vapour diffusion with diethyl ether, from which crystals suitable for X-ray analysis were obtained. Yield: 52%. ^1H NMR (400.13 MHz, 298 K, $\text{DMSO-}d_6$): δ 8.92 [d, 1H, CH of $\text{C}_5\text{H}_4\text{N}$], 8.27–8.24 [m, 2H, $2\times\text{CH}$ of $\text{C}_6\text{H}_4\text{NO}_2$], 8.10 [d, 1H, CH of $\text{C}_5\text{H}_4\text{N}$], 7.93 [br.s, 1H, CH of $\text{C}_5\text{H}_4\text{N}$], 7.76 [t, 1H, $\text{C}_5\text{H}_4\text{N}$], 7.54 [d, 2H, $2\times\text{CH}$ of $\text{C}_6\text{H}_4\text{NO}_2$], 6.00 [s, 6H, $6\times\text{CH}$ of C_6H_6], 4.37 [m, 6H, $3\times\text{NCH}_2\text{N}$ of PTA], 3.98 [s, 6H, $3\times\text{PCH}_2\text{N}$ of PTA]. ^{13}C NMR (100.61 MHz, $\text{DMSO-}d_6$): δ 169.9 [C of CON], 158.8 [C of $\text{C}_5\text{H}_4\text{N}$], 155.9 [CH of $\text{C}_5\text{H}_4\text{N}$], 154.6 [C of $\text{C}_6\text{H}_4\text{NO}_2$], 143.9 [C of $\text{C}_6\text{H}_4\text{NO}_2$], 139.2 [CH of $\text{C}_5\text{H}_4\text{N}$], 129.4 [CH of $\text{C}_5\text{H}_4\text{N}$], 127.8 [$2\times\text{CH}$ of $\text{C}_6\text{H}_4\text{NO}_2$], 127.2 [CH of $\text{C}_5\text{H}_4\text{N}$], 124.2 [$2\times\text{CH}$ of $\text{C}_6\text{H}_4\text{NO}_2$], 85.9 [$6\times\text{CH}$ of C_6H_6], 72.8 [$3\times\text{NCH}_2\text{N}$ of PTA], 52.2 [$3\times\text{PCH}_2\text{N}$ of PTA]. ^{31}P NMR (126 MHz, $\text{DMSO-}d_6$): δ -39.1 [s, PTA], -144.1 [sept, PF_6]. ESI-MS (+ve mode): $[\text{Ru}(\eta^6\text{-benzene})(\text{L}^1)\text{PTA}]^+$: 579.1 (m/z). Anal. Calcd for $\text{C}_{25}\text{H}_{30}\text{F}_6\text{N}_6\text{O}_4\text{P}_2\text{Ru}$: C, 39.74; H, 4.00; N, 11.12. Found: C, 39.56; H, 4.32; N, 10.89.

2.2.1.3 Synthesis of $[\text{Ru}(\eta^6\text{-}p\text{-cymene})(\text{L}^2)\text{Cl}]$ [5]

0.05 g of $[(\eta^6\text{-}p\text{-cymene})\text{RuCl}(\mu\text{-Cl})_2]$ (0.08 mmol) was dissolved in 20 mL of dichloromethane and the ligand (HL^2) [4-(N-(2-pyridyl)carbamoyl)pyridine] (0.03 g, 0.16 mmol), dissolved in methanol was added dropwise. The mixture was stirred at room temperature for 4 h. The resulting solution was then filtered and evaporated *in vacuo* to ca. 5 mL. Addition of excess diethyl ether to the filtrate leads to the formation of an orange coloured precipitate. The precipitate was filtered, washed with hexane and dried in open air affording the title compound as an orange solid. Yield: 54%. ^1H NMR (400.13 MHz, 298 K, CDCl_3): δ 9.03 [br s, 1H, CH of $\text{C}_5\text{H}_4\text{N}$ of 4-aminopyridine], 8.37 [broad, 2H, CH of $\text{C}_5\text{H}_4\text{N}$ of 4-aminopyridine], 8.05 [d, 1H, CH of $\text{C}_5\text{H}_4\text{N}$ of picolinic acid], 7.97 [t, 1H, CH of $\text{C}_5\text{H}_4\text{N}$ of picolinic acid], 7.58 [t, 1H, CH of $\text{C}_5\text{H}_4\text{N}$ of picolinic acid], 6.81 [d, 2H, CH of $\text{C}_5\text{H}_4\text{N}$ of 4-aminopyridine], 5.49 [d, 1H, CH of C_6H_4], 5.32 [d, 2H, CH of C_6H_4], 5.28 [d, 1H, CH of C_6H_4], 2.46 [sept, 1H, $\text{CH}(\text{CH}_3)_2$], 2.23 [s, 3H, $\text{C}_6\text{H}_4\text{CH}_3$], 1.05 [d, 3H, $\text{CH}(\text{CH}_3)_2$], 0.99 [d, 3H, $\text{CH}(\text{CH}_3)_2$]. ESI-MS (+ve mode): $[\text{Ru}(\eta^6\text{-}p\text{-cymene})(\text{L}^2)]^+$: 434.1 (m/z).

2.2.1.4 Synthesis of $[\text{Ru}(\eta^6\text{-}p\text{-cymene})(\text{HL}^2)(\text{PTA})][\text{PF}_6]_2$ [6]· CH_3OH .

A 10 mL methanolic solution of 1,3,5-triaza-7-phosphoadamantane (0.35 g, 0.22 mmol) was added dropwise to a solution of complex **5** (0.1 g, 0.22 mmol) dissolved in a mixture of methanol and dichloromethane (10 mL + 10 mL). The resulting solution was then stirred overnight at room temperature and filtered. The filtrate was then evaporated to dryness to obtain the crude product as a yellow solid. Yield: 78%. The obtained compound was then dissolved in methanol (0.5 g, 0.08 mmol) and a methanolic solution of NH_4PF_6 (0.03 g, 0.18 mmol) was then added to it. The resulting solution was allowed to stir for 2 h at room temperature. The mixture was then filtered and concentrated to 5 mL and kept at 0°C overnight. Yellow coloured crystals suitable for single crystal XRD were obtained from the reaction mixture. Yield: 70%. ^1H NMR (400.13 MHz,

298 K, DMSO-*d*₆): δ 9.00 [d, 1H, CH of C₅H₄N], 8.64 [d, 2H, 2×CH of substituted 4-aminopyridine], 8.36 [t, 1H, CH of C₅H₄N], 8.21 [d, 1H, CH of C₅H₄N], 7.92 [d, 1H, CH of C₅H₄N], 7.87 [d, 2H, 2×CH of substituted 4-aminopyridine], 6.29 [d, 1H, CH of C₆H₄], 6.06 [d, 1H, CH of C₆H₄], 5.87 [d, 1H, CH of C₆H₄], 5.78 [d, 1H, CH of C₆H₄], 4.41 [m, 6H, 3×NCH₂N], 3.99 [m, 6H, 3×PCH₂N], 2.43 [s, 3H, C₆H₄CH₃], 2.26 [sept, 1H, CH of CH(CH₃)₂], 0.99 [d, 3H, CH(CH₃)₂], 0.73 [d, 3H, CH(CH₃)₂]. ¹³C NMR (100.61 MHz, DMSO-*d*₆): δ 168.6 [C of CON], 156.7 [C of substituted 4-aminopyridine], 153.0 [2×CH of substituted 4-aminopyridine], 142.5 [CH of C₅H₄N], 141.0 [CH of C₅H₄N], 129.8 [CH of C₅H₄N], 127.5 [CH of C₅H₄N], 122.4 [CH of substituted 4-aminopyridine], 121.0 [CH of substituted 4-aminopyridine], 101.6 [C of C₆H₄], 90.9 [C of C₆H₄], 87.9 [2×CH of C₆H₄], 78.5 [2×CH of C₆H₄], 71.2 [3×NCH₂N of PTA], 49.9–48.5 [3×PCH₂N of PTA], 30.6 [C₆H₄CH₃], 21.9 [CH(CH₃)₂], 20.9 [CH(CH₃)₂], 18.4 [CH of CH(CH₃)₂]. ³¹P NMR (DMSO-*d*₆, 126 MHz): δ -38.9, -144.2 [sept, PF₆]. ESI-MS (+ve mode): 296.1 (m/z): [Ru(η^6 -*p*-cymene)(L²)²⁺]. Anal. Calcd for C₂₈H₃₉F₁₂N₆O₂P₃Ru: C, 36.81; H, 4.30; N, 9.20. Found: C, 36.90; H, 4.54; N, 9.45.

2.2.1.5 Synthesis of [Ru(η^6 -*p*-cymene)(L³)Cl] [7]

0.1 g of [(η^6 -*p*-cymene)RuCl(μ -Cl)]₂ (0.16 mmol) was dissolved in 50 mL of methanol and the methanolic solution of the ligand (HL³) [3-(N-(2-pyridyl)carbamoyl)pyridine] (0.06 g, 0.32 mmol) was added dropwise in to that. The mixture was stirred at room temperature for 4 h. The resulting solution was then filtered. The filtrate was evaporated *in vacuo* to ca. 5 mL. An excess of diethyl ether was added to accomplish precipitation. The precipitate was filtered, washed with hexane and dried in open air affording compound **7** as an orange solid. Yield: 42%. ¹H NMR (400.13 MHz, 298 K, CDCl₃): δ 9.54 [s, 1H CH of substituted 3-aminopyridine], 9.02 [s, 1H, CH of C₅H₄N], 8.76 [d, 1H, CH of C₅H₄N], 8.36 [d, 1H, CH of substituted 3-aminopyridine], 8.12 [d, 1H, CH of substituted 3-aminopyridine], 7.96 [t, 1H, CH of C₅H₄N], 7.54 [t, 1H, CH of C₅H₄N], 7.22 [t, 1H, CH of substituted 3-aminopyridine], 5.65 [d, 1H, CH of C₆H₄], 5.57 [d, 1H, CH of

C_6H_4], 5.49 [d, 1H, CH of C_6H_4], 5.30 [d, 1H, CH of C_6H_4], 2.55 [sept, 1H, $CH(CH_3)_2$], 2.26 [s, 3H, $C_6H_4CH_3$], 1.14 [d, 3H, $CH(CH_3)_2$], 1.05 [d, 3H, $CH(CH_3)_2$]. ESI-MS (+ve mode): $[Ru(\eta^6\text{-}p\text{-cymene})(L^3)]^+$: 434.0 (m/z).

2.2.1.6 Synthesis of $[Ru(\eta^6\text{-}p\text{-cymene})(L^3)(PTA)][BF_4]$ [8]

To a solution of complex **7** (0.1 g, 0.22 mmol) dissolved in methanol (20 mL), a 10 mL methanolic solution of 1,3,5-triaza-7-phosphoadamantane (0.35 g, 0.22 mmol) was added dropwise. The resulting mixture was stirred overnight at room temperature and filtered. The filtrate was then evacuated *in vacuo* to obtain the crude product as an orange coloured solid. Yield: 70%. The orange solid was then dissolved in a mixture of dichloromethane and methanol (5 mL + 5 mL) and a methanolic solution of $NaBF_4$ (0.006 g, 0.05 mmol) was added to it. The resulting solution was then stirred at room temperature for 2 h and then filtered. The filtrate was then concentrated *in vacuo* to 2 mL and kept for vapour diffusion with diethyl ether to obtain orange coloured crystals of compound **8**. Yield: 65%. 1H NMR (400.13 MHz, 298 K, $DMSO-d_6$): δ 8.98 [d, 1H, CH of C_5H_4N], 8.68 [s, 1H, CH of substituted 3-aminopyridine], 8.40 [br, s, 1H, CH of C_5H_4N], 8.29 [t, 1H, CH of substituted 3-aminopyridine], 8.07 [d, 1H, CH of substituted 3-aminopyridine], 7.84 [t, 1H, CH of C_5H_4N], 7.76 [d, 1H, CH of C_5H_4N], 7.54 [br.t, 1H, CH of substituted 3-aminopyridine], 6.31 [d, 1H, CH of C_6H_4], 5.94 [d, 1H, CH of C_6H_4], 5.79 [d, 1H, CH of C_6H_4], 5.39 [d, 1H, CH of C_6H_4], 4.45 [m, 6H, $3 \times NCH_2N$], 4.07–3.85 [m, 6H, $3 \times PCH_2N$], 2.37 [s, 3H, $C_6H_4CH_3$], 2.15 [sept, 1H, CH of $CH(CH_3)_2$], 0.93 [d, 3H, $CH(CH_3)_2$], 0.75 [d, 3H, $CH(CH_3)_2$]. ^{13}C NMR (100.61 MHz, $DMSO-d_6$): δ 167.0 [C of CON], 157.2 [CH of C_5H_4N], 156.3 [CH of C_5H_4N], 154.2 [C of substituted 3-aminopyridine], 147.5 [C of C_5H_4N substituted 3-aminopyridine], 144.5 [CH of C_5H_4N], 140.6 [CH of substituted 3-aminopyridine], 133.5 [CH of C_5H_4N], 129.3 [CH of C_5H_4N], 118.7 [CH of substituted 3-aminopyridine], 115.2 [CH of substituted 3-aminopyridine], 101.8 [C of C_6H_4], 93.5 [C of C_6H_4], 91.3 [CH of C_6H_4], 88.8 [CH of C_6H_4], 87.5 [C of C_6H_4], 79.4–70.6 [$3 \times PCH_2N$ of PTA], 53.7–46.2 [$3 \times NCH_2N$ of PTA], 30.2 [$C_6H_4CH_3$], 21.9 [$CH(CH_3)_2$], 21.1 [$CH(CH_3)_2$],

17.9 [CH of CH(CH₃)₂]. ³¹P NMR (DMSO-*d*₆, 126 MHz): δ -39.1. ESI-MS (+ve mode): [Ru(η⁶-*p*-cymene)(L³)(PTA)]⁺: 591.1 (m/z). Anal. Calcd for C₂₇H₃₄BF₄N₆OPRu: C, 47.87; H, 5.06; N, 12.41. Found: C, 47.53; H, 5.31; N, 12.47.

2.2.2 X-ray crystallography

2.2.2.1 X-ray crystallography of compound 2

X-ray single crystals of complex **2** were immersed in cryo-oil, mounted in Nylon loops and measured at a temperature of 150 K on a Bruker AXS-KAPPA APEX II with graphite monochromated Mo-Kα (λ = 0.71073) radiation. Data were collected using omega scans of 0.5° per frame and a full sphere of data was obtained. Cell parameters were retrieved using Bruker SMART^[27] software and refined using Bruker SAINT^[28] on all the observed reflections. Absorption corrections were applied using SADABS.^[29] Structures were solved by direct methods by using the SHELXS-97 package^[30] and refined with SHELXL-2014/7.^[31] Calculations were performed using the WinGX System-Version 2014.1.^[32] Least squares refinement with anisotropic thermal motion parameters for all the nonhydrogen atoms and isotropic for the remaining atoms was employed. All hydrogen atoms bonded to carbon were included in the model at the geometrically calculated positions and refined using a riding model. U_{iso}(H) was defined as 1.2U_{eq} of the parent carbon atoms for phenyl and methylene residues and 1.5U_{eq} of the parent carbon atoms for the methyl groups. There was some void in the structure which, despite the negligible volume and number of electrons (63 Å³ and 3 electrons per unit cell), was corrected with PLATON/SQUEEZE (Table 2.1).^[33]

2.2.2.2 X-ray crystallography of compound 4

X-ray single crystal structural data of compound **4** was collected on a Bruker D8 Venture PHOTON 100 CMOS diffractometer equipped with an INCOATEC microfocus source and graphite monochromated MoKα radiation (λ = 0.71073 Å) operating at 50 kV and 30 mA. The program SAINT85 was used for the integration of diffraction profiles and absorption

correction was done with the SADABS86 program. The structure was solved by SIR 9287 and refined by the full matrix least-squares method using the SHELXL-201388 and WinGX system, v 2013.3.89. All the nonhydrogen atoms were located from the difference Fourier map and refined anisotropically. All the hydrogen atoms were fixed by HFIX and placed in ideal positions and included in the refinement process using the riding model with isotropic thermal parameters. The potential solvent accessible area or void space was calculated using the PLATON multipurpose crystallographic software.

2.2.2.3 X-ray crystallography compound 6 and 8

Single crystal X-ray structural studies of **6** and **8** were carried out on a CCD Agilent Technologies (Oxford Diffraction) SUPER NOVA diffractometer. Data for the crystal **6** and **8** were collected at 293(2) K and 150(2) K respectively using graphite-monochromated MoK α radiation ($\lambda = 0.71073$ Å). The strategy for the data collection was evaluated by using the CrysAlisPro CCD software. The data were collected by the standard ‘phi–omega scan techniques and were scaled and reduced using CrysAlis-Pro RED software. The structures were elucidated by direct methods using SHELXS-97 and refined by full matrix least squares with SHELXL-97, refining on F^2 .^[31] The positions of all the atoms were obtained by direct methods. All non-hydrogen atoms were refined anisotropically. The remaining hydrogen atoms were placed in geometrically constrained positions and refined with isotropic temperature factors, generally $1.2U_{eq}$ of their parent atoms.

2.2.3 Protein binding experiments

Protein binding studies of the synthesised complexes were carried out by tryptophan fluorescence quenching experiments using human serum albumin (HSA). The excitation wavelength for HSA was at 280 nm, and the quenching of the emission intensity of the tryptophan residues of HSA at 345 nm was monitored using the complexes as a quencher with increased concentration. The excitation and emission slit widths and scan rates were

kept constant throughout the experiment. A 10 μM stock solution of HSA was prepared using 50 mM Tris buffer solution and stored at 4°C for further use. Stock solutions of 5 mM strength were made using synthesized compounds. Fluorometric titration was carried out taking 2 mL of the protein solution and the fluorescence intensity was measured as blank. For titration, each time, 10 μL of the stock solution was added to the protein solution and the fluorescence

intensity was measured. For all the four complexes, up to 100 μL of the solution was added to measure fluorescence quenching. The fluorescence quenching data were further analyzed by using the Stern–Volmer equation, which again can be expressed in terms of the bimolecular quenching rate constant and the average life time of the fluorophore as shown in the following equation:

$$\frac{F_0}{F} = 1 + k_q\tau_0[Q] = 1 + K_{SV}[Q]$$

where F_0 and F are the fluorescence intensities in the absence and presence of a quencher, k_q is the bimolecular quenching rate constant, τ_0 is the average lifetime of a fluorophore in the absence of a quencher and $[Q]$ is the concentration of a quencher (metal complexes). K_{SV} is the Stern–Volmer quenching constant in M^{-1} .

2.2.4 Inhibition of the Trx-R enzyme

The inhibition of the Trx-R enzyme was carried out using DTNB as a substrate according to the protocol given by Sigma Aldrich with subsequent modifications. Colorimetric assays were performed with a microplate reader to determine the inhibition of Trx-R. The compound was dissolved to make stock solution in DMSO (5 mM). Mammalian thioredoxin reductase, supplied in 50 mM Tris-HCl (pH = 7.4), 10 mM EDTA, 300 mM NaCl and 10% glycerol was diluted 20 times. The reaction mixture in each well consists of working buffer [180 μL ; 100 mM potassium phosphate with 10 mM EDTA and 0.24 mM nicotinamide adenine dinucleotide phosphate (NaDPH)], 1x assay buffer (8 μL), TrxR enzymes (2 μL), and the positive control (cisplatin) or the ruthenium complex. The reaction mixture was incubated for 15 min at 298 K and then 100 mM

DMSO solution (6 μL) of DTNB was added. The formation of 5-thio-2-nitrobenzoic acid (5-TNB) was monitored with a microplate reader at 412 nm after 15 and 30 min. Non-interference with the assay component was ensured by a negative control experiment with an enzyme free solution. The following equation was used to determine the TrxR enzyme activity.

$$\text{Unit/mL} = [\Delta A_{412}/\text{min}(\text{TrxR}) \times \text{dil} \times \text{vol}] / \text{enz}_{\text{vol}}$$

$\Delta A_{412} \text{ min}^{-1}$ = change in absorbance at 412 nm per minute, $\Delta A_{412} \text{ min}^{-1}$ (TrxR) = [$\Delta A_{412} \text{ min}^{-1}$ (sample) – $\Delta A_{412} \text{ min}^{-1}$ (blank, without enzyme)], dil = sample dilution factor, vol = volume of the reaction mixture and enz_{vol} = volume of the enzyme.

2.2.5 Supplementary materials

CCDC 1036656, 1449639, 1477542 and 1444481 contain the supplementary crystallographic data for **2**, **4**, **6** and **8** respectively. These data can be obtained free of charge *via* <http://www.ccdc.cam.ac.uk/conts/retrieving.html>, or from the Cambridge Crystallographic Data Centre, 12 Union Road, Cambridge CB2 1EZ, UK; fax: (+44) 1223-336-033; or e-mail: deposit@ccdc.cam.ac.uk.

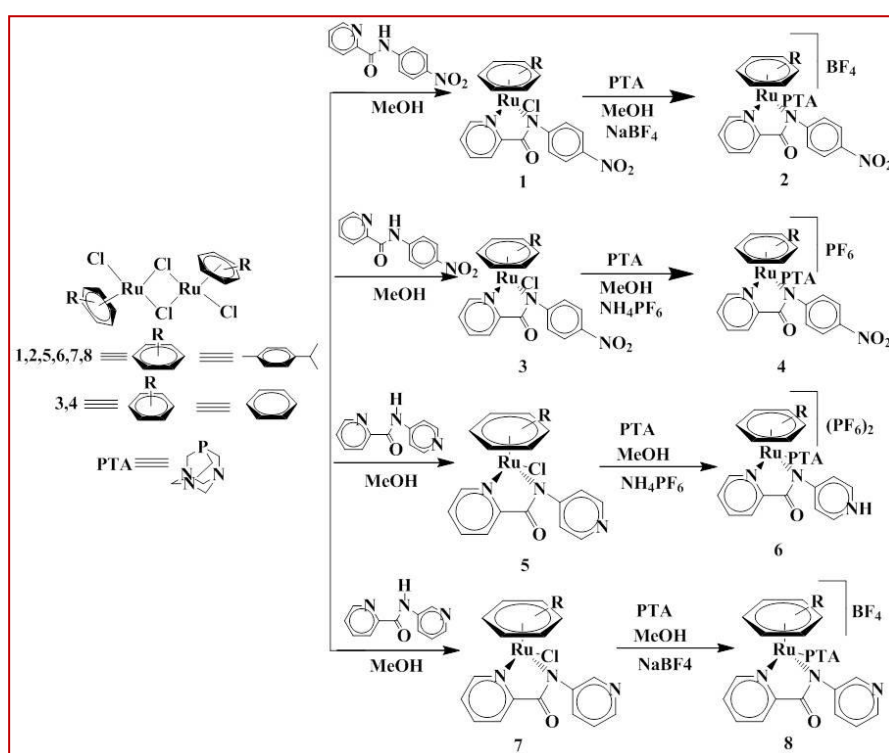
2.3 Results and discussion

2.3.1 Syntheses of complexes

Room temperature substitution of a chloride ligand in ruthenium(II) complexes with the general formula $[\text{Ru}(\eta^6\text{-arene})(\text{L})\text{Cl}]$ (**HL**¹ = pyridine-2-carboxylic acid(4-nitro-phenyl)-amide, $\eta^6\text{-arene}$ = *p*-cymene **1** and **HL**¹ = pyridine-2-carboxylic acid(4-nitro-phenyl)-amide, $\eta^6\text{-arene}$ = benzene **3**, **HL**² = 4-(N-(2-pyridyl)carbamoyl)pyridine, $\eta^6\text{-arene}$ = *p*-cymene, **5** **HL**³ = 3-(N-(2-pyridyl)carbamoyl)pyridine, $\eta^6\text{-arene}$ = *p*-cymene **7**) with 1,3,5-triaza-7-phosphadamantane (PTA) yielded water soluble complexes $[\text{Ru}(\eta^6\text{-arene})(\text{L})(\text{PTA})]^+$ [**2**, **4**, **8**] and $[\text{Ru}(\eta^6\text{-arene})(\text{HL})(\text{PTA})]^{++}$ [**6**] (Scheme 2.1).

Compound **2** and compound **8** were recrystallized in presence of tetrafluoroborate ions in a dichloromethane and methanol mixture to generate single crystals of $[\text{Ru}(\eta^6\text{-}i\text{p}\text{-cymene})(\text{L}^1)(\text{PTA})]\text{BF}_4$ **2** and single

crystals of $[\text{Ru}(\eta^6\text{-}p\text{-cymene})(\text{L}^3)(\text{PTA})]\text{BF}_4$ **8** for solid state characterization whereas single crystals for compound **4** and compound **6** were obtained in the presence of NH_4PF_6 as $[\text{Ru}(\eta^6\text{-benzene})(\text{L}^1)(\text{PTA})]\text{PF}_6$ and $[\text{Ru}(\eta^6\text{-}p\text{-cymene})(\text{HL}^2)(\text{PTA})](\text{PF}_6)_2$, respectively. All the PTA compounds were obtained as yellow/yellow-orange powders in moderate to good yields (52%–78%). Complex $[\text{Ru}(\eta^6\text{-}p\text{-cymene})(\text{L}^2)\text{Cl}]$ **5** and $[\text{Ru}(\eta^6\text{-}p\text{-cymene})(\text{L}^3)\text{Cl}]$ **7** were prepared by the reaction of N-substituted picolinamide with $[(\eta^6\text{-}p\text{-cymene})\text{RuCl}(\mu\text{-Cl})_2]$ using a method identical as for complexes **1** and **3**.



Scheme 2.1: Synthesis of compounds $[\text{Ru}(\eta^6\text{-}p\text{-cymene})(\text{L}^1)(\text{PTA})][\text{BF}_4]$ **2**, $[\text{Ru}(\eta^6\text{-benzene})(\text{L}^1)(\text{PTA})][\text{PF}_6]$ **4**, $[\text{Ru}(\text{HL}^2)(\eta^6\text{-}p\text{-cymene})(\text{PTA})][\text{PF}_6]_2$ **6**, and $[\text{Ru}(\eta^6\text{-}p\text{-cymene})(\text{L}^3)(\text{PTA})][\text{BF}_4]$ **8**.

The ^1H NMR spectra for complexes **2** and **4** display peaks at 8.98 to 7.57 ppm typical of the aromatic ring for ligand L^1 (Fig.2.1-Fig.2.2).

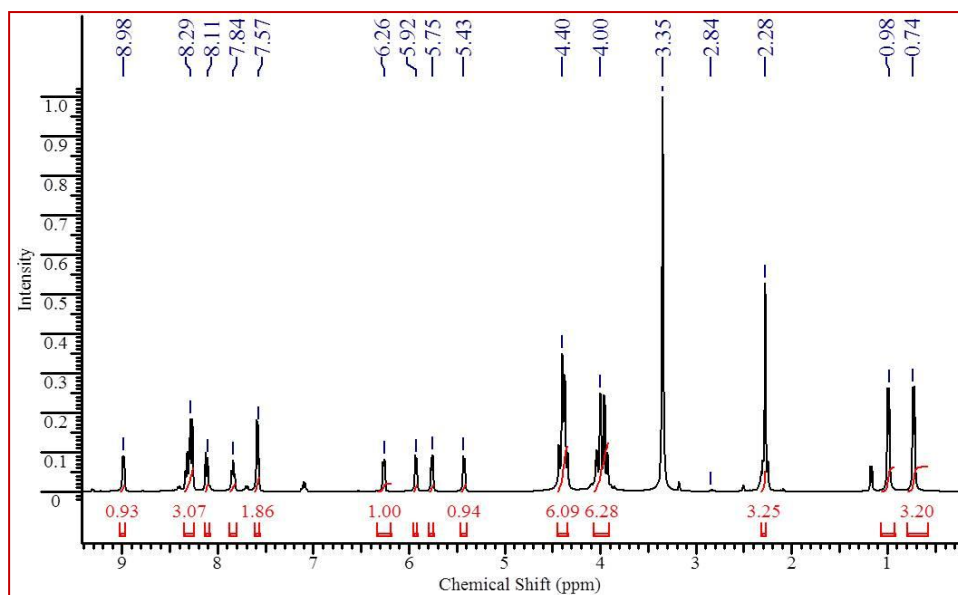


Fig.2.1: ^1H NMR spectra of complex 2.

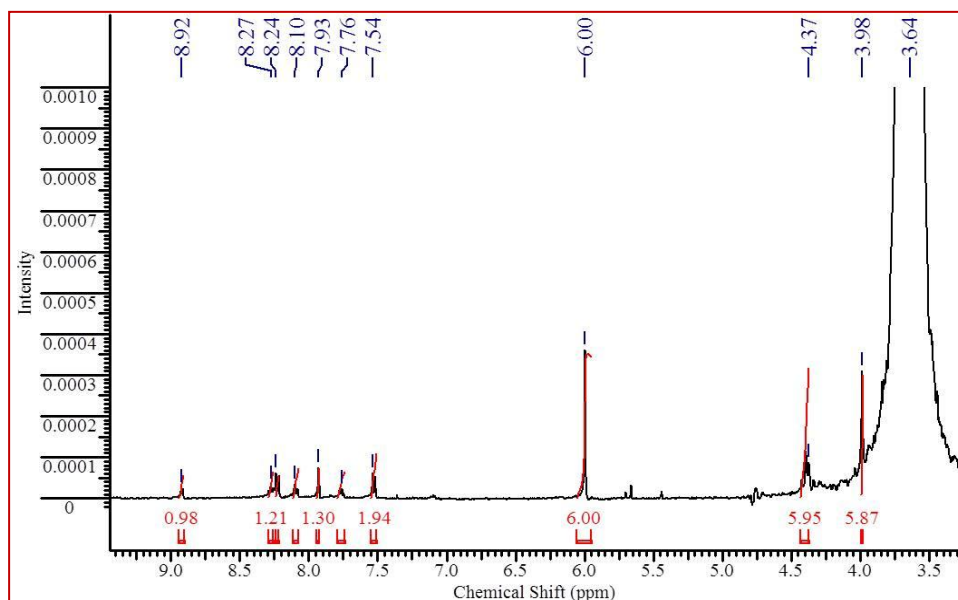


Fig.2.2: ^1H NMR spectra of complex 4.

The lack of an NH signal indicates the deprotonation of the ligand. The signals of the arene ring are observed in the range of 6.26 to 5.43 ppm and at 2.84, 2.28, 0.98 and 0.72 ppm for *p*-cymene and 6.0 ppm for the coordinated benzene ring. The resonance due to the PTA is shifted towards the lower field with respect to uncoordinated PTA, confirming the coordination. Although free PTA shows only two singlets in the ^1H NMR, two sets of multiplets were observed for the synthesized complexes as

reported earlier.^[34] Pyridinyl signals for the ligand **HL**² in compounds **5** and **6** are observed in the range of 9.03 to 6.81 ppm (Fig.2.3 and Fig.2.4).

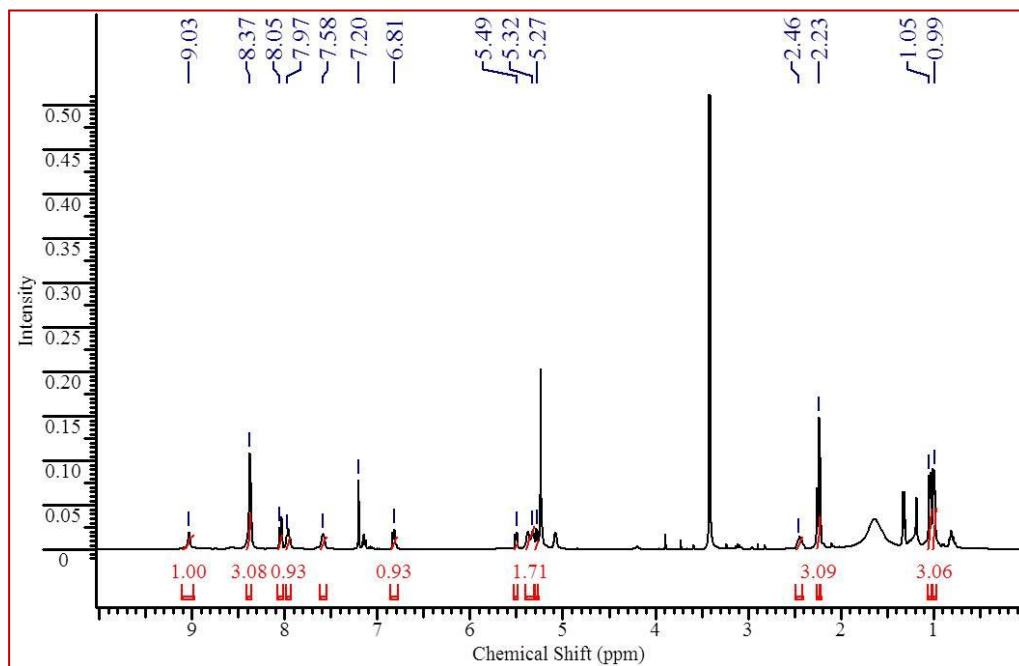


Fig.2.3: ¹H NMR spectra of complex **5**.

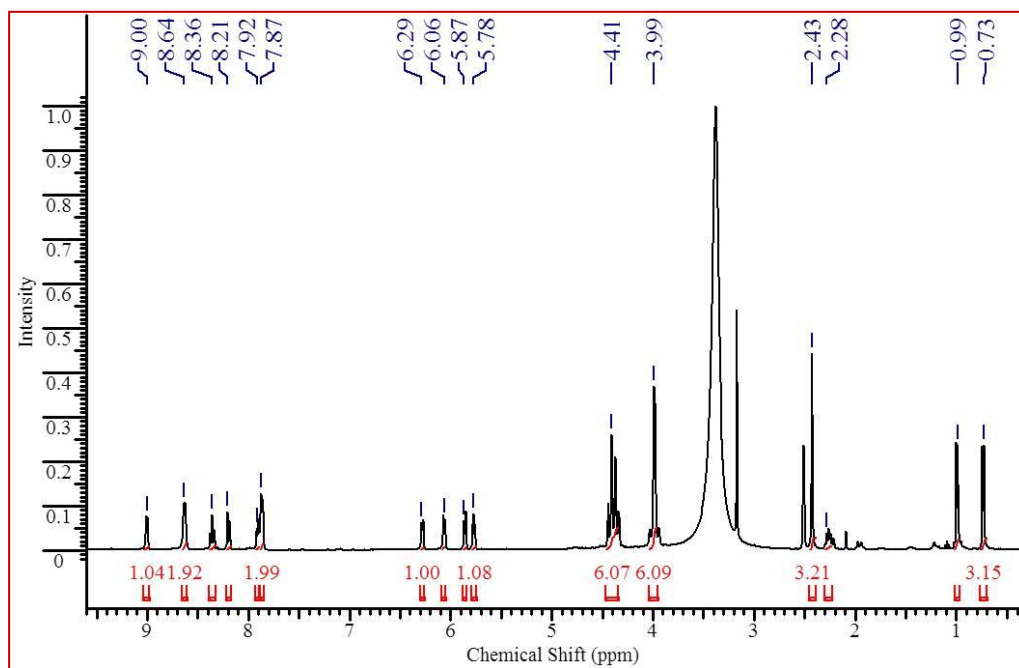


Fig.2.4: ¹H NMR spectra of complex **6**.

Similar peaks in the range of 9.54 to 7.22 were observed for ligand **L**³ in compounds **7** and **8** (Fig.2.5 and Fig.2.6).

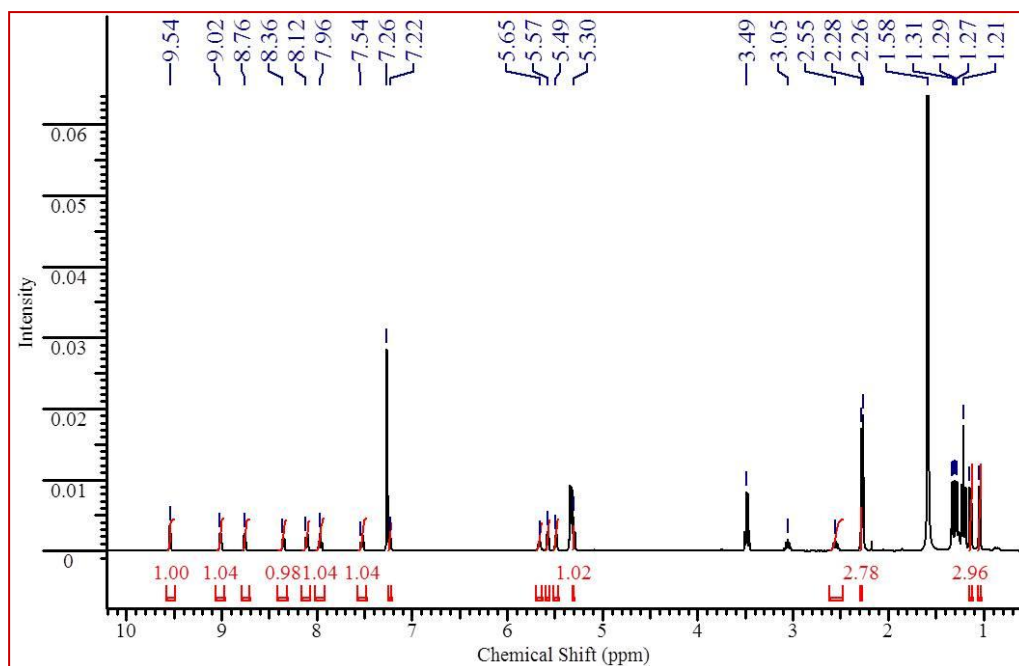


Fig.2.5: ^1H NMR spectra of complex **7**.

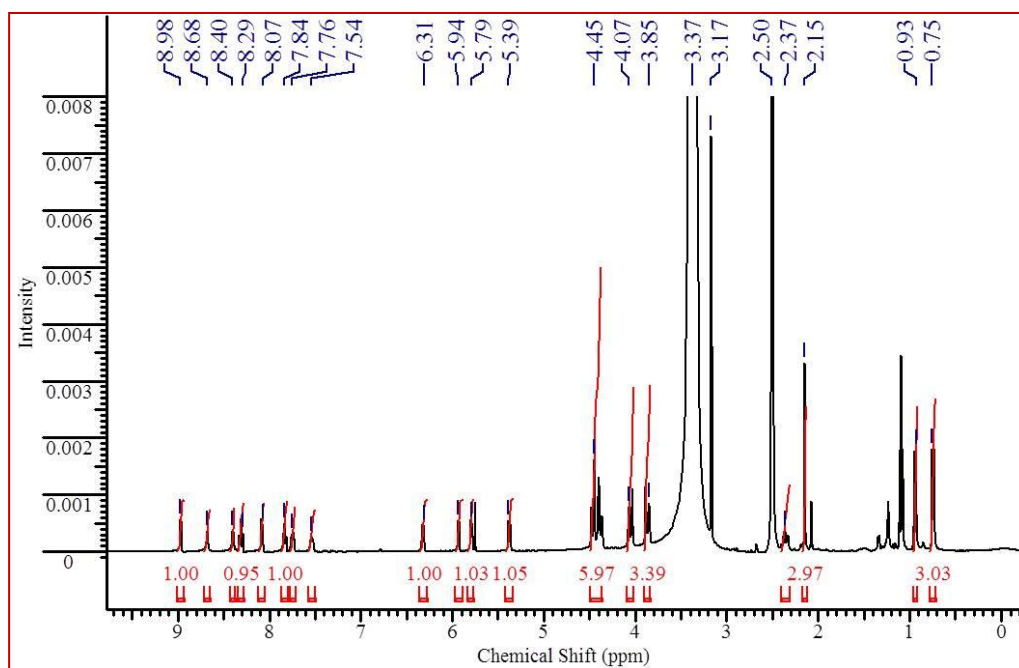


Fig.2.6: ^1H NMR spectra of complex **8**.

The ^{13}C spectra for compounds **2**, **4**, **6** and **8** also corroborate the proposed structure (Fig.2.7-Fig.2.10).

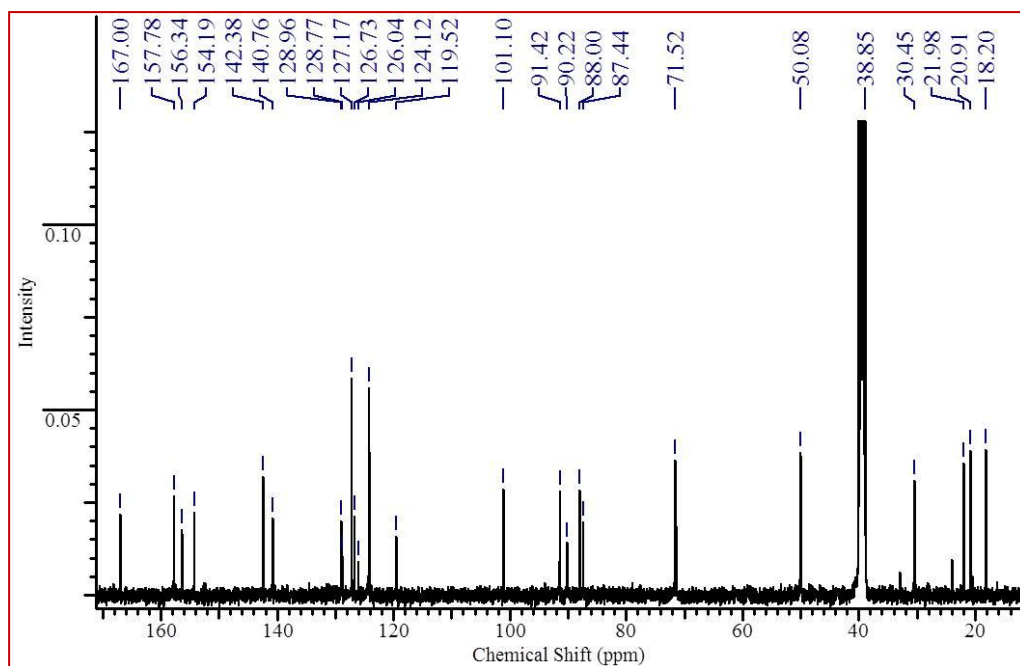


Fig.2.7: ^{13}C NMR spectra of complex 2.

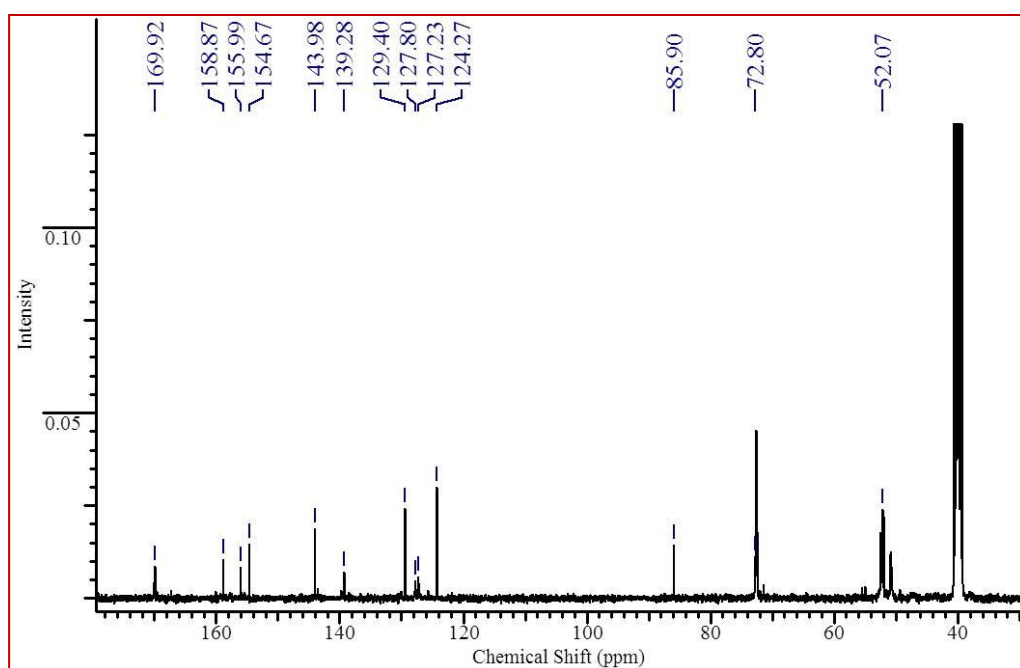


Fig.2.8: ^{13}C NMR spectra of complex 4.

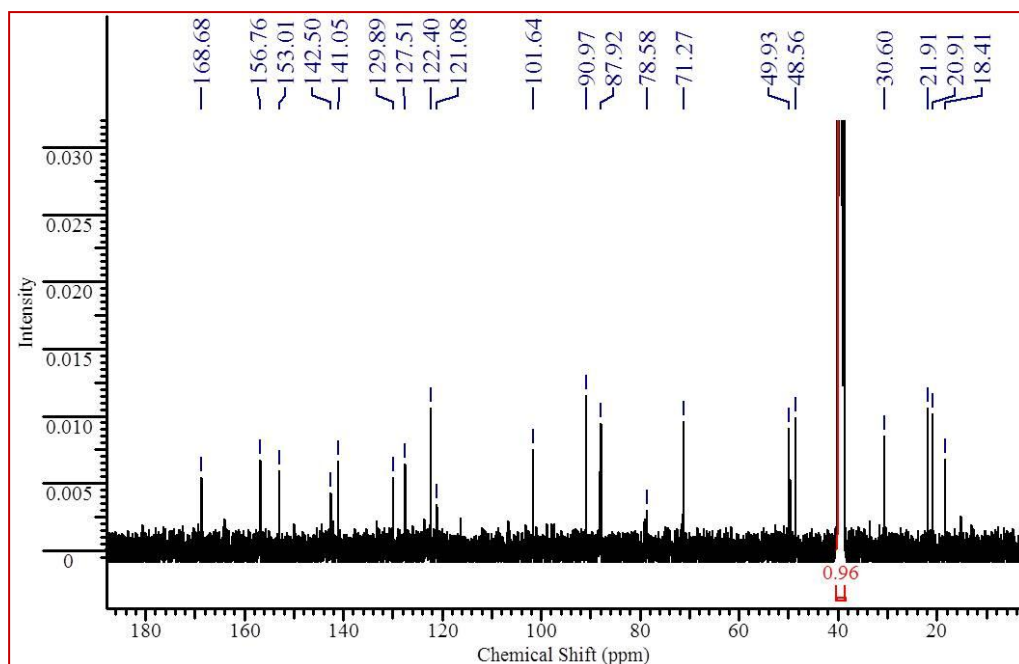


Fig.2.9: ^{13}C NMR spectra of complex **6**.

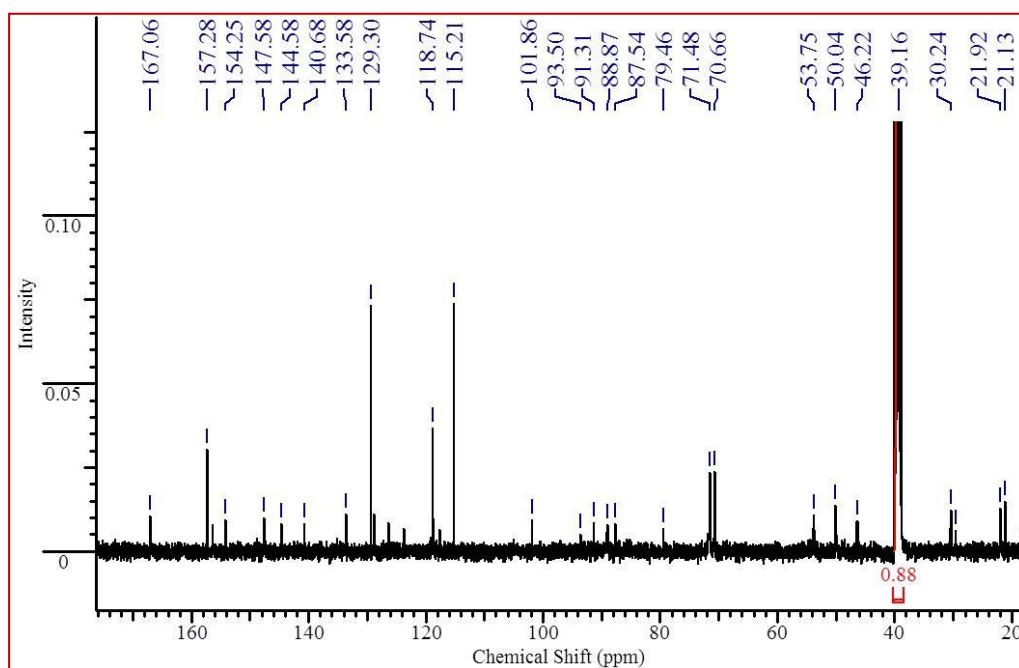


Fig.2.10: ^{13}C NMR spectra of complex **8**.

The ^{31}P NMR spectra of compounds **2**, **4**, **6** and **8** show peaks in the range of -30 to -39 ppm as reported earlier (Fig.2.11-Fig.2.14).^[10]

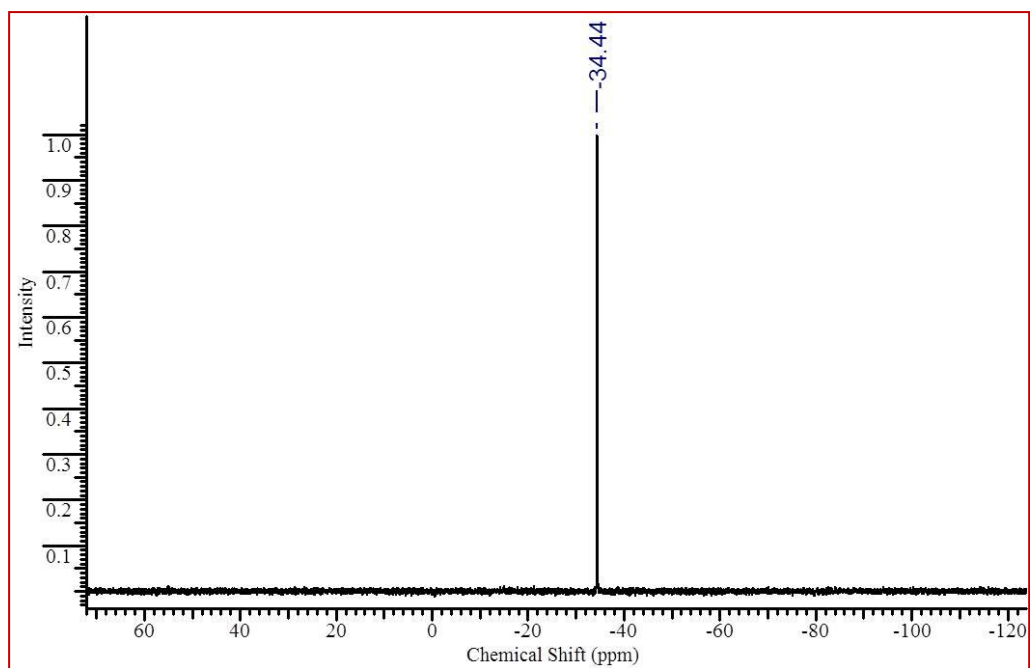


Fig.2.11: ^{31}P NMR spectra of complex 2.

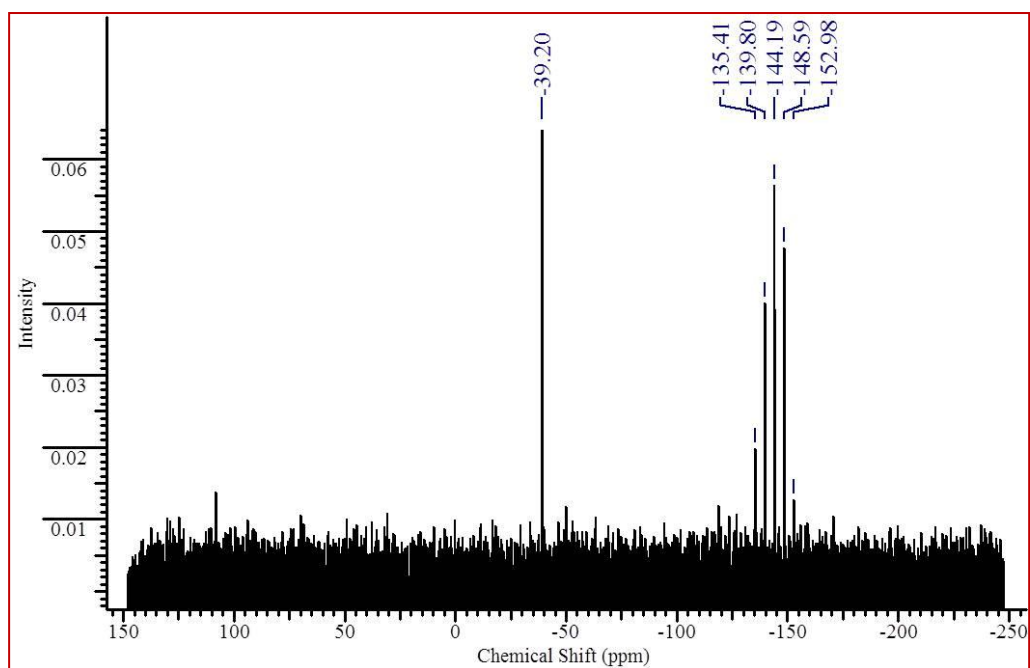


Fig.2.12: ^{31}P NMR spectra of complex 4.

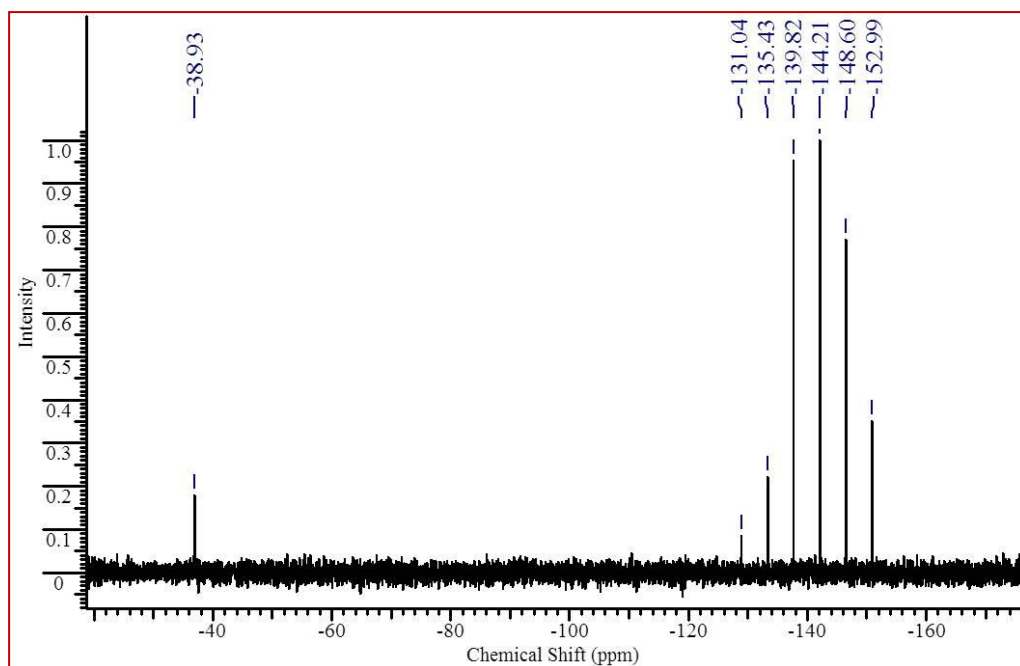


Fig.2.13: ^{31}P NMR spectra of complex **6**.

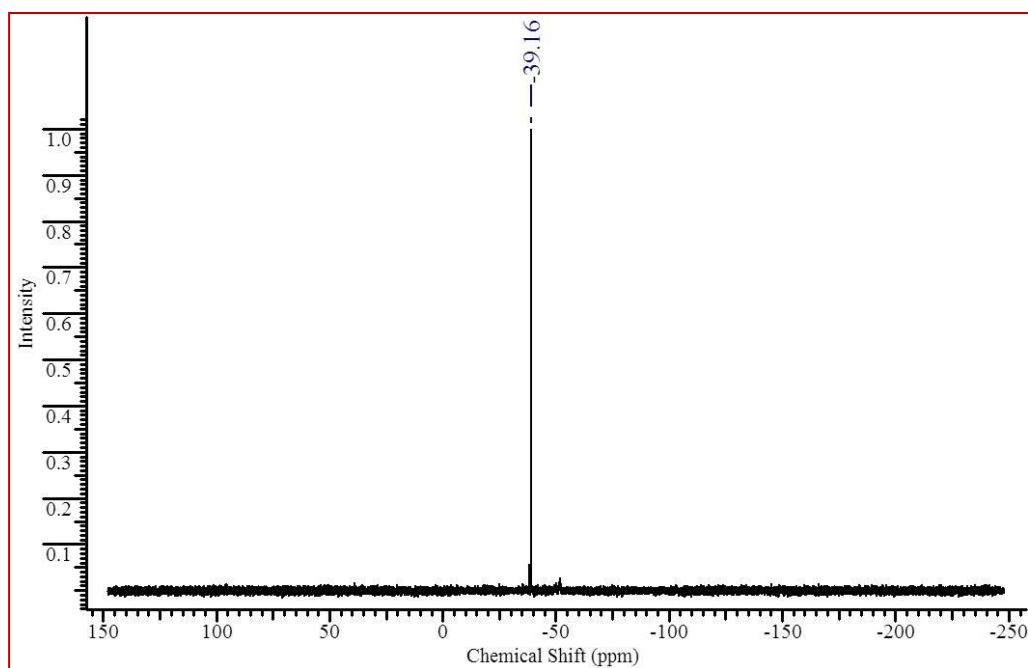


Fig.2.14: ^{31}P NMR spectra of complex **8**.

The ESI mass spectra of **2**, **4**, **6**, **8** revealed two main peak envelopes. The higher one corresponds to $[\text{Ru}(\text{arene})(\text{L})(\text{PTA})]^+$ and the other to $[\text{Ru}(\text{arene})(\text{L})]^+$ (Fig.2.15-Fig.2.18).

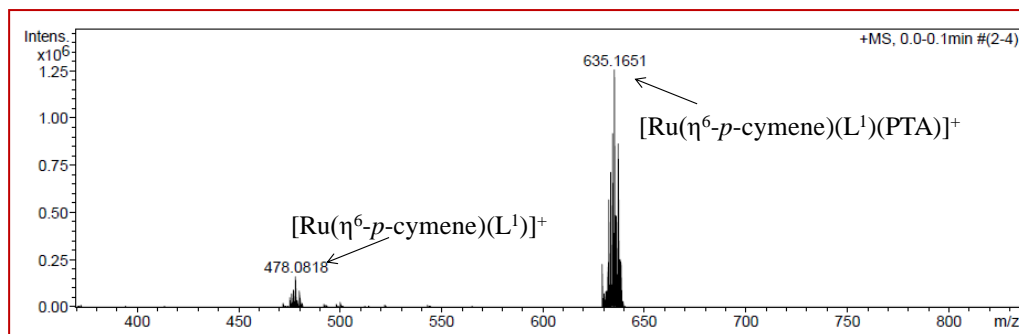


Fig.2.15: ESI-MS of complex 2.

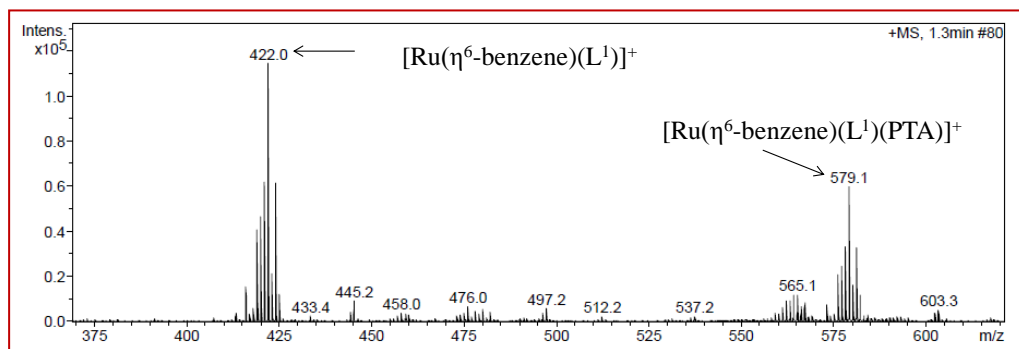


Fig.2.16: ESI-MS of complex 4.

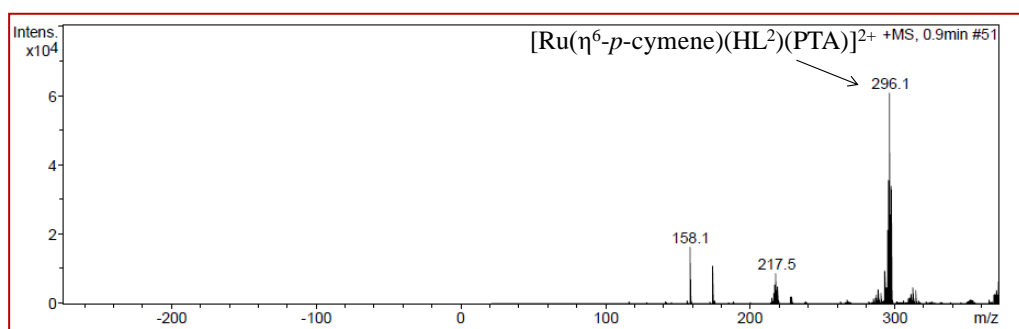


Fig.2.17: ESI-MS of complex 6.

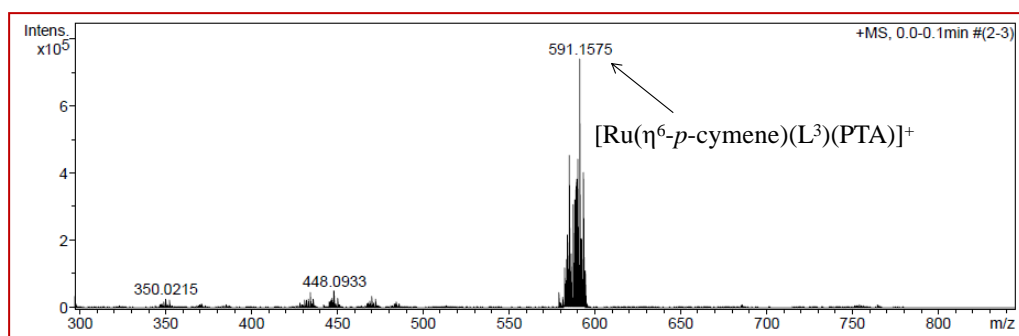


Fig.2.18: ESI-MS of complex 8.

Compounds 5 and 7 produce ESI-MS peaks for the $[\text{Ru}(p\text{-cym})(\text{L})]^+$ moiety (Fig.2.19-Fig.2.20).

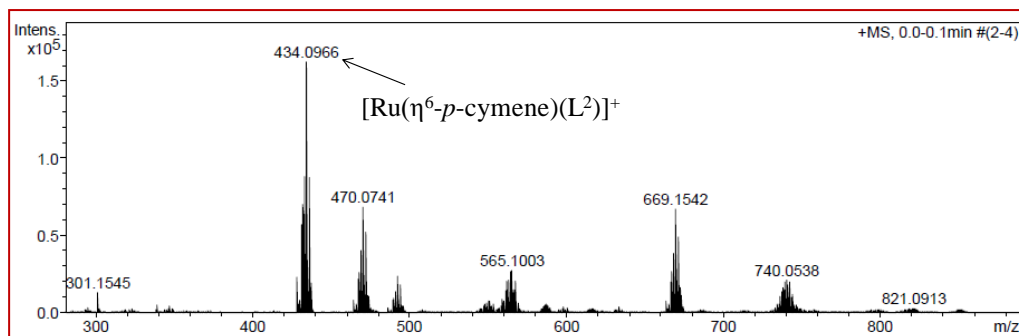


Fig.2.19: ESI-MS of complex 5.

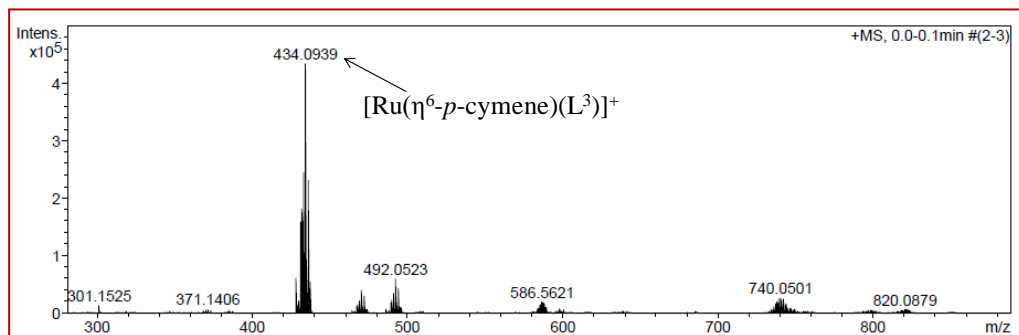


Fig.2.20: ESI-MS of complex 7.

The solid state structures of the four compounds (**2**, **4**, **6** and **8**) were investigated by X-ray crystallography. All the compounds possess the characteristic pseudo-octahedral geometry. The η^6 π -bonded arene ring occupying three coordination positions of the octahedron, along with two coordination sites occupied by the nitrogen donor of the N-substituted picolinamide moiety and the other coordination site, is occupied by the PTA ligand through the phosphorus donor. The asymmetric unit of **2** comprises one complex cation, one BF_4 anion and two water molecules (Fig. 2.21).

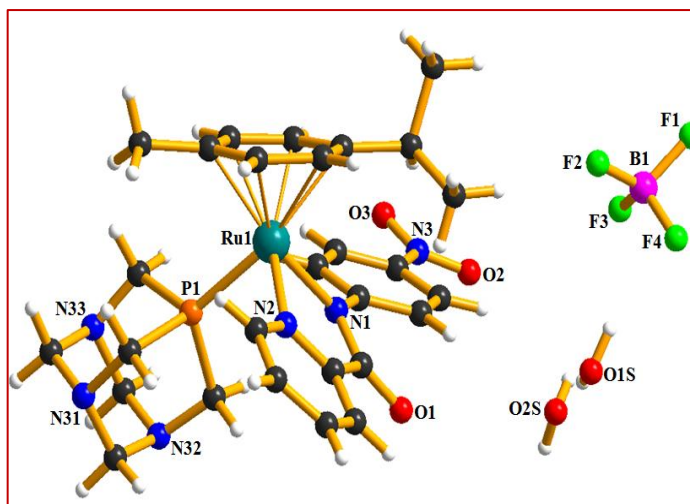


Fig.2.21: The solid state crystal structure of compound **2** with partial atomic numbering scheme. Key bond lengths (Å) and angles (°): $Ru(1)-P(1)$: 2.3112(7); $Ru(1)-N(1)$: 2.118(2); $Ru(1)-N(2)$: 2.072(2); $Ru(1)-C_{centroid}$: 1.735; $P(1)-Ru(1)-N(1)$: 87.54(7); $P(1)-Ru(1)-N(2)$: 86.90(7); $N(1)-Ru(1)-N(2)$: 77.80(9).

The $(L^1)^-$ ligand binds the metal in a N,N-chelating fashion, thus giving rise to a five-membered RuNCCN metallacycle, the ruthenium coordination environment being then fulfilled by the P-atom of PTA and by the π -bonded aromatic ring of *p*-cymene. Bond distances and angles are in the range of those found in other ruthenium compounds and PTA or arene derivatives.^[14] As a result of steric restrictions, the anionic organic ligand is twisted, as measured by the angle (25.03°) between the least-squares planes of its aromatic and pyridinyl rings; in addition, the least-squares planes of the cymene and of the metallacycle rings are 49.84° apart. The Ru–P bond is nearly orthogonal to the metallacycle (88.95°), but markedly away from the plane of the arene (130.40°). The isolated ruthenium complexes form a 1D hydrogen bonded chain along the *b*-axis through C32–H32A \cdots O3 and C34–H34B \cdots O3. The counter BF_4^- anion and two water molecules as the solvent of crystallization cemented these parallel chains through further hydrogen bonding [C22–H22 \cdots F1, C27–H27B \cdots F1, C12–H12 \cdots F1, C30–H30C \cdots F2, C31–H31A \cdots F3, O1S–H1A \cdots F3, C25–H25 \cdots F4, C33–H33A \cdots O1S, O2S–H2A \cdots N31] for a 2D hydrogen bonded polymer in the *bc*-plane.

Complex **4** also has a similar kind of structure to compound **2** (Fig. 2.22). However, the twisting in the anionic ligand is much greater here which is

found to be 56.3° between the least-squares planes of its aromatic and pyridinyl rings.

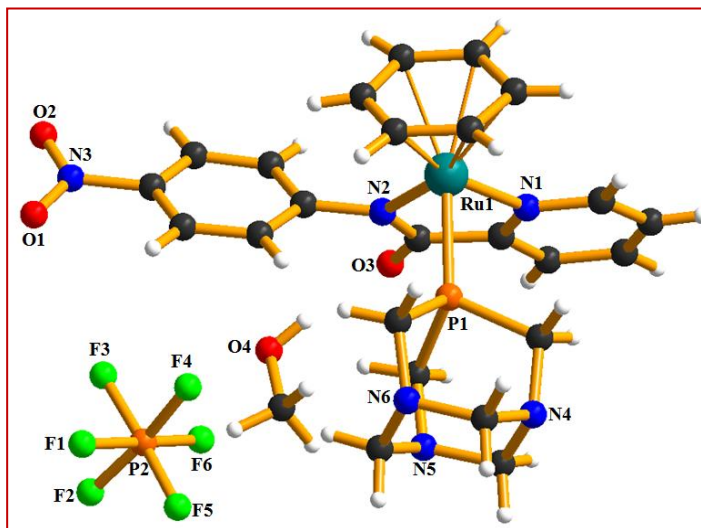


Fig.2.22: The solid state crystal structure of compound **4** with partial atomic numbering scheme. Key bond lengths (Å) and angles ($^\circ$): $Ru(1)-P(1)$: 2.327(1); $Ru(1)-N(1)$: 2.092(3); $Ru(1)-N(2)$: 2.096(3); $Ru(1)-C_{centroid}$: 1.735; $P(1)-Ru(1)-N(1)$: 87.37(8); $P(1)-Ru(1)-N(2)$: 88.84(8); $N(1)-Ru(1)-N(2)$: 76.9(1).

In complex **4**, every complex molecule is found to be interacting with three other surrounding molecules through $C13-H13 \cdots O1$, $C21-H21 \cdots O1$, $C6-H6 \cdots O2$, $C11-H11 \cdots N4$, $C9-H9 \cdots N5$. It gives a complicated 3D packing which is further reinforced by an octahedral PF_6^- counteranion [$C2-H2 \cdots F3$, $H19-H19 \cdots F3$, $C17-H17A \cdots F2$ and $C22-H22 \cdots F1$] and one methanol as solvent molecules.

Complex **6** has been shown to crystallize in the monoclinic space group $P2_1/n$. Two pyridyl rings in the ligand were found to be twisted at an angle of 37.43° (Fig.2.23). A methanol molecule is also observed as a solvent of crystallization. However, the most interesting observation is the presence of two hexafluorophosphate ions per ruthenium centre indicating the neutral nature of the substituted ligand.

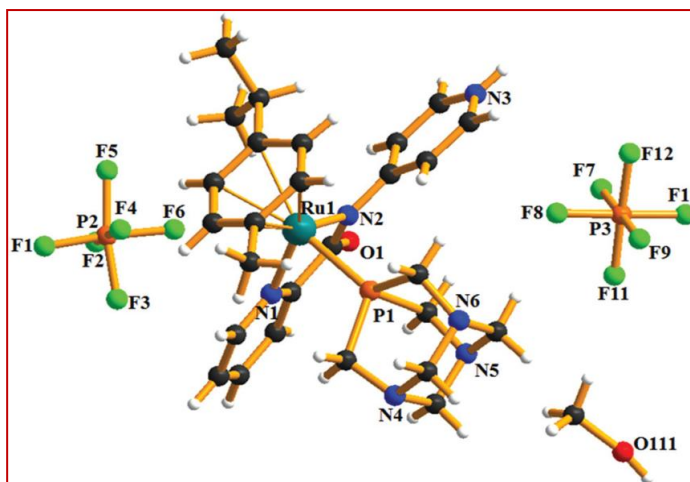
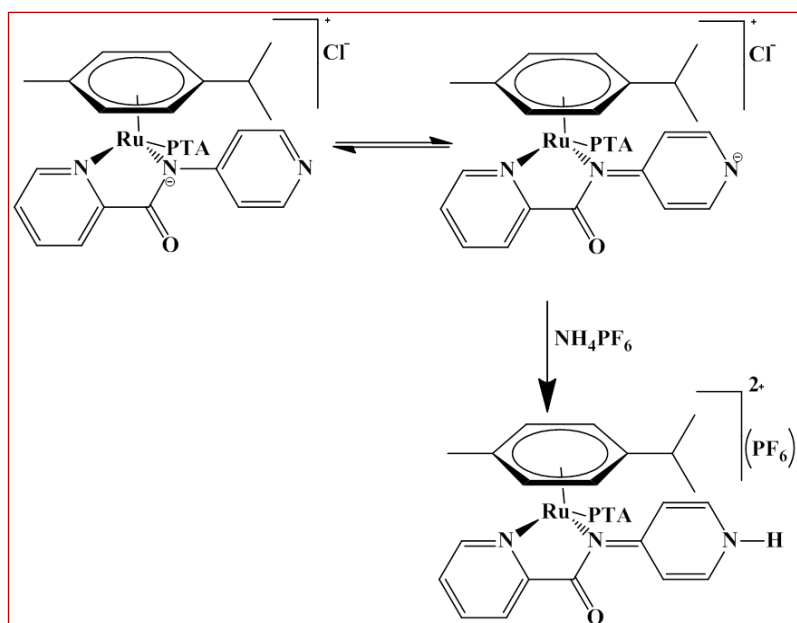


Fig.2.23: The solid state crystal structure of compound **6** with partial atomic numbering scheme. Key bond lengths (Å) and angles (°): $Ru(1)-P(1)$: 2.319(1); $Ru(1)-N(1)$: 2.086(3); $Ru(1)-N(2)$: 2.115(3); $Ru(1)-C_{centroid}$: 1.736; $P(1)-Ru(1)-N(1)$: 85.14(9); $P(1)-Ru(1)-N(2)$: 89.38(9); $N(1)-Ru(1)-N(2)$: 77.9(1).

A closer observation of the crystal structure reveals a comparatively shorter C–N bond distance of the amino pyridyl fraction of the ligand [C7–N2 1.396(5) Å] along with the C8–C9 and C10–C11 bond distance in the pyridyl ring [1.365(6) and 1.366(6) Å, respectively] indicating the protonation of the 4-pyridyl nitrogen in the presence of an ammonium salt during the complexation, which essentially leads to the change of the valence-bond representation of the ligand as per Scheme 2.2.



Scheme 2.2: Valence bond tautomerism of compound.

Protonation at the 4-pyridyl nitrogen atom gives a partial double bond character to the C7–N2 bond making it comparatively labile in nature. A similar kind of observation is reported earlier for an alkyl pyridine palladium complex.^[35] This subtle change in the system makes the ligand relatively weaker with respect to complex **8**, which is evident through a comparatively longer bond length between the donating nitrogen atom and the ruthenium centre [N(1)–Ru(1) and N(2)–Ru(2)]. There are two crystallographically independent PF₆[−] ions present. One of them connects three ruthenium cationic complexes through C25–H25A···F1, C23–H23A···F2, C2–H2···F6 and C15–H15···F4. The other PF₆[−] connects four such complexes through C27–H27A···F8, C18–H18···F7, C25–H25B···F9, C24–H24A···F12 and C11–H11···F12. The N-pyridyl hydrogen has been shown to form a strong hydrogen bond with methanol molecules which act as a solvent of crystallization through N3–H3N···O111 [1.896 Å]. All these hydrogen bonds lead to the formation of a 3D-hydrogen bonded network.

Complex **8** crystallized in the triclinic space group C2/c. Two pyridyl rings in the ligand were found to be twisted at an angle of 45.91° (Fig. 2.24).

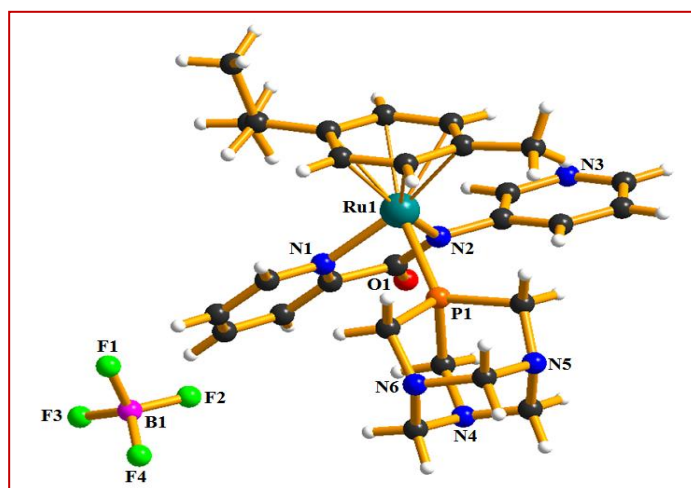


Fig.2.24: The solid state crystal structure of compound **8** with partial atomic numbering scheme. Key bond lengths (Å) and angles (°): Ru(1)–P(1): 2.319(1); Ru(1)–N(1): 2.079(3); Ru(1)–N(2): 2.100(3); Ru(1)–C_{centroid}: 1.736; P(1)–Ru(1)–N(1): 83.70(9); P(1)–Ru(1)–N(2): 90.30(8); N(1)–Ru(1)–N(2): 77.2(1).

One BF_4^- ion per ruthenium centre is observed indicating that the ligand has a uninegative charge unlike compound **6**. This is due to the inability to stabilize the alternative valence bond structure as per the previous case by the pyridyl N-atom at 3-position. Each BF_4^- ion is connected to six complex units *via* hydrogen bonds, *viz.* C18–H18 \cdots F3, C24–H24B \cdots F3, C26–H26B \cdots F2, C27–H27B \cdots F3, C25–H25B \cdots F1, C19–H19 \cdots F1, C1–H1 \cdots F1 and C3–H3 \cdots F1. Furthermore each molecule is connected to two different molecules through amide O atoms *via* hydrogen bonding [C9–H9 \cdots O1, C8–H8 \cdots O1, C23–H23B \cdots O1] and PTA N-atoms [C24–H24A \cdots N6]. Altogether it forms a hydrogen bonded 3D network stabilized by counter anions.

2.3.2 Conductivity measurements

In order to investigate the probable structures of compounds **6** and **8** in solution, the conductivity of their solution was measured. The conductivity values for compound **6** in acetonitrile and water were found to be $270 \text{ } \Omega^{-1} \text{ cm}^2 \text{ mol}^{-1}$ and $280 \text{ } \Omega^{-1} \text{ cm}^2 \text{ mol}^{-1}$ attesting the 1:2 composition of the complex with the retention of the dicationic nature of the ruthenium complex moiety. On the other hand, compound **8** shows a molar conductance around $106 \text{ } \Omega^{-1} \text{ cm}^2 \text{ mol}^{-1}$ indicative of the 1:1 composition as per the solid state crystal structure.^[36] The conductance measurement of compounds **5** and **7** provides the value corresponding to a non-electrolyte, which is in agreement with the solid state structure.

2.3.3 Protein binding studies

As a potential candidate for a tumour growth inhibition agent, we were interested to study the interaction of the synthesized complexes with different biomolecules. All the complexes have shown interesting interactions with serum albumin which is important because of its ability to carry active molecules in the blood through their non-covalent conjugation. These active molecules are a group of proteins which can bind metal ions and complexes and transport through blood streams. A fluorescence quenching experiment was carried out to understand the mechanism of

action between the synthesized complexes and HSA (Human Serum Albumin). The high sensitivity of the tryptophan moiety and its surrounding local environment present in the albumin towards the intrinsic fluorescence spectra of proteins can provide certain useful information on the structure and dynamics, which is often utilized in the study of protein folding and association reactions. Separate solutions of HSA were titrated against the addition of different compounds. In the case of HSA binding, addition of the reported compounds to the respective protein solution causes a significant decrease in the initial fluorescence intensity for compounds **2**, **4**, **6** and **8** (Fig.2.25). In the case of compounds **2** and **4**, plots $[F_0/F$ vs. $[Q]]$ with an upward curvature towards the y-axis were obtained, signifying concurrent quenching by collision as well as by complex formation with the same quencher.^[37] To gain further insight into the quenching process, the fluorescence quenching data were analysed with the Stern–Volmer equation as described in the Experimental section.

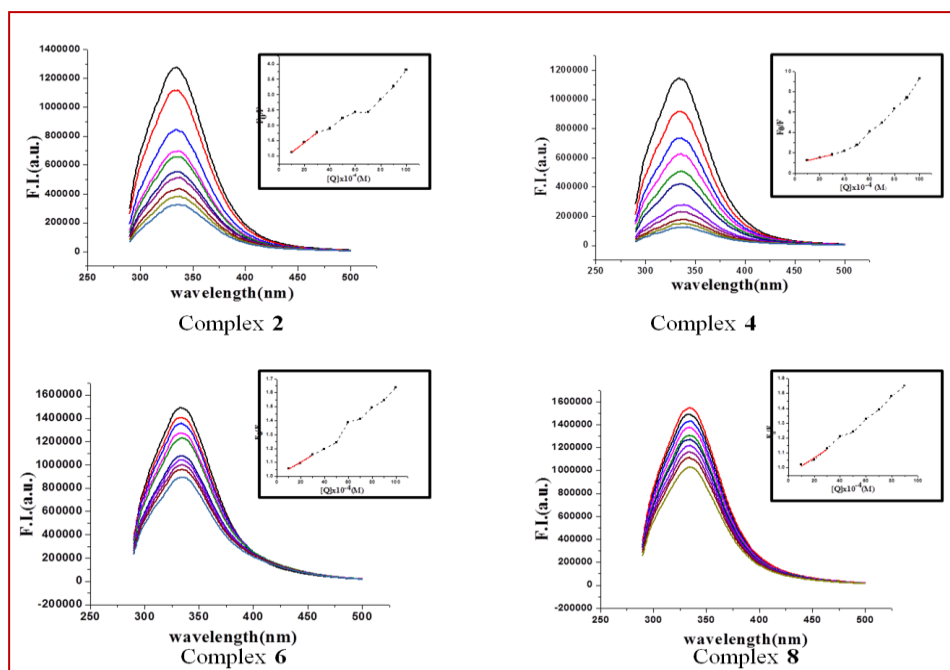


Fig 2.25: Fluorescence quenching of HSA by Complex **2**, **4**, **6** and **8**.

The value of K_{SV} obtained from the linear plot of F_0/F vs. $[Q]$ follows the order $2 > 4 > 8 > 6$. The nitro-substituted ligand based complexes (**2** and **4**) are capable of quenching tryptophan fluorescence more strongly with respect to the pyridyl ligand based complexes (**6** and **8**). This may be due to

the presence of a substituted phenyl ring instead of a pyridyl group, which may lead to stronger hydrophobic interactions with the protein. Similarly *p*-cymene complex **2** has been found to be more interactive with the protein due to the enhanced hydrophobic interaction of the methyl and isopropyl groups of *p*-cymene with the tryptophan site.^[38] The K_q values obtained for all the complexes are found to be in the range of 8.04×10^{11} – 6.41×10^{13} L mol⁻¹ S⁻¹, indicating the involvement of a static quenching mechanism.^[39] To determine the binding constant and the number of binding sites, the Scatchard equation was employed, which is given by

$$\log \frac{[F_0 - F]}{F} = \log K_a + n \log [Q]$$

where K_a and n are the binding constant and the number of binding sites, respectively, and F_0 and F are the fluorescence intensities in the absence and presence of the quencher respectively. Thus, a plot of $\log[(F_0 - F)/F]$ versus $\log[Q]$ can be used to determine the value of the binding constant (from the intercept) and the number of binding sites (from the slope). Using the Scatchard plot, binding constants and n values were also calculated for all the compounds which are presented in Table 2.1. The values of n for all the complexes are in the range ~ 1 , indicating comparable binding properties of the complexes with HSA.

Table 2.1: Various parameters obtained from HSA interaction with the prepared complexes.

Complex	$K_{sv}(M^{-1})$	$K_q(M^{-1}S^{-1})$	$K_a(M^{-1})$	n
Compound 2	3.21×10^4	5.19×10^{12}	2.24×10^5	1.23
Compound 4	2.87×10^4	4.64×10^{12}	1.14×10^7	1.55
Compound 6	4.97×10^3	8.04×10^{11}	1.41×10^4	1.09
Compound 8	5.60×10^3	8.28×10^{11}	4.87×10^4	1.24

2.3.4 Growth inhibition of ruthenium–arene complexes

The antiproliferative activities of compounds **2**, **4**, **6**, and **8** were studied against three cell lines *viz.* breast cancer cell line MCF 7, ovarian carcinoma cell line A2780 and lung cancer cell line A549. SRB assay had been utilized to obtain the results in terms of GI₅₀ (concentration of drug that produces 50% inhibition of the cells), TGI (concentration of the drug that produces total inhibition of the cells) and LC₅₀ (concentration of the

drug that kills 50% of the cells). All cancer cells were exposed for 24 h to increasing concentrations of the complexes, and their proliferation was determined. Adriamycin, a chemotherapeutic drug was used as a positive control. Though compounds **2**, **4** and **8** do not show much cell growth inhibition, however, quite interestingly compound **6** has shown remarkable cell growth inhibition properties against all cell lines almost to the tune of Adriamycin in terms of molar concentration. All the data are summarized in Fig 2.26 and Table 2.2.

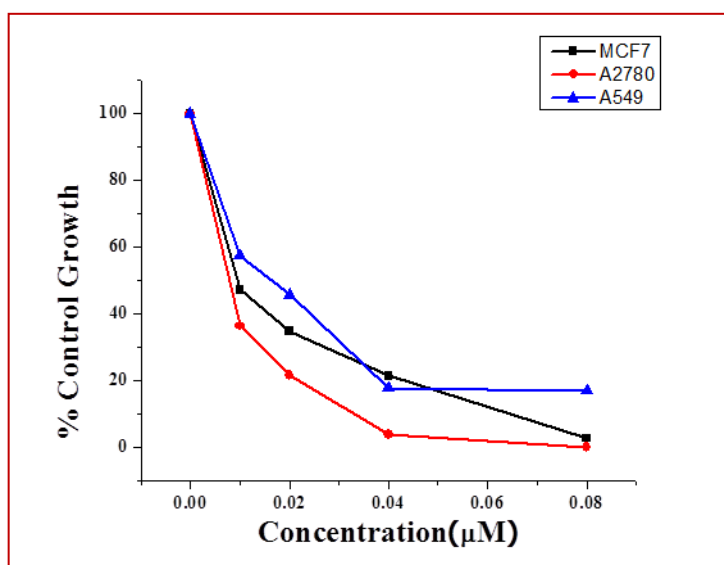


Fig.2.26: Analysis of GI_{50} value of compound **6** against different cell lines using adriamycin as positive control.

Table 2.2: GI_{50} value (nM) of the prepared complexes in human cancer cells

Complex	MCF7	A2780	A549
Complex 2	>80	>80	>80
Complex 4	>80	>80	>80
Complex 6	<0.1	<0.1	<0.1
Complex 8	>80	>80	>80
Adriamycin	<0.1	<0.1	<0.1

2.3.5 Stability study of compounds **6** and **8**

To understand what might be leading compound **6** to be so active against cancer cell lines whereas a similar compound **8** is non-active, solution stability study of complexes **6** and **8** was carried out. Many a times, cleavage of the M–L bond is found to be the first step for the activation of Ru-complexes in solution.^[40] Thus it is of considerable interest to know the nature of the species generated in solution which is responsible for its cytotoxic behaviour. Thus, the hydrolytic behaviour of compound **6** was studied to check its stability under pseudopharmacological conditions. The decomposition nature of the compound was studied in 5 mM NaCl solution (corresponding to the low intracellular NaCl concentration in cells) and in 100 mM NaCl solution (corresponding to the higher NaCl levels in blood plasma). Compound **6** was dissolved in aqueous NaCl ($c = 5$ or 100 mM in D_2O containing 10% $DMSO-d_6$) and maintained at 37°C for 7 days. Decomposition of the compound was monitored using ^{31}P NMR spectroscopy. Compound **6** underwent immediate transformation in both the solutions (5 mM and 100 mM NaCl) with the substitution of the picolinamide ligand with two chloride ions to form $[Ru(p\text{-cym})(PTA)Cl_2]$ which is evident from the typical ^{31}P singlet peak at -35.5 ppm (Fig. 2.27 and 2.28).^[41]

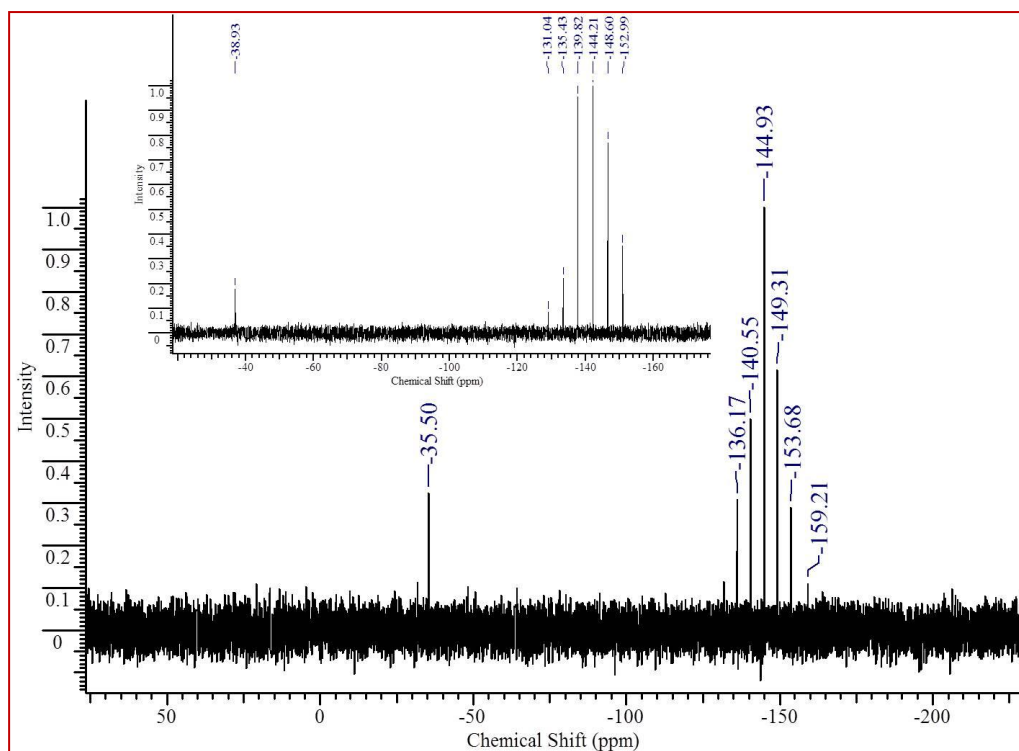


Fig.2.27: ^{31}P NMR of compound **6** in 100mM NaCl solution after 7 days. ^{31}P NMR of compound **6** in 10% DMSO- d_6 [inset].

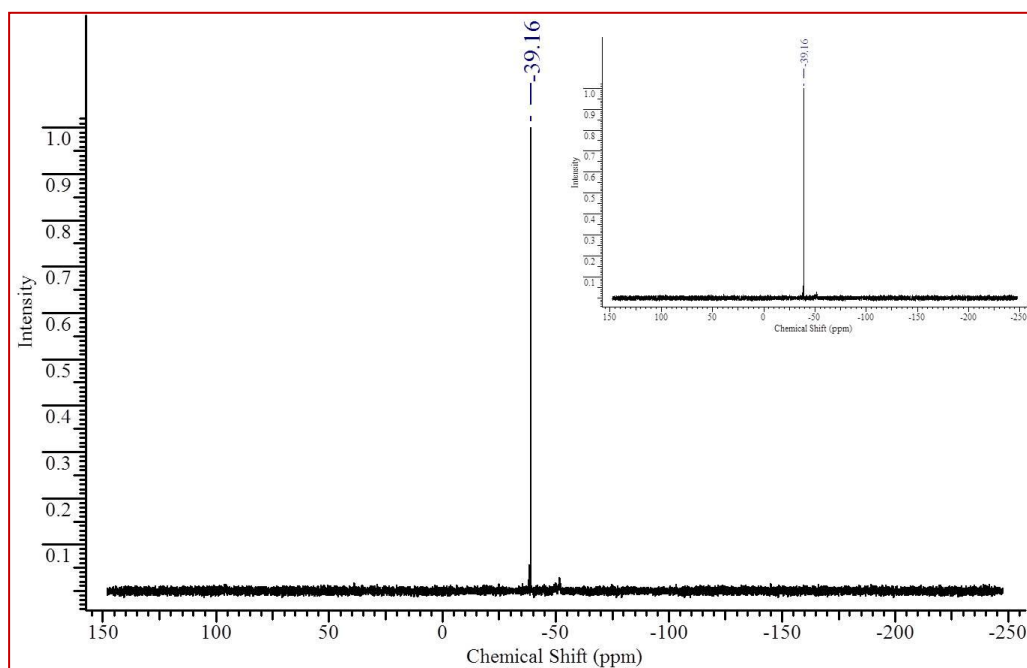


Fig.2.28: ^{31}P NMR of compound **8** in 5 mM NaCl solution after 7 days. ^{31}P NMR of compound **8** in 10% DMSO- d_6 [inset].

Whereas no peak, corresponding to the starting complex **6** at -38.9 ppm, was observed. By analysing the ^{31}P NMR data, it can be said that compound **6** is unstable in intracellular NaCl concentration in cells as well as in extracellular blood plasma. It undergoes instant transformation to

form RAPTA-C predominantly. However, a similar study with complex **8** has shown that the compound is quite stable at both 5 mM and 100 mM concentrations of NaCl without showing any other ^{31}P peak even after 7 days except the characteristic one for complex **8** itself at -37.8 ppm (Fig.2.29). These results are in agreement with the observation of solid state structure determination where a

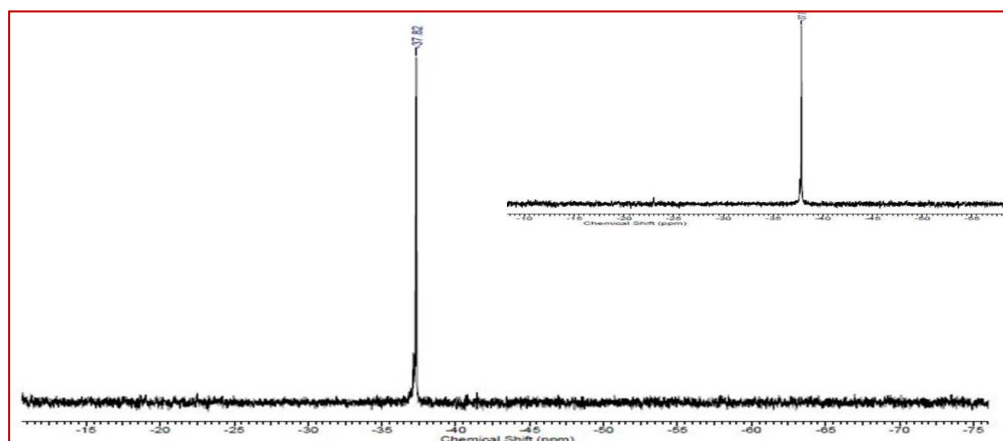


Fig.2.29: ^{31}P NMR of compound **8** in 100mM NaCl solution after 7 days. ^{31}P NMR of compound **8** in 10% DMSO- d_6 [inset].

valence bond tautomer of ligand **HL**² gets stabilized making the substituted picolinamide ligand the weaker one with respect to ligand **HL**³ in complex **8**. Perhaps this dissociation of the ligand plays some important role in the observed antiproliferative properties of complex **6**. Complex **6** has shown a tendency to form $[\text{Ru}(p\text{-cym})(\text{PTA})\text{Cl}_2]$ in NaCl solution; therefore to check the possibility that if $[\text{Ru}(p\text{-cym})(\text{PTA})\text{Cl}_2]$ is the actual active species for the antiproliferative properties of complex **6**, we have performed the cytotoxicity study of $[\text{Ru}(p\text{-cym})(\text{PTA})\text{Cl}_2]$ against all three cancer cell lines. It has been observed that the GI_{50} values for $[\text{Ru}(p\text{-cym})(\text{PTA})\text{Cl}_2]$ are quite high against all the three cell lines. Thus, it can be concluded that $[\text{Ru}(p\text{-cym})(\text{PTA})\text{Cl}_2]$ is not the entity responsible for the antiproliferative activity of compound **6**. In physiological medium, after the ligand gets liberated from the coordination sphere owing to its labile nature, some other biomolecules like thioredoxin reductase, which is already present in the physiological medium, might get attached to the ruthenium centre, activating the compound to act as an antiproliferative agent.

2.3.6 Mammalian Trx-R inhibition

To further investigate the possible pathway by which compound **6** shows growth inhibition properties, we have determined the mammalian thioredoxin reductase inhibition properties of the synthesized complexes. Mammalian thioredoxin reductases (TrxR) are large homodimeric proteins that play an important role in intracellular redox metabolism, along with a few other biochemical systems.^[23] Thioredoxin reductases are characterized by broad substrate specificity and by easily accessible redox centres. In mammalian TrxR, the redox centre consists of a cysteine selenocysteine redox pair that approaches the N-terminal active site of the other subunit for electron transfer.^[42] The active site selenolate group, after reduction, manifests a large propensity to react with “soft” metal ions, making TrxR a likely pharmacological target for a vast array of metallodrugs. This is probably the reason why various gold(I) and platinum(II) compounds were earlier reported to be potent inhibitors of mammalian thioredoxin reductase.^[43,44] Recent studies suggest that some ruthenium complexes also show Trx-R inhibition owing to its ‘soft’ nature.^[42,45] Complexes **2**, **4**, **6** and **8** have been tested for TrxR inhibition at various concentrations. Whereas compounds **2**, **4** and **8** have shown very little activity towards Trx-R, compound **6** was found highly active against the enzyme. The IC₅₀ value was found to be 11.07 μM which might be due to the weakly bound substituted picolinamide ligand which dissociates easily in the presence of thioredoxin reductase with a selenocysteine redox centre. The selenocysteine group might get coordinated to the ruthenium centre inducing the inhibition of the enzyme which might be a plausible reason for the inherent tumor growth inhibition properties of compound **6**.

2.4 Conclusion

Four new ruthenium(II) complexes containing an N-substituted picolinamide ligand with amphiphilic PTA ligands have been synthesized and characterised. All the complexes are water soluble and their interactions with HSA protein molecules have been explored. Cytotoxicity values for the prepared compounds have been evaluated for different cell

lines. Compounds **2**, **4** and **8** have the general molecular formula $[\text{Ru}(\eta^6\text{-arene})(\text{L})(\text{PTA})]\text{X}$ where the ligands (L) behave as monoanionic ligands, whereas in compound **6** the ligand takes a valence bond tautomerized protonated form which behaves as a neutral polar ligand making the complex dicationic in nature. Interestingly among the four compounds, compound **6** shows very promising antiproliferative activity against all the three cell lines with the GI_{50} value comparative to Adriamycin, a cytotoxic drug in the nM scale. To understand the mechanistic pathway, protein binding studies, hydrolysis and ligand substitution and mammalian Trx-R inhibition studies were carried out for all the complexes. Although all the compounds show significant binding with the HSA protein, only compound **6** strongly inhibits Trx-R activity which probably has some correlation with its strong antiproliferative properties.

2.5 References

- [1] Singh, A. K., Pandey, D. S., Xu, Q., Braunstein, P. (2014), Recent advances in supramolecular and biological aspects of arene ruthenium(II) complexes, *Coord. Chem. Rev.*, 270-271, 31-56. (DOI: 10.1016/j.ccr.2013.09.009)
- [2] Hartinger, C. G., Dyson, P. J. (2009), Bioorganometallic chemistry- from teaching paradigms to medicinal applications, *Chem. Soc. Rev.*, 38, 391-401. (DOI: 10.1039/b707077m)
- [3] Furrer, J., Fink, S. G. (2016), Thiolato-bridged dinuclear arene Ruthenium complexes and their potential as anticancer drugs, *Coord. Chem. Rev.*, 309, 36-50. (DOI: 10.1016/j.ccr.2015.10.007)
- [4] Therrin, B. (2015), Biologically relevant arene ruthenium metallal assemblies, *Cryst. Eng. Comm.*, 17, 484-491. (DOI: 10.1039/c4ce02146k)
- [5] Liu, H. K., Sadler, P. J. (2011), Metal complexes as DNA intercalators, *Acc. Chem. Res.*, 44, 349-359. (DOI: 10.1021/ar100140e)
- [6] Yan, Y. K., Melchart, M., Habtemariam, A., Sadler, P. J. (2005), Organometallic chemistry, biology and medicine: ruthenium arene

- anticancer complexes, *Chem. Commun.*, 4764-4776. (DOI: 10.1039/b508531b)
- [7] (a) Habtemariam, A., Melchart, M., Fernández, R., Parsons, S., Oswald, D. H. I., Parkin, A., Fabbiani, P. A. F., Davidson, E. J., Dawson, A., Aird, E. H., Jodrell, I. D., Sadler, P. J. (2007), Structure-activity relationships for cytotoxic ruthenium(II) arene complexes containing N,N-, N,O-, and O,O-chelating ligands, *J. Med. Chem.*, 49, 6858-6868. (DOI: 10.1021/jm060596m), (b) Uršič, M., Lipeč, T., Meden, A., Turel, I. (2017), Synthesis and structural evaluation of organo-ruthenium complexes with β -Diketonates, *Molecules*, 22, 326-337. (DOI: 10.3390/molecules22020326)
- [8] Kurzwernhart, A., Kandioller, W., Bartel, C., Bächler, S., Trondl, R., Mühlgassner, G., Jakupec, M. A., Arion, V. B., Marko, D., Keppler, B. K., Hartinger, C. G. (2012), Targeting the DNA-topoisomerase complex in a double-strike approach with a topoisomerase inhibiting moiety and covalent DNA binder, *Chem. Commun.*, 4839-4841. (DOI: 10.1039/c2cc31040f)
- [9] Guo, W., Zheng, W., Luo, Q., Li, X., Zhao, Y., Xiong, S., Wang, F. (2013), Transferrin serves as a mediator to deliver organometallic ruthenium(II) anticancer complexes into cells, *Inorg. Chem.*, 52, 5328-5338. (DOI: 10.1021/ic4002626)
- [10] Pettinari, R., Marchetti, F., Condello, F., Pettinari, C., Lupidi, G., Scopelliti, R., Mukhopadhyay, S., Riedel, T., Dyson, P. J. (2014), Ruthenium(II)-arene RAPTA type complexes containing curcumin and bisdemethoxycurcumin display potent and selective anticancer activity, *Organometallics*, 33, 3709-3715. (DOI: 10.1021/om500317b)
- [11] Pettinari, R., Pettinari, C., Marchetti, F., Skelton, B. W., White, A. H., Bonfili, L., Cuccioloni, M., Mozzicafreddo, M., Cecarini, V., Angeletti, M., Nabissi, M., Eleuteri, A. M. (2014), Arene-ruthenium(II) acylpyrazolonato complexes: apoptosis-promoting

- effects on human cancer cells, *J. Med. Chem.*, *57*, 4532-4542. (DOI: 10.1021/jm500458c)
- [12] Kilpin, K. J., Cammack, S. M., Clavel, C. M., Dyson, P. J. (2012), Ruthenium(II) arene PTA (RAPTA) complexes: impact of enantiomerically pure chiral ligands, *Dalton Trans.*, *42*, 2008-2014. (DOI: 10.1039/c2dt32333h)
- [13] Kilpin, K. J., Clavel, C. M., Edafe, F., Dyson, P. J. (2012), Naphthalimide-tagged ruthenium-arene anticancer complexes: combining coordination with intercalation, *Organometallics*, *31*, 7031-7039. (DOI: 10.1021/om3007079)
- [14] Vock, C. A., Renfrew, A. K., Scopelliti, R., Juillerat- Jeanneret, L., Dyson, P. J. (2008), Influence of the diketonato ligand on the cytotoxicities of $[\text{Ru}(\eta^6\text{-}p\text{-cymene})\text{-(R}_2\text{acac)(PTA)}]^+$ complexes (PTA = 1,3,5-triaza-7-phosphaadamantane), *Eur. J. Inorg. Chem.*, 1661-1671. (DOI: 10.1002/ejic.200701291)
- [15] Ang, W. H., Daldini, E., Scolaro, C., Scopelliti, R., Juillerat- Jeanneret, L., Dyson, P. J. (2006), Development of organometallic ruthenium-arene anticancer drugs that resist hydrolysis, *Inorg. Chem.*, *45*, 9006-9013. (DOI: 10.1021/ic061008y)
- [16] Vock, C. A., Renfrew, A. K., Scopelliti, R., Juillerat- Jeanneret, L., Dyson, P. J. (2008), Influence of the diketonato ligand on the cytotoxicities of $[\text{Ru}(\eta^6\text{-}p\text{-cymene})\text{-(R}_2\text{acac)(PTA)}]^+$ complexes (PTA = 1,3,5-triaza-7-phosphaadamantane), *Eur. J. Inorg. Chem.*, 1661-1671. (DOI: 10.1002/ejic.200701291)
- [17] Govender, P., Sudding, L. C., Clavel, M. C., Dyson, P. J., Therrien, B., Smith, G. S. (2013), The influence of RAPTA moieties on the antiproliferative activity of peripheral-functionalised poly(salicyladiminato) metallodendrimers, *Dalton Trans.*, *42*, 1267-1277. (DOI: 10.1039/c2dt31337e)
- [18] Almodares, Z., Lucas, S. J., Crossley, B. D., Basri, A. D., Pask, C. M., Hebden, A. J., Phillips, R. M., McGowan, P. C. (2014), Rhodium, iridium, and ruthenium half-sandwich picolinamide complexes as anticancer agents, *Inorg. Chem.*, *53*, 727-736. (DOI: 10.1021/ic401529u)

- [19] Lucas, S. J., Lord, R. M., Wilson, R. L., Phillips, R. M., Sridharan, V., McGowan, P. C. (2012), Synthesis of iridium and ruthenium complexes with (N,N), (N,O) and (O,O), coordinating bidentate ligands as potential anti-cancer agents, *Dalton Trans.*, 41, 13800-13802. (DOI: 10.1039/c2dt32104a)
- [20] van Rijt, S. H., Hebden, A. J., Amaresekera, T. Deeth, R. J., Clarkson, G. J., Parsons, S., McGowan, P. C., Sadler, P. J. (2009), Amide linkage isomerism as an activity switch for organometallic osmium and ruthenium anticancer complexes, *J. Med. Chem.*, 52, 7753-7764. (DOI: 10.1021/jm900731j)
- [21] Mokesch, S., Novak, M. S., Roller, A., Jakupec, M. A., Kandioller, W., Keppler, B. K. (2015), 1,3-dioxindan-2-carboxamides as bioactive ligand scaffolds for the development of novel organometallic anticancer drugs, *Organometallics*, 34, 848-857. (DOI: 10.1021/om501032s)
- [22] Dyson, P. J., Sava, G. (2006), Metal-based antitumour drugs in the post genomic era, *Dalton Trans.*, 1929-1933. (DOI: 10.1039/b601840h)
- [23] Casini, A., Gabbiani, C., Sorrentino, F., Rigobello, M. P., Bindoli, A., Geldbach, T. J., Marrone, A., Re, N., Hartinger, C. G., Dyson, P. J., Messori, L. (2008), Emerging protein targets for anticancer metallodrugs: inhibition of thioredoxin reductase and cathepsin B by antitumor Ruthenium(II)-arene compounds, *J. Med. Chem.*, 51, 6773-6781. (DOI: 10.1021/jm8006678)
- [24] Camm, K. D., El-Sokkary, A., Gott, A. L., Stockley, P. G., Belyaeva, T., McGowan, P. C. (2009), Synthesis, molecular structure and evaluation of new organometallic ruthenium anticancer agents, *Dalton Trans.*, 10914-10925. (DOI: 10.1039/b918902e)
- [25] Li, R., Martin, M. P., Liu, Y., Wang, B., Patel, A. R., Zhu, J., Sun, N., Pireddu, R., Lawrence, N. J., Li, J., Haura, E. B., Sung, S., Guida, W. C., Schonbrunn, E., Sebt, M. S. (2012), Fragment-based and structure-guided discovery and optimization of Rho kinase

- inhibitors, *J. Med. Chem.*, **55**, 2474-2478. (DOI: 10.1021/jm201289r)
- [26] Sanghamitra, N. J. M, Adwankar, M. K., Juvekar, A. S., Khurajjam, V., Wycliff, C., Samuelson, A. G. (2011), Copper(I) complexes of modified nucleobases and vitamin B3 as potential chemotherapeutic agents: *In vitro* and *in vivo* studies, *Indian J. Chem., Sect. A: Inorg., Bio-inorg., Phys., Theor. Anal. Chem.*, **50**, 465-473. (DOI: <http://hdl.handle.net/123456789/11243>)
- [27] SMART & SAINT Software Reference manuals, version 5.0, Bruker AXS Inc., Madison, WI, 1998.
- [28] SAINT, Area Detector Integration Software, Siemens Analytical Instruments Inc., Madison, WI, USA, 1995.
- [29] G. M. Sheldrick, SADABS, Program for semi-empirical absorption correction, University of Göttingen, Göttingen, Germany, 1997.
- [30] Sheldrick, G. M., Schneider, T. R. (1997), [16] SHELXL: Highresolution refinement, *Methods in Enzymology*, **277**, 319–343. (DOI: 10.1016/S0076-6879(97)77018-6)
- [31] Sheldrick, G. M. (2008), A short history of SHELX, *Acta Crystallogr. Sect. A: Fundam. Crystallogr.*, **64**, 112-122. (DOI: 10.1107/S0108767307043930)
- [32] Farrugia, L. J. (1999), WinGX suite for small-molecule single-crystal crystallography, *J. Appl. Crystallogr.*, **32**, 837-838. (DOI: 10.1107/S0021889899006020)
- [33] Spek, A. L. (2003), Single-crystal structure validation with the program PLATON, *Appl. Crystallogr.*, **36**, 7-13. (DOI: 10.1107/S0021889802022112)
- [34] Seršen, S., Kljun, J., Kryeziu, K., Panchuk, R., Alte, B., Körner, W., Heffeter, P., Berger, W., Turel, I. (2015), Structure-related mode-of-action differences of anticancer organoruthenium complexes with β -Diketonates, *J. Med. Chem.*, **58**, 3984-3996. (DOI: 10.1021/acs.jmedchem.5b00288)
- [35] Boyd, P. D. W., Wright, L. J., Zafar, M. N. (2011), Extending the range of neutral N-Donor ligands available for metal catalysts: N-[1-alkylpyridin-4(1H)-ylidene]amides in palladium-catalyzed cross-

- coupling reactions, *Inorg. Chem.*, 250, 10522-10524. (DOI: 10.1021/ic201527s)
- [36] Ali, I., Wani, A. W., Saleem, K. (2013), Empirical formulae to molecular structures of metal complexes by molar conductance, *Synth. React. Inorg. Met.-Org. Chem.*, 43(9), 1162-1170. (DOI: 10.1080/15533174.2012.756898)
- [37] Alagesan, M., Nattamai, S. P., Bhuvanesh, S. P., Dharmaraj, N. (2014), An investigation on new ruthenium(II) hydrazone complexes as anticancer agents and their interaction with biomolecules, *Dalton Trans.*, 43, 6087-6099. (DOI: 10.1039/c3dt51949j)
- [38] Ganeshpandian, M., Loganathan, R., Suresh, E., Riyasdeen, A., Akbarshad, M. A., Palaniandavar, M. (2014), New ruthenium(II) arene complexes of anthracenylappended diazacycloalkanes: effect of ligand intercalation and hydrophobicity on DNA and protein binding and cleavage and cytotoxicity, *Dalton Transactions*, 43, 1203-1219. (DOI: 10.1039/c3dt51641e)
- [39] Das, M., Nasani, R., Saha, M., Mobin, S. M., Mukhopadhyay, S. (2015), Nickel(II) complexes with a flexible piperazinyl moiety: studies on DNA and protein binding and catecholase like properties, *Dalton Trans.*, 44, 2299-2310. (DOI: 10.1039/c4dt02675f)
- [40] Mitra, R., Samuelson, A. G. (2015), Substitution-modulated anticancer activity of half- sandwich ruthenium(II) complexes with heterocyclic ancillary ligands, *Eur. J. Inorg. Chem.*, 3536-3546. (DOI: 10.1002/ejic.201402205)
- [41] Scolaro, C., Hartinger, C. G., Allardyce, C. S., Keppler, B. K., Dyson, P. J. (2008), Hydrolysis study of the bifunctional antitumour compound RAPTA-C, $[\text{Ru}(\eta^6\text{-}p\text{-cymene})\text{Cl}_2(\text{pta})]$, *J. Inorg. Biochem.*, 102, 1743-1748. (DOI: 10.1016/j.jinorgbio.2008.05.004)
- [42] Mura, P., Camalli, M., Bindoli, A., Sorrentino, F., Casini, A., Gabbiani, C., Corsini, M., Zanello, P., Rigobello, M. P., Messori, L. (2007), Activity of rat cytosolic thioredoxin reductase is strongly decreased by *trans*-[Bis(2-amino-5-methylthiazole)tetrachlororuthenate(III)]: first report of relevant

- thioredoxin reductase inhibition for a ruthenium compound, *J. Med. Chem.*, 50, 5871-5874. (DOI: 10.1021/jm0708578)
- [43] Coronello, M., Mini, E., Caciagli, B., Cinellu, M. A., Bindoli, A., Gabbiani, C., Messori, L. (2005), Mechanisms of cytotoxicity of selected organogold(III) compounds, *J. Med. Chem.*, 48, 6761-6765. (DOI: 10.1021/jm050493o)
- [44] C. Marzano, V. Gandin, A. Folda, G. Scutari, A. Bindoli and M. P. Rigobello, Inhibition of thioredoxin reductase by auranofin induces apoptosis in cisplatin-resistant human ovarian cancer cells, *Free Radical Biol. Med.*, 2007, 872-881. (DOI: 10.1016/j.freeradbiomed.2006.12.021)
- [45] Casini, A., Gabbiani, C., Sorrentino, F., Rigobello, M. P., Bindoli, A., Geldbach, T. J., Marrone, A., Re, N., Hartinger, C. G., Dyson, P. J., Messori, L. (2008), Emerging protein targets for anticancer metallodrugs: inhibition of thioredoxin reductase and cathepsin B by antitumor ruthenium(II)-arene compounds, *J. Med. Chem.*, 51, 6773-6781. (DOI: 10.1021/jm8006678)

Chapter 3
Ruthenium(II) Arene NSAID Complexes:
Inhibition of Cyclooxygenase and
Antiproliferative Activity Against Cancer
Cell Lines

3.1 Introduction

Research on the development of metal based therapeutics has been increased many folds which is recognized in the astronomical jump in number of related publications in the last twenty years.^[1] The advancement of platinum based anticancer drugs has attracted much attention in the development of more cytotoxic platinum complexes which can be examined as possibly the next generation of metallodrugs for cancer therapy.^[2] However, the cytotoxicity of platinum complexes brings on several severe side effects which need to be treated simultaneously. As an alternative a new class of ruthenium complexes was introduced in the late eighties and nineties which have been found to be quite active against cancerous growth.^[3] Among them, imidazolium *trans*-[tetrachlorido(dimethylsulfoxide)-(1*H*-imidazole) ruthenate(III)] (NAMI-A) has shown prominent cytotoxicity selectively against metastatic tumors and completed clinical trials very recently.^[4] Two other complexes *viz.* indazolium *trans*-[tetrachloridobis(1*H*-indazole) ruthenate(III)] (KP1019) and its sodium salt KP1339 have also shown considerable activity against various primary tumors.^[5] Apart from these, ruthenium(II)–arene complexes have shown remarkable activity against primary and metastatic tumors with various ligands.^[6] The advantage of ruthenium–arene complexes over platinum complexes could be in its lower cytotoxicity (at least in some cases) which may lead to a situation where it can be well tolerated by the patient. The emergence of these new ruthenium complexes with anticancer properties opens up the possibility of tagging various biologically active molecules or their derivatives as ligands or as part of ligands to improve the efficacy of the molecule.^[7] Non-steroidal anti-inflammatory drugs (NSAIDs) are a group of molecules which have been reported to be active against cancer cells with chemopreventive properties.^[8] NSAIDs mostly target cyclooxygenase (COX-1 and COX-2)^[9] and lipoxygenase (LOX)^[10] which are commonly upregulated (particularly COX-2) in malignant tumors.^[11] COX-1 and COX-2 are mainly involved in the formation of prostaglandin H₂, which afterward forms prostaglandin,^[12,13] whereas LOX is involved in the formation of

cis/trans conjugated hydroxyeicosatetraenoic acids (HETEs).^[14] The role of COX-1 has been found in renal blood flow, microcirculation of gastric mucosa and normal platelet function;^[15] whereas, the role of COX-2 has been earmarked for mitogenesis.^[16,17] On the other hand, the role of LOX in the formation of 12(S)-HETE, which plays a significant role in angiogenic activity through the migration of endothelial cells, is also well known.^[18] Because of all the above reasons, COX and LOX remain key anticancer targets where NSAIDs can play a vital role. The chemopreventive properties of NSAIDs have been also observed because of their role in glucose metabolism, up-regulation of PUMA (p53 up-regulated modulator of apoptosis), decrease of epidermal growth factor (EGF) and up-regulation of the expression of the tumor suppressor gene.^[19,20] Though there are several reports where ruthenium–arene complexes have been tested for the inhibition of key enzymes and proteins along with their anticancer potential, similar studies with NSAIDs are limited.^[21] However, it is worth mentioning that there are other reports where transition metal–NSAID non-organometallic complexes have been synthesized and tested for cytotoxic and antiproliferative properties.^[22] Interestingly, to the best of literature review, there is no report available where the anticancer properties of the synthesized ruthenium arene NSAID complexes have been ever correlated with the efficacy of COX and/or LOX inhibition. In this particular chapter, the synthesis of four new ruthenium–arene NSAID complexes and their inhibition activity against COX and LOX enzymes and antiproliferative activity against different cancer cell lines have been represented. Additionally, docking studies have been performed to understand the relative molecular level interactions of Ru(II) complexes with the COX-2 enzyme as compared to free NSAIDs.

3.2 Experimental section

3.2.1 Materials and methods

All the required chemicals were purchased from Sigma and used without further purification. The specifications of all the instruments used for analysis purpose were same as described in the section 2.2.1 of the chapter

2. COX and LOX inhibition study has been carried out according to the given protocol.^[23,24]

3.2.1.1 Synthesis of [Ru(η^6 -*p*-cymene)(nap)Cl] [9]

To a solution of [Ru(η^6 -*p*-cymene)Cl₂]₂ (0.1 g, 0.16 mmol) in CH₂Cl₂ (50 mL), a methanolic solution (10 mL) of the potassium salt of naproxen (0.08 g, 0.33 mmol) was added dropwise and stirred overnight at room temperature. The resulting orange coloured solution was evaporated to dryness and extracted with CH₂Cl₂ (3×10 mL) to remove KCl. The CH₂Cl₂ extract was evaporated *in vacuo* to obtain a yellow solid as the product. Crystals of the product suitable for X-ray crystallographic analysis were obtained *via* vapour diffusion of diethyl ether in dichloromethane solution. ¹H NMR (400.13 MHz, 298 K, CDCl₃) δ : 7.58 [d, 3H, CH of C₁₀H₆], 7.32 [d, 1H, CH of C₁₀H₆], 7.04 [d, 2H, CH of C₁₀H₆], 5.45 [d, 2H, CH of C₆H₄], 5.23 [d, 2H, CH of C₆H₄], 3.82 [s, 4H, OCH₃ and CH of CH₃(CH)COOH], 2.76 [m, 1H, CH(CH₃)₂], 2.18 [s, 3H, C₆H₄CH₃], 1.37 [br.s, 3H, CH₃(CH)COOH], 1.18 [d, 6H, CH(CH₃)₂]. ¹³C NMR (100.61 MHz, CDCl₃) δ : 193.4 [C of COOH], 157.4 [C of C₁₀H₆], 135.3 [C of C₁₀H₆], 133.6 [C of C₁₀H₆], 129.2 [CH of C₁₀H₆], 128.9 [C of C₁₀H₆], 126.9 [CH of C₁₀H₆], 126.7 [CH of C₁₀H₆], 126.2 [CH of C₁₀H₆], 118.7 [CH of C₁₀H₆], 105.5 [CH of C₁₀H₆], 100.6 [C of C₆H₄], 94.3 [C of C₆H₄], 81.3 [2×CH of C₆H₄], 80.5 [2×CH of C₆H₄], 55.3 [OCH₃], 48.0 [CH of CH(CH₃)COOH], 31.4 [C₆H₄CH₃], 22.2 [CH(CH₃)₂], 18.8 [CH₃ of CH(CH₃)COOH], 18.1 [CH of CH(CH₃)₂]. Anal. calcd for C₂₄H₂₇ClO₃Ru: C, 57.65; H, 5.44. Found: C, 57.80; H, 5.80. ESI-MS (+ve mode): [Ru(η^6 -*p*-cymene)(nap)]⁺: 465.1 (m/z).

3.2.1.2 Synthesis of [Ru(η^6 -*p*-cymene)(diclo)Cl] [10]

A methanolic solution (10 mL) of the sodium salt of diclofenac (0.1 g, 0.33 mmol) was added to a solution of [Ru(η^6 -*p*-cymene)Cl₂]₂ (0.1 g, 0.16 mmol), dissolved in CH₂Cl₂ (50 mL) with stirring. The mixture was allowed to stir overnight to yield an orange coloured solution with a white precipitate of NaCl. The solvent was removed *in vacuo* and the product was

extracted in dichloromethane (3×10 mL). Diethyl ether was added (10 mL) to afford a yellow precipitate. The precipitate was dried *in vacuo* to afford a yellow powder. Crystals of the product suitable for X-ray crystallographic analysis were obtained *via* the vapour diffusion of diethyl ether in dichloromethane solution. ¹H NMR (400.13 MHz, 298 K, CDCl₃) δ: 7.31 [d, 2H, CH of C₆H₃], 7.15 [d, 1H, CH of C₆H₄], 7.09 [t, 1H, CH of C₆H₃], 6.96 [m, 1H, CH of C₆H₄], 6.92 [m, 1H, CH of C₆H₄], 6.51 [s, 1H, CH of C₆H₄], 5.60 [d, 2H, CH of C₆H₄], 5.39 [d, 2H, CH of C₆H₄], 3.54 [s, 2H, CH₂ of CH₂COOH], 2.90 [m, 1H, CH(CH₃)₂], 2.27 [s, 3H, C₆H₄CH₃], 1.30 [m, 6H, CH(CH₃)₂]. ¹³C NMR (100.61 MHz, CDCl₃) δ: 190.0 [C of COOH], 142.9 [C of C₆H₄], 138.1 [2×C of C₆H₄ and CH of C₆H₄], 130.9 [CH of C₆H₄], 129.2 [C of C₆H₃], 128.8 [CH of C₆H₄], 127.7 [CH of C₆H₃], 123.9 [CH of C₆H₃], 121.7 [C of C₆H₃], 118.1 [2×CH of C₆H₃], 99.7 [C of C₆H₄ (*p*-cymene)], 93.9 [C of C₆H₄ (*p*-cymene)], 81.3 [CH of C₆H₄ (*p*-cymene)], 80.5 [CH of C₆H₄ (*p*-cymene)], 77.8 [CH of C₆H₄ (*p*-cymene)], 76.8 [CH of C₆H₄ (*p*-cymene)], 31.4 [C₆H₄CH₃], 30.5 [CH₂ of CH₂COOH], 22.3 [CH(CH₃)₂], 18.7 [CH of CH(CH₃)₂]. Anal. calcd for C₂₄H₂₄Cl₃NO₂Ru: C, 50.94; H, 4.27. Found: C, 50.80; H, 4.51. ESI-MS (+ve mode): [Ru(η⁶-*p*-cymene)(diclo)]⁺: 532.0 (m/z).

3.2.1.3 Synthesis of [Ru(η⁶-*p*-cymene)(ibu)Cl] [11]

[Ru(η⁶-*p*-cymene)Cl₂]₂ (0.1 g, 0.16 mol) was dissolved in dry CH₂Cl₂ (50 mL). The sodium salt of ibuprofen (0.04 g, 0.16 mmol) was added with stirring. The mixture was allowed to stir overnight to afford a yellow coloured solution. The mixture was evaporated to dryness and extracted with CH₂Cl₂. The CH₂Cl₂ was reduced *in vacuo* to a volume of *ca.* 5 mL. An excess of diethyl ether was added to afford the title compound as an orange solid. ¹H NMR (400.13 MHz, 298 K, CDCl₃) δ: 7.26 [d, 2H, CH of C₆H₄ (ibuprofen)], 7.08 [d, 2H, CH of C₆H₄(ibuprofen)], 5.54 [d, 2H, CH of C₆H₄ (*p*-cymene)], 5.31 [d, 2H, CH of C₆H₄ (*p*-cymene)], 3.35 [q, 1H, CH of CH(CH₃)COOH], 2.84 [m, 1H, CH(CH₃)₂], 2.44 [d, 2H, CH₂CH(CH₃)₂], 2.28 [s, 3H, C₆H₄CH₃], 1.84 [m, 1H, CH(CH₃)₂], 1.34 [d, 3H, CH(CH₃)COOH], 0.98 [d, 6H, CH(CH₃)₂], 0.89 [d, 6H, CH(CH₃)₂]

(ibuprofen)]; ^{13}C NMR (100.61 MHz, CDCl_3) δ : 175.9 [C of COOH], 139.9 [C of C_6H_4 (ibuprofen)], 138.9 [C of C_6H_4 (ibuprofen)], 129.4 [$2\times\text{CH}$ of C_6H_4 (ibuprofen)], 127.5 [CH of C_6H_4 (ibuprofen)], 126.5 [CH of C_6H_4 (ibuprofen)], 106.8 [C of C_6H_4 (*p*-cymene)], 100.5 [C of C_6H_4 (*p*-cymene)], 86.8 [$2\times\text{CH}$ of C_6H_4 (*p*-cymene)], 85.9 [$2\times\text{CH}$ of C_6H_4 (*p*-cymene)], 44.7 [CH_2 of $\text{CH}_2\text{CH}(\text{CH}_3)_2$], 44.7 [CH of $\text{CH}(\text{CH}_3)\text{COOH}$], 30.0 [CH of $\text{CH}(\text{CH}_3)_2$], 24.4 [$\text{C}_6\text{H}_4\text{CH}_3$], 22.6 [$\text{CH}(\text{CH}_3)_2$ (ibuprofen)], 21.9 [$\text{CH}(\text{CH}_3)_2$ (*p*-cymene)], 19.0 [$\text{CH}_3(\text{CH})\text{COOH}$], 18.3 [CH of $\text{CH}(\text{CH}_3)_2$]. Anal. calcd for $\text{C}_{23}\text{H}_{31}\text{ClO}_2\text{Ru}$: C, 58.03; H, 6.56. Found: C, 57.37; H, 6.88. ESI-MS (+ve mode): $[\text{Ru}(\eta^6\text{-}p\text{-cymene})(\text{ibu})]^+$: 441.1 (m/z).

3.2.1.4 Synthesis of $[\text{Ru}(\eta^6\text{-}p\text{-cymene})(\text{asp})\text{Cl}]$ [12]

A methanolic solution (10 mL) of 2-acetoxy potassium benzoate (0.07 g, 0.32 mmol) was added to a solution of $[\text{Ru}(\eta^6\text{-}p\text{-cymene})\text{Cl}_2]_2$ (0.1 g, 0.16 mmol), dissolved in CH_2Cl_2 (50 mL) with stirring. The mixture was allowed to stir overnight to yield an orange solution with a white precipitate of KCl. The solvent was removed *in vacuo* and the product was extracted in dichloromethane (3×10 mL). Diethyl ether was added (10 mL) to afford a yellow precipitate which was further washed with diethyl ether (3×5 mL) and dried *in vacuo* to afford a yellow powder. ^1H NMR (400.13 MHz, 298 K, CDCl_3) δ : 7.76 [m, 1H, C_6H_4 of *p*-cymene], 7.29 [m, 1H, C_6H_4], 6.93 [d, 1H, C_6H_4], 6.78 [d, 1H, C_6H_4], 5.63 [d, 2H, C_6H_4 of *p*-cymene], 5.40 [d, 2H, C_6H_4 of *p*-cymene], 2.87 [m, 1H, $\text{CH}(\text{CH}_3)_2$], 2.27 [s, 6H, 3Hs of $\text{C}_6\text{H}_4\text{CH}_3$ and 3Hs of COOCH_3], 1.34 [d, 6H, $\text{CH}(\text{CH}_3)_2$]. ^{13}C NMR (100.61 MHz, CDCl_3) δ : 206.5 [C of COOH], 168.8 [C of COOCH_3], 149.2 [C of C_6H_4], 134.8 [CH of C_6H_4], 132.5 [CH of C_6H_4], 129.7 [CH of C_6H_4], 124.7 [CH of C_6H_4], 122.3 [C of C_6H_4], 117.5 [C of C_6H_4], 115.8 [C of C_6H_4], 98.7 [$2\times\text{CH}$ of C_6H_4], 97.3 [$2\times\text{CH}$ of C_6H_4], 29.8 [$\text{C}_6\text{H}_4\text{CH}_3$], 21.3 [COOCH_3], 20.1 [CH of $\text{CH}(\text{CH}_3)_2$], 17.6 [$\text{CH}(\text{CH}_3)_2$], 17.4 [$\text{CH}(\text{CH}_3)_2$]. Anal. calcd for $\text{C}_{19}\text{H}_{21}\text{ClO}_4\text{Ru}$: C, 50.72; H, 4.70. Found: C, 50.46; H, 4.88. ESI-MS (+ve mode): $[\text{Ru}(\eta^6\text{-}p\text{-cymene})(\text{asp})\text{Cl}]$: 414.1 (m/z).

3.2.2 X-ray crystallography

3.2.2.1 X-ray crystallography of complex 9 and 10

The description of instrumentation of X-ray crystallography for complex **9** and **10** is same as described in Section 2.2.2.2.

3.2.3 Growth inhibition study

The procedure for SRB assay is same as discussed in chapter 2.

3.2.4 Stability studies in DMSO

In order to check the stability of the prepared compounds in solution state, 1-2 mg of the sample was dissolved in DMSO-*d*₆ and its NMR was recorded after 0.5, 3, 24 and 48 h. To check the stability of the prepared compounds by ESI-MS, the compounds were dissolved in DMSO-MeOH mixture and ESI-MS was recorded after 15 mins.

3.2.5 Assay of Cyclooxygenase (COX)

The assay mixture for COX contained Tris-HCl buffer, glutathione, hemoglobin and enzyme. The reaction was started by the addition of arachidonic acid. Then the reaction was stopped after 1 min incubation at 37°C by addition of 0.2 mL of 10% TCA in 1 N HCl, mixed and 0.2 mL of TBA was added. The contents were heated in a boiling water bath for 20 min, cooled and centrifuged at 1,000 rpm for 3 min. The supernatant was measured at 532 nm for COX activity. The experiments were carried out in triplicate manner for all the samples and graph was plotted taking the average of the three observations.

3.2.6 Assay of Lipoxygenase (LOX)

The assay mixture for 15-lipoxygenase contained 2.75 mL of phosphate buffer of pH 6.5, 0.2 mL of sodium linoleate and 50 µl of enzyme. The increase in OD was measured at 280 nm. The experiments were carried out in triplicate manner for all the samples and graph was plotted taking the average of the three observations.

3.2.7 DNA binding experiments

DNA binding studies of the prepared compounds were carried out using ct-DNA by fluorescence spectroscopy. A stock solution of ct-DNA was prepared in tris-HCl buffer and ethidium bromide was added to it. First, fluorescence spectra of DNA bound EB were obtained at the excitation and emission wavelengths of 515 nm and 602 nm respectively. The titration quenching experiment was carried out by keeping the concentration of DNA in buffer constant and adding 10 μ L of the sample solution at a time. After addition of the sample solution, the solution was kept for 5 min and then fluorescence intensity was measured. The quenching efficiency was calculated from Stern-Volmer eq.

3.2.8 Protein binding experiments

The procedure for protein binding experiments is same as described in section 2.2.3 in chapter 2.

3.2.9 Interaction with Amino acids

Reactivity of the prepared compounds with amino acids was examined using ESI-MS spectroscopy. 2 mg of the compound was mixed with equimolar amount of different amino acids *viz.* His, Met, Cys. The mixture was dissolved in MeOH and ESI-MS spectra was recorded after 0.5, 24, 48 h.

3.2.10 Docking Studies

3.2.10.1 AutoDock simulation method

AutoDock 4.2 MGL tools and Lamarckian Generic algorithm (LGA) were used for proteinfixed ligand-flexible docking calculations.^[25] The conformation of complexes were taken from their X-ray crystal structures. A two-step docking protocol was employed to perform the docking experiment. In the first step, both the ligand and protein were prepared. The torsion angle and the flexibility issues of the ligand were optimized. For the protein, all the water molecules and the metal ions were removed from the extracted crystal structure. All polar and non-polar hydrogen atoms and the

Gasteiger charge were added in to the crystal structure of the protein. In the second step, all possible binding sites of the receptor were determined by the co-crystallized ligand present in the active site of the proteins (for naproxen PDB: 3q7d;^{9[26]} for diclofenac PDB: 5ikq^[27]). Auto grid version 4.2 was used to calculate the grid parameters and the grid size was set to 40×40×40 points with grid spacing of 0.375 Å. Twenty search attempts (*i.e.*, ga_run parameter) were performed for each ligand. The maximum number of energy evaluations before the termination of LGA run was 250,000 and the maximum number of generations of LGA run before termination was 27,000. Other docking parameters were set to the default values of AutoDock 4.2 program.

3.2.10.2. Gold simulation method:

The docking simulation was performed by using the Gold 5.5 (Hermes 1.8.2) simulation software. The X-Ray crystallographic structures of the both proteins (PDB id: 3q7d and 5ikq) were extracted from protein data bank. Both the proteins were prepared by Gold 5.5 software by removing the water molecules followed by structural refinement study, respectively. Additionally, hydrogen atoms were added up to the crystal structure. All possible binding sites of the receptor were determined by the co-crystallized ligand present in the active site of the proteins. The grid was selected based on the ligands co-crystallized with the protein. The grid size for PDB 3q7d and 5ikq was considered as -33.555×41.327×18.997, and 26.992×41.680×14.356, respectively. Thirty GA run was selected for all the docking experiments.^[28] The docked complexes were visualized by Pymol 1.3 software.

3.2.11 Supplementary materials

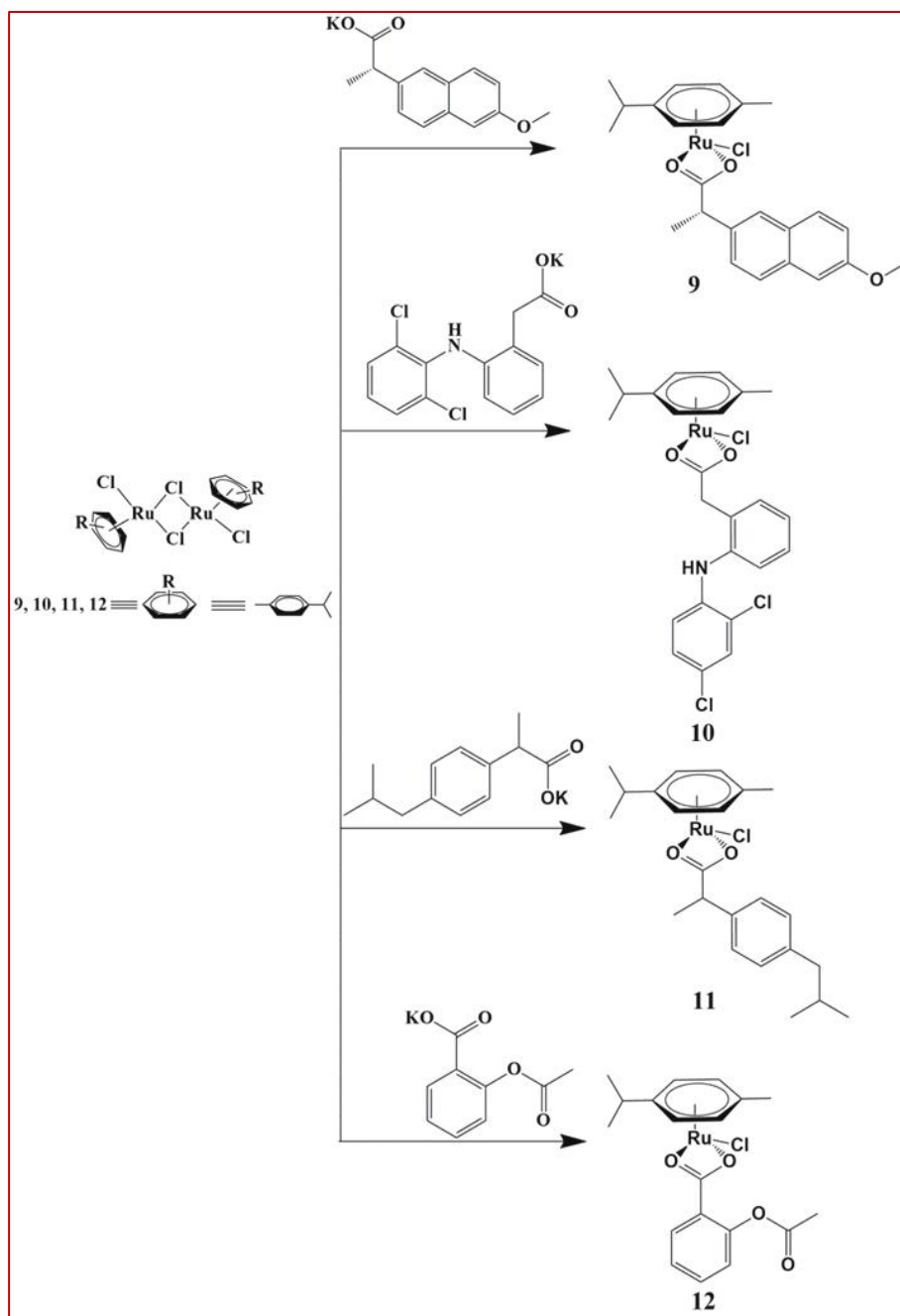
CCDC 1529590 and 1477975 contain the supplementary crystallographic data for **9** and **10** respectively. These data can be obtained free of charge *via* <http://www.ccdc.cam.ac.uk/conts/retrieving.html>, or from the Cambridge Crystallographic Data Centre, 12 Union Road, Cambridge CB2 1EZ, UK; fax: (+44) 1223-336-033; or e-mail: deposit@ccdc.cam.ac.uk.

3.3 Results and discussion

3.3.1 Synthesis of complexes

Ruthenium complexes **9**, **10**, **11** and **12** were obtained in moderate yields when the potassium salt of the respective ligands was mixed with a solution of $[(\eta^6\text{-}p\text{-cymene})\text{RuCl}_2]_2$ and stirred overnight at room temperature [for complexes **9**, **11** and **12**], whereas complex **10** was obtained after overnight stirring of the mixture of sodium salt of the ligand and $[(\eta^6\text{-}p\text{-cymene})\text{RuCl}_2]_2$ at room temperature (Scheme 3.1).

The IR spectra of the complexes have been analyzed to understand the possible mode of binding by carboxylate ions. In the IR spectra, complexes show bands in the region of 1502–1594 cm^{-1} and 1379–1385 cm^{-1} for antisymmetric and symmetric vibrations respectively, indicating the chelating nature of carboxylates.^[29–31]



Scheme 3.1: Synthesis of compounds $[Ru(\eta^6\text{-}p\text{-cymene})(\text{nap})Cl]$ **9**, $[Ru(\eta^6\text{-}p\text{-cymene})(\text{diclo})Cl]$ **10**, $[Ru(\eta^6\text{-}p\text{-cymene})(\text{ibu})Cl]$ **11**, and $[Ru(\eta^6\text{-}p\text{-cymene})(\text{asp})Cl]$ **12**.

The ^1H NMR spectra of complexes **9**, **10**, **11** and **12** show a typical band for the *p*-cymene moiety in the range of 5.47–5.63 and 5.26–5.40 ppm for ring protons and 2.80–2.87, 2.20–2.27 and 1.18–1.84 ppm for side chain protons. The aromatic protons for NSAID moieties are observed as multiplets in the range of 6.49–7.76 ppm. Signals for aliphatic protons for the NSAID moieties appear in the appropriate regions indicating the formation of Ru(II)–NSAID complexes (Fig.3.1–Fig.3.4).

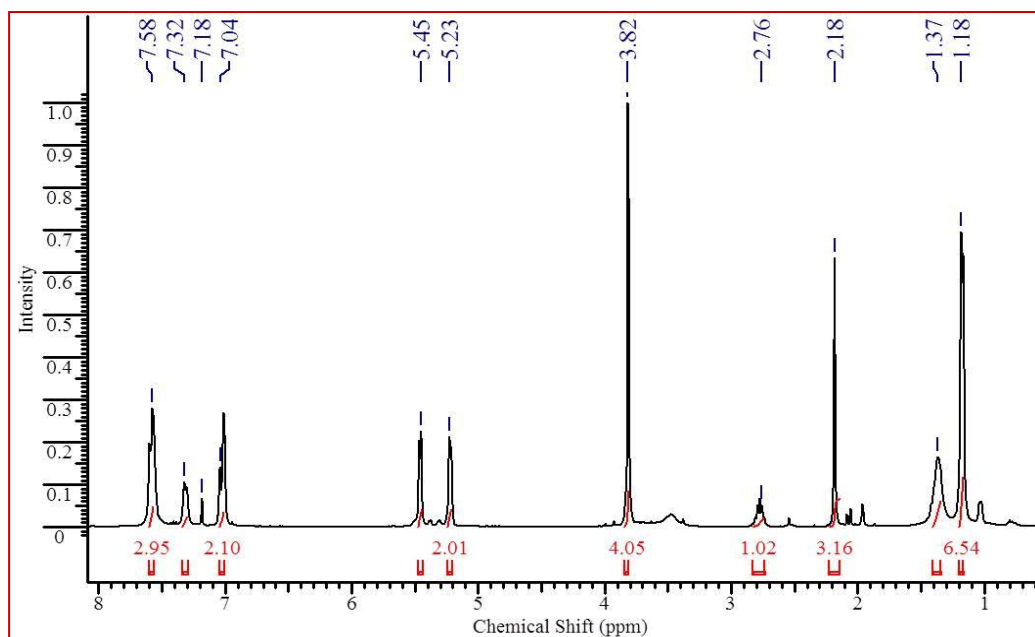


Fig.3.1: ^1H NMR spectra of complex 9.

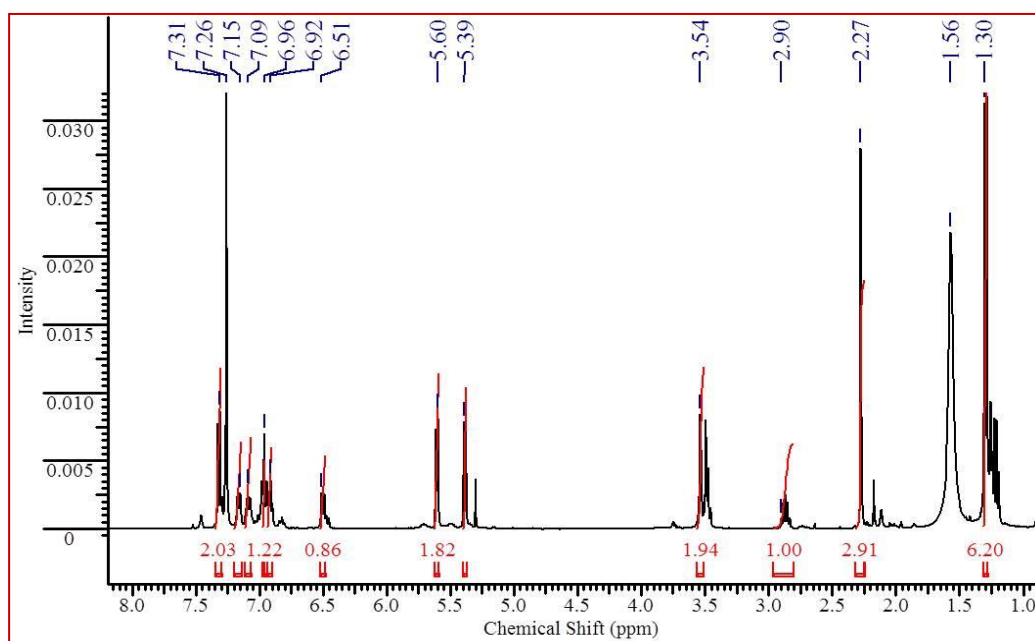


Fig.3.2: ^1H NMR spectra of complex 10.

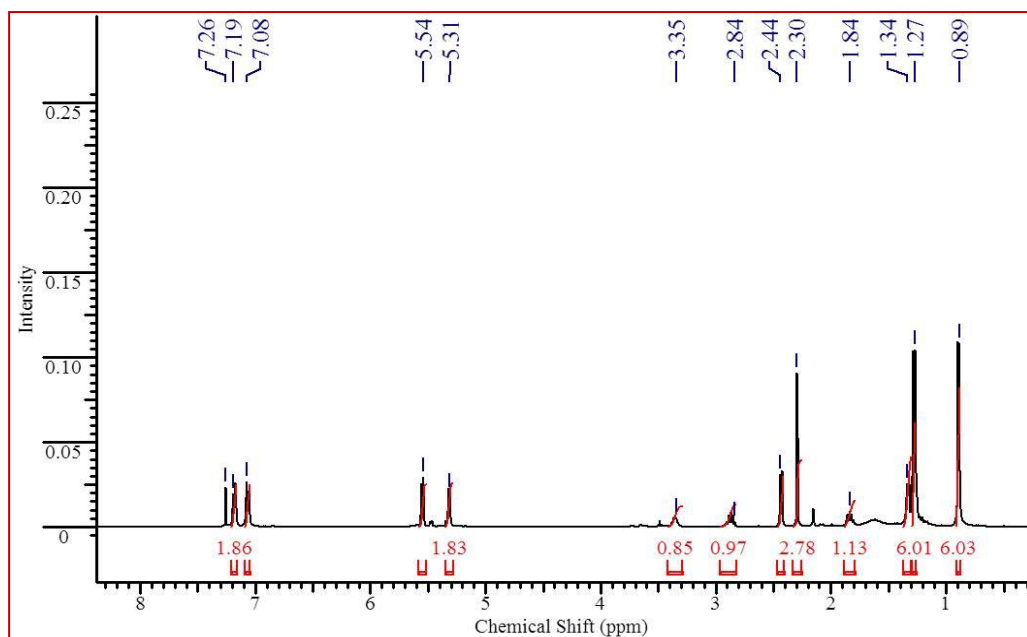


Fig.3.3: ^1H NMR spectra of complex **11**.

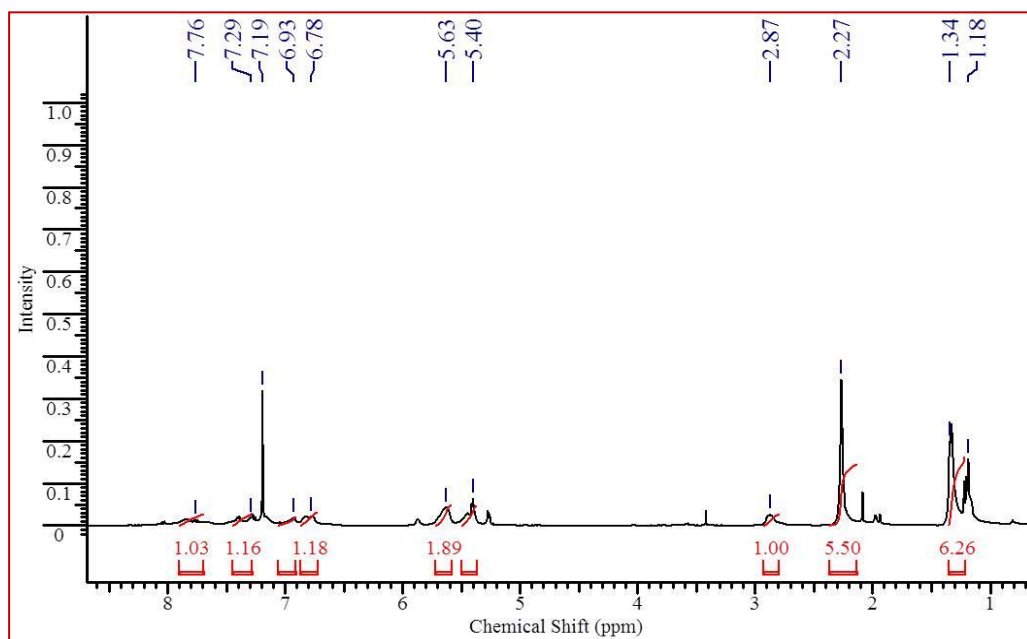


Fig.3.4: ^1H NMR spectra of complex **12**.

The ^{13}C NMR spectra of complexes **9–12** also corroborate with the proposed structure (Fig.3.5-Fig.3.8).

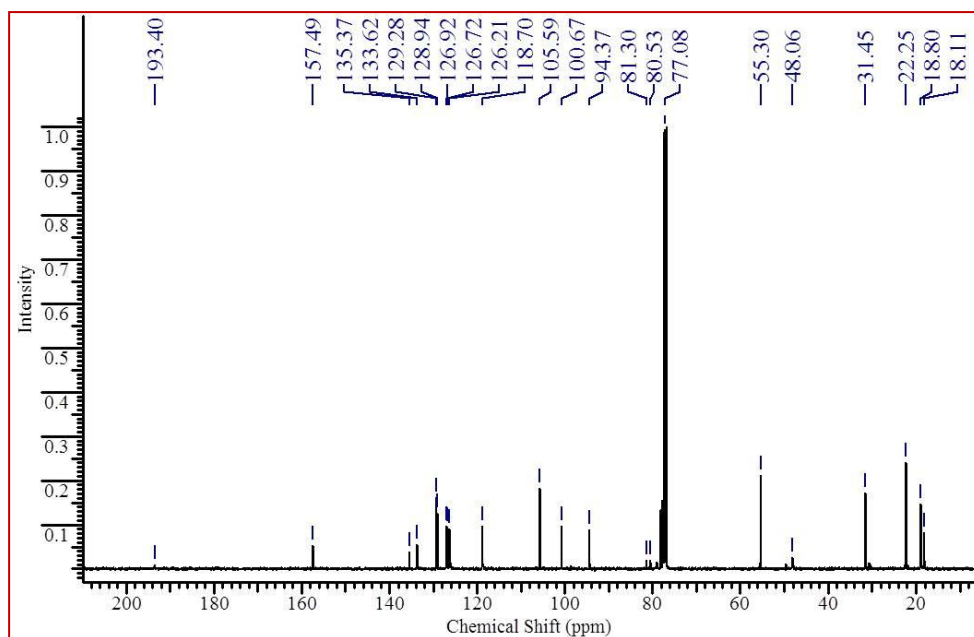


Fig.3.5: ^{13}C NMR spectra of complex 9.

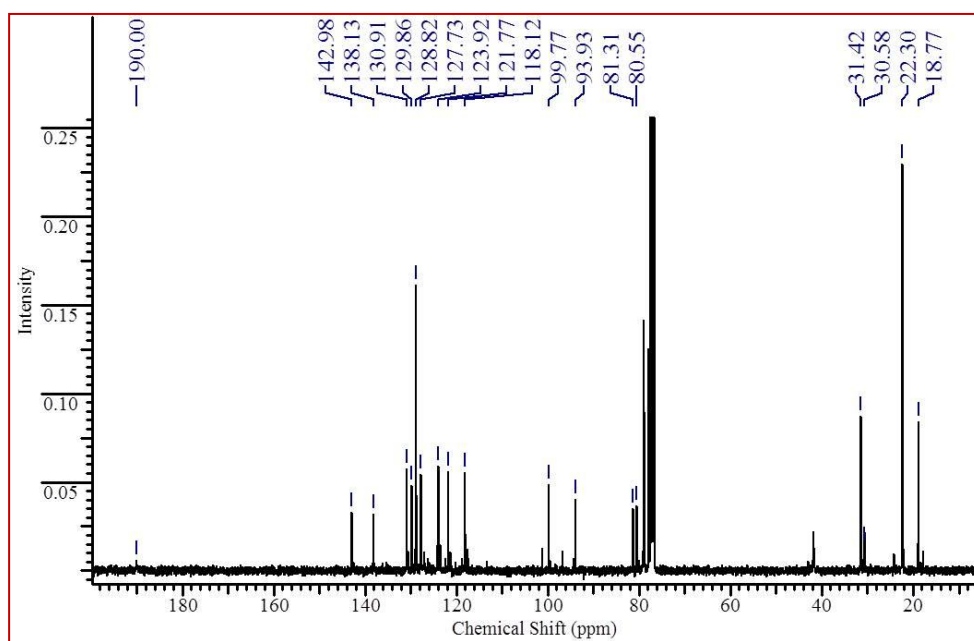


Fig.3.6: ^{13}C NMR spectra of complex 10.

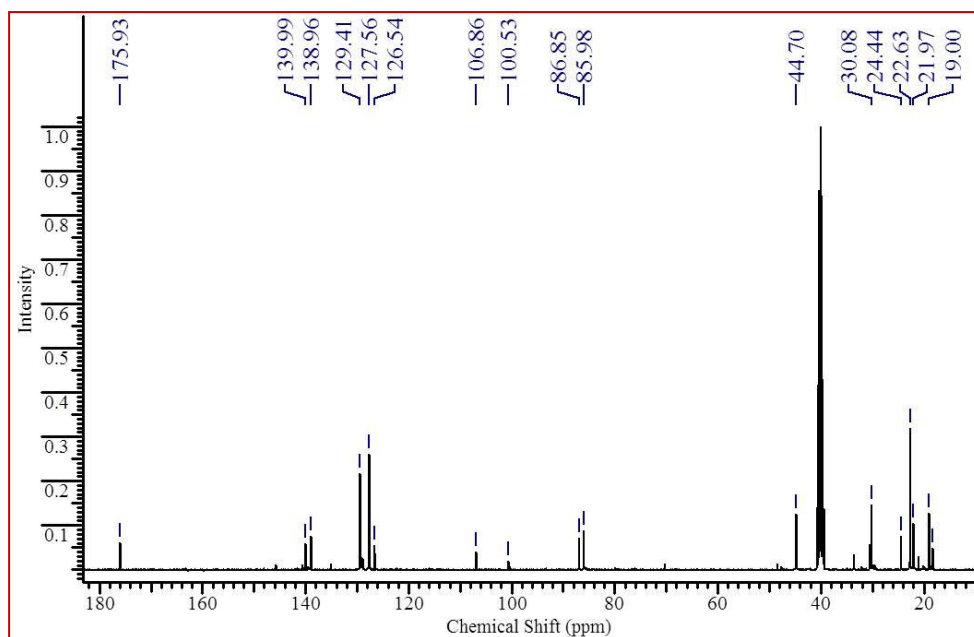


Fig.3.7: ^{13}C NMR spectra of complex **11**.

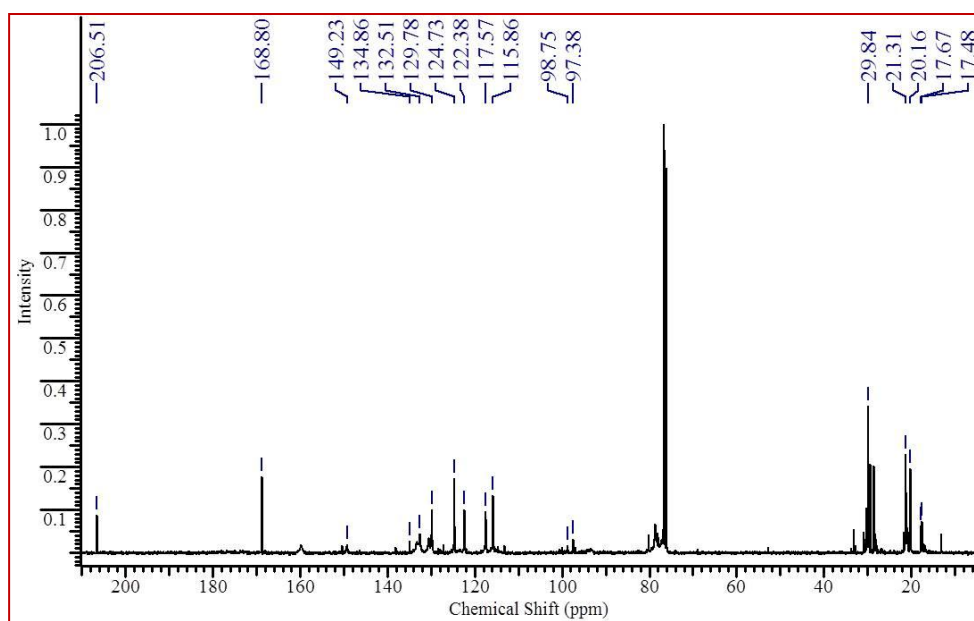


Fig.3.8: ^{13}C NMR spectra of complex **12**.

The ESI-MS of **9**, **10**, **11** and **12** show one main peak envelope corresponding to the $[\text{Ru}(\eta^6\text{-}p\text{-cymene})(\text{NSAID-H})]^+$ moiety after the dissociation of the labile chloro ligand (Fig.3.9-Fig.3.12).

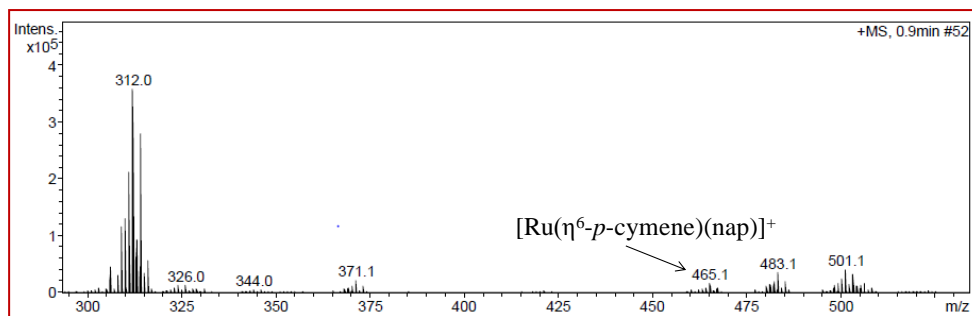


Fig.3.9: ESI-MS of complex **9**.

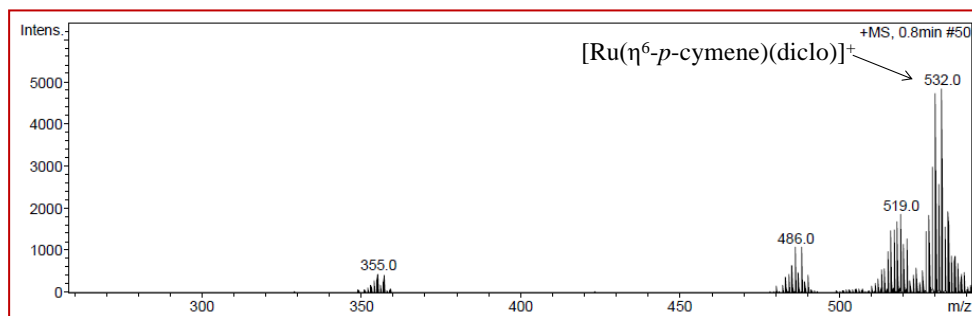


Fig.3.10: ESI-MS of complex **10**.

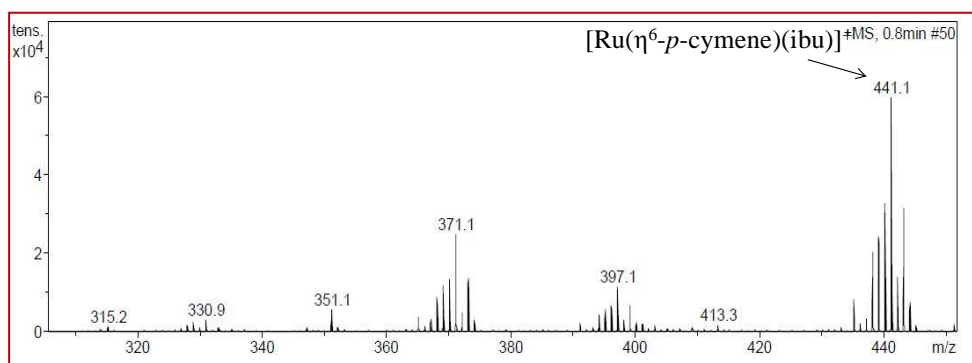


Fig.3.11: ESI-MS of complex **11**.

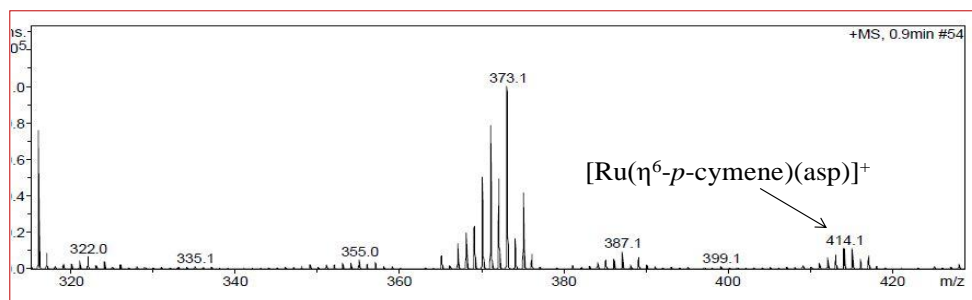


Fig.3.12: ESI-MS of complex **12**.

The solid state structures of complexes **9** and **10** have been investigated by X-ray crystallography. Both the complexes possess a pseudo-octahedral geometry and the η^6 π -bonded arene ring occupies three coordination positions of the octahedron. Two coordination sites are occupied by naproxen carboxylate and diclofenac carboxylate groups in a chelating

fashion for complexes **9** and **10**, respectively. The sixth coordination position is occupied by the chloro ligand. All the relevant bond lengths and bond angles of complexes **9** and **10** are given in the caption of Fig. 3.13,

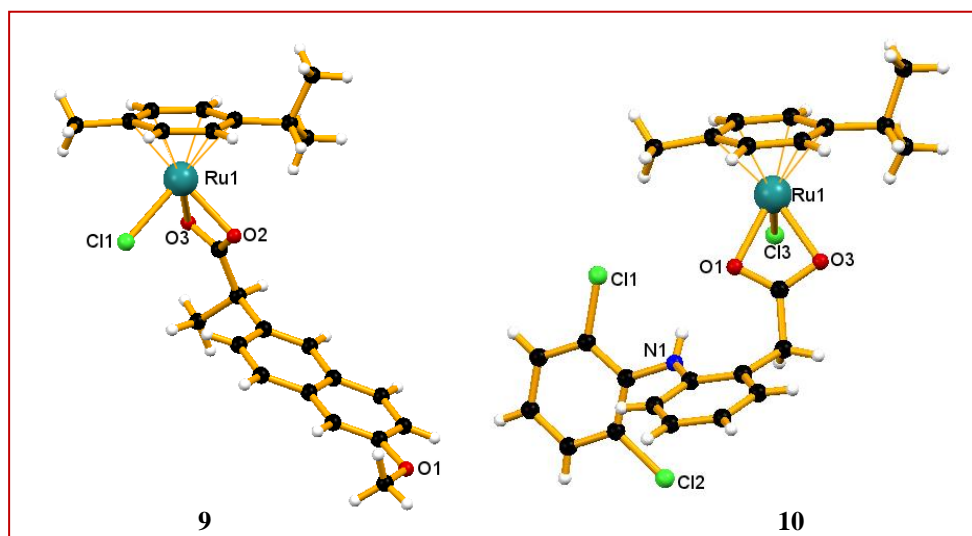


Fig.3.13: The solid state crystal structure of compound **9** and **10** with partial atomic numbering scheme. Key bond lengths (Å) and angles (°) of complex **9**: Ru(1)–O(1): 2.208(7); Ru(1)–O(2): 2.179(4); Ru(1)–Cl: 2.402(2); Ru(1)–C_{centroid}:1.417; O(1)–Ru(1)–O(2): 60.0(2); Cl(1)–Ru(1)–O(1): 85.0(1); Cl(1)–Ru(1)–O(2): 84.4(1). Key bond lengths (Å) and angles (°) of complex **10**: Ru(1)–O(1): 2.161(2); Ru(1)–O(2): 2.153(2); Ru(1)–Cl: 2.3704(8); Ru(1)–C_{centroid}:1.406; O(1)–Ru(1)–O(2): 60.16(6); Cl(1)–Ru(1)–O(1): 84.93(5); Cl(1)–Ru(1)–O(2): 84.04(5).

3.3.2 Growth inhibition study of Ru(II)–NSAID complexes

The anticancer activities of the reported complexes as well as free NSAID ligands have been tested against three different cancer cell lines *viz.*, lung cancer cell line A549, breast cancer cell line MCF7 and cervix cancer cell line HeLa. The results were obtained in terms of GI₅₀ (concentration of the drug that produces 50% inhibition of the cells), TGI (concentration of the drug that produces total inhibition of the cells) and LC₅₀ (concentration of the drug that kills 50% of the cells) using the sulforhodamine B (SRB) assay. All cancer cells were exposed for 24 h to increasing concentrations of the complexes as well as free NSAID ligands and their proliferations are reported in terms of GI₅₀ values as values for LC₅₀ and TGIs against all the three cell lines were >80 nm. Adriamycin, a chemotherapeutic drug, was used as a positive control. It is interesting to note that although free NSAID ligands have not shown any significant antiproliferative activity against any

of the three cell lines, complexes **9**, **10** and **11** have shown marked antiproliferative activity against A549 and MCF7 cells in a nanomolar concentration. Complexes **10** and **11** are quite active against HeLa cell lines but complex **9** is relatively inactive. Complex **12** has not shown any growth inhibition property in any of the cell lines. All the related data are compiled in Fig. 3.14 and Table 3.1.

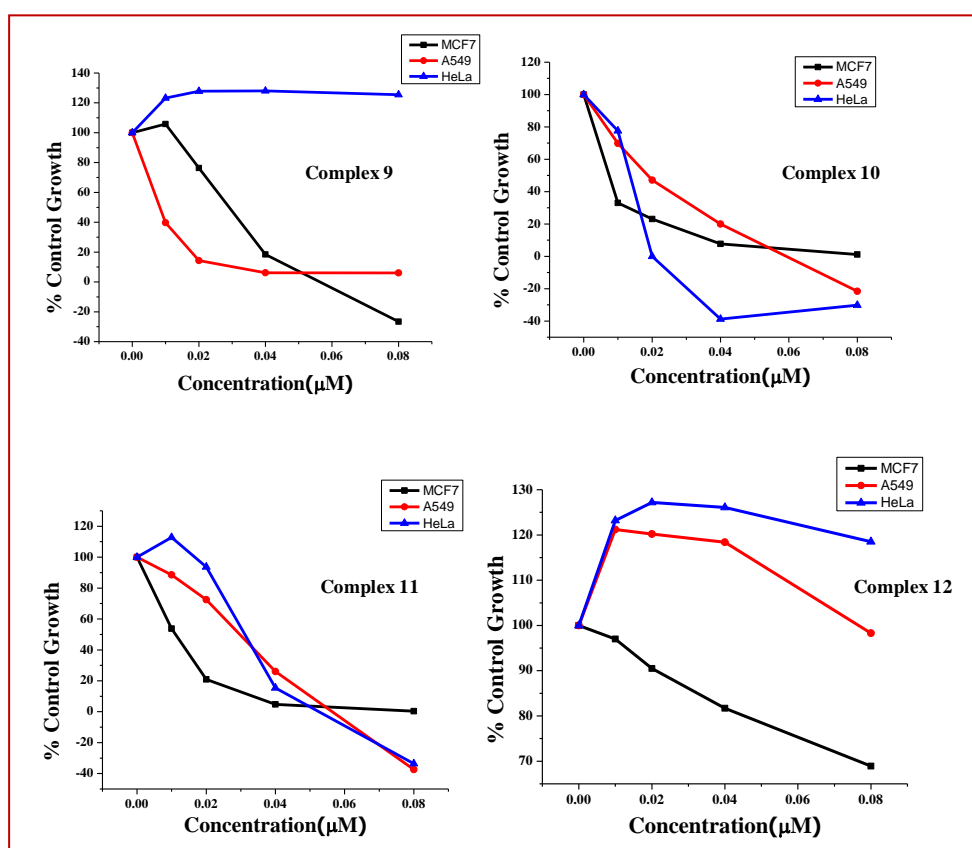


Fig.3.14: Analysis of the GI_{50} value of complexes **9**, **10**, **11** and **12** against different cancer cell lines.

Table 3.1: GI_{50} value (nM/mL) of the prepared complexes in human cancer cell lines.

Complex	A549	MCF7	HeLa
Naproxen	Inactive	>80	>80
Complex 9	<0.1	<0.1	>80
Diclofenac	49.6	>80	74.8
Complex 10	<0.1	<0.1	<0.1
Ibuprofen	Inactive	>80	Inactive
Complex 11	<0.1	<0.1	<0.1
Aspirin	Inactive	Inactive	Inactive
Complex 12	>80	>80	>80
Adriamycin	<0.1	<0.1	<0.1

A closer look at the GI_{50} value obtained signifies that complex **10** and **11** have shown comparable antiproliferative activity against different cell lines followed by complex **9**. As free NSAIDs are non-cytotoxic against the reported cancerous cell lines, it is obvious that the vacant coordination sites of the Ru(II) centre is definitely occupied either by some solvent molecules or by different biomolecules (*e.g.* enzyme or protein molecule) present in the physiological system, which make the compounds significantly cytotoxic in nature against the same cancerous cell lines. A closer look at the fragmentation of the Ru-NSAID complexes revealed the formation of non-toxic $[Ru(\eta^6\text{-}p\text{-cymene})(DMSO)Cl]^+$ in 1% DMSO medium by ESI-MS. Therefore, coordination by some biomolecules in the vacant position must be the driving force behind the antiproliferative activity of the fragmented species. Though it is very difficult to establish any kind of structure–activity relationship without further investigations, one obvious point is that the reported complexes are more cytotoxic against all the cell lines than many other metal–NSAID complexes as reported earlier.^[32]

3.3.3 Stability study in DMSO

As DMSO is the most widely utilized solvent for the preparation of stock solution for biophysical and biological testing, the stability of all the complexes has been tested in DMSO solution. In the case of ruthenium complexes, most of the time it is observed that DMSO can act as a very good ligand coordinating to the ruthenium center through sulphur or oxygen atoms.^[33] Stability studies by ESI-MS indicate that the complexes are unstable in the DMSO–MeOH mixture as the peak corresponding to $[Ru(\eta^6\text{-}p\text{-cymene})(NSAID-H)]^+$ becomes insignificant and a new peak emerges at m/z 565.1 which corresponds to a methoxido-bridge dimeric species $[Ru_2(\eta^6\text{-}p\text{-cymene})_2(OCH_3)_3]^+$ after 30 minutes (Fig.3.15).

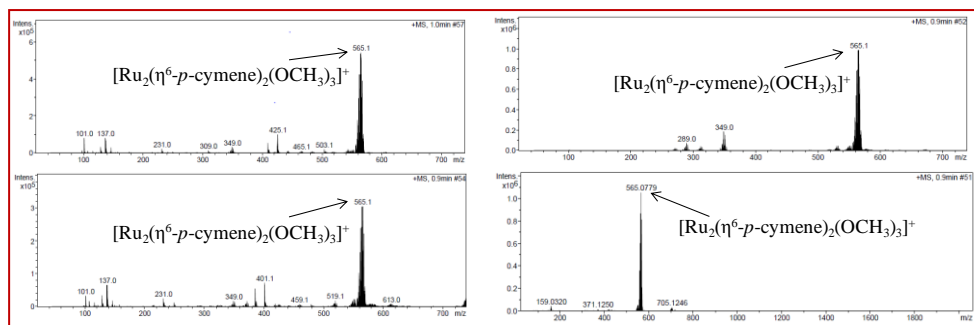


Fig.3.15: ESI-MS spectra of compound **9**, **10**, **11** and **12** in DMSO–MeOH. Complexes were dissolved in a 1% DMSO–MeOH mixture at room temperature and ESI-MS were recorded after 15 minutes at the same temperature.

A similar kind of observation has been also reported previously.^[34] However, when the ESI-MS spectra are recorded after dissolving the complexes in DMSO and immediately diluted to 1% with water, a peak at m/z 349.0 becomes the major peak corresponding to the species $[\text{Ru}(\eta^6\text{-}p\text{-cymene})(\text{DMSO})\text{Cl}]^+$ after 1 h (Fig.3.16).

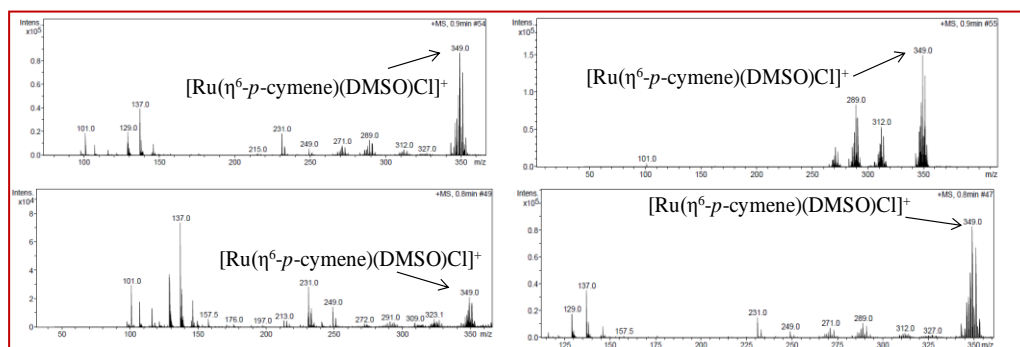


Fig.3.16: ESI-MS of Compound **9**, **10**, **11** and **12** in 1% DMSO-media.

The identification of the fragmented species similar to the biological conditions could not be established completely as the sixth coordination position could have been taken up either by different solvent molecules (DMSO or water) or some bioligands or chloride ions. Furthermore, an additional peak in the negative mode corresponding to free ligands indicates the release of NSAID as a carboxylate from the ruthenium centre in the reaction medium under both the conditions. To verify further, ^1H NMR spectra of all the complexes were recorded after dissolution of the sample in $\text{DMSO-}d_6$ (Fig.3.17). However, complexes **9** and **10** seem to be stable up to 12 h and the subsequent development of additional peaks

corresponding to free carboxylic acid protons for naproxen and diclofenac has been observed; for complexes **11** and **12**, additional peaks, indicating the presence of free NSAIDs, have been observed only after 30 minutes of the dissolution of the sample in DMSO- d_6 .

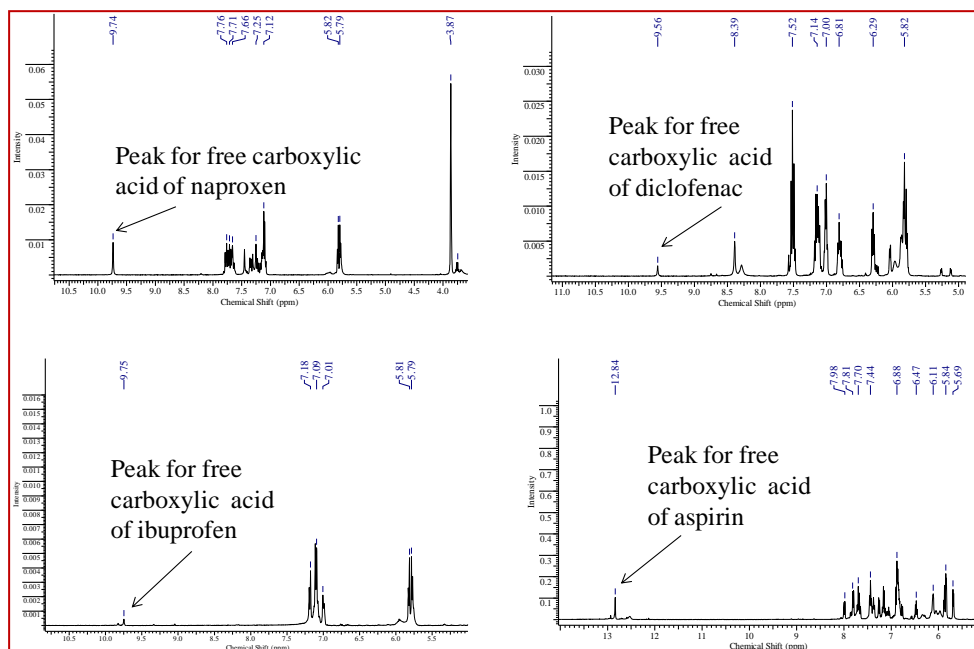


Fig.3.17: ^1H NMR spectra of compound **9**, **10**, **11** and **12** in DMSO- d_6 . 2 mg of the particular complex was dissolved in DMSO- d_6 at room temperature and its ^1H NMR was after 0.5, 3, 24 and 48 h.

Furthermore, the ^{13}C spectrum of all the complexes in DMSO- d_6 after 12 h revealed two peaks for carboxylic acid carbon, one for ruthenium coordinated carboxylic acid and another for the free carboxylic acid at 186.1 (ruthenium bound) and 175.9 (free) (Fig.3.18).

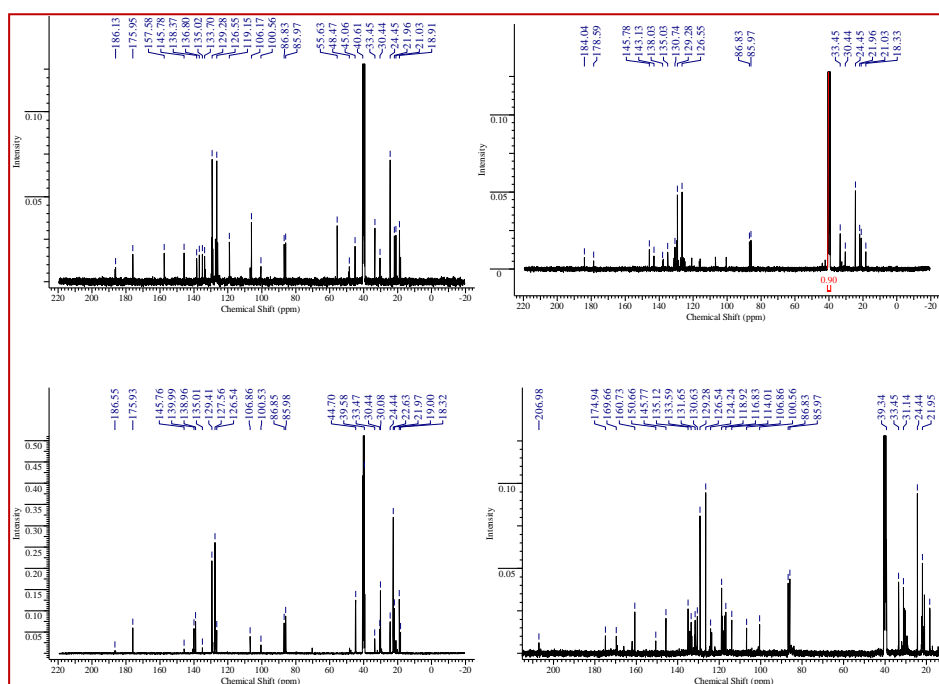


Fig.3.18: ^{13}C NMR spectra of complex **9**, **10**, **11** and **12** in $\text{DMSO-}d_6$. This indicates partial dissociation of the NSAID molecule from the coordination sphere of ruthenium in pure 100% DMSO solution.

3.3.4 COX inhibition studies

Since NSAIDs exert a chemopreventive effect by inhibiting prostaglandin and leukotriene synthesis, which were derived from the enzymatic transformation of arachidonic acid *via* cyclooxygenase and lipoxygenase pathways, a standardized method was adopted to find out whether there exists any correlation between the inhibition of COX and LOX activity and observed antiproliferative activity of the complexes. When hPBMCs are induced with ox-LDL groups to activate the arachidonic acid pathway, the total COX activity is significantly increased compared to normal hPBMCs. hPBM cells, induced by ox-LDL, upon treatment with different concentrations of free NSAIDs or complexes at different concentrations (25 μM and 50 μM), inhibit the total COX activity in a dose dependent manner compared to ox-LDL challenged groups. Moreover, it is interesting to mention that the extent in the decrease of the total COX activity caused by the complexes is more than that of the free NSAIDs. Although at 25 μM , none of the complexes has shown any significant activity, at the concentration of 50 μM , complexes **9** and **10** show moderate inhibition of

total COX activity, whereas significant inhibition has been observed for complexes **11** and **12** (Fig.3.19).

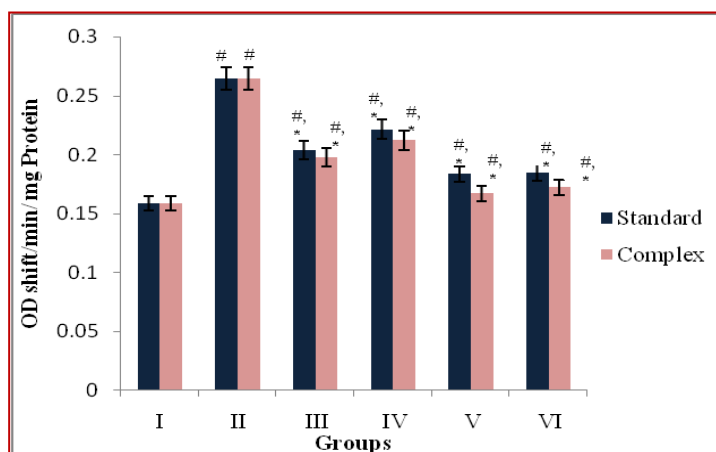


Fig.3.19: Effect of complexes on total COX activity at 50 μ M concentration. hPBMCs stimulated with 50 μ g/ml of ox-LDL served as the ox-LDL control group. The cells were pretreated with 50 μ M concentration of complexes and standards prior to ox-LDL challenge. Values are expressed as average of 6 samples \pm SEM. #Statistical difference with normal group at $P < 0.05$. *Statistical difference with group II at $P < 0.05$. Group I - Normal, Group II - ox-LDL, Group III - ox-LDL + naproxen/ox-LDL + Complex **9**, Group IV - ox-LDL + diclofenac/ox-LDL + Complex **10**, Group V - ox-LDL + ibuprofen/ox-LDL + Complex **11**, Group VI - ox-LDL + aspirin/ox-LDL + Complex **12**.

However, all the free NSAIDs have shown lesser inhibition activity than the respective complexes both at 25 μ M and 50 μ M. A comparison between the antiproliferative activity and COX inhibition activity of complexes **9**, **10** and **11** reveals that although complexes **9** and **10** possess almost similar antiproliferative activity, complex **9** has shown higher activity towards COX enzyme inhibition than complex **10**. However, complex **11** has shown high antiproliferative as well as relatively better COX inhibition property. There are various reports where naproxen or aspirin has been used to prepare metal complexes with different transition metals *e.g.* Co, Mo, Mn, and Rh and their cytotoxicity as well as COX-1 and/or COX-2 inhibition property have been evaluated against different cancerous cell lines.^[35] In all the cases, metal-NSAID complexes have shown better activity than free NSAID analogues. Again, cisplatin has been conjugated with different NSAIDs (indomethacin and ibuprofen) to overcome cisplatin-related

resistance as well as superior COX inhibition activity compared to free NSAIDs.^[36]

3.3.5 LOX inhibition studies

Lipoxygenase belongs to the family of key enzymes which are involved in the biosynthesis of leukotrienes that have an important role in the pathophysiology of several inflammatory diseases. 15-LOX activity is significantly increased in the mononuclear cell culture after treatment with ox-LDL. Pretreatment with free NSAIDs or complexes at different concentrations (25 μ M and 50 μ M) significantly decrease 15-LOX activity in hPBMCs compared to the ox-LDL control. Between the two different concentrations taken *i.e.* 25 μ M and 50 μ M, a significant reduction in 15-LOX activity has been shown at a concentration of 50 μ M for all the complexes as compared to the free NSAIDs; however, complexes **11** and **12** have shown superior activity compared to complexes **9** and **10**.

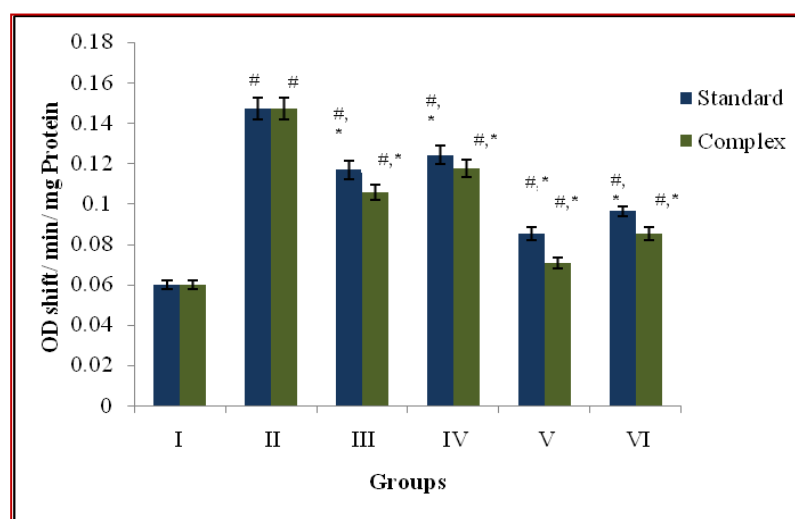


Fig.3.20: Effect of complexes on 15-LOX at 50 μ M concentration. hPBMCs stimulated with 50 μ g/ml of ox-LDL served as the ox-LDL control group. The cells were pretreated with 50 μ M concentration of complexes and Standards prior to ox-LDL challenge. Values are expressed as average of 6 samples \pm SEM. #Statistical difference with normal group at $P < 0.05$. *Statistical difference with group II at $P < 0.05$. Group I - Normal, Group II - ox-LDL, Group III - ox-LDL + naproxen/ox-LDL + Complex **9**, Group IV - ox-LDL + diclofenac/ox-LDL + complex **10**, Group V - ox-LDL + ibuprofen/ox-LDL + complex **11**, Group VI - ox-LDL + aspirin/ox-LDL + complex **12**.

Again, complexes **11** and **12** have reduced the 15-LOX activity more significantly than their counter part free NSAIDs at 50 μM concentrations.

3.3.6 DNA binding study

As the reported complexes have shown considerable antiproliferative activity, the DNA binding ability of the complexes was tested with ct-DNA through fluorescence quenching due to ethidium bromide displacement. Although complexes **9**, **10**, and **12** seem to be non-interactive with DNA, complex **11** has shown increased quenching of fluorescence at 605 nm with increase in the concentration of the metal complex (Fig.3.21).

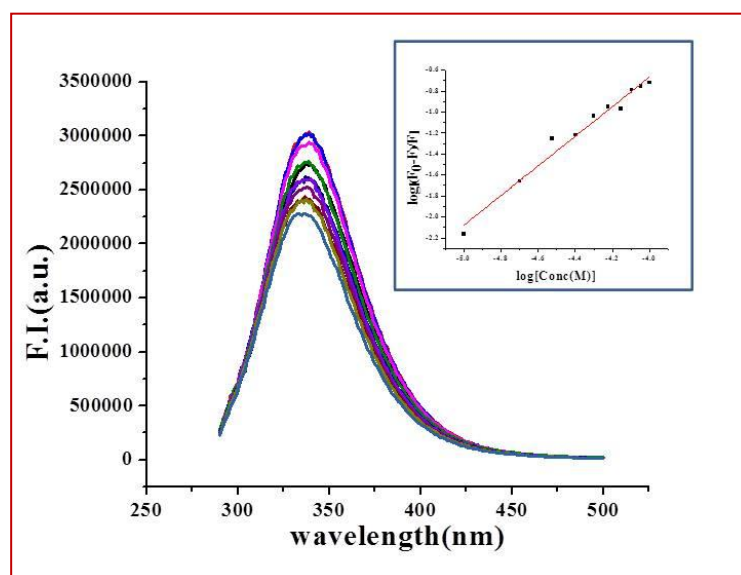


Fig.3.21: Fluorescence quenching of ct-DNA by compound 11.

Analyzing the Stern–Volmer plot, the k_q value has been found to be $1.1 \times 10^3 \text{ M}^{-1} \text{ s}^{-1}$ while the binding constant value (K_b) has been obtained from the Scatchard equation as $2.29 \times 10^4 \text{ M}^{-1}$. The values indicate that complex **11** is able to displace EB from the EB–DNA conjugate as a result of their competition for the DNA-intercalating sites, suggesting the intercalation of the complex to ct-DNA. Thus, antiproliferative activity shown by complex **11** might have been at least partially due to the interaction of DNA in the biological system.

3.3.7 Protein binding studies

The binding of prospective drug molecules with plasma proteins are very important as transport of drugs occurs through the bloodstream *via* the interaction with plasma proteins.^[37] All the complexes were subjected to interact with Bovine Serum Albumin (BSA) and their interactions with protein have been monitored through quenching of an emission peak arising out of the tryptophan residue of BSA.

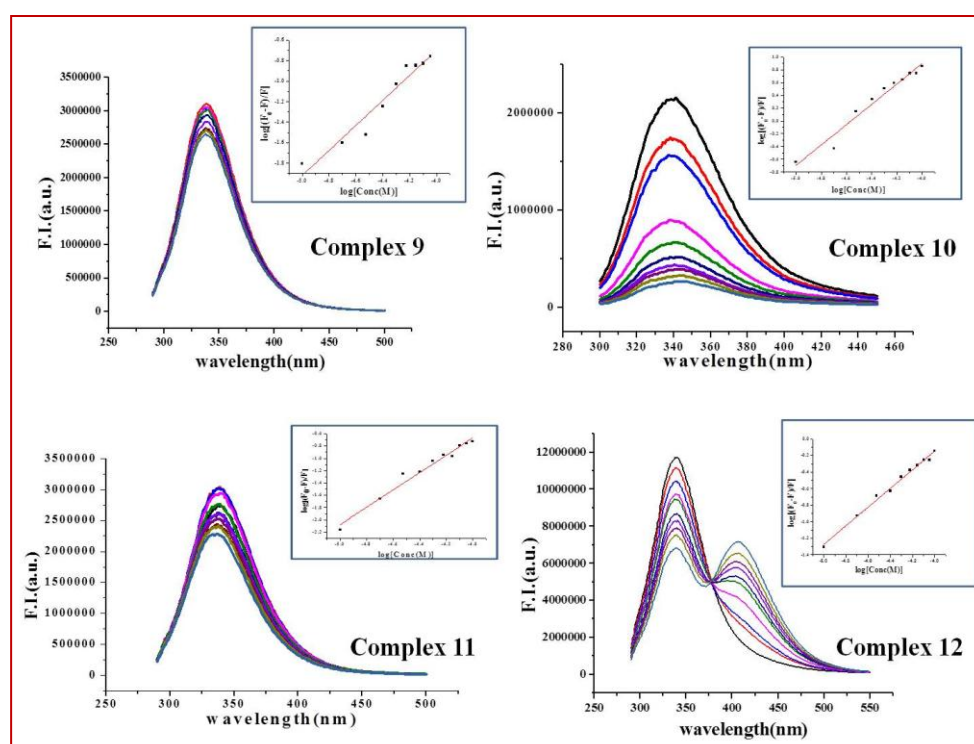


Fig.3.22: Fluorescence quenching of HSA by Complex 9, 10, 11 and 12.

Separate solutions of BSA were titrated against the addition of different complexes. In the case of BSA binding, the addition of reported complexes to the respective protein solution causes a significant decrease of the initial fluorescence intensity (Fig.3.22). To get further insight into the quenching process, the fluorescence quenching data were analyzed with the Stern–Volmer equation. The k_q values obtained for all the complexes are found to be in the range of 2.99×10^{11} – $1.04 \times 10^{13} \text{ M}^{-1} \text{ s}^{-1}$, indicating the involvement of the static quenching mechanism. The binding constant (K_a) and the number of binding sites (n) have been determined by the Scatchard plot. The values of n for all the complexes are in the range ~ 1 , indicating the

comparable binding property of the complexes. All the relevant data are compiled in Table 3.2.

Table 3.2: Various parameters obtained from BSA interaction with the prepared complexes.

BSA	$K_{sv}(M^{-1})$	$K_q(M^{-1}s^{-1})$	$K_a(M^{-1})$	n
Complex 9	4.97×10^3	8.04×10^{11}	1.41×10^4	1.09
Complex 10	6.45×10^4	1.04×10^{13}	1.69×10^7	1.58
Complex 11	1.85×10^3	2.99×10^{11}	9.55×10^4	1.41
Complex 12	6.76×10^3	1.09×10^{12}	2.33×10^4	1.12

3.3.8 Interaction with amino acids

Very often, metallodrugs interact with different protein molecules present in the biological system upon intravenous administration. Proteins can play a significant role either in the delivery of metal-based anticancer drugs to their cellular targets or in deactivating them before reaching the target. Thus, the interactions between the prepared complexes and amino acids were studied to look into the possible interaction with biomolecules and metabolization. In order to investigate in detail the binding mode, the complexes were mixed with different amino acids and ESI-MS were recorded after 1 h and 24 h. It shows that amino acids *viz.* histidine, methionine, and cysteine gradually bind to the ruthenium centre by substituting the coordinated ligand. The reaction between histidine and ruthenium complexes gives a peak at m/z 389.8, which is assigned as $[Ru(cym)(His)-H]^+$ (Fig.3.23).

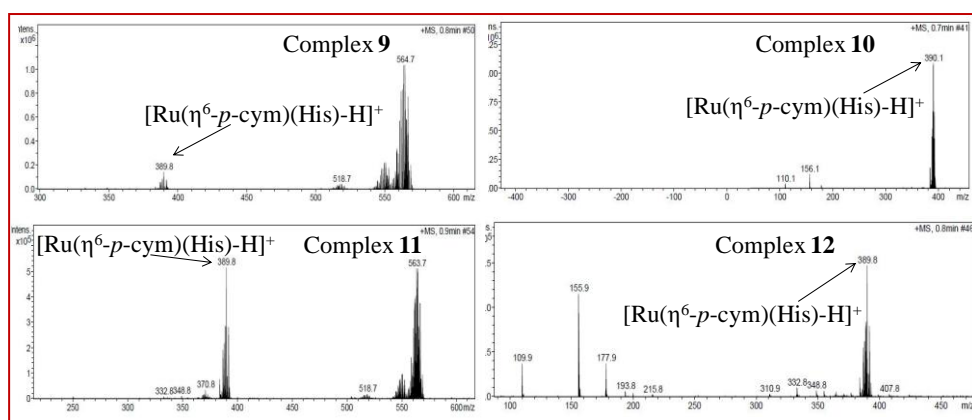


Fig.3.23: ESI-MS of Histidine Adduct by Compound 9, 10, 11 and 12.

The reaction with cysteine shows a peak at m/z 355.7, confirming the formation of $[\text{Ru}(\eta^6\text{-}p\text{-cym})(\text{Cys})\text{-H}]^+$ (Fig.3.24).

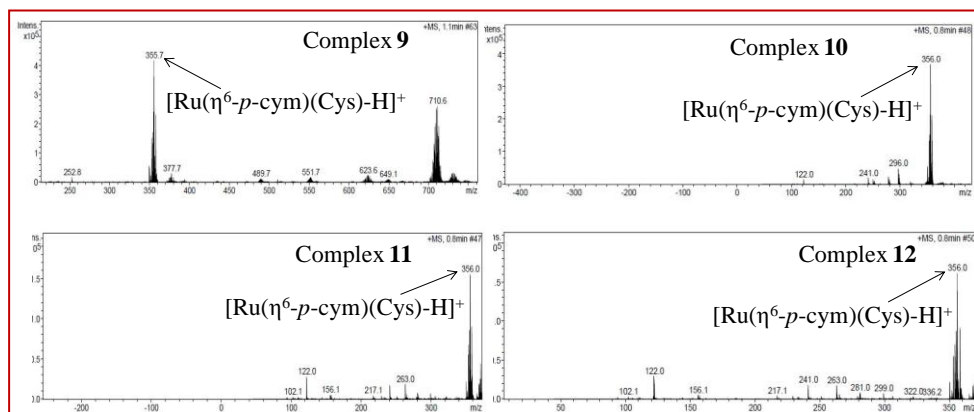


Fig.3.24: ESI-MS of Cysteine adduct by Compound 9, 10, 11 and 12.

Whereas methionine gives a peak at m/z 383.8 corroborating the structure $[\text{Ru}(\text{cym})(\text{Met})\text{-H}]^+$ (Fig.3.25).

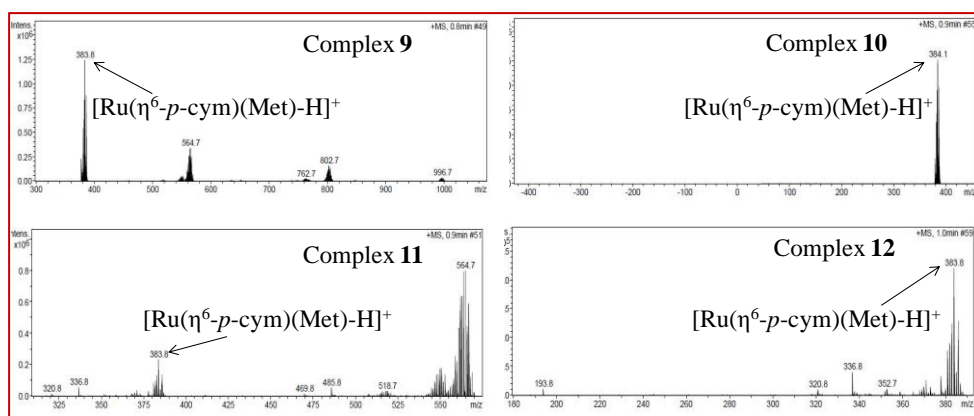


Fig.3.25: ESI-MS of Methionine adduct by Compound 9, 10, 11 and 12.

When the ESI-MS spectra were recorded after 1h, the peak of the ruthenium complex coordinated to amino acids was obtained along with the peak of the parent complex as the major one. But when ESI-MS spectra were recorded after 24 h for the same reaction mixture, it was found that the peak of the amino acid coordinated to complex becomes the major peak as no peak of the parent complex has been observed. This observation shows that amino acids replace the ligand (NSAIDs) from the Ru-centre with time. To perform a comparative study among all the amino acids, each of the complexes was mixed with histidine, methionine and cysteine in a 1:1:1 ratio and their ESI-MS spectra were recorded after 24 h. Relative abundance ESI-MS spectra show that complexes bind with all the amino

acids; however the preference for binding has been histidine > methionine > cysteine (Fig.3.26).

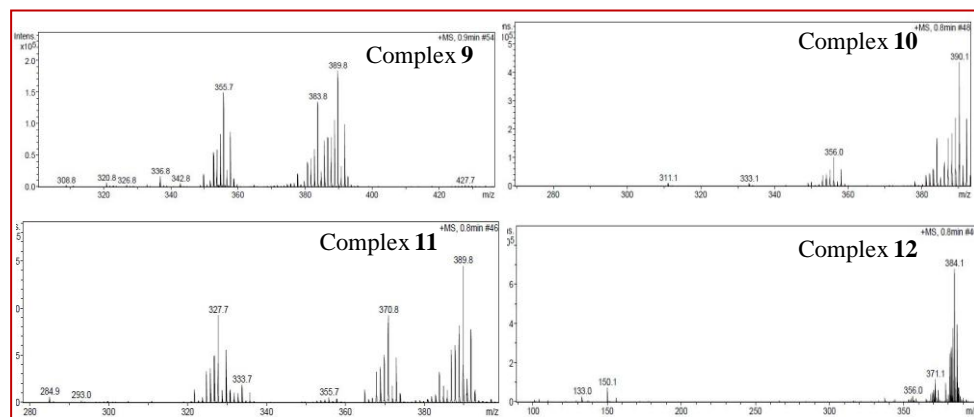


Fig.3.26: ESI-MS of Mixture of [Histidine+Cysteine+Methionine] Adduct by Compound **9**, **10**, **11** and **12**. (clockwise from right)

The preference for His indicates the enhanced stability of the formed adducts compared to their Met and Cys analogues.^[38]

3.3.9 Docking analysis

To understand the possible molecular interactions of the synthesized complexes with COX, docking studies of complexes **9** and **10** with COX-2 have been carried out. The conformation of complexes was taken from their single crystal X-ray structures. The protein conformation was obtained from the X-ray structures of COX-2 as co-crystallized with two NSAIDs such as naproxen (PDB: 3q7d)^[39] and diclofenac (PDB: 5ikq).^[40] For the docking studies, the co-crystallized ligands were removed and the free protein was used for binding with Ru(II) complexes as well as with free NSAIDs. These two particular crystals of the protein were chosen specially to correlate the binding affinities of Ru(II) complexes containing naproxen and diclofenac ligands used in the present study and these complexes were also found to be relatively stable under the experimental conditions in organic solvents. The molecular interactions of COX-2 with free ligands (NSAIDs) were also studied in addition to the interactions with Ru(II) complexes to understand the relative feasibility of interactions. Two independent molecular docking simulation methods such as AutoDock and Gold were used to understand the binding pattern and to have reliable

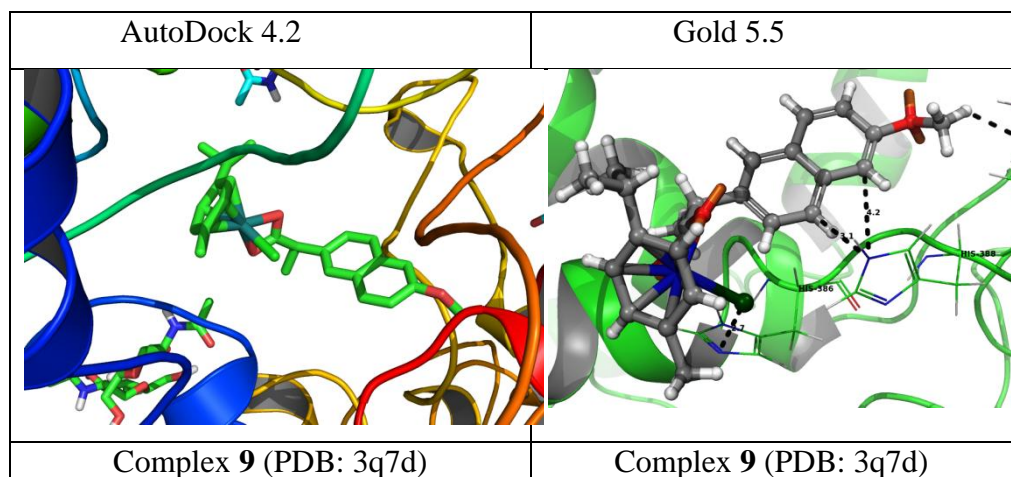
results for their interactions. To understand the compatibility of Ru(II) complexes as well as ligands towards both of the cocrystallized proteins (PDB: 3q7d and 5ikq), docking studies with all possible combinations have been performed and the results are shown in Table 3.4.

Table 3.4: Summary of molecular interactions of complex **9**, complex **10** and their corresponding ligands with COX-2.

Target	Compounds	AutoDock 4.2		Gold 5.5	
		Binding Energy (Kcal mol ⁻¹)	Interactions	Gold Score (GS)	Interactions
3q7d	Complex 9	-8.5	--	64.86	H386 A, H388 A, L391 A
	Naproxen	-6.38	V228.A, N537.A	50.92	A199 A, L390 A, H388 A, H207 A
	Complex 10	-7.41	S530.A	58.17	H386A, H388 A
	Diclofenac	-6.73	R376.A	44.28	H207 A, Q203 A, H388 A
5ikq	Complex 9	-9.83	--	65.16	S530 A
	Naproxen	-6.83	R120.A, Y355.A	46.76	H207 A, N382 A
	Complex 10	-9.09	--	52.32	H207 A, W387 A, H388 A, N382 A
	Diclofenac	-7.07	S530.A	47.42	S530 A, Y385 A, M522 A

While AutoDock provided the calculated Gibbs free energy for the interactions, Gold provided GoldScore (GS) as the fitness scoring pattern to understand the relative strength of interactions. Interestingly, the outcomes from both of these methods are in good agreement and match well with their experimentally observed COX inhibition results. For example,

complex **9** exhibited higher binding affinity than complex **10** towards both the co-crystallized proteins as reflected by its higher binding energy values ($-8.5 \text{ kcal mol}^{-1}$ and $-9.8 \text{ kcal mol}^{-1}$) as well as the higher GS score (64.86 and 65.16) as shown in Table 3.4. However, both complexes **9** and **10** exhibited significantly higher binding affinities than the corresponding free ligands naproxen and diclofenac towards COX-2. The higher affinities of Ru(II)-complexes as compared to the corresponding free NSAID ligands are probably due to the higher extent of different non-bonded interactions of complexes with proximal amino acid residues of proteins at their binding sites. In addition to H-bonding interactions, other non-bonded interactions such as halogen bonding and pi-pi stacking interactions were also detected to strengthen their binding affinities. For example, complex **9** showed the pi-pi interaction with H386A and H388A residues (PDB: 3q7d). Additionally, a hydrogen bonding interaction was detected with L391A of COX-2 (PDB: 3q7d). Similarly, a hydrogen bonding interaction was detected for complex **9** with S530 in COX-2 (PDB: 5ikq). For complex **10**, additional halogen bonding interaction was detected between the chloro group of the ligand and N382A (2.8 \AA ; PDB: 3q7d). Some representative molecular interactions with protein are shown in Fig.3.27.



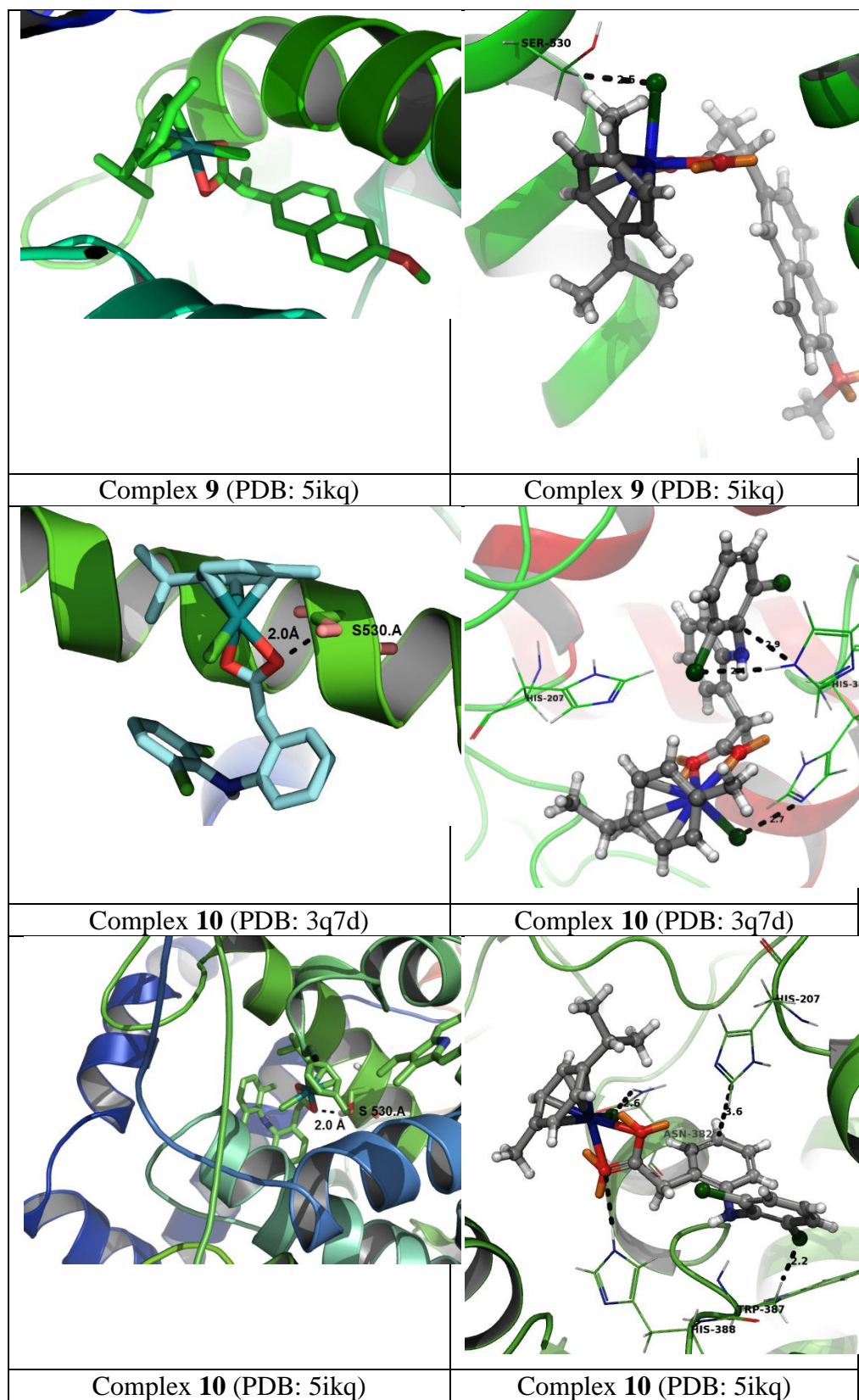


Fig. 3.27: Docking interaction illustration of the selected ligands as well as complexes with COX-2.

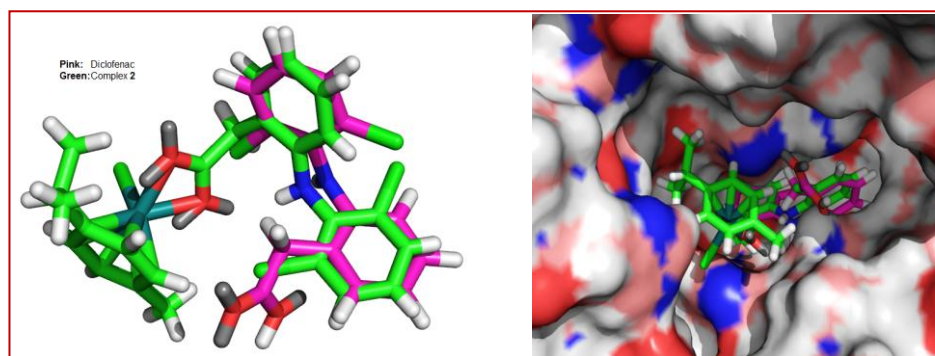


Fig.3.28: *Overlay diagrams for the binding of complex 10 and free diclofenac at the binding site of COX-2 (PDB: 5ikq) showing their binding precision as obtained by Gold simulation.*

It should be noted that such molecular modelling for ruthenium (η^6 -cymene) complexes for their relative COX-2 binding affinities was also performed using Gold software as reported recently.^[41] Our findings using docking simulations are in agreement with the experimental observations on the relative inhibition of COX and LOX by complexes **9** and **10**. The COX inhibition studies as well as their relative anti-proliferative activities are more important as these two complexes were relatively more stable in DMSO under experimental conditions unlike complexes **11** and **12**.

3.4 Conclusion

In a nutshell herein the synthesis of four ruthenium arene NSAID complexes viz. $[\text{Ru}(\eta^6\text{-}p\text{-cymene})(\text{nap})\text{Cl}]$ **9**, $[\text{Ru}(\eta^6\text{-}p\text{-cymene})(\text{diclo})\text{Cl}]$ **10**, $[\text{Ru}(\eta^6\text{-}p\text{-cymene})(\text{ibu})\text{Cl}]$ **11** and $[\text{Ru}(\eta^6\text{-}p\text{-cymene})(\text{asp})\text{Cl}]$ **12** have been described. Complexes **10** and **11** have shown remarkable antiproliferative activity against the lung cancer cell line A549, breast cancer cell line MCF7 and cervical cancer cell line HeLa to the tuning of anticancer drug adriamycin in terms of the nanomolar concentration. Complex **9** has shown effective antiproliferative activity against the lung cancer cell line A549 and breast cancer cell line MCF7. However, it is relatively inactive against the cervical cancer cell line HeLa. Here, it is worth mentioning that complex **11** is more effective in the inhibition of the cyclooxygenase

enzyme, followed by complex **10** and complex **9** indicating a possible correlation between the inhibition of COX and anticancer property. The stability study of the complexes in methanol indicates the tendency of the NSAID ligands to dissociate from the Ru(II) centre in solution and different biomolecules or solvent molecules get attached to the fragmented Ru(II) centre, making the complexes promisingly cytotoxic in nature. The extent of dissociation is different depending upon the nature of NSAIDs and the solvent used. However, from the stability study it seems that the complexes may act as pro-drugs which may get converted in the biological system to some unknown entity. Furthermore, all the complexes have shown adequate binding towards plasma protein. The outcome of this study certainly testifies to the importance of using NSAID ligands in metal complexes to target COX and LOX enzymes to stimulate anticancer and anti-proliferative activities in metal complexes in an effective way.

3.5 References

- [1] (a) Morais, T. S., Valente, A., Tomaz, A. I., Marques, F., Garcia, M. H. (2016), Tracking antitumor metallodrugs: promising agents with the Ru(II)- and Fe(II)-cyclopentadienyl scaffolds, *Future Med. Chem.*, 8, 527-544. (DOI: doi.org/10.4155/fmc.16.7) (b) Wani, W. A., Prashar, S., Shreaz, S., S. Gómez-Ruiz. (2016), Nanostructured materials functionalized with metal complexes: in search of alternatives for administering anticancer metallodrugs, *Coord. Chem. Rev.* 312, 67–98. (DOI: 10.1016/j.ccr.2016.01.001); (c) Barry, N. P. E., Sadler, P. J. (2014), 100 years of metal coordination chemistry: from Alfred Werner to anticancer metallodrugs, *Pure Appl. Chem.*, 86, 1897-1910. (DOI: doi.org/10.1515/pac-2014-0504) (d) Allardyce, C. S., Dyson, P. J. (2016), Metal-based drugs that break the rules, *Dalton Trans.*, 45, 3201-3209. (DOI: 10.1039/c5dt03919c)
- [2] Sava, G.; Bergamo, A., Dyson, P. J. (2011), Metal-based

- antitumour drugs in the post-genomic era: what comes next? Dalton Trans., 40, 9069-9075. (DOI: 10.1039/c1dt10522a) (b) Mitra, K. (2016), Platinum complexes as light promoted anticancer agents: a redefined strategy for controlled activation, Dalton Trans., 45, 19157-19171. (DOI: 10.1039/c6dt03665a) (c) Gao, C., Zhang, Y., Chen, J., Wang, T., Qian, Y., Yang, B., Dong, P., Zhang, Y. (2016), Targeted drug delivery system for platinum-based anticancer drugs, Mini-Rev. Med. Chem., 16, 872-891. (DOI: 10.2174/1389557516666151120115947) (d) Gibson, D. (2016), Platinum(IV) anticancer prodrugs- hypotheses and facts, Dalton Trans., 45, 12983-12991. (DOI: 10.1039/c6dt01414c)
- [3] Bergamo, A., Sava, G. (2015), Linking the future of anticancer metal-complexes to the therapy of tumour metastases, Chem. Soc. Rev., 44, 8818-8835. (DOI: 10.1039/c5cs00134j)
- [4] Rademaker-Lakhai, J. M., van den Bongard, D., Pluim, D., Beijnen, J. H., Schellens, J. H. M. (2004), A phase I and pharmacological study with imidazolium-trans-DMSO-imidazole- tetrachlororuthenate, a novel ruthenium anticancer agent, Clin. Cancer Res., 10, 3717-3727. (DOI: 10.1158/1078-0432.CCR-03-0746); (b) Velders, A. H., Bergamo, A., Alessio, E., Zangrando, E., Haasnoot, J. G., Casarsa, C., Cocchietto, M., Zorzet, S., Sava, G. (2004), Synthesis and chemical-pharmacological characterization of the antimetastatic NAMI-A-type Ru(III) complexes (Hdmtp)[*trans*-RuCl₄(dmsos)(dmtp)],(Na)[*trans*-RuCl₄(dmsos)(dmtp)],and[*mer*-RuCl₃(H₂O)(dmsos)(dmtp)] (dmtp=5,7 Dimethyl[1,2,4]triazolo[1,5-*a*] pyrimidine), J. Med. Chem., 47, 1110-1121. (DOI: 10.1021/jm030984d)
- [5] Trondl, R., Heffeter, P., Kowol, C. R., Jakupec, M. A., Bergerand, W., Keppler, B. K. (2014), NKP-1339, the first ruthenium-based anticancer drug on the edge to clinical

- application, *Chem. Sci.*, 5, 2925-2932. (DOI: 10.1039/c3sc53243g)
- [6] (a) Bergamo, A., Sava, G., (2011), Ruthenium anticancer compounds: myths and realities of the emerging metal-based drugs, *Dalton Trans.*, 40, 7817-7823. (DOI: 10.1039/c0dt01816c) (b) Casini, A., Gabbiani, C., Sorrentino, F., Rigobello, M. P., Bindoli, A., Geldbach, T. J., Marrone, A., Re, N., Hartinger, C. G., Dyson, P. J., Messori, L. (2008), Emerging protein targets for anticancer metallodrugs: inhibition of thioredoxin reductase and cathepsin B by antitumor ruthenium(II)-arene compounds, *J. Med. Chem.*, 51, 6773-6781. (DOI: 10.1021/jm8006678) (c) Yan, Y. K., Melchart, M., Habtemariam, A., Sadler, P. J. (2005), Organometallic chemistry, biology and medicine: ruthenium arene anticancer complexes, *Chem. Commun.*, 4764-4776. (DOI: 10.1039/b508531b) (d) Mandal, P., Malviya, N., Guedes da Silva, M. F. C., Dhankhar, S. S., Nagaraja, C. M., Mobin, S. M., Mukhopadhyay, S. (2016), Fine tuning through valence bond tautomerization of ancillary ligands in ruthenium(II) arene complexes for better anticancer activity and enzyme inhibition properties, *Dalton Trans.*, 45, 19277-19289. (DOI: 10.1039/c6dt02969h)
- [7] (a) Kurzwernhart, A., Kandioller, W., Bartel, C., Bächler, S., Trondl, R., Mühlgassner, G., Jakupec, M. A., Arion, V. B., Marko, D., Keppler, B. K., Hartinger, C. G. (2012), Targeting the DNA-topoisomerase complex in a double-strike approach with a topoisomerase inhibiting moiety and covalent DNA binder, *Chem. Commun.*, 48, 4839-4841. (DOI: 10.1039/c2cc31040f) (b) Ang, W. H., Parker, L. J., Luca, A. D., Juillerat-Jeanneret, L., Morton, C. J., Bello, M. L., Parker, M. W., Dyson, P. J. (2009), Rational design of an organometallic glutathione transferase inhibitor, *Angew. Chem., Int. Ed.*, 48, 3854-3857. (DOI:

- 10.1002/anie.200900185)
- [8] Banti, C. N., Hadjikakou, S. K. (2016), Non-Steroidal anti-inflammatory drugs (NSAIDs) in metal complexes and their effect at the cellular level, *Eur. J. Inorg. Chem.*, 19, 3048-3071. (DOI: 10.1002/ejic.201501480)
- [9] Boodram, J. N., Mcgregor, I. J., Bruno, P. M., Cressey, P. B., Hemann, M. T., Suntharalingam, K. (2016), Breast cancer stem cell potent copper(II)-non-steroidal anti-inflammatory drug complexes, *Angew. Chem., Int. Ed.*, 55, 2845-2850. (DOI: 10.1002/anie.201510443)
- [10] Feng, J., Du, X., Liu, H., Sui, X., Zhang, C., Tang, Y., Zhang, J. (2014), Manganese-mefenamic acid complexes exhibit high lipoxygenase inhibitory activity, *Dalton Trans.*, 43, 10930-10939. (DOI: 10.1039/c4dt01111b)
- [11] Markworth, J. F., Vella, L., Lingard, B. S., Tull, D. L., Rupasinghe, T. W., Sinclair, A. J., Maddipati, K. R., Smith, D. C. (2013), Human inflammatory and resolving lipid mediator responses to resistance exercise and ibuprofen treatment, *Am. J. Physiol.: Regul., Integr. Comp. Physiol.*, 305, R1281-R1296. (DOI: 10.1152/ajpregu.00128.2013)
- [12] (a) Wallace, J. M. (2002), Nutritional and botanical modulation of the inflammatory cascade-eicosanoids, cyclooxygenases, and lipoxygenases-as an adjunct in cancer therapy, *Integr. Cancer Ther.*, 1, 7-37. (DOI: 10.1177/153473540200100102) (b) Kaur, J., Vaish, V., Sanyal, S. N. (2012), COX-2 as a molecular target of colon cancer chemoprevention: promise and reality, *Biomed. Aging Pathol.*, 2, 67-72. (DOI: 10.1016/j.biomag.2012.07.007)
- [13] Viegas, A., Manso, J., Corvo, M. C., Marques, M. M. B., Cabrita, E. J. (2011), Binding of ibuprofen, ketorolac, and diclofenac to COX-1 and COX-2 studied by saturation transfer difference NMR, *J. Med. Chem.*, 54, 8555-8562. (DOI: 10.1021/jm201090k)

- [14] (a) Luci, D. K., Jameson II, J. B., Yasgar, A., Diaz, G., Joshi, N., Kantz, A., Markham, K., Perry, S., Kuhn, N., Yeung, J., E. H. Kerns, L. Schultz, M. Holinstat, J. L. Nadler, D. A. Taylor-Fishwick, A. Jadhav, A. Simeonov, T. R. Holman and D. J. Maloney, (2014), Synthesis and structure-activity relationship studies of 4-((2-hydroxy-3-methoxybenzyl)amino) benzenesulfonamide derivatives as potent and selective inhibitors of 12-lipoxygenase, *J. Med. Chem.*, 57, 495-506. (DOI: 10.1021/jm4016476) (b) Czapski, G. A., Czubowicz, K., Strosznajder, J. B., Strosznajder, R. P. (2016), The Lipoxygenases: their regulation and implication in alzheimer's disease, *Neurochem. Res.*, 41, 243-257. (DOI: 10.1007/s11064-015-1776-x)
- [15] Vitale, P., Tacconelli, S., Perrone, M. G., Malerba, P., Simone, L. Scilimati, A., Lavecchia, A., Dovizio, M., Marcantoni, E., Bruno, A., Patrignani, P. (2013), Synthesis, pharmacological characterization, and docking analysis of a novel family of diarylisoxazoles as highly selective cyclooxygenase-1 (COX-1) inhibitors, *J. Med. Chem.*, 56, 4277-4299. (DOI: 10.1021/jm301905a)
- [16] Mont, F. J., Leval, X. De, Michaux, C., Renard, J. F., Winum, J. Y., Montero, J. L., Damas, J., Dogné, J. M., Pirotte, B. (2004), Design, synthesis, and pharmacological evaluation of pyridinic analogues of nimesulide as cyclooxygenase-2 selective inhibitors, *J. Med. Chem.*, 47, 6749-6759. (DOI: 10.1021/jm0494801)
- [17] Masferrer, J. (2001), Approach to angiogenesis inhibition based on cyclooxygenase-2, *Cancer J.*, 7, S144-S150.
- [18] Kim, T. Y., Kim, J., Choo, H. Y. P., Kwon, H. J. (2016), *Biochem. Biophys. Res. Commun.*, Inhibition of 5-lipoxygenase suppresses vascular endothelial growth factor-induced angiogenesis in endothelial cells, 478, 1117-1122. (DOI: 10.1016/j.bbrc.2016.08.078)

- [19] Ishihara, A. T., Hoshino, T., Namba, T., Tanaka, K. I., Mizushima, T. (2007), Involvement of up-regulation of PUMA in non-steroidal anti-inflammatory drug-induced apoptosis, *Biochem. Biophys. Res. Commun.*, 356, 711-717. (DOI: 10.1016/j.bbrc.2007.03.034)
- [20] Zhang, Y., Tortorella, M. D., Liao, J., Qin, Chen, T., Luo, J., Chen, Guan, J., Talley, J. J., Tu, Z. (2015), Synthesis and evaluation of novel erlotinib–NSAID conjugates as more comprehensive anticancer agents, *ACS Med. Chem. Lett.*, 6, 1086-1090. (DOI: 10.1021/acsmchemlett.5b00286)
- [21] Morris, R. E., Aird, R. E., Murdoch, P. D. S., Chen, J. H. Cummings, H., Hughes, N. D., Parsons, S., Parkin, A., Boyd, G., Jodrell, D. I., Sadler, P. J. (2001), Inhibition of cancer cell growth by ruthenium(II) arene complexes, *J. Med. Chem.*, 44, 3616-3621. (DOI: 10.1021/jm010051m) (b) Seuanes, G. C., Moreira, M. B., Petta, T., Freire de Moraes Del Lama, M. P., Beraldo de Moraes, L. A., Moraes de Oliveira, A. R., Naal, R. M. Z. G., Nikolaou, S. (2015), Novel binuclear μ -oxo diruthenium complexes combined with ibuprofen and ketoprofen: Interaction with relevant target biomolecules and anti-allergic potential, *J. Inorg. Biochem.*, 153, 178-185. (DOI: 10.1016/j.jinorgbio.2015.08.004) (c) Santos, R. L. S. R., Bergamo, A., Sava, G., Silva, D. O. (2012), Synthesis and characterization of a diruthenium(II,III)–ketoprofen compound and study of the in vitro effects on CRC cells in comparison to the naproxen and ibuprofen derivatives, *Polyhedron*, 42, 175-181. (DOI: 10.1016/j.poly.2012.05.012) (d) Huang, S., Liang, Y., Huang, C., Su, W., Lei, X., Liu, Y., Xiao, Q. (2016), Systematical investigation of binding interaction between novel ruthenium(II) arene complex with curcumin analogs and ct DNA, *Luminescence*, 31, 1384-1394. (DOI: 10.1002/bio.3119) (e) Lopes, C. S. J., Damasceno, J. L., Oliviera, P. F., Guedes, A. P. M., Tavares, D. C., Deflon, V.

- M., Lopes, N. P., Pivatto, M., Batista, A. A., Maia, P. I. S., Poelhsitz, G. V. (2015), Ruthenium(II) complexes containing anti-inflammatory drugs as ligands: synthesis, characterisation and *in vitro* cytotoxicity activities on cancer cell lines, *J. Braz. Chem. Soc.*, 26, 1838-1847. (DOI: 10.5935/0103-5053.20150161)
- [22] Păunescu, E., McArthur, S., Soudani, M., Scopelliti, R. Dyson, P. J. (2016), Nonsteroidal anti-inflammatory organometallic anticancer compounds, *Inorg. Chem.*, 55, 1788-1808. (DOI: 10.1021/acs.inorgchem.5b02690) (b) Psomas, J., Kessissoglou, P. (2013), Quinolones and non-steroidal anti-inflammatory drugs interacting with copper(II), nickel(II), cobalt(II) and zinc(II): structural features, biological evaluation and perspectives, *Dalton Trans.*, 42, 6252-6276. (DOI: 10.1039/c3dt50268f) (c) Totta, X., Hatzidimitriou, A. G., Papadopoulos, A. N., Psomas, G. (2016), Nickel(II) complexes of the non-steroidal anti-inflammatory drug tolfenamic acid: Synthesis, structure, antioxidant activity and interaction with albumins and calf-thymus DNA, *Polyhedron*, 117, 172-183. (DOI: 10.1016/j.poly.2016.05.050) (d) Perdih, D. F., Tangoulis, V., Turel, I., Kessiosglou, D. P., Psomas, G. (2011), Interaction of copper(II) with the non-steroidal anti-inflammatory drugs naproxen and diclofenac: Synthesis, structure, DNA- and albumin binding, *J. Inorg. Biochem.*, 105, 476-489. (DOI: 10.1016/j.jinorgbio.2010.08.013)
- [23] Shimizu, T., Kondo, K., Hayaishi, O. (1981), Role of prostaglandin endoperoxides in the serum thiobarbituric acid reaction, *Arch Biochem Biophys.*, 206, 271-276. (DOI: 0003-9861/81/020271)
- [24] Axelrod, B., Cheesbrough, T. M., Laakso, S. (1981), Lipoxygenase-1 from soyabean seed inhibiting the activity of pancreatic lipase, *Methods Enzymol.*, 71, 441-451. (DOI: 10.1016/0076-6879(81)71054-1)

- [25] Morris, G. M., Goodsell, D. S., Halliday, R. S., Huey, R., Hart, W. E., Belew R. K., Olson, A. J. (1998), Automated docking using a lamarckian genetic algorithm and an empirical binding free energy function, *J. Comput Sci.*, 19(14), 1639-1662. (DOI: 10.1002/(SICI)1096-987X(19981115)19:14<1639::AID-JCC10>3.0.CO;2-B)
- [26] Duggan, K. C., Hermanson, D. J., Musee, J., Prusakiewicz, J. J., Scheib, J. L., Carter, B. D., Banerjee, S., Oates, J. A., Marnett, L. J. (2011), (*R*)-Profens are substrate-selective inhibitors of endocannabinoid oxygenation by COX-2, *Nat. Chem. Biol.*, 7, 803-809. (DOI: 10.1038/nchembio.1821)
- [27] Orlando, B. J., Malkowski, M. G. (2016), Substrate-selective inhibition of cyclooxygenase-2 by fenamic acid derivatives is dependent on peroxide tone, *J. Biol. Chem.*, 291, 15069-15081. (DOI: 10.1074/jbc.M116.725713)
- [28] Jones, G., Willet, P., Glen, R. C., Leach, A. R., Taylor, R. (1997), Development and validation of a genetic algorithm for flexible docking, *J. Mol. Biol.*, 267, 727-748. (DOI: 10.1006/jmbi.1996.0897)
- [29] Chen, Z. N., Deng, R. W., Wu, J. G. (1992), Synthesis, characterization, and anti inflammatory activity of naproxen complexes with rare earth (III), *J. Inorg. Biochem.*, 47, 81-87. (DOI: 10.1016/0162-0134(92)84044-N)
- [30] Nakamoto, K., (2009), Infrared and raman spectra of inorganic and coordination compounds, theory and applications in inorganic chemistry. 6th ed. John Wiley & Sons, Inc.: Hoboken, New Jersey.
- [31] e Silva, I. M. P., Profirio, D. M., de Paivo, R. E. F., Lancellotti, M., Formig, A. L. B., Corbi, P. P. (2013), A silver complex with ibuprofen: Synthesis, solid state characterization, DFT calculations and antibacterial assays, *J. Mol. Struct.*, 1049, 1-6. (DOI: 10.1016/j.molstruc.2013.06.034)
- [32] (a) Tabrizi, L., Chiniforoshan, H., McArdle, P. (2015),

Synthesis, crystal structure and spectroscopy of bioactive Cd(II) polymeric complex of the non-steroidal anti-inflammatory drug diclofenac sodium: Antiproliferative and biological activity, *Spectrochim. Acta, Part A*, 136, 429-436. (DOI: 10.1016/j.saa.2014.09.053) (b) Intini, F. P., Zajac, J., Novohradsky, V., Saltarella, T., Pacifico, C., Brabec, V., Natile, G., Kasparkova, J. (2017), Novel antitumor platinum(II) conjugates containing the nonsteroidal anti-inflammatory agent diclofenac: synthesis and dual mechanisms of antiproliferative effects, *Inorg. Chem.*, 56(3), 1483-1497. (DOI: 10.1021/acs.inorgchem.6b02553) (c) Rehman, H. U., Freitas, T. E., Gomes, R. N., Colquhoun, A., Silva, D. O. (2016), Axially-modified paddlewheel diruthenium(II,III)-ibuprofenato metallodrugs and the influence of the structural modification on U87MG and A172 human glioma cell proliferation, apoptosis, mitosis and migration, *J. Inorg. Biochem.*, 165, 181-191. (DOI: 10.1016/j.jinorgbio.2016.10.003) (d) Božić, B. DJ., Rogan, J. R., Poleti, D. D., Trišović, N. P., Božić, B. DJ., Ušćumlić, G. S. (2012), Synthesis, characterization and antiproliferative activity of transition metal complexes with 3-(4,5-Diphenyl-1,3-oxazol-2-yl)propanoic acid (Oxaprozin), *Chem. Pharm. Bull.*, 2012, 60(7), 865-869. (DOI: 10.1248/cpb.c12-00185) (e) Zawidlak-Węgrzyńska, B., Kawalec, M., Bosek, I., Łqeczyk-Juzwa, M., Adamus, G., Rusin, A., Filipczak, P., Głowala-Kosińska, M., Wolanńska, K., Krawczyk, Z., Kurcok, P. (2010), Synthesis and antiproliferative properties of ibuprofen-oligo(3-hydroxybutyrate) conjugates, *Eur. J. Med. Chem.*, 2010, 45, 1833-1842. (DOI: 10.1016/j.ejmech.2010.01.020) (f) El-Gamel, N. E. A. (2009), *J. Coord. Chem.*, The interactions of metal ions with nonsteroidal anti-inflammatory drugs (oxicams), 62(14), 2239-2260. (DOI: 10.1080/00958970902822630) (g) Gkaniatsou, E. I., Banti, C.

- N., Kourkoumelis, N., Skoulika, S., Manoli, M., Tasiopoulos, A. J., Hadjikakou, S. K. (2015), Novel mixed metal Ag(I)-Sb(III)-metallotherapeutics of the NSAIDs, aspirin and salicylic acid: Enhancement of their solubility and bioactivity by using the surfactant CTAB, *J. Inorg. Biochem.*, 150, 108-119. (DOI: 10.1016/j.jinorgbio.2015.04.014)
- [33] Patra, M., Joshi, T., Pierroz, V., Ingram, K., Kaiser, M., Ferrari, S., Springler, B., Kieser, J., Gasser, G. (2013), DMSO-mediated ligand dissociation: renaissance for biological activity of *N*-Heterocyclic-[Ru(η^6 -arene)Cl₂] drug candidates, *Chem.-Eur. J.*, 19, 14768-14772. (DOI: 10.1002/chem.201303341)
- [34] Gould, R. O., Stephenson, T. A., Tocher, D. A. (1984), Synthesis and reactions of some triple alkoxo- and thioato-bridged arene ruthenium(II) complexes. X-ray structure determination of [Ru₂(η -C₆H₆)₂(OMe)₃][BPh₄], *J. Organomet. Chem.*, 263, 375-384. (DOI: 10.1016/0022-328X(84)85040-8)
- [35] Cressey, P. B., Eskandari, A., Bruno, P. M., Lu, C., Hemann, M. T., Suntharalingam, K. (2016), The potent inhibitory effect of a naproxen-appended cobalt(III)-cyclam complex on cancer stem cells, *Chem Bio Chem*, 17, 1713-1718. (DOI: 10.1002/cbic.201600368) (b) Rubner, G., Bendsdorf, K., Wellner, A., Bergemann, S., Ott, I., Gust, R. (2010), [Cyclopentadienyl]metallocarbonyl complexes of acetylsalicylic acid as neo-anticancer agents, *Eur. J. Med. Chem.*, 45, 5157-5163. (DOI: 10.1016/j.ejmech.2010.08.028)
- [36] Neumann, W., Crews, B. C., Sárosi, M. B., Daniel, C. M., Ghebreselasie, K., Scholz, M. S., Marnett, L. J., Hey-Hawkins, E. (2015), Conjugation of cisplatin analogues and cyclooxygenase inhibitors to overcome cisplatin resistance, *Chem Med Chem*, 2015, 10, 183-192. (DOI: 10.1002/cmdc.201402353)
- [37] Ganeshpandian, M., Loganathan, R., Suresh, E., Riyasdeen, A.,

- Akbarsha, M. A., Palaniandavar, M. (2014), New ruthenium(II) arene complexes of anthracenyl appended diazacycloalkanes: effect of ligand intercalation and hydrophobicity on DNA and protein binding and cleavage and cytotoxicity, *Dalton Trans.*, 43, 1203-1209. (DOI: 10.1039/c3dt51641e)
- [38] Hanif, M., Henke, H., Meier, S. M., Martic, S., Labib, M., Kandioller, W., Jakupec, M. A., Arion, V. B., Kraatz, B. H., Keppler, B. K., Hartinger, C. G. (2010), Is the reactivity of M(II)-arene complexes of 3-Hydroxy-2(1H)-pyridones to biomolecules the anticancer activity determining parameter?, *Inorg. Chem.*, 49, 7953-7963. (DOI: 10.1021/ic1009785)
- [39] Duggan, K. C., Hermanson, D. J., Musee, J., Prusakiewicz, J. J., Scheib, J. L., Carter, B. D., Banerjee, S., Oates, J. A., Marnett, L. J. (2011), (*R*)-Profens are substrate-selective inhibitors of endocannabinoid oxygenation by COX-2, *Nat. Chem. Biol.*, 7, 803-809. (DOI: 10.1038/nchembio.663)
- [40] Orlando, B. J., Malkowski, M. G. (2016), Substrate-selective inhibition of cyclooxygenase-2 by fenamic acid derivatives is dependent on peroxide tone, *J. Biol. Chem.*, 291, 15069-15081. (DOI: 10.1074/jbc.M116.725713)
- [41] Aman, F., Hanif, M., Siddiqui, W. A., Ashraf, A., Filak, L. K., Reynisson, J., Söhnle, T., Jamieson, S. M. F., Hartinger, C. G. (2014), Anticancer ruthenium(η^6 -*p*-cymene) complexes of nonsteroidal anti-inflammatory drug derivatives, *Organometallics*, 33, 5546-5553. (DOI: 10.1021/om500825h)

Chapter 4

RAPTA Type Complexes Containing N-substituted Tetrazole Scaffolds: Synthesis, Characterization and Antiproliferative Activity

4.1 Introduction

Design of potential therapeutics based on metal-drug synergism has attracted much attention in recent years. This can be achieved by combination of a drug molecule of known therapeutic value with a biologically relevant metal in a single molecule, leading to new chemical entity with enhanced activity, decreased toxicity, and more controlled pharmacokinetic properties than each separate component.^[1] Inclusion of various heterocycles in the coordination atmosphere of ruthenium(II) has been explored in recent times as probable combination of metal-ligands which may show improved anti-cancer properties. Apart from KP1019^[2,3] and NAMI-A^[4,5], where Ru(III) centre is attached with 1*H*-indazole and imidazole moiety respectively, there are several reports where Ru(II)-arene scaffold has been used to attachazole ligands with known biological significance. Ruthenium and osmium complexes of the general formula $[(\eta^6\text{-}p\text{-cymene})\text{M}(\text{oxine})(\text{Hazole})]\text{X}$, where Hazole = pyrazole (Hpz), indazole (Hind), imidazole (Him), benzimidazole (Hbzim), have shown excellent cytotoxic effects in different cancer cell lines with IC₅₀ values ranging from 3.3 to 9.4 μM .^[6] Ru(II)-cyclopentadienyl CTZ complex, $[\text{RuC}_p(\text{PPh}_3)_2(\text{CTZ})](\text{CF}_3\text{SO}_3)$, where CTZ= Clotrimazole, has shown remarkable antiproliferative as well as antiparasitic activity in recent reports.^[7]

Combretastatin A-4, isolated from the bark of the South African tree *Combretum caffrum*, has shown interesting antiproliferative activity against different cancer cell lines.^[8] Recently it is reported that combretastatin A-4 inhibits the polymerization of tubulin molecule by binding with colchicines, which in result arrests the cell mitosis pathway.^[9] But one drawback of combretastatin is that, it isomerizes to thermodynamically more stable *trans* isomer in the physiological system, resulting the loss of its cytotoxic nature.^[10] Therefore, to retain the appropriate spatial arrangements, olefin bond has been substituted by different heterocyclic moieties like imidazole,^[11] pyrazole,^[12] thiazole^[13] and many more. Literature studies reveal that the

3', 4', 5' -trimethoxy substitution pattern on the A-ring, *cis*-olefin configuration at the bridge and presence of 4' -methoxy group at the B-ring are crucial for cytotoxicity, whereas the presence of 3' hydroxy moiety is not necessary for potent activity (Fig. 4.1).^[14,15]

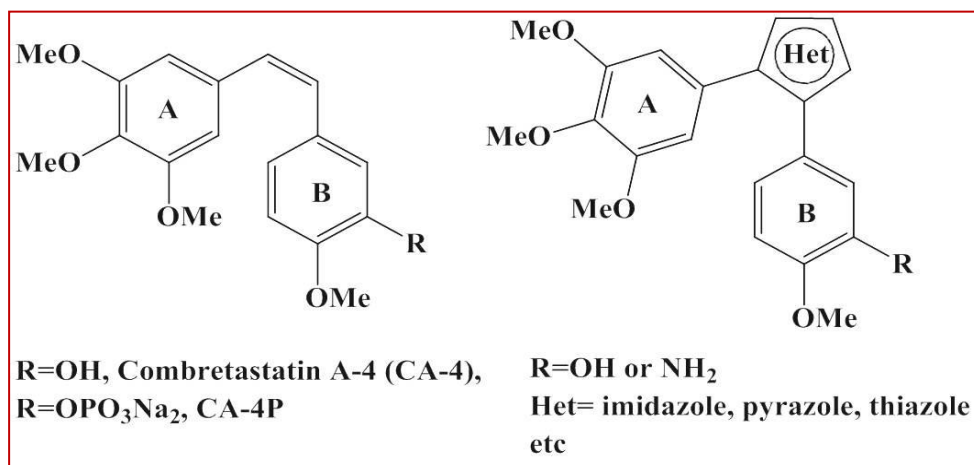
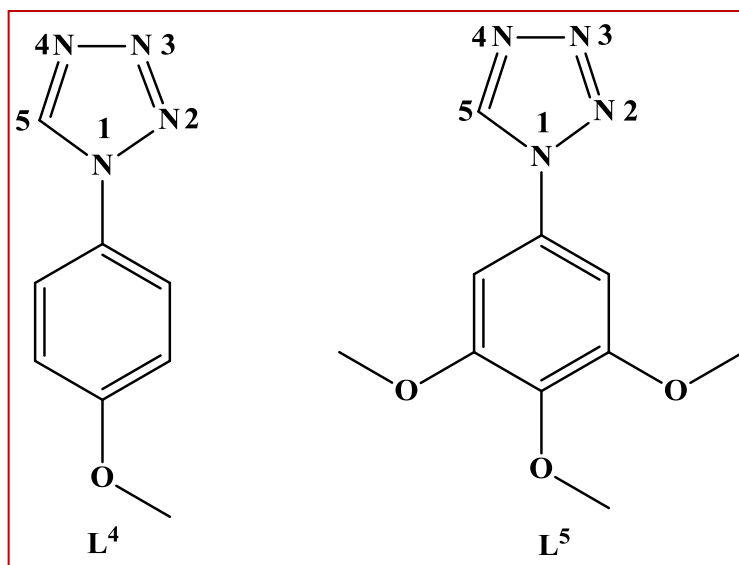


Fig. 4.1: Structure of combretastatin.

Continuing with the aim of preparing new Ru(II)-arene based anticancer metallodrugs, this chapter is focussed on Ru(II)-arene based complexes with different azole moiety as co-ligands. Two new tetrazole ligands 1-(4-methoxy-phenyl)-1*H*-tetrazole (**L⁴**) and 1-(3,4,5-trimethoxy-phenyl)-1*H*-tetrazole (**L⁵**) (Scheme 4.1) were chosen in such a way, where the 2-position of the tetrazole is of the “pyrazole” type and the 4-position is of the “imidazole” type, and **L⁴** contains 4-methoxy group, whereas **L⁵** contains 3, 4, 5-methoxy groups, so that combination of azole ligands and PTA moiety at the Ru(II) centre may show some interesting antiproliferative activity.



Scheme 4.1: Structures of ligand L^4 and L^5 .

Herein synthesis and characterization of four Ru(II)-arene complexes containing different tetrazole ligands [**13**, **15**, **17**, **19**] and their PTA analogues [**14**, **16**, **18**, **20**] have been reported. All the compounds have been tested for their antiproliferative activities against different cell lines. Interestingly most of the ruthenium compounds have shown higher antiproliferative activity than the free tetrazole ligands. To understand the possible mechanism, interaction of synthesized ruthenium compounds have been explored with different biomolecules and their stability in physiological system have been also investigated.

4.2 Experimental section

4.2.1 Materials and methods

All the chemical reagents required were purchased from Sigma and used without further purification. The specifications of all the instruments used for analysis purpose were same as described in the section 2.2.1 of the chapter 2. Ligand L^4 and L^5 have been prepared by reported procedure.^[16] Sulforhodamine B (SRB) growth inhibition (GI₅₀) assays were carried out by the Advanced Center for Treatment, Research and Education in Cancer (ACTREC), Mumbai, by following the literature procedure.^[17]

4.2.1.1 Synthesis of [Ru(η^6 -*p*-cymene)(L⁴)Cl₂] [13]

To a solution of [Ru(η^6 -*p*-cymene)Cl₂]₂ (0.1 g, 0.16 mol) in CH₂Cl₂ (50mL), a methanolic solution (10 mL) of L⁴ (0.07g, 0.33mmol) was added drop wise and stirred overnight at room temperature. The resulting orange coloured solution was evaporated to dryness to obtain orange solid as the product. Single crystal of complex **13** for solid state crystallisation was obtained by vapour diffusion of diethyl ether into a saturated solution of the compound in CH₂Cl₂. Yield: 74%. ¹H NMR (400.13MHz, 298K, CDCl₃) δ : 9.23 [s, 1H, CH of C₈H₈N₄O], 7.55 [d, 2H, 2 \times CH of C₈H₈N₄O], 7.05 [d, 2H, 2 \times CH of C₈H₈N₄O], 5.79 [d, 2H, 2 \times CH of C₆H₄], 5.53 [d, 2H, 2 \times CH of C₆H₄], 3.89 [s, 3H, CH₃ of C₈H₈N₄O], 3.13 [sept, 1H, CH(CH₃)₂], 2.36 [s, 3H, C₆H₄CH₃], 1.33 [d, 6H, CH(CH₃)₂]. ¹³C NMR (100.61MHz, CDCl₃) δ : 161.1 [C of C₁₀H₁₂N₄O₃], 143.1 [CH of C₁₀H₁₂N₄O₃], 126.0 [C of C₁₀H₁₂N₄O₃], 122.8 [2 \times CH of C₁₀H₁₂N₄O₃], 115.2 [2 \times CH of C₁₀H₁₂N₄O₃], 103.7 [C of C₆H₄], 99.2 [C of C₆H₄], 82.9 [2 \times CH of C₆H₄], 81.3 [2 \times CH of C₆H₄], 55.8 [C of OCH₃], 30.7 [CH(CH₃)₂], 22.2 [2 \times CH(CH₃)₂], 18.9 [C₆H₄CH₃]. ESI-MS (+ve mode): [Ru(η^6 -*p*-cymene)(L⁴)Cl]⁺: 447.4 (m/z). Anal. Calcd for C₁₈H₂₂Cl₂N₄ORu (%): C, 44.82; H, 4.60; N, 11.61. Found: C, 45.48; H, 4.66; N, 11.47.

4.2.1.2 Synthesis of [Ru(η^6 -*p*-cymene)(L⁴)(PTA)Cl]PF₆ [14]

To a solution of compound **13** (0.1 g, 0.20 mmol) dissolved in methanol (20 mL), a 10 mL methanolic solution of 1,3,5-triaza-7-phosphoadamantane (0.03 g, 0.20 mmol) was added dropwise. The resulting mixture was stirred overnight at room temperature and filtered. The filtrate was then evaporated *in vacuo* to obtain the product as an orange coloured solid. A mixture of complex **14** (0.05g, 0.07mmol) and NH₄PF₆ (0.01g, 0.07 mmol) in 20 mL methanol was stirred for 2 h and filtered. The filtrate was kept overnight at 4°C, from which single crystal of complex **14** was obtained. Yield: 59%. ¹H NMR (400.13MHz, 298K, DMSO-*d*₆) δ : 9.64 [s, 1H, CH of C₈H₈N₄O], 7.69 [d, 2H, 2 \times CH of C₈H₈N₄O], 6.99 [d, 2H, 2 \times CH of C₈H₈N₄O], 6.10 [d, 1H, CH of C₆H₄], 6.04 [d, 1H, CH of C₆H₄], 5.80 [d, 1H, CH of C₆H₄], 5.73 [d, 1H, CH of C₆H₄], 4.52 [s, 6H,

6×CH of C₆H₆], 4.27 [s, 6H, 3×NCH₂N], 3.41 [s, 3H, CH₃ of C₈H₈N₄O], 2.67[sept, 1H, CH(CH₃)₂], 2.10 [br.s, 3H, C₆H₄CH₃], 1.18 [d, 3H, CH(CH₃)₂], 1.07 [d, 3H, CH(CH₃)₂]. ¹³C NMR (100.61MHz, DMSO-*d*₆) δ: 160.4 [C of C₁₀H₁₂N₄O₃], 142.6[CH of C₁₀H₁₂N₄O₃], 126.5 [C of C₁₀H₁₂N₄O₃], 123.4[2×CH of C₁₀H₁₂N₄O₃], 115.5 [2×CH of C₁₀H₁₂N₄O₃], 104.6 [C of C₆H₄], 95.4 [C of C₆H₄], 88.4[2×CH of C₆H₄], 85.1 [2×CH of C₆H₄], 72.5 [3×NCH₂N of PTA], 56.1 [C of OCH₃], 52.1 [3×PCH₂N of PTA], 33.4 [CH(CH₃)₂], 24.4 [2×CH(CH₃)₂], 20.0 [C₆H₄CH₃]. ³¹P NMR (DMSO-*d*₆, 126 MHz): δ -32.8, -144.0 [sept, PF₆]. ESI-MS (+ve mode): [Ru(η⁶-*p*-cymene)(L⁴)(PTA)Cl]⁺ : 604.1 (m/z). Anal. Calcd for C₂₄H₃₄ClF₆N₇OP₂Ru(%): C, 38.48; H, 4.58; N, 13.09. Found: C, 38.55; H, 4.66; N, 12.34.

4.2.1.3 Synthesis of [Ru(η⁶-benzene)(L⁴)Cl₂] [15]

To a solution of [Ru(η⁶-benzene)Cl₂]₂ (0.1 g, 0.2 mol) in methanol (50mL), a methanolic solution (10mL) of L⁴ (0.07g, 0.4mmol) was added dropwise and refluxed overnight. The resulting orange coloured solution was evaporated to dryness and extracted with chloroform to obtain orange solid as the product. Crystals of the product suitable for X-ray crystallographic analysis were obtained *via* vapour diffusion from dichloromethane and diethyl ether. Yield: 67%. ¹H NMR (400.13MHz, 298K, CDCl₃) δ: 9.17 [s, 1H, CH of C₈H₈N₄O], 7.55 [d, 2H, 2×CH of C₈H₈N₄O], 7.05 [d, 2H, 2×CH of C₈H₈N₄O], 5.94 [s, 6H, 6×CH of C₆H₆], 3.88 [s, 3H, CH₃ of C₈H₈N₄O]. ¹³C NMR (100.61MHz, CDCl₃) δ: 161.3 [C of C₈H₈N₄O], 142.9 [CH of C₈H₈N₄O], 125.9 [C of C₈H₈N₄O], 122.9 [2×CH of C₈H₈N₄O], 115.3 [2×CH of C₈H₈N₄O], 84.4 [6×CH of C₆H₆], 55.7 [C of OCH₃]. ESI-MS (+ve mode): [Ru(η⁶-benzene)(L⁴)Cl]⁺: 391.0 (m/z). Anal. Calcd for C₁₄H₁₄Cl₂N₄ORu(%): C, 39.45; H, 3.31; N, 13.14. Found: C, 40.16; H, 3.50; N, 13.08.

4.2.1.4 Synthesis of [Ru(η⁶-benzene)(L⁴)(PTA)Cl]Cl [16]

A methanolic solution (10 mL) of 1,3,5-triaza-7-phosphoadamantane (0.03 g, 0.23 mmol) was added dropwise to a solution of compound **15** (0.1 g,

0.23 mmol) dissolved in a mixture of methanol and dichloromethane (10 mL+10 mL). The resulting solution was then stirred overnight at room temperature and filtered. The filtrate was then evaporated to dryness to obtain the crude product as a yellow solid. The isolated compound was recrystallized from chloroform ether mixture. Yield: 54%. ^1H NMR (400.13MHz, 298K, DMSO- d_6) δ : 9.98 [s, 1H, CH of $\text{C}_8\text{H}_8\text{N}_4\text{O}$], 7.80 [d, 1H, CH of $\text{C}_8\text{H}_8\text{N}_4\text{O}$], 7.36 [br.s, 2H, 2 \times CH of $\text{C}_8\text{H}_8\text{N}_4\text{O}$], 7.20 [d, 1H, CH of $\text{C}_8\text{H}_8\text{N}_4\text{O}$], 5.73 [s, 6H, 6 \times CH of C_6H_6], 4.43 [s, 6H, 3 \times NCH $_2$ N], 4.20 [s, 6H, 3 \times PCH $_2$ N], 3.84 [s, 3H, CH $_3$ of $\text{C}_8\text{H}_8\text{N}_4\text{O}$]. ^{13}C NMR (100.61MHz, DMSO- d_6) δ : 160.4 [C of $\text{C}_8\text{H}_8\text{N}_4\text{O}$], 142.6 [CH of $\text{C}_8\text{H}_8\text{N}_4\text{O}$], 128.7 [C of $\text{C}_8\text{H}_8\text{N}_4\text{O}$], 123.4 [2 \times CH of $\text{C}_8\text{H}_8\text{N}_4\text{O}$], 115.5 [2 \times CH of $\text{C}_8\text{H}_8\text{N}_4\text{O}$], 86.9 [6 \times CH of C_6H_6], 72.7 [3 \times NCH $_2$ N of PTA], 56.1 [C of OCH $_3$], 52.0 [3 \times PCH $_2$ N of PTA]. ^{31}P NMR (DMSO- d_6 , 126 MHz): δ -31.8. ESI-MS (+ve mode): $[\text{Ru}(\eta^6\text{-benzene})(\text{L}^4)(\text{PTA})\text{Cl}]^+$: 548.1 (m/z). Anal. Calcd for $\text{C}_{20}\text{H}_{26}\text{Cl}_2\text{N}_7\text{OPRu}(\%)$: C, 41.17; H, 4.49; N, 16.81. Found: C, 41.16; H, 4.50; N, 17.08.

4.2.1.5 Synthesis of $[\text{Ru}(\eta^6\text{-}p\text{-cymene})(\text{L}^5)\text{Cl}_2]$ [17]

Complex **17** was obtained following the same procedure as complex **13**, using the ligand L^5 . The crude compound was dissolved in CH_2Cl_2 and further recrystallized by layering with diethyl ether. Yield : 76%. ^1H NMR (400.13MHz, 298K, CDCl_3) δ : 9.19 [s, 1H, CH of $\text{C}_{10}\text{H}_{12}\text{N}_4\text{O}_3$], 6.83 [s, 1H, CH of $\text{C}_{10}\text{H}_{12}\text{N}_4\text{O}_3$], 6.75 [s, 1H, CH of $\text{C}_{10}\text{H}_{12}\text{N}_4\text{O}_3$], 5.72 [d, 2H, 2 \times CH of C_6H_4], 5.43 [d, 2H, 2 \times CH of C_6H_4], 3.88 [s, 3H, CH $_3$ of $\text{C}_{10}\text{H}_{12}\text{N}_4\text{O}_3$], 3.83 [br, 6H, 2 \times CH $_3$ of $\text{C}_{10}\text{H}_{12}\text{N}_4\text{O}_3$], 3.08 [sept, 1H, CH(CH $_3$) $_2$], 2.27 [s, 3H, $\text{C}_6\text{H}_4\text{CH}_3$], 1.24 [d, 6H, CH(CH $_3$) $_2$]. ^{13}C NMR (100.61MHz, CDCl_3) δ : 154.1 [2 \times C of $\text{C}_{10}\text{H}_{12}\text{N}_4\text{O}_3$], 143.2 [CH of $\text{C}_{10}\text{H}_{12}\text{N}_4\text{O}_3$], 139.7 [C of $\text{C}_{10}\text{H}_{12}\text{N}_4\text{O}_3$], 128.5 [C of $\text{C}_{10}\text{H}_{12}\text{N}_4\text{O}_3$], 103.81 [2 \times CH of $\text{C}_{10}\text{H}_{12}\text{N}_4\text{O}_3$], 99.3 [C of C_6H_4], 98.8 [C of C_6H_4], 82.9 [2 \times CH of C_6H_4], 81.3 [2 \times CH of C_6H_4], 61.0 [C of OCH $_3$], 56.6 [2 \times C of OCH $_3$], 30.7 [CH(CH $_3$) $_2$], 22.1 [2 \times CH(CH $_3$) $_2$], 18.8 [$\text{C}_6\text{H}_4\text{CH}_3$]. ESI-MS (+ve mode): $[\text{Ru}(\eta^6\text{-}p\text{-cymene})(\text{L}^5)\text{Cl}]^+$: 507.4 (m/z). Anal. Calcd for

$C_{20}H_{26}Cl_2N_4O_3Ru$ (%): C, 44.29; H, 4.83; N, 10.33. Found: C, 44.53; H, 4.91; N, 10.89.

4.2.1.6 Synthesis of $[Ru(\eta^6\text{-}p\text{-cymene})(L^5)(PTA)Cl]Cl$ [18]

To a solution of complex **17** (0.1 g, 0.18 mmol) dissolved in methanol (20 mL), a 10 mL methanolic solution of 1,3,5-triaza-7-phosphoadamantane (0.03 g, 0.18 mmol) was added dropwise. The resulting mixture was stirred overnight at room temperature and filtered. The filtrate was then evaporated *in vacuo* to obtain the crude product as an orange coloured solid. The isolated compound was further recrystallized from methanol and diethyl ether mixture. Yield: 57%. 1H NMR (400.13MHz, 298K, DMSO- d_6) δ : 10.08 [s, 1H, CH of $C_{10}H_{12}N_4O_3$], 7.26 [s, 2H, 2 \times CH of $C_{10}H_{12}N_4O_3$], 5.76 [d, 2H, 2 \times CH of C_6H_4], 5.73 [d, 2H, 2 \times CH of C_6H_4], 4.43 [s, 6H, 3 \times NCH $_2$ N], 4.18 [s, 6H, 3 \times PCH $_2$ N], 3.89 [s, 6H, 2 \times OCH $_3$ of $C_{10}H_{12}N_4O_3$], 3.74 [s, 3H, CH $_3$ of $C_{10}H_{12}N_4O_3$], 2.58 [sept, 1H, CH(CH $_3$) $_2$], 1.89 [s, 3H, C_6H_4 CH $_3$], 1.13 [d, 6H, CH(CH $_3$) $_2$]. ^{13}C NMR (100.61MHz, DMSO- d_6) δ : 154.1 [2 \times C of $C_{10}H_{12}N_4O_3$], 142.8 [CH of $C_{10}H_{12}N_4O_3$], 138.5 [C of $C_{10}H_{12}N_4O_3$], 129.2 [C of $C_{10}H_{12}N_4O_3$], 126.5 [2 \times CH of $C_{10}H_{12}N_4O_3$], 99.7 [C of C_6H_4], 95.4 [C of C_6H_4], 88.4 [2 \times CH of C_6H_4], 85.1 [2 \times CH of C_6H_4], 72.7 [3 \times NCH $_2$ N of PTA], 60.7 [C of OCH $_3$], 56.9 [2 \times C of OCH $_3$], 52.1 [3 \times PCH $_2$ N of PTA], 30.5 [CH(CH $_3$) $_2$], 24.4, 22.1 [2 \times CH(CH $_3$) $_2$], 18.3 [C_6H_4 CH $_3$]. ^{31}P NMR (DMSO- d_6 , 126 MHz): δ -34.4. ESI-MS (+ve mode): $[Ru(\eta^6\text{-}p\text{-cymene})(L^5)(PTA)]^+$: 664.1 (m/z). Anal. Calcd for $C_{26}H_{38}Cl_2N_7O_3PRu$ (%): C, 44.64; H, 5.48; N, 10.14. Found: C, 44.53; H, 5.91; N, 10.89.

4.2.1.7 Synthesis of $[Ru(\eta^6\text{-benzene})(L^5)Cl_2]$ [19]

Compound **19** was obtained from the same procedure as compound **15** using the ligand L^5 . Crystals of the product suitable for X-ray crystallographic analysis were obtained *via* vapour diffusion of diethyl ether in dichloromethane solution. Yield : 62%. 1H NMR (400.13MHz, 298K, CDCl $_3$) δ : 9.24 [s, 1H, CH of $C_{10}H_{12}N_4O_3$], 6.84 [s, 2H, 2 \times CH of $C_{10}H_{12}N_4O_3$], 5.96 [s, 6H, 6 \times CH of C_6H_6], 3.92 [s, 6H, 2 \times OCH $_3$ of

$C_{10}H_{12}N_4O_3$], 3.90 [s, 3H, OCH_3 of $C_{10}H_{12}N_4O_3$]. ^{13}C NMR (100.61MHz, $CDCl_3$) δ : 154.2 [$2\times C$ of $C_{10}H_{12}N_4O_3$], 143.0 [CH of $C_{10}H_{12}N_4O_3$], 139.8 [C of $C_{10}H_{12}N_4O_3$], 128.4 [C of $C_{10}H_{12}N_4O_3$], 98.8 [$2\times CH$ of $C_{10}H_{12}N_4O_3$], 84.5 [$6\times CH$ of C_6H_6], 61.1 [C of OCH_3], 56.6 [$2\times C$ of OCH_3]. ESI-MS (+ve mode): $[Ru(\eta^6\text{-benzene})(L^5)Cl]^+$: 451.0 (m/z). Anal. Calcd for $C_{16}H_{18}Cl_2N_4O_3Ru$ (%): C, 39.52; H, 3.73; N, 11.52. Found: C, 40.16; H, 3.50; N, 12.08.

4.2.1.8 Synthesis of $[Ru(\eta^6\text{-benzene})(L^5)(PTA)Cl]Cl$ [20]

A methanolic solution (10mL) of 1,3,5-triaza-7-phosphoadamantane (0.03 g, 0.20 mmol) was added dropwise to a solution of compound **19** (0.1 g, 0.20 mmol) dissolved in a mixture of methanol and dichloromethane (10 mL + 10 mL). The resulting solution was then stirred overnight at room temperature and filtered. The filtrate was then evaporated to dryness to obtain the crude product as a yellow solid. The obtained compound was further recrystallized from chloroform and diethyl ether mixture. Yield : 54%. 1H NMR (400.13MHz, 298K, $DMSO-d_6$) δ : 10.06 [s, 1H, CH of $C_{10}H_{12}N_4O_3$], 7.36 [s, 1H, CH of $C_{10}H_{12}N_4O_3$], 7.24 [s, 1H, CH of $C_{10}H_{12}N_4O_3$], 5.73 [s, 6H, $6\times CH$ of C_6H_6], 4.43 [s, 6H, $3\times NCH_2N$], 4.20 [s, 6H, $3\times PCH_2N$], 3.88 [s, 6H, $2\times OCH_3$ of $C_{10}H_{12}N_4O_3$], 3.72 [s, 3H, OCH_3 of $C_{10}H_{12}N_4O_3$]. ^{13}C NMR (100.61MHz, $DMSO-d_6$) δ : 154.0 [$2\times C$ of $C_{10}H_{12}N_4O_3$], 142.8 [CH of $C_{10}H_{12}N_4O_3$], 138.5 [C of $C_{10}H_{12}N_4O_3$], 129.8 [C of $C_{10}H_{12}N_4O_3$], 128.7 [$2\times CH$ of $C_{10}H_{12}N_4O_3$], 99.7 [$6\times CH$ of C_6H_6], 72.6 [$3\times NCH_2N$ of PTA], 60.7 [C of OCH_3], 56.8 [$2\times C$ of OCH_3], 52.2 [$3\times PCH_2N$ of PTA]. ^{31}P NMR ($DMSO-d_6$, 126 MHz): δ -31.8. ESI-MS (+ve mode): $[Ru(\eta^6\text{-benzene})(L^5)(PTA)Cl]^+$: 608.1 (m/z). Anal. Calcd for $C_{22}H_{30}Cl_2N_7O_3PRu$ (%): C, 41.06; H, 4.70; N, 15.24. Found: C, 40.86; H, 4.50; N, 15.08.

4.2.2 X-ray crystallography

The description of instrumentation of X-ray crystallography for complex **13**, **14**, **15** and **19** is same as described in Section 2.2.2.2.

4.2.3 Protein binding experiments

Protein binding studies of the reported compounds were performed by tryptophan fluorescence quenching experiments using bovine serum albumin (BSA). The excitation wavelength for BSA was at 280 nm and the quenching of the emission intensity of the tryptophan residues of BSA at 345 nm was monitored using the complexes as quencher with increased concentration. The excitation and emission slit widths and scan rates were kept constant throughout the experiment. A 10 μ M stock solution of BSA was prepared using 50 mM tris buffer solution and stored at 4°C for further use. Stock solutions of 5 mM strength were prepared using synthesized compounds. Fluorimetric titration was carried out taking 2 mL of the protein solution and fluorescence intensity was measured as blank. For titration, each time, 10 μ L of the stock solution was added to the protein solution and fluorescence intensity was measured. For all the eight complexes, up to 100 μ L of the solution was added to measure fluorescence quenching. The fluorescence quenching data was further analyzed by the Stern–Volmer equation, which again can be expressed in terms of bimolecular quenching rate constant and average life time of the fluorophore as shown in following equation.

$$\frac{F_0}{F} = 1 + k_q \tau_0 [Q] = 1 + K_{SV} [Q]$$

where F_0 and F are the fluorescence intensities in the absence and the presence of a quencher, k_q is the bimolecular quenching rate constant, τ_0 is the average lifetime of fluorophore in the absence of a quencher and $[Q]$ is the concentration of a quencher (metal complexes). K_{SV} is the Stern–Volmer quenching constant in M^{-1} .

4.2.4 Supplementary materials

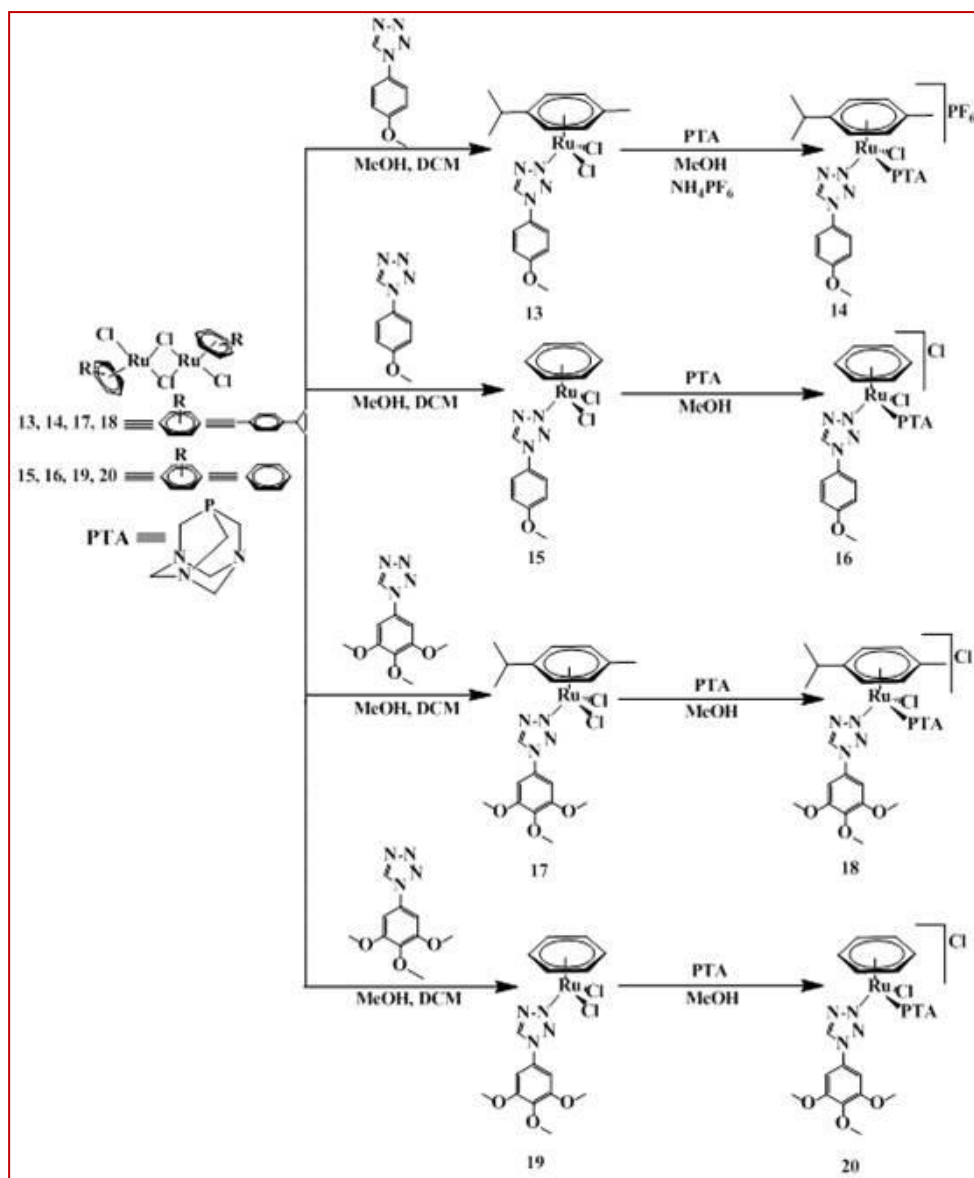
CCDC 1477974, 1556306, 1572600 and 1572631 contain the supplementary crystallographic data for **13**, **14**, **15** and **19** respectively. These data can be obtained free of charge *via* <http://www.ccdc.cam.ac.uk/conts/retrieving.html>, or from the Cambridge

Crystallographic Data Centre, 12 Union Road, Cambridge CB2 1EZ, UK;
fax: (+44) 1223-336-033; or e-mail: deposit@ccdc.cam.ac.uk.

4.3 Results and discussions

4.3.1 Synthesis and characterization of Complexes

N-substituted tetrazole ligands have been envisaged to stabilize a neutral ruthenium complex which may penetrate the cell membrane more easily in its neutral form. The monomethoxy or trimethoxy scaffold as N-substitution has been conceived as several organic molecules with this kind of scaffold have shown interesting anticancer properties in various cells.^[18] The dichloro ruthenium *p*-cymene complexes **13** and **17** have been prepared when a solution of dimeric $[(\eta^6\text{-}p\text{-cymene})\text{RuCl}_2]_2$ were stirred overnight with the respective ligands [ligand **L**⁴ for complex **13** and ligand **L**⁵ for complex **17**] at room temperature (Scheme 4.2).



Scheme 4.2: Synthesis of complex 13-20.

The reaction mixture was evaporated to dryness to get the complexes **13** and **17** as orange solid and the compounds were recrystallized further from suitable solvents. Synthesis of dichloro analogues of ruthenium benzene complexes required further drastic condition. Refluxing the methanolic solution of $[(\eta^6\text{-benzene})\text{RuCl}_2]_2$ and the corresponding ligands [ligand L^4 for complex **15** and ligand L^5 for complex **19**] for 24h furnished the desired products **15** and **19**. The solid obtained after the evaporation of the reaction mixture was again dissolved in chloroform and filtered. The filtrate was evaporated to dryness to get the complex **15** and **19** as yellow solid. Complex **13**, **15** and **19** were further recrystallised from vapour diffusion of

diethyl ether into a DCM extract of the corresponding complexes to obtain suitable single crystals for X-ray diffraction study.

Room temperature substitution of a chloride ligand in ruthenium(II) complexes with the general formula $[\text{Ru}(\eta^6\text{-arene})(\text{L})\text{Cl}_2]$ ($\text{L}^4 = 1\text{-}(4\text{-methoxyphenyl})\text{-}1H\text{-tetrazole}$, $\eta^6\text{-arene} = p\text{-cymene}$ **13**, $\eta^6\text{-arene} = \text{benzene}$ **15** and $\text{L}^5 = 1\text{-}(3,4,5\text{-Trimethoxyphenyl})\text{-}1H\text{-tetrazole}$, $\eta^6\text{-arene} = p\text{-cymene}$ **17**, $\eta^6\text{-arene} = \text{benzene}$ **19**) with 1,3,5-triaza-7-phosphoadamantane (PTA) yielded water soluble complexes $[\text{Ru}(\text{L})(\eta^6\text{-arene})(\text{PTA})\text{Cl}]\text{Cl}$ [**14**, **16**, **18** and **20**] (Scheme 4.2). Compound **14** was further treated with NH_4PF_6 in a mixture of methanol and dichloromethane to get single crystals of $[\text{Ru}(\text{L}^4)(\eta^6\text{-}p\text{-cymene})(\text{PTA})\text{Cl}]\text{PF}_6$ for solid state characterization. All the complexes are air stable and soluble in dichloromethane, methanol and DMSO. All the compounds with PTA as coligand are soluble in water, whereas dichloro analogues are less soluble in water. All the complexes have been characterized by ^1H and ^{13}C NMR spectroscopy, ESI-MS and elemental analyses. Furthermore, complex **13**, **14**, **15**, and **19** were additionally characterized by single crystal X-ray diffraction. The ^1H NMR spectra of **13**, **14**, **17**, **18** show typical band for *p*-cymene moiety at 5.72-6.10 and 5.43-5.73 ppm for ring protons and 2.67-3.13, 1.89-2.36 and 1.07-1.33 ppm for side chain protons (Fig.4.2-Fig.4.5), whereas complex **15**, **16**, **19**, **20** give singlet peak in the region 5.73-6.84 for benzene ring protons (Fig. 4.6-Fig.4.9).

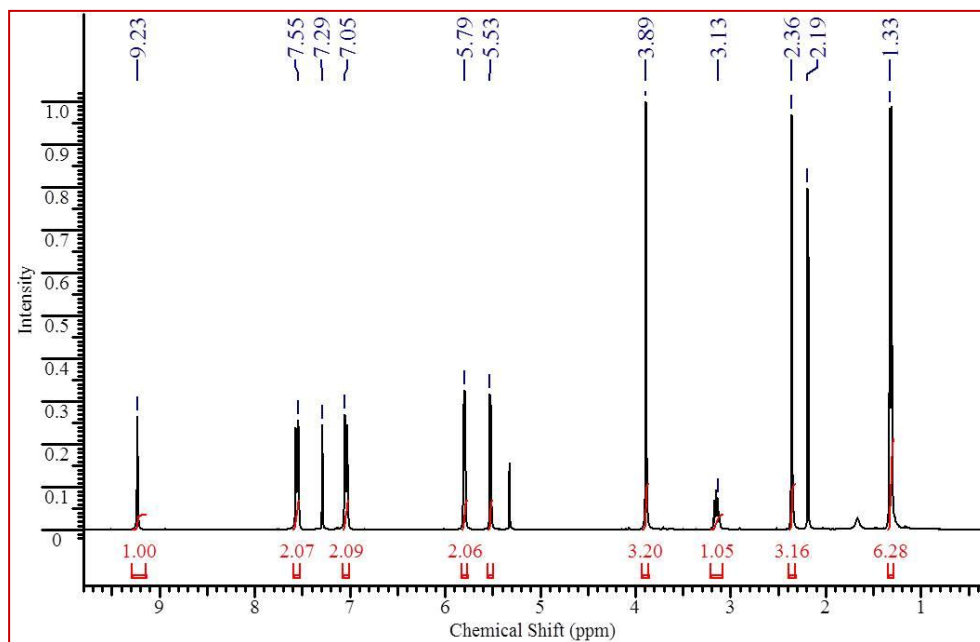


Fig. 4.2: ^1H NMR spectra of complex **13**.

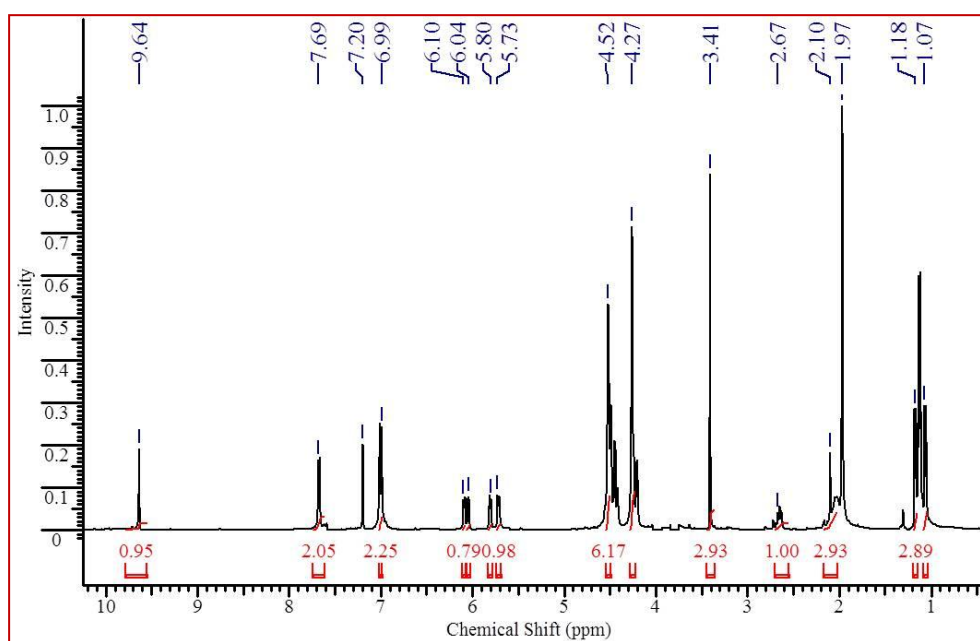


Fig. 4.3: ^1H NMR spectra of complex **14**.

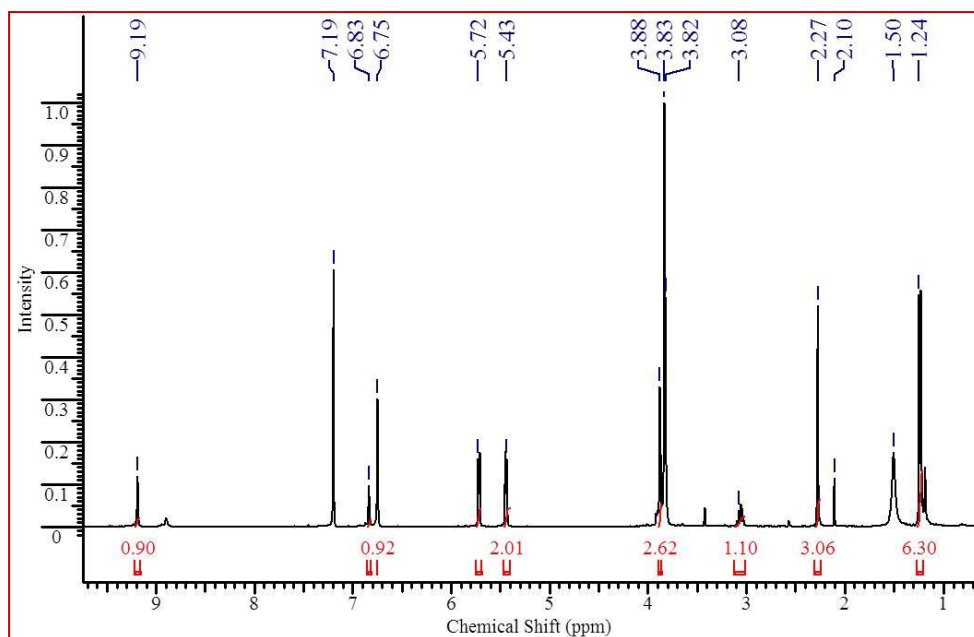


Fig. 4.4: ^1H NMR spectra of complex 17.

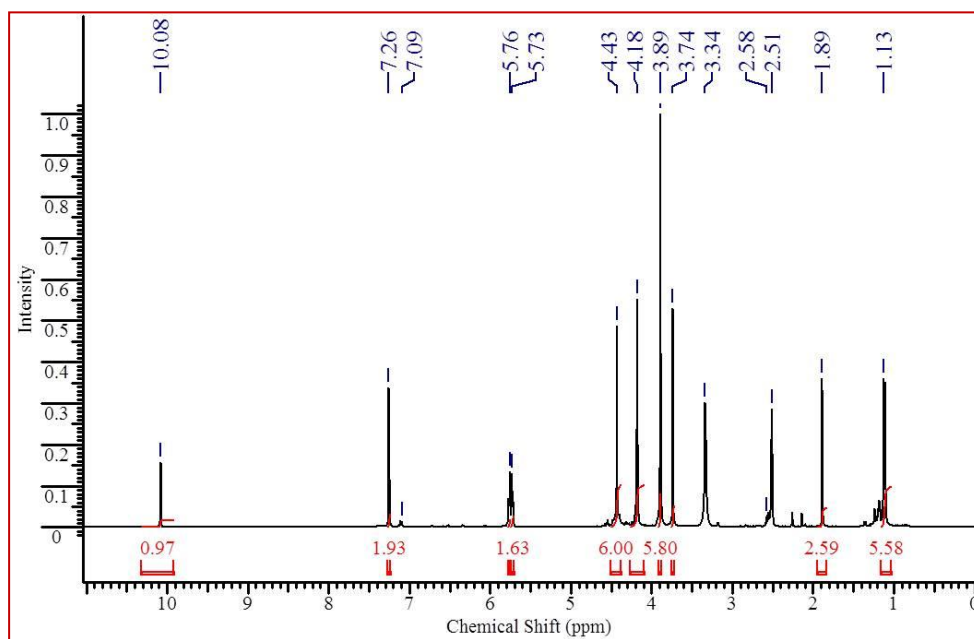


Fig. 4.5: ^1H NMR spectra of complex 18.

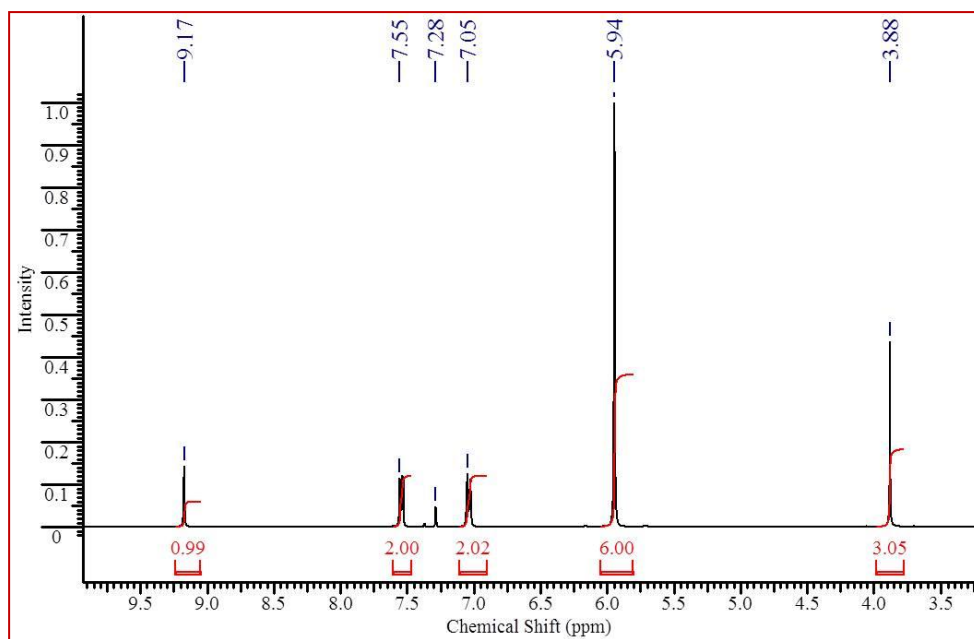


Fig.4.6: ^1H NMR spectra of complex 15.

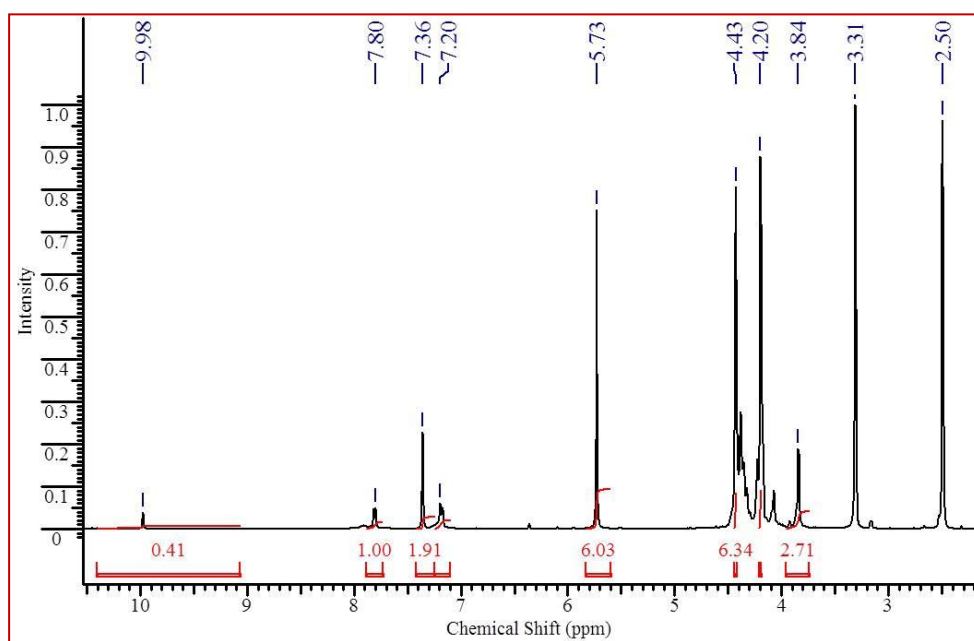


Fig.4.7: ^1H NMR spectra complex 16.

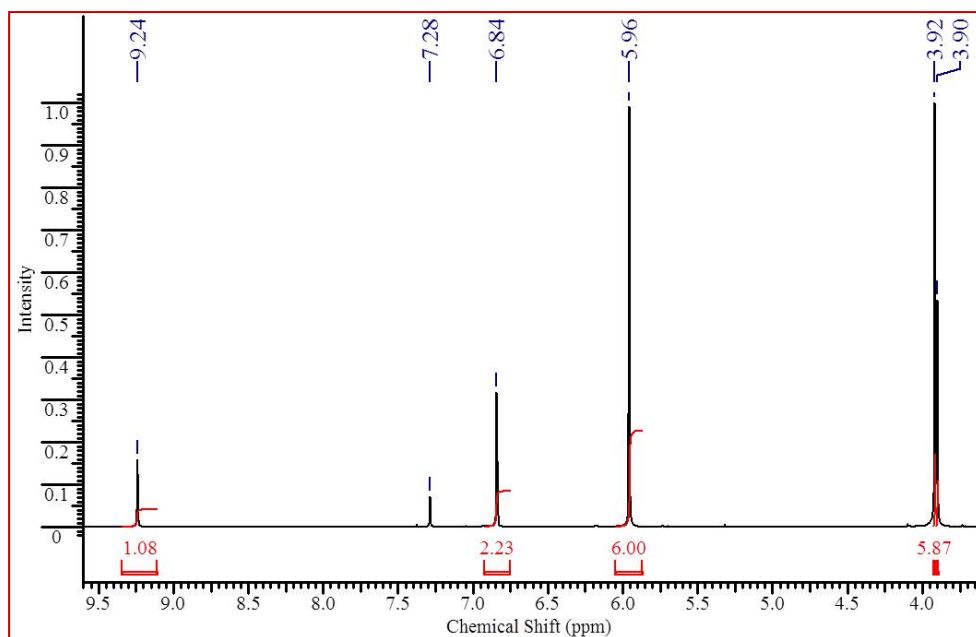


Fig.4.8: ^1H NMR spectra of complex 19.

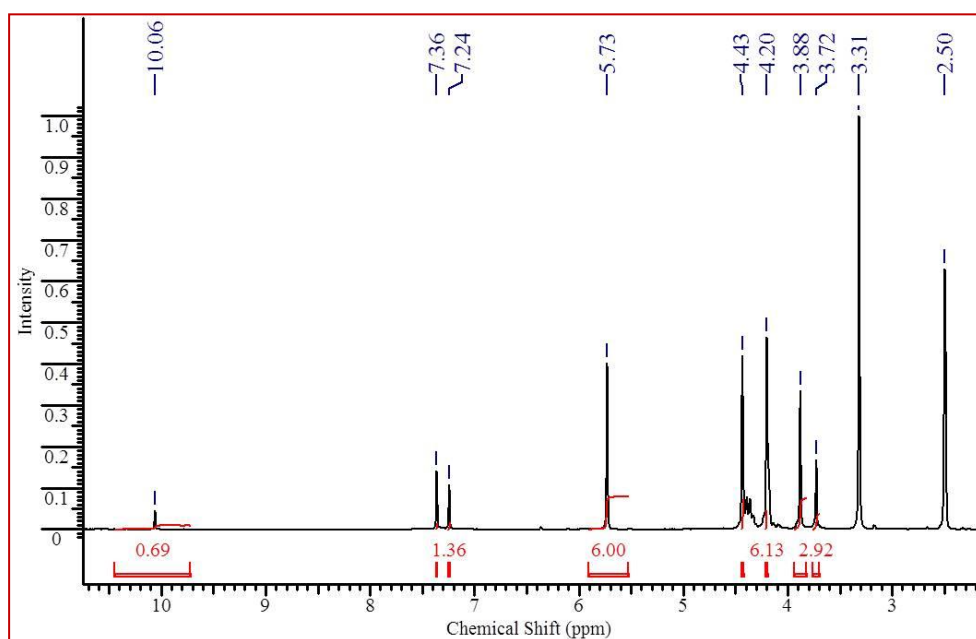


Fig.4.9: ^1H NMR spectra of complex 20.

^{13}C NMR spectra of all the complexes corroborate with the proposed structures (Fig.4.10-Fig.4.17).

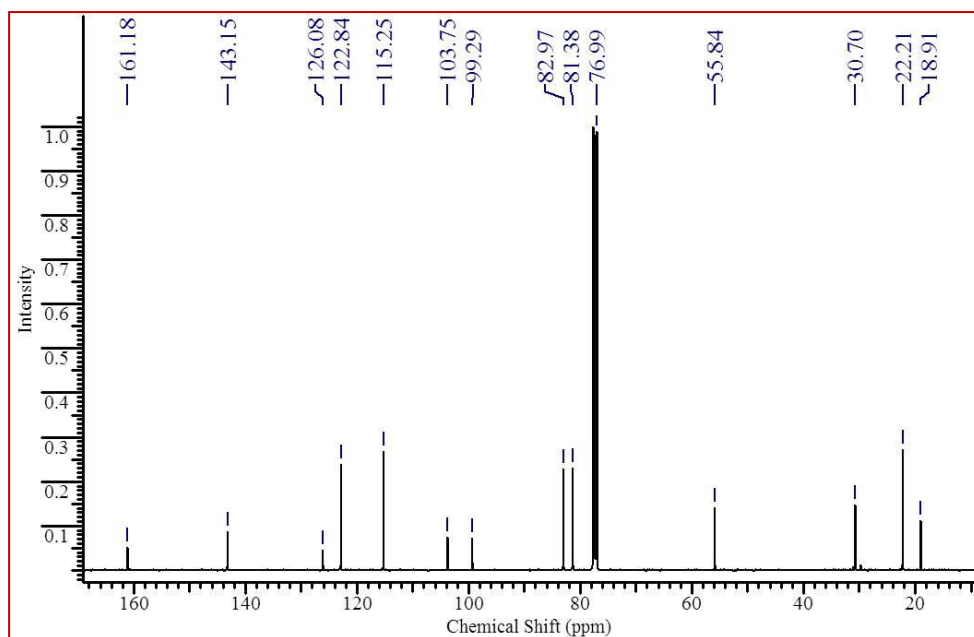


Fig.4.10: ^{13}C NMR spectra of complex 13.

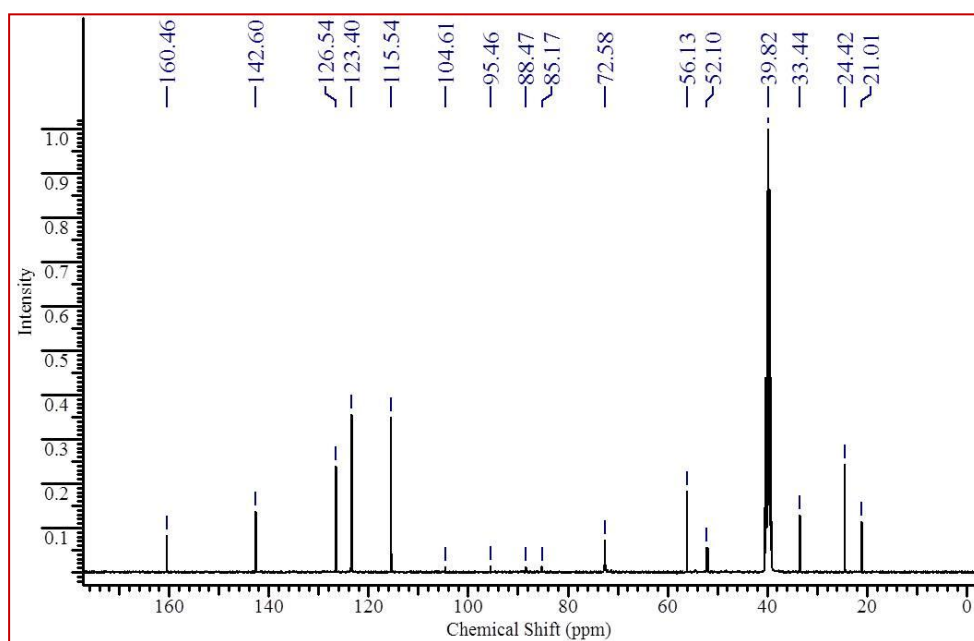


Fig.4.11: ^{13}C NMR spectra of complex 14.

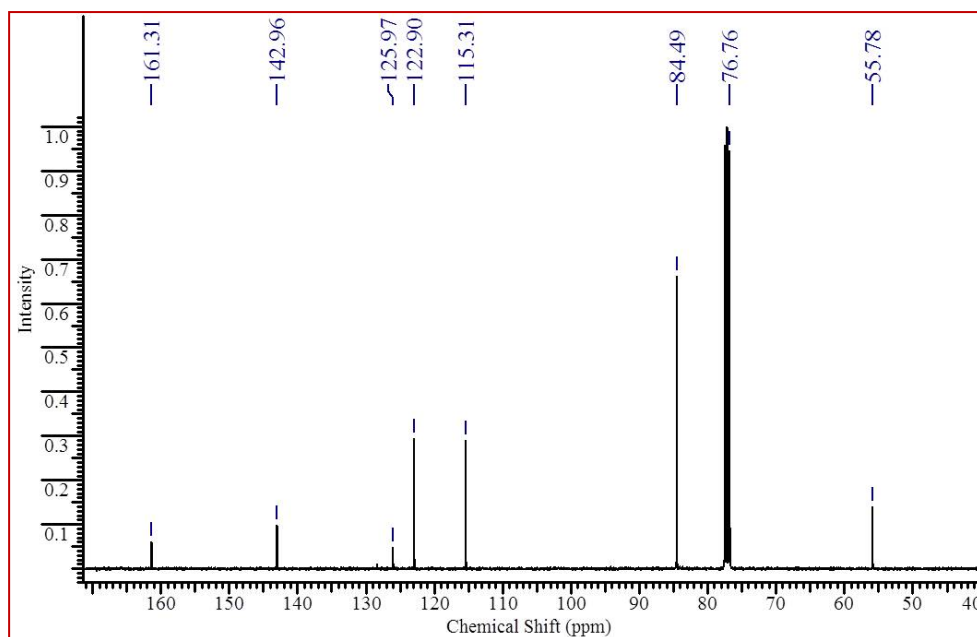


Fig.4.12: ^{13}C NMR spectra of complex 15.

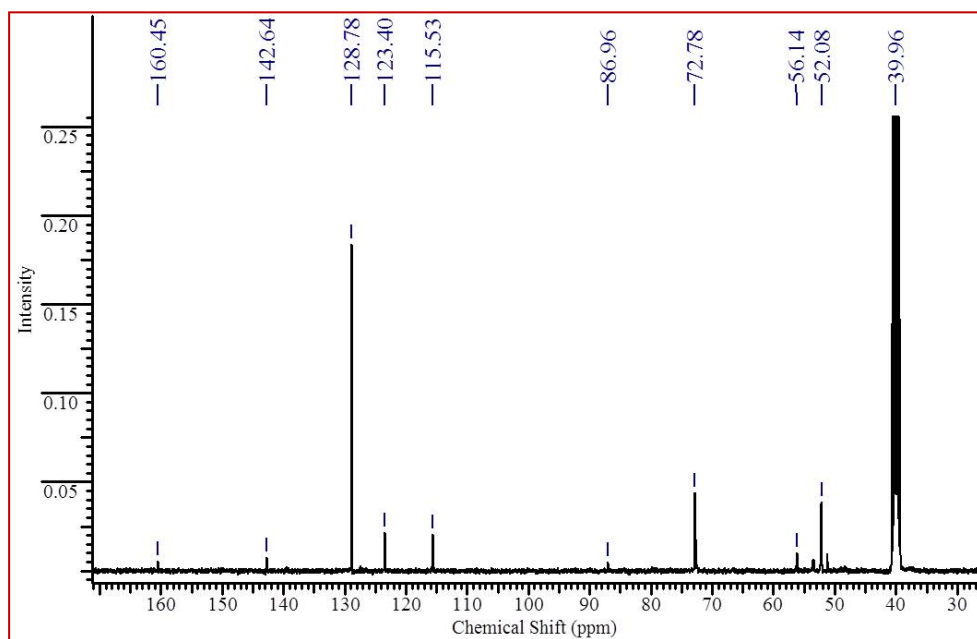


Fig.4.13: ^{13}C NMR spectra of complex 16.

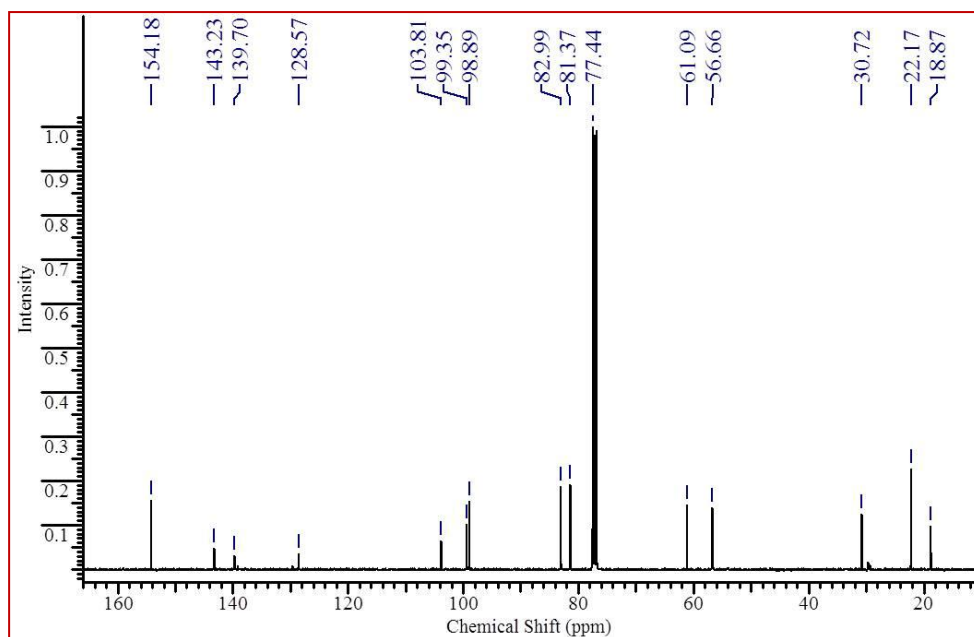


Fig.4.14: ^{13}C NMR spectra of complex 17.

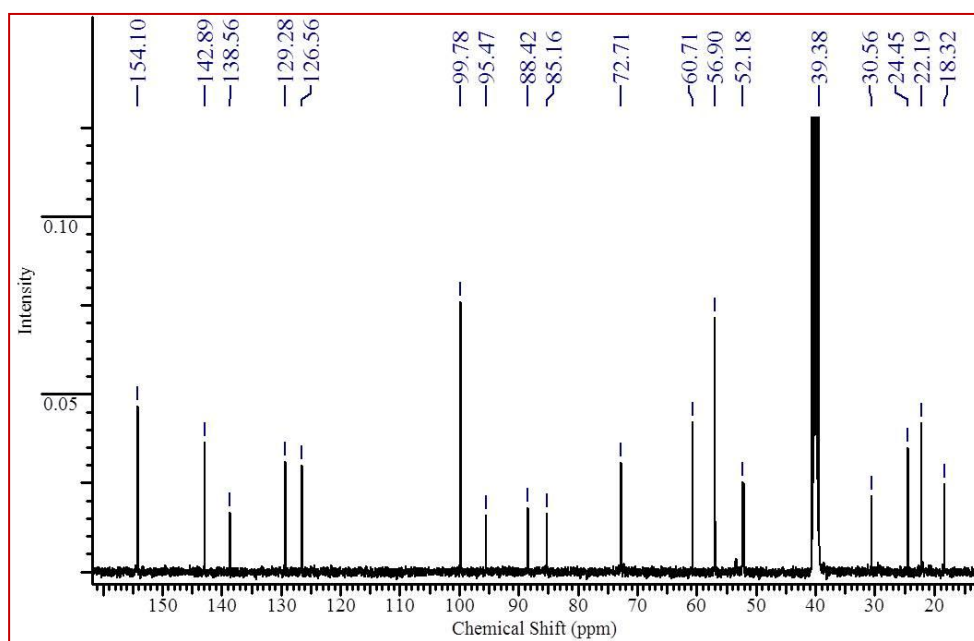


Fig.4.15: ^{13}C NMR spectra of complex 18.

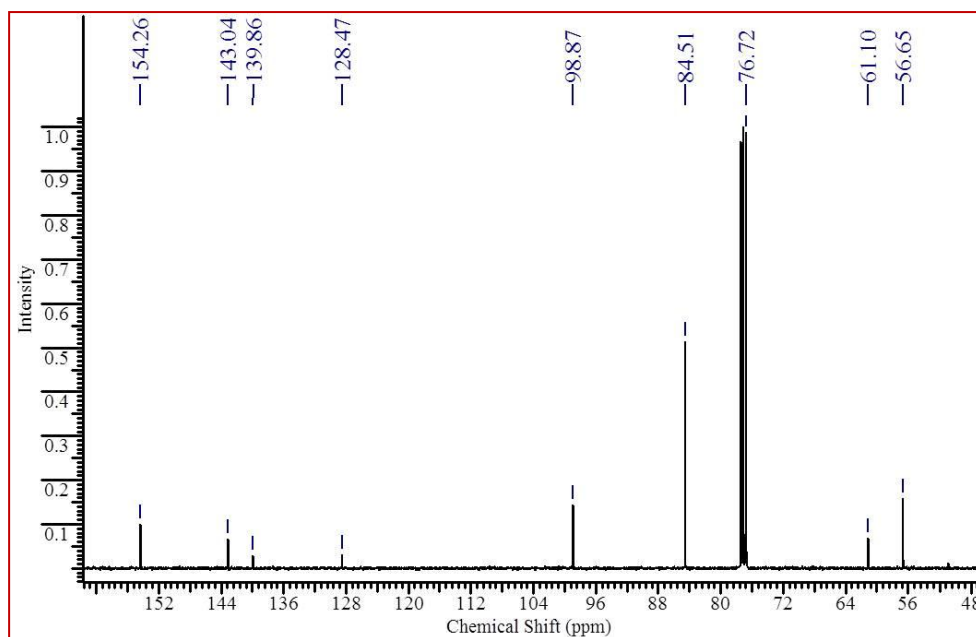


Fig.4.16: ^{13}C NMR spectra of complex **19**.

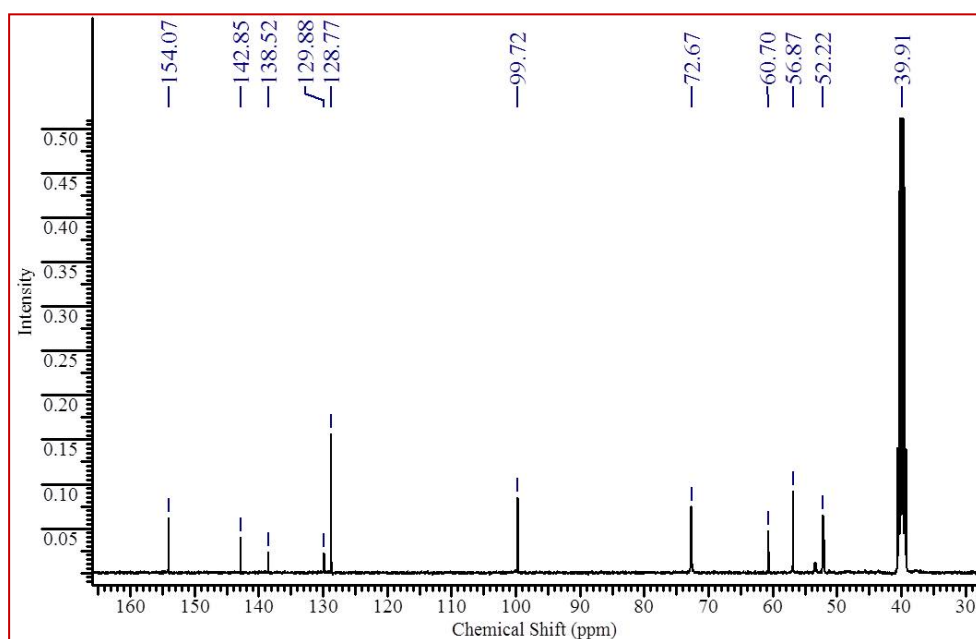


Fig.4.17: ^{13}C NMR spectra of complex **20**.

The ^{31}P NMR spectra of compounds **14**, **16**, **18** and **20** show peaks in the range of -31 to -34 ppm corresponding to the P atom of PTA ligand as reported earlier (Fig.4.18-Fig.4.21).^[19] Again, complex **14** shows an additional septet peak in the range -144 ppm, confirming the presence of $-\text{PF}_6$ moiety in the crystal.

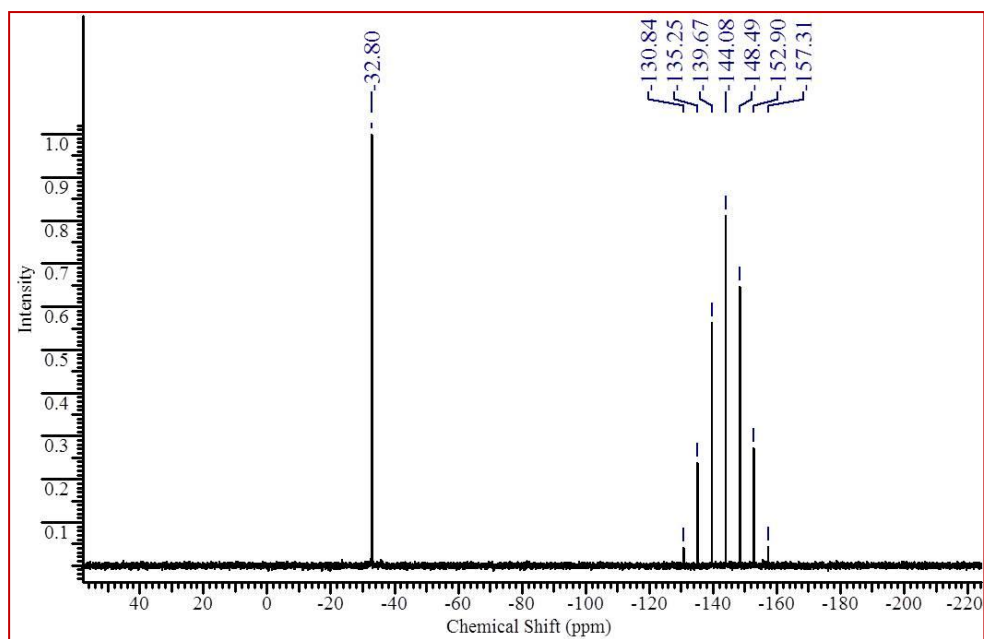


Fig.4.18: ^{31}P NMR spectra of complex 14.

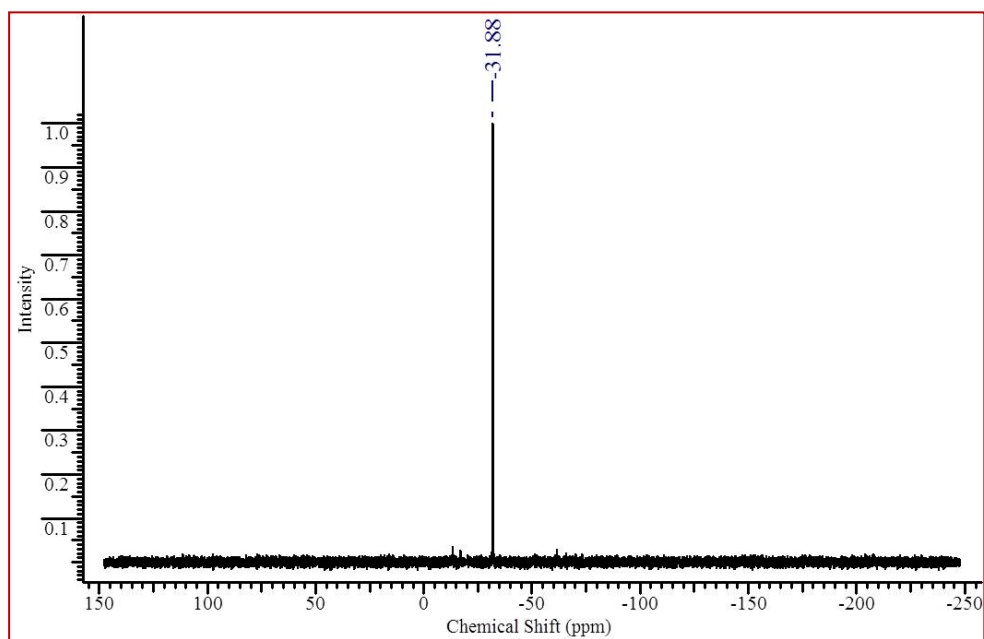


Fig.4.19: ^{31}P NMR spectra of complex 16.

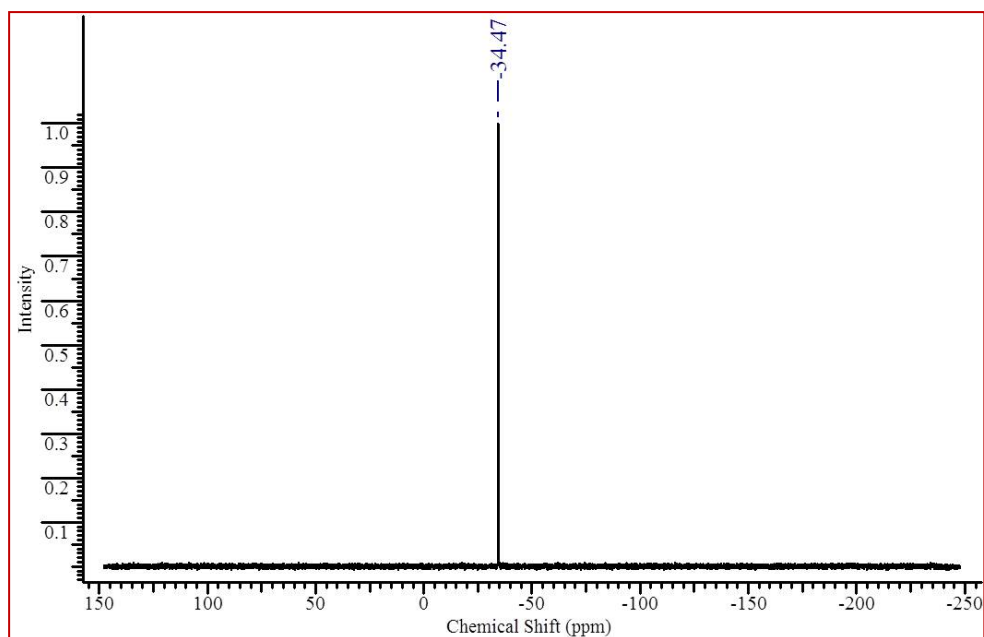


Fig.4.20: ^{31}P NMR spectra of complex 18.

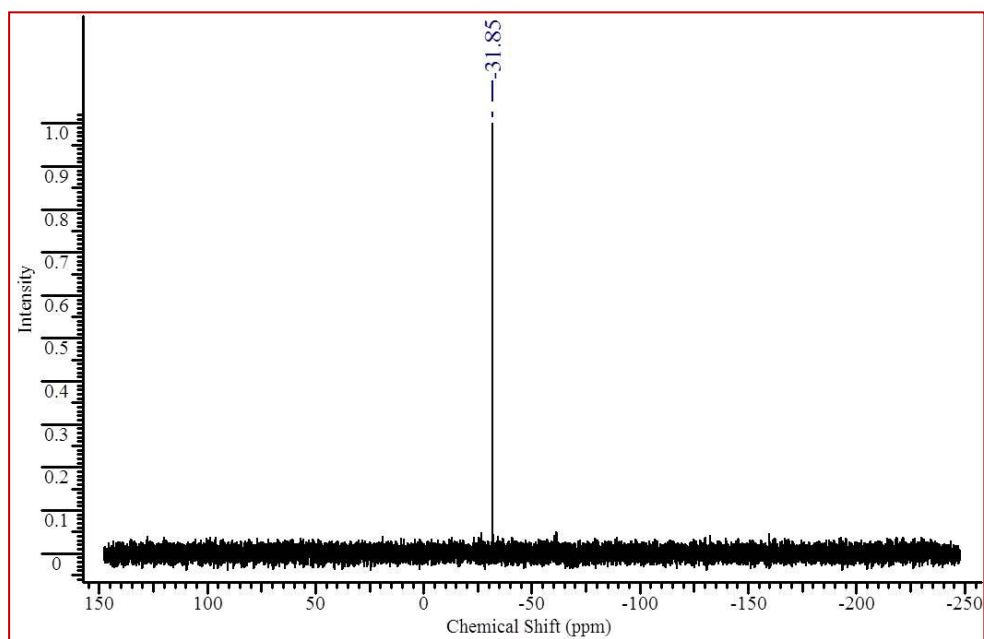


Fig.4.21: ^{31}P NMR spectra of complex 20.

The ESI-MS of **13**, **15**, **17** and **19** show one main peak envelope corresponding to $[\text{Ru}(\eta^6\text{-}p\text{-cymene})(\text{L})\text{Cl}]^+$ moiety after the dissociation of one labile chloride ligand (Fig.4.22-Fig.4.25),

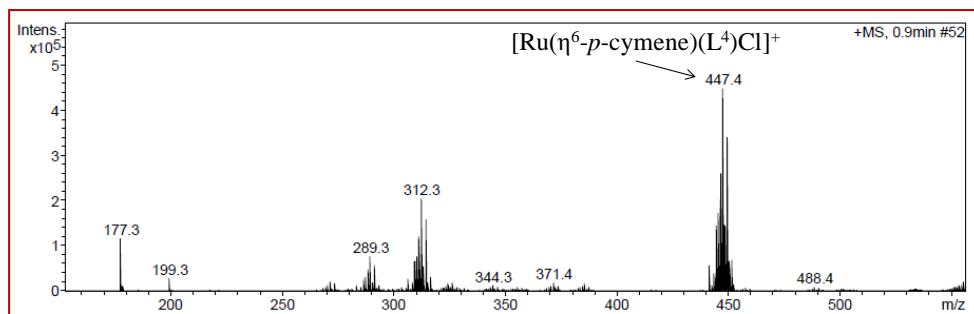


Fig.4.22: ESI-MS spectra of complex 13.

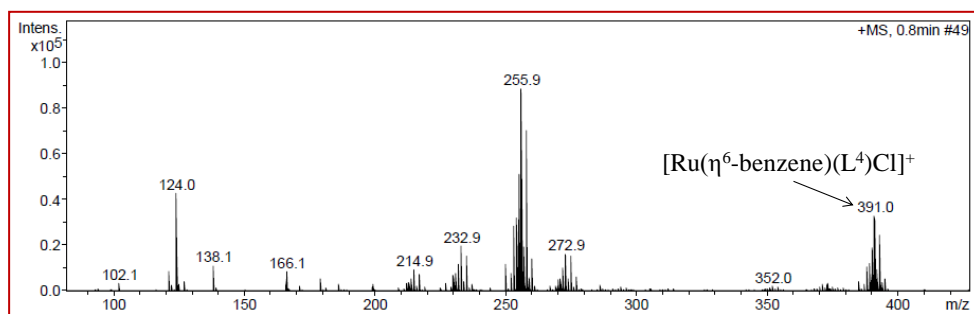


Fig.4.23: ESI-MS spectra of complex 15.

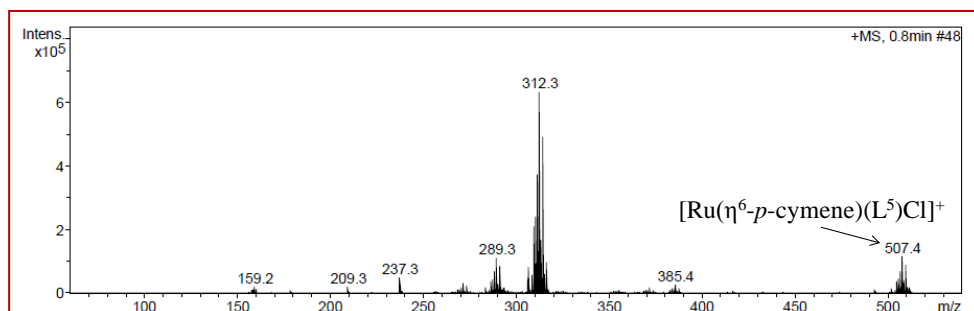


Fig.4.24: ESI-MS spectra of complex 17.

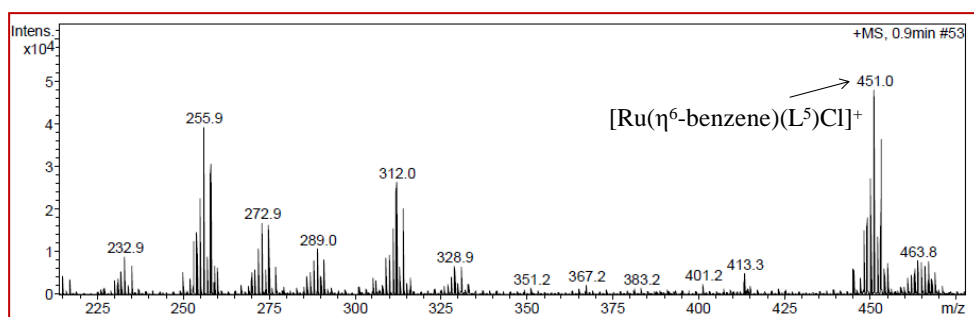


Fig.4.25: ESI-MS spectra of complex 19.

whereas complex 14, 16, 18 and 20 reveal single peak envelope analogous to $[\text{Ru}(\eta^6\text{-}p\text{-cymene})(\text{PTA})\text{Cl}]^+$ cationic complex moiety (Fig.4.26-Fig.4.29).

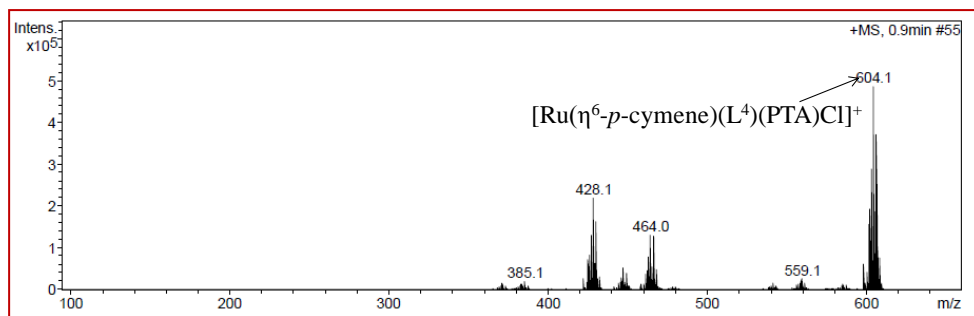


Fig.4.26: ESI-MS spectra of complex **14**.

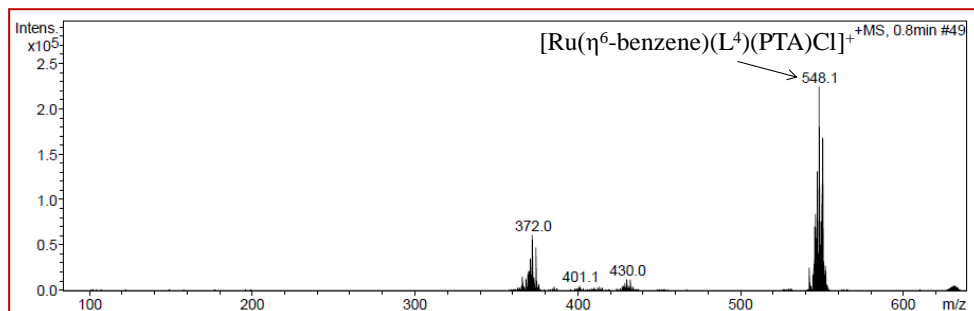


Fig.4.27: ESI-MS spectra of complex **16**.

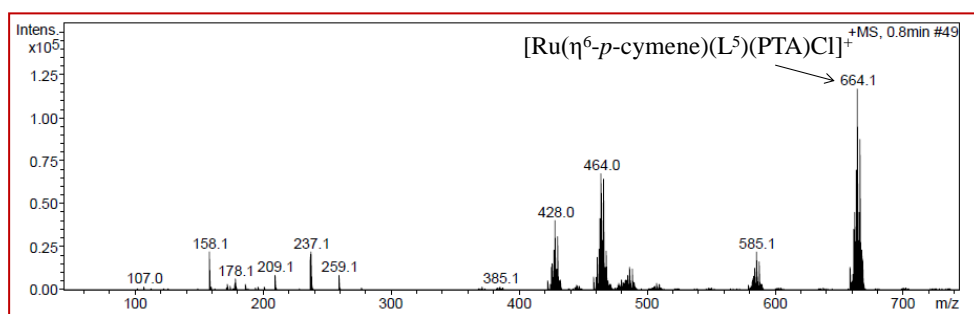


Fig.4.28: ESI-MS spectra of complex **18**.

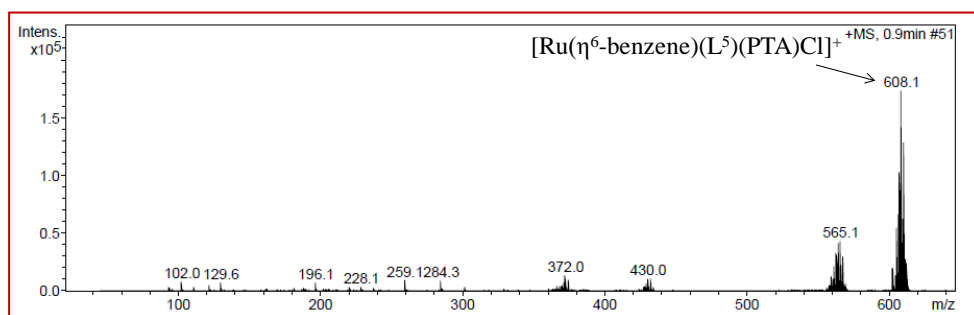


Fig.4.29: ESI-MS spectra of complex **20**.

The solid state structures of complexes **13**, **14**, **15** and **19** have been investigated by X-ray crystallography. All the complexes possess pseudo-octahedral geometry and the η^6 π -bonded arene ring occupies three coordination positions of octahedron. For complex **13**,

15 and **19**, one coordination site is occupied by either 1-(4-methoxyphenyl)-1*H*-tetrazole [for complex **13** and **15**] or 1-(3,4,5-Trimethoxyphenyl)-1*H*-tetrazole [for complex **19**] and other two coordination sites are occupied by two chloride ligands [Fig.4.30-Fig. 4.32].

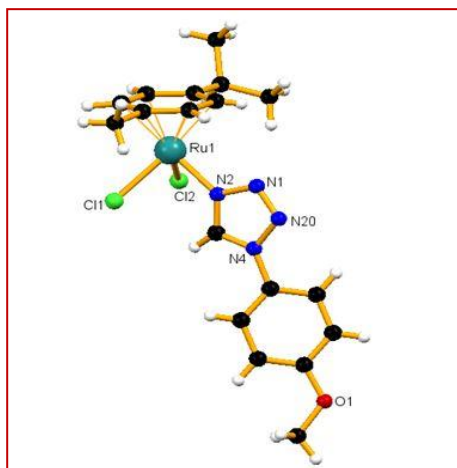


Fig.4.30: The solid state crystal structure of compound **13** with partial atomic numbering scheme. Key bond lengths (Å) and angles (°): $Ru(1)-N(1)$: 2.104(3); $Ru(1)-Cl(1)$: 2.425(2); $Ru(1)-Cl(2)$: 2.412(2); $Ru(1)-C_{centroid}$: 1.666; $Cl(1)-Ru(1)-Cl(2)$: 87.83(4); $Cl(1)-Ru(1)-N(2)$: 85.11(8); $Cl(2)-Ru(1)-N(2)$: 82.71(8).

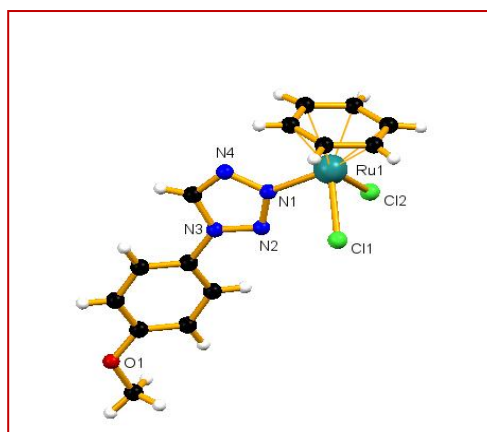


Fig.4.31: The solid state crystal structure of compound **15** with partial atomic numbering scheme. Key bond lengths (Å) and angles (°): $Ru(1)-N(1)$: 2.107(2); $Ru(1)-Cl(1)$: 2.4166(7); $Ru(1)-Cl(2)$: 2.4084(7); $Ru(1)-C_{centroid}$: 1.418; $Cl(1)-Ru(1)-Cl(2)$: 87.43(2); $Cl(1)-Ru(1)-N(2)$: 83.85(6); $Cl(2)-Ru(1)-N(2)$: 84.23(5).

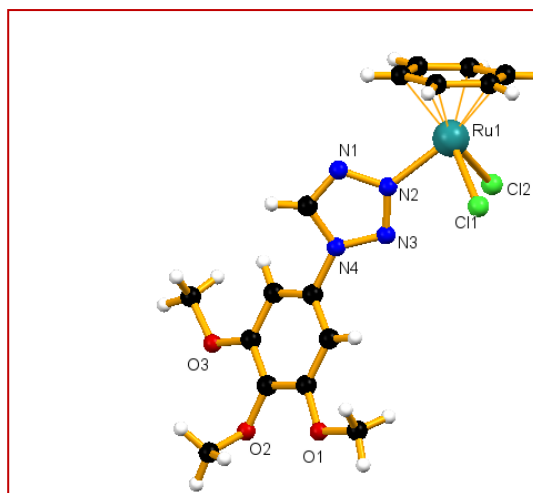


Fig.4.32: The solid state crystal structure of compound **19** with partial atomic numbering scheme. Key bond lengths (Å) and angles (°): $Ru(1)-N(1)$: 2.110(2); $Ru(1)-Cl(1)$; 2.4124(19); $Ru(1)-Cl(2)$: 2.4162(18); $Ru(1)-C_{centroid}$:1.425; $Cl(1)-Ru(1)-Cl(2)$: 88.19(4); $Cl(1)-Ru(1)-N(2)$: 85.22(6); $Cl(2)-Ru(1)-N(2)$: 84.05(6).

In case of complex **14**, one coordination centre is occupied by 1-(4-methoxyphenyl)-1*H*-tetrazole, one is occupied with chloride ligand and the sixth coordination site is occupied by PTA ligand. Complex **14** possesses one PF_6 moiety as counter anion in the crystal lattice [Fig.4.33].

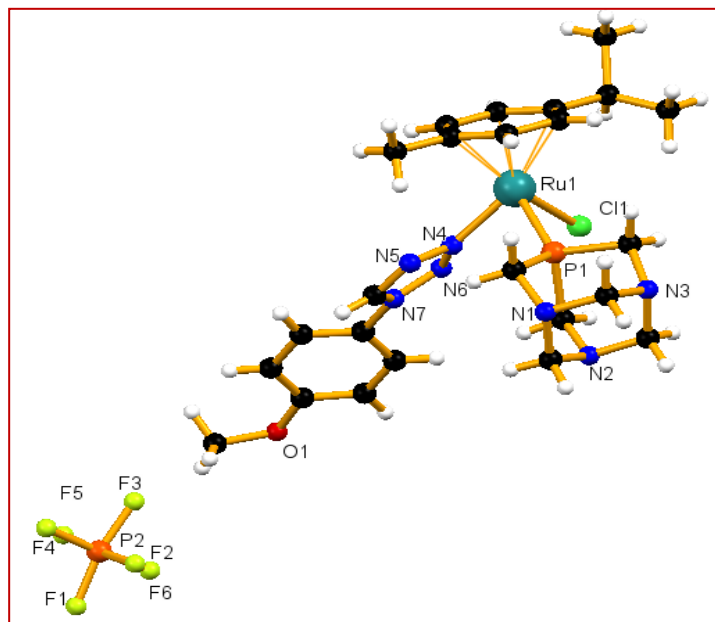


Fig.4.33: The solid state crystal structure of compound **14** with partial atomic numbering scheme. Key bond lengths (Å) and angles (°): $Ru(1)-P(1)$: 2.3099(14); $Ru(1)-N(1)$; 2.103(3); $Ru(1)-Cl(1)$: 2.3952(14); $Ru(1)-C_{centroid}$:1.717; $Cl(1)-Ru(1)-N(4)$: 86.51(7); $N(4)-Ru(1)-P(1)$: 85.28(7); $P(1)-Ru(1)-Cl(1)$: 83.93(3).

4.3.2 Growth inhibition study of prepared complexes

The anticancer activities of the reported complexes as well as free tetrazole ligands have been tested against three different cancer cell lines *viz.*, T Cell leukemia cell line Jurkat, breast cancer cell line MCF7 and cervix cancer cell line HeLa. Results were obtained in terms of GI_{50} (concentration of drug that produces 50% inhibition of the cells), TGI (concentration of the drug that produces total inhibition of the cells) and LC_{50} (concentration of the drug that kills 50% of the cells) using sulforhodamine B (SRB) assay. The cancer cell lines MCF7 and HeLa are widely used to test the effectiveness of ruthenium arene complexes whereas studies on Jurkat cell with ruthenium arene complexes are scarcely reported. All cancer cells were exposed for 24 h to increasing concentrations of the complexes as well as free tetrazole ligands and their proliferation are reported in terms of GI_{50} values. Adriamycin, a chemotherapeutic drug was used as a positive control. It is interesting to report that, although both the free tetrazole ligands are inactive in all the three cell lines, Ru(II) compounds coordinated to those ligands have shown improved cytotoxicity against different cell lines. Complex **13**, **14**, and **17** and have shown substantial antiproliferative activity against HeLa Cell lines, whereas, complex **18** has shown significant antiproliferative activity against Jurkat cell line. In case of Ru(II)-benzene complexes; although complex **19** is either inactive or has shown cytotoxicity at a very higher concentration against all the cell lines, incorporation of PTA ligand by substituting Cl ligand in complex **19** *i.e.* complex **20** has shown quite improved antiproliferative activity against Jurkat and MCF7 cell lines. Whereas between the complexes **15** and **16**, complex **15** has shown good antiproliferative activity against Hela cell line, however incorporation of PTA ligand does not give any improved activity in case of complex **16**. Although there are various reports of Ru(II)-arene chloro complexes as well as RAPTA complexes containing monodentate N-donor ligand with IC_{50} values in μM scale, reports on such type of complexes with GI_{50} value in μM scale are hardly published so far.^[20] The reported complexes which have shown remarkable antiproliferative activities against different cancer cell lines, the difference in numerical

values in terms of GI_{50} parameter are within error margin (in nanomolar level) therefore deduction of any Structure Activity Relationship (SAR) among the reported complexes are not possible without further investigation. However, what is observed is that the introduction of PTA ligand in the ruthenium center has increased the antiproliferative activity in most of the cases against Jurkat and MCF-7 cell lines. However, no such trend is observed in case of HeLa cell lines. All the related data are presented in Table 4.1.

Table 4.1: GI_{50} value ($\mu\text{M}/\text{mL}$) of the prepared complexes in human cancer cell lines.

Complex	Jurkat	MCF7	HeLa
13	>80	>80	1×10^{-4}
14	>80	>80	6.31×10^{-5}
15	inactive	>80	1.46×10^{-4}
16	>80	>80	>80
17	>80	>80	1.3×10^{-4}
18	1.08×10^{-4}	>80	>80
19	inactive	>80	>80
20	6.42×10^{-5}	6.88×10^{-5}	>80
Adriamycin	<0.1	<0.1	<0.1

4.3.3 Protein binding studies

Binding of prospective drug molecules with plasma proteins are very significant as transport of drugs occur through the bloodstream *via* interaction with plasma proteins.^[21] All the complexes were subjected to interact with bovine serum albumin (BSA) and their interactions with protein have been examined through quenching of emission peak arising out of tryptophan residue of BSA. Separate solutions of BSA were titrated against addition of different complexes. In case of BSA binding, addition of reported complexes to the respective protein solution causes significant decrease of initial fluorescence intensity. To get further insight in the

quenching process, the fluorescence quenching data were analyzed with Stern-Volmer equation. The k_q values obtained for all the complexes are found to be in the range of $3.80 \times 10^{11} - 1.31 \times 10^{12} \text{ L mol}^{-1} \text{ s}^{-1}$, indicating the involvement of static quenching mechanism. The binding constant (K_a) and number of binding sites (n) have been determined by Scatchard plot. The value of n for all the complexes are in the range ~ 1 , indicating comparable binding property of the complexes. All the relevant data are compiled in Table 4.2.

Table 4.2: Various parameters obtained from BSA interaction with the prepared complexes.

BSA	$K_{sv}(\text{M}^{-1})$	$K_q(\text{M}^{-1}\text{s}^{-1})$	$K_a(\text{M}^{-1})$	n
Complex 13	8.12×10^3	1.31×10^{12}	2.62×10^4	1.12
Complex 14	3.33×10^3	5.39×10^{11}	3.03×10^2	0.75
Complex 15	2.35×10^3	3.80×10^{11}	1.31×10^2	0.45
Complex 16	5.31×10^3	8.60×10^{11}	2.29×10^7	1.85
Complex 17	2.65×10^3	4.30×10^{11}	5.59×10^3	1.08
Complex 18	4.46×10^3	7.22×10^{11}	3.00×10^2	0.48
Complex 19	7.10×10^3	1.15×10^{12}	2.71×10^4	1.13
Complex 20	3.83×10^3	6.20×10^{11}	1.28×10^5	1.38

4.3.4 Stability study of reported complexes

To understand what might be leading Ru(II)-PTA complexes **14**, **16**, **18**, **20** to be active in different ways against different cancer cell lines, solution stability study of all the four complexes were performed. Very often, it has been observed that dissociation of the M–L bond is the first step for the activation of Ru-complexes in solution.^[22] Thus it is of considerable interest to know the nature of the species generated in solution which is responsible for its cytotoxic behaviour. Thus, the hydrolytic behaviour of the prepared complexes was studied to check its stability under

pseudopharmacological conditions. The decomposition nature of the complexes were studied in 5 mM NaCl solution (corresponding to the low intracellular NaCl concentration in cells) and in 100 mM NaCl solution (corresponding to the higher NaCl levels in blood plasma). Complexes were dissolved in aqueous NaCl ($c = 5$ or 100 mM in D_2O containing 10% $DMSO-d_6$) and maintained at $37^\circ C$ for 7 days. Decomposition of the complexes was monitored using ^{31}P NMR spectroscopy. Complex **14** and **18** undergo partial transformation immediately in both the solutions (5 mM and 100 mM NaCl) with the substitution of the tetrazole ligand with one chloride ions to form $[Ru(p\text{-cym})(PTA)Cl_2]$ which is evident from the typical ^{31}P singlet peak at -30 - -33 ppm along with the parent peak; whereas, complex **16** and **20** also undergo partial substitution by the chloride ligand at a relatively slower rate [after 5-6 days]. The difference in dissociation rate might have some influence for the Ru(II)-PTA complexes to show different degree of antiproliferative activity despite of their structural similarities.

4.4 Conclusion

In this chapter, synthesis of eight new Ru(II)-arene complexes containing two different N-substituted tetrazole co-ligands, which have been selected because of previous reports where heterocyclic ligands have shown enhanced anticancer properties in similar complexes, have been reported. All the compounds have been characterized with different analytical techniques, out of which four complexes have been characterized by X-ray crystallography in solid state. The antiproliferative activities against different cell lines as well as interaction with different biomolecules of the complexes have been explored. In some cases with the introduction of PTA ligands in coordination sphere enhances the water solubility of the complexes and in turn the anticancer activity also increases in terms of GI_{50} values. While the N-substituted tetrazole ligands have mainly shown inactivity against all the cell lines, many of the ruthenium complexes have shown considerable activity. However, the difference in GI_{50} values for different compounds varies to the tune of nanomolar level which prevents

to draw any conclusive structure activity relationship out of the available data. Further investigation is in progress to determine the mechanistic pathway of the active compounds against different cell lines.

4.5 References:

- [1] (a) Albada, B., Metzler-Nolte, N. (2016), Organometallic-peptide bioconjugate: synthetic strategies and medical applications, *Chem. Rev.*, 116(19), 11797-11839. (DOI: 10.1021/acs.chemrev.6b00166)
(b) Fricker, S. P. (2007), Metal based drugs: from serendipity to design, *Dalton Trans.*, 4903-4917. (DOI: 10.1039/B705551J)
- [2] Bijelic, A., Theiner, S., Keppler, B. K., Rompel, A. (2016), X-ray structure analysis of indazolium trans-[tetrachlorobis (1*H*-indazole) ruthenate (III)] (KP 1019) bound to human serum albumin reveals two ruthenium binding sites and provides insights into the drug binding mechanism, *J. Med. Chem.*, 59(12), 5894-5903. (DOI: 10.1021/acs.jmedchem.6b00600)
- [3] Hartinger, C. G., Jakupec, M. A., Zorbas-Seifried, S., Groessl, M., Egger, A., Berger, W., Zorbas, H., Dyson, P. J., Keppler, B. K. (2008), KP1019, A new redox-active anticancer agent-preclinical development and results of a clinical phase I study in tumor patients, *Chem. Biodiversity*, 5, 2140-2155. (DOI: 10.1002/cbdv.200890195)
- [4] Sava, G., Zorzet, S., Turrin, C., Vita, F., Soranzo, M., Zabucchi, G., Cocchietto, M., Bergamo, A., DiGiovine, S., Pezzoni, G., Sartor, L., Garbisa, S. (2003), Dual action of NAMI-A in inhibition of solid tumor metastasis: selective targeting of metastatic cells and binding to collagen, *Clin. Cancer Res.*, 9, 1898-1905. (DOI: clincancerres.aacrjournals.org/content/9/5/1898)
- [5] Rademaker-Lakhai, J. M., van den Bongard, D., Pluim, D., Beijnen, J. H., Schellens, J. H. M. (2004), A Phase I and pharmacological study with imidazolium-*trans*-DMSO-imidazole-tetrachlororuthenate, a novel ruthenium anticancer agent, *Clin. Cancer Res.*, 10, 3717-3727. (DOI: clincancerres.aacrjournals.org/content/10/11/3717)

- [6] Schuecker, R., John, R., Jakupec, M. A., Arion, V. B., Keppler, B.K. (2008), Water-soluble mixed-ligand ruthenium(II) and osmium(II) arene complexes with high antiproliferative activity, *Organometallics*, 27, 6587–6595. (DOI: 10.1021/om800774t)
- [7] (a) Arce, E. R., Sarniguet, C, Moraes, T. S., Vieites, M, Tomaz, A. I., Medeiros, A., Comini, M. A., Varela, J., Cerecetto, H., González, M., Marques, F., García, M. H., Otero, L., Gambino, D. (2015), A new ruthenium cyclopentadienyl azole compound with activity on tumor cell lines and trypanosomatid parasites, *J. Coord. Chem.*, 68(16), 2923–2937. (DOI: 10.1080/00958972.2015.1062480) (b) Martínez, A., Carreon, T., Iniguez, E., Anzellotti, A, Sánchez, A., Tyan, M., Sattler, A., Herrera, L., Maldonado, R. A., Sánchez-Delgado, R. A. (2012), Searching for new chemotherapies for tropical diseases: ruthenium–clotrimazole complexes display high *in vitro* activity against *leishmania major* and *trypanosoma cruzi* and low toxicity toward normal mammalian cells, *J. Med. Chem.*, 55(8), 3867-3877. (DOI: 10.1021/jm300070h)
- [8] Pettit, G. R., Singh, S. B., Hamel, E., Lin, C. M., Alberts, D. S., Garcia-Kendall, D. (1989), Isolation and structure of the strong cell growth and tubulin inhibitor combretastatin A-4, *Experientia*, 45, 209-211. (DOI: 10.1007/BF01954881)
- [9] Romagnoli, R., Baraldi, P. G., Prencipe, F., Oliva, P., Baraldi, S., Tabrizi, M. A., Lopez-Cara, L. C., Ferla, S., Brancale, A., Hamel, E., Ronca, R., Bortolozzi, R., Mariotto, E., Basso, G., Viola, G. (2016), Design and synthesis of potent *in vitro* and *in vivo* anticancer agents based on 1-(3',4',5'-trimethoxyphenyl)-2-Aryl-1*H*-imidazole, *Sci. Rep.* 6:26602, 1-17. (DOI: 10.1038/srep26602)
- [10] Bisby, R. H., Botchway, S. W., Hadfield, J. A., McGowan, A. T., Parker, A. W., Scherer, K. M. (2012), Fluorescence lifetime imaging of E-combretastatin uptake and distribution in live mammalian cells, *Eur. J. Cancer*. 48, 1896-1903. (DOI: 10.1016/j.ejca.2011.11.025)
- [11] Bellina, F., Cauteruccio, S., Monti, S., Rossi, R. (2006), Novel imidazole-based combretastatin A-4 analogues: Evaluation of their *in vitro* antitumor activity and molecular modeling study of their

- binding to the colchicine site of tubulin, *Bioorg. Med. Chem. Lett.* 16, 5757-5762. (DOI: 10.1016/j.bmcl.2006.08.087)
- [12] Wang, L., Woods, K. W., Li, Q., Barr, K. J., McCroskey, R. W., Hannick, S. M., Gherke, L., Credo, R. B., Hui, Y., Marsh, K., Warner, R., Lee, J. Y., Zielinski-Mozng, N., Frost, D., Rosenberg, S. H., Sham, H. L. (2002), Potent, orally active heterocycle-based combretastatin A-4 analogues: synthesis, structure-activity relationship, pharmacokinetics, and in vivo antitumor activity evaluation, *J. Med. Chem.* 45, 1697-1711. (DOI: 10.1021/jm010523x)
- [13] Romagnoli, R., Baraldi, P. G., Cara, C. L., Salvador, M. K., Bortolozzi, R., Basso, G., Viola, G., Balzarini, J., Brancale, A., Fu, X., Li, J., Zhang, S., Hamel, E. (2011), One-pot synthesis and biological evaluation of 2-pyrrolidinyl-4-amino-5-(3',4',5'-trimethoxybenzoyl)thiazole: a unique, highly active antimicrotubule agent, *Eur. J. Med. Chem.* 46, 6015-6024. (DOI: 10.1016/j.ejmech.2011.10.013)
- [14] Tron, G. C., Pirali, T., Sorba, G., Pagliai, F., Busacca, S., Genazzani, A. A. (2006), Medicinal chemistry of Combretastatin A4: present and future directions, *J. Med. Chem.*, 49(11), 3033-3044. (DOI: 10.1021/jm0512903)
- [15] Shan, Y., Zhang, J., Liu, Z., Wang, M., Dong, Y. (2011), Developments of combretastatin A-4 derivatives as anticancer agents, *Curr. Med. Chem.*, 18(4), 523-538. (DOI: 10.2174/092986711794480221)
- [16] Romagnoli, R., Baraldi, P. G., Salvador, M. K., Preti, D., Tabrizi, M. A., Brancale, A., Fu, X., Li, J., Zhang, S., Hamel, E., Bortolozzi, R., Basso, G., Viola, G. (2012), Synthesis and evaluation of 1,5-disubstituted tetrazoles as rigid analogues of combretastatin A-4 with potent antiproliferative and antitumor activity, *J. Med. Chem.* 55, 475-488. (DOI: 10.1021/jm2013979)
- [17] Sanghamitra, N. J. M, Adwankar, M. K., Juvekar, A. S., Khurajjam, V., Wycliff, C., Samuelson, A. G. (2011), Copper(I) complexes of modified nucleobases and vitamin B3 as potential chemotherapeutic

- agents: *In vitro* and *in vivo* studies, Indian J. Chem., Sect. A: Inorg., Bio-inorg., Phys., Theor. Anal. Chem., 50, 465-473. (DOI: <http://hdl.handle.net/123456789/11243>)
- [18] (a) Yan, J., Hu, J., An, B., Huang, L., Li, X. (2017), Design, synthesis, and biological evaluation of cyclic-indole derivatives as anti-tumor agents via the inhibition of tubulin polymerization, Eur. J. Med. Chem. 125, 663-675 (DOI: [dx.doi.org/10.1016/j.ejmech.2016.09.056](https://doi.org/10.1016/j.ejmech.2016.09.056)) (b) Gerova, M. S., Stateva, S. R., Radonova, E.M., Kalenderska, R. B., Rusew, R.I., Nikolova, R. P., Chaney, C. D., Shivachev, B. L., Apostolova, M. D., Petrov, O. I. (2016), Combretastatin A-4 analogues with benzoxazolone scaffold: Synthesis, structure and biological activity, Eur. J. Med. Chem., 120, 121-133 (DOI: [10.1016/j.ejmech.2016.05.012](https://doi.org/10.1016/j.ejmech.2016.05.012)) (c) Mowery, P., Mejia, F. B., Franceschi, C. L., Kean, M. H., Kwansare, D. O., Lafferty, M. M., Neerukonda, N. D., C. E., Rolph, Truax, N. J., Pelkey, E. T. (2017), Synthesis and evaluation of the anti-proliferative activity of diaryl-3-pyrrolin-2-ones and fused analogs, Bioorg. Med. Chem. Lett., 27, 191-195. (DOI: [10.1016/j.bmcl.2016.11.076](https://doi.org/10.1016/j.bmcl.2016.11.076))
- [19] Mandal, P., Malviya, N., Guedes da Silva, M. F.C., Dhankhar, S. S., Nagaraja, C. M., Mobin, S. M., Mukhopadhyay, S. (2016), Fine tuning through valence bond tautomerization of ancillary ligands in ruthenium(II) arene complexes for better anticancer activity and enzyme inhibition properties, Dalton Trans. 45, 19277-19289. (DOI: [10.1039/c6dt02969h](https://doi.org/10.1039/c6dt02969h))
- [20] (a) Renfrew, A. K., Juillerat-Jeanneret, L., Dyson, P. J. (2011), Adding diversity to ruthenium(II)-arene anticancer (RAPTA) compounds via click chemistry: The influence of hydrophobic chains, J. Organomet. Chem., 696, 772-779. (DOI: [10.1016/j.jorganchem.2010.09.067](https://doi.org/10.1016/j.jorganchem.2010.09.067)) (b) Chuklin, P., Chalermpanaphan, V., Nhugeaw, T., Saithong, S., Chainok, K., Phongpaichit, S., Ratanaphan, A., Leesakul, N. (2017), Synthesis, X-ray structure of organometallic ruthenium (II) *p*-cymene complexes based on P- and N- donor ligands and their *in vitro* antibacterial and

- anticancer studies, *J. Organomet. Chem.*, 846, 242-250. (DOI: 10.1016/j.jorganchem.2017.06.017) (c) Grau, J., Noe, V., Ciudad, C., Prieto, M. J., Font-Bardia, M., Calvet, T., Moreno, V. (2012), New π -arene ruthenium(II) piano-stool complexes with nitrogen ligands, *J. Inorg. Biochem.*, 109, 72-81. (DOI: 10.1016/j.jinorgbio.2012.01.003) (d) Vock, C. A., Scolaro, C., Phillips, A. D., Scopelliti, R., Sava, G., Dyson, P. J. (2006), Synthesis, characterization, and *in vitro* evaluation of novel ruthenium(II) η^6 -arene imidazole complexes, *J. Med. Chem.*, 49, 5552-5561. (DOI: 10.1021/jm060495o)
- [21] Ganeshpandian, M., Loganathan, R., Suresh, E., Riyasdeen, A., Akbarsha, M. A., Palaniandavar, M. (2014), New ruthenium(II) arene complexes of anthracenyl appended diazacycloalkanes: effect of ligand intercalation and hydrophobicity on DNA and protein binding and cleavage and cytotoxicity, *Dalton Trans.* 43, 1203-1219. (DOI: 10.1039/c3dt51641e)
- [22] Mitra, R., Samuelson, A. G. (2014), Substitution-modulated anticancer activity of half-sandwich Ruthenium(II) complexes with heterocyclic ancillary ligands, *Eur. J. Inorg. Chem.*, 22, 3536-3546. (DOI: 10.1002/ejic.201402205)

Chapter 5

RAPTA Complexes Containing Ferrocenamide Ligands: Synthesis, Characterisation and Antiproliferative Activity Against Cancer Cell Lines

5.1 Introduction

In the quest of a metal based anticancer drug, introduction of a second metal atom in designing a prospective molecule as potential agent has been explored in recent times.^[1-4] Ferrocene based bimetallic complexes have been studied extensively owing to its favourable electronic properties, negligible intrinsic toxicity of the ferrocenyl group and ease of functionalization.^[5-7] Moreover, oxidation of ferrocene produces ferrocenium cation, which has the ability to show cytotoxic activity against different cancerous cell lines by oxidative DNA cleavage involving Reactive Oxygen Species (ROS).^[8-10] Jaouen *et al* reported analogue of breast cancer drug tamoxifen, known as ferrocifen from 1-[4-(2-dimethylaminoethoxy)]-1-(phenyl-2-ferrocenylbut-1-ene), which has shown high antiproliferative activity owing to its combined action of the organic molecule with Fenton chemistry at the Fe centre.^[11-14] Ferroquine, ferrocene conjugated analogue of chloroquine, has been found to be more effective as antimalarial drug than chloroquine itself.^[15]

In order to develop heterometallic anticancer drug with synergistic effect between two metal atoms, ferrocene molecule has been coupled with various transition metal atoms. Ferrocenyl ethynyl and ferrocenyl *N*-heterocyclic carbene gold(I) complexes have been reported to show significant cytotoxicity against different cancer cell lines.^[16,17] Recently, ferrocene conjugated platinum(II) complexes have been found as cytotoxic agents showing similar activity as cisplatin against MCF7 and A2780 cancer cells.^[18,19] Few ferrocene complexes containing rhodium, iridium and palladium metal have displayed growth inhibition property similar to that of the widely used chemotherapeutic agent, cisplatin.^[20-23] Although there are a number of reports where ruthenium and ferrocene have been combined together and their antiproliferative activity have been evaluated^[24-30], reports on synthesis and biological activity of RAPTA type complexes incorporating ferrocene derivatives are only handful.^[31]

In many cases, cancer cells are overexpressed with peptide receptors than the normal cells. Therefore,

attachment of a cytotoxic drug to a peptide moiety can be a promising strategy for tumour targeting in terms of therapeutic as well as diagnostic purpose.^[32] This targeted anticancer approach will result in therapeutic agents with increased tumour selectivity and decreased toxicity in normal tissues.^[33] Recently few reports have been published where picolinamide or carboxamide complexes have shown interesting anticancer properties due to their dynamic coordinating nature to the metal centre.^[34,35]

Considering all the above facts, combining the advantage of ferrocenyl moiety with RAPTA type of complexes in presence of amide ligands has been taken up. Chapter 5 describes synthesis of two ferrocenyl picolinamide ligands (**HL**⁷ and **HL**⁸) followed by generation of two Ru-Fc compounds taking **HL**⁷ and **HL**⁸ as coligands and their RAPTA analogues. All the complexes have been tested for their antiproliferative activity against different cell lines and their electrochemical properties as well as DNA binding affinity have also been evaluated.

5.2 Experimental Section

5.2.1 Materials and methods

All the required chemicals were purchased from Sigma and used without further purification. The specifications of all the instruments used for analysis purpose were same as described in the section 2.2.1 of the chapter 2. Sulforhodamine B (SRB) growth inhibition (GI₅₀) assays were carried out by the Advanced Centre for Treatment, Research and Education in Cancer (ACTREC), Mumbai, by following the literature procedure described in chapter 2.

5.2.1.1 Synthesis of [C₅H₅FeC₅H₄-C₆H₄-NHCO-C₅H₄N].C₇H₈ [**HL**⁷]

Dark orange crystals of 4-ferrocenyl aniline (0.74 g, 2.5 mmol) was added into a solution of pyridine-2-carboxylic acid (0.3 g, 2.5 mmol) dissolved in pyridine (1.0 mL). The mixture was stirred under heating at 110°C for 30 min. In to the hot mixture, 0.65 mL of triphenyl phosphite (2.5 mmol) was

added and stirred under heating at 110°C for 4 h. The reaction mixture was cooled and 2 mL DCM was added to it. Then the mixture was added in to 5 mL of distilled water. Finally the mixture was extracted with 5 mL of 1:1 (v/v) aq. HCl, from which crude product was obtained in DCM extract. Single crystal for the ligand **HL**⁷ was obtained from the slow diffusion of diethyl ether to the toluene solution of the complex. ¹H NMR (400.13 MHz, DMSO-*d*₆): 9.34 [s, 1H, C₅H₄CONH], 8.76 [d, 1H NC₅H₄], 8.17 [d, 1H, NC₅H₄], 8.08, [t, 1H, NC₅H₄], 7.87 [d, 2H, C₆H₄], 7.69 [t, 1H, NC₅H₄], 7.55 [d, 2H, C₆H₄], 7.16 [t, 2H, C₇H₈], 6.74 [m, 3H, C₇H₈], 4.78 [br.s, 2H, C₅H₄], 4.33 [br.s, 2H, C₅H₄], 4.03 [s, 5H, C₅H₅]. ¹³C NMR (100.61 MHz, DMSO-*d*₆): δ162.7 [C of CONH], 157.7 [CH of C₅H₄N], 150.3 [C of C₅H₄N], 148.9 [C of C₆H₄], 138.6 [CH of C₅H₄N], 136.6 [C of C₇H₈], 129.8 [C of C₆H₄ and 2×CH of C₇H₈], 127.3 [2×CH of C₆H₄ and 2×CH of C₇H₈], 126.5 [CH of C₅H₄N and CH of C₇H₈], 122.7 [CH of C₅H₄N], 115.6 [2×CH of C₆H₄], 85.1 [C of C₅H₄], 69.7 [5×CH of C₅H₅], 69.1 [2×CH of C₅H₄], 66.4 [2×CH of C₅H₄]. Anal. Calcd for C₂₉H₂₆FeN₂O: C, 73.43; H, 5.52; N: 5.91. Found: C, 73.53; H, 5.73; N, 5.43.ESI-MS (+ve mode): [C₂₂H₁₈FeN₂O+H]⁺ 383.1 (m/z).

5.2.1.2 Synthesis of [C₅H₅FeC₅H₄-C₆H₄-NHCO-C₉H₆N] [**HL**⁸]

HL⁸ was prepared following the similar procedure as **HL**⁷ using isoquinoline-1-carboxylic acid. Single crystal for the ligand **HL**⁸ was obtained by the slow diffusion of hexane in to the DCM solution. ¹H NMR (400.13 MHz, CDCl₃): 10.27 [s, 1H, NC₉H₆CONH], 9.69 [d, 1H, C₉H₆N], 8.47 [d, 1H, C₉H₆N], 7.79 [m, 2H, C₆H₄], 7.68 [m, 4H, C₉H₆N], 7.46 [d, 2H, C₆H₄], 4.59 [br.s, 2H, C₅H₄], 4.25 [br.s, 2H, C₅H₄], 3.99 [s, 4H, C₅H₅]. ¹³C NMR (100.61 MHz, CDCl₃): δ: 165.0 [C of CONH], 158.8 [C of C₉H₆N], 142.8 [C of C₆H₄], 135.2 [CH of C₉H₆N], 132.9 [C of C₉H₆N], 131.3 [CH of C₉H₆N], 130.5 [C of C₆H₄], 125.9 [2×CH of C₆H₄], 124.2 [CH of C₉H₆N], 123.1 [CH of C₉H₆N], 122.6 [CH of C₉H₆N], 122.2 [C of C₉H₆N], 121.9 [CH of C₉H₆N], 115.1 [2×CH of C₆H₄], 80.9 [C of C₅H₄], 65.1 [5×CH of C₅H₅], 64.4 [2×CH of C₅H₄], 61.7 [2×CH of C₅H₄]. Anal.

Calcd for $C_{26}H_{20}FeN_2O$: C, 72.24; H, 4.66; N, 6.48. Found: C, 72.34; H, 4.80; N: 6.46. ESI-MS (+ve mode) : $[C_{26}H_{20}FeN_2O+H]^+$: 433.1(m/z).

5.2.1.3 Synthesis of $[Ru(\eta^6\text{-}p\text{-cymene})(L^7)Cl]$ [21]

To a solution of $[Ru(\eta^6\text{-}p\text{-cymene})Cl_2]_2$ (0.1g, 0.16 mmol) in dichloromethane (20 mL), ligand **HL**⁷ (0.12g, 0.33 mmol) was added. The mixture was stirred at room temperature for 24 h. The product was isolated by precipitation with diethyl ether and dried *in vacuo* to afford a red-orange crystalline powder. ¹H NMR (400.13 MHz, *d*₄-MeOH): 8.75 [d, 1H, NC₅H₄], 8.19 [d, 2H, CH of C₆H₄], 8.15 [t, 1H, NC₅H₄], 8.01 [d, 1H, NC₅H₄], 7.68 [t, 1H, NC₅H₄], 7.29 [d, 2H, C₆H₄], 5.94 [d, 1H, CH of C₆H₄], 5.69 [d, 1H, CH of C₆H₄], 5.65 [d, 1H, CH of C₆H₄], 5.17 [d, 2H, CH of C₆H₄], 4.31 [m, 5H, C₅H₄], 3.94 [d, 2H, C₅H₄], 3.82 [d, 2H, C₅H₅], 2.24 [sept, 1H, CH(CH₃)₂], 2.04 [s, 3H, C₆H₄CH₃], 0.84 [d, 3H, CH(CH₃)₂], 0.65 [d, 3H, CH(CH₃)₂]. ¹³C NMR (100.61 MHz, DMSO-*d*₆): δ 167.3 [C of CONH], 156.4 [CH of C₅H₄N], 155.2 [C of C₅H₄N], 145.9 [C of C₆H₄], 140.6 [CH of C₅H₄N], 135.2 [C of C₆H₄], 130.1 [2×CH of C₆H₄], 129.4 [CH of C₅H₄N], 126.7 [CH of C₅H₄N], 110.9 [2×CH of C₆H₄], 109.4 [C of C₆H₄], 99.9 [C of C₆H₄], 90.2 [2×CH of C₆H₄], 88.1 [2×CH of C₆H₄], 85.3 [C of C₅H₄], 72.8 [5×CH of C₅H₅], 72.4 [2×CH of C₅H₄], 65.5 [2×CH of C₅H₄], 30.9 [C₆H₄CH₃], 22.3 [CH(CH₃)₂], 21.2 [CH(CH₃)₂], 18.2 [CH of CH(CH₃)₂]. Anal. Calcd for $C_{32}H_{31}ClFeN_2ORu$: C, 58.95; H, 4.79; N, 4.30. Found: C, 58.80; H, 4.80; N, 4.47. ESI-MS (+ve mode): $[Ru(\eta^6\text{-}p\text{-cymene})(L^7)]^+$: 617.1 (m/z).

5.2.1.4 Synthesis of $[Ru(\eta^6\text{-}p\text{-cymene})(L^7)PTA]BPh_4$ [22]

To a solution of complex **21** (0.1g, 0.15mmol), dissolved in 20mL of methanol, a methanolic solution of 1,3,5-triaza-7-phosphoadamantane (0.23g, 0.15mmol) was added dropwise and stirred overnight at room temperature. The resulting solution was evaporated to dryness to get the crude product as yellow solid. The crude product (0.03g, 0.04mmol) was then dissolved in a mixture of dichloromethane and methanol and a solution of sodium tetraphenylborate (0.01g, 0.04mmol) was added

dropwise to that. The resulting solution was stirred for 2h and then filtered. The filtrate was kept for vapour diffusion with diethyl ether, from which orange coloured crystalline compound was obtained. ^1H NMR (400.13 MHz, DMSO- d_6): 8.95 [d, 1H, NC $_5$ H $_4$], 8.29 [t, 1H, NC $_5$ H $_4$], 8.06 [d, 1H, NC $_5$ H $_4$], 7.82 [t, 1H, NC $_5$ H $_4$], 7.58 [d, 2H, C $_6$ H $_4$], 7.25 [d, 2H, C $_6$ H $_4$], 7.18 [br.s, 8H, B(C $_6$ H $_5$) $_4$], 6.93 [t, 8H, B(C $_6$ H $_5$) $_4$], 6.79 [t, 4H, B(C $_6$ H $_5$) $_4$], 6.33 [d, 1H, CH of C $_6$ H $_4$], 5.89 [d, 1H, CH of C $_6$ H $_4$], 5.77 [d, 1H, CH of C $_6$ H $_4$], 5.31 [d, 1H, CH of C $_6$ H $_4$], 4.81-3.89 [m, 12H from PTA and 9H from C $_5$ H $_5$ FeC $_5$ H $_4$], 2.34 [m, 1H, CH(CH $_3$) $_2$], 2.11 [s, 3H, C $_6$ H $_4$ CH $_3$], 0.95 [d, 3H, CH(CH $_3$) $_2$], 0.78 [d, 3H, CH(CH $_3$) $_2$]. ^{13}C NMR (100.61 MHz, DMSO- d_6): δ 167.0 [C of CONH], 164.7-163.2 [4 \times C of C $_24$ H $_20$ B], 156.7 [CH of C $_5$ H $_4$ N], 150.2 [C of C $_5$ H $_4$ N], 141.2 [C of C $_6$ H $_4$], 136.1 [CH of C $_5$ H $_4$ N], 135.2 [4 \times CH of C $_24$ H $_20$ B], 129.6 [C of C $_6$ H $_4$], 129.0 [4 \times CH of C $_24$ H $_20$ B], 127.0 [2 \times CH of C $_6$ H $_4$], 126.7 [2 \times CH of C $_7$ H $_8$], 126.4 [CH of C $_5$ H $_4$ N], 125.9 [4 \times CH of C $_24$ H $_20$ B], 122.1 [CH of C $_5$ H $_4$ N and], 117.8 [2 \times CH of C $_6$ H $_4$], 102.2 [C of C $_6$ H $_4$], 92.5 [C of C $_6$ H $_4$], 88.2 [2 \times CH of C $_6$ H $_4$], 85.3 [C of C $_5$ H $_4$], 79.6 [2 \times CH of C $_6$ H $_4$], 72.2 [3 \times NCH $_2$ N of PTA], 70.0 [5 \times CH of C $_5$ H $_5$], 69.5 [2 \times CH of C $_5$ H $_4$], 66.6 [2 \times CH of C $_5$ H $_4$], 50.6-49.2 [3 \times PCH $_2$ N of PTA], 30.8 [C $_6$ H $_4$ CH $_3$], 22.5 [CH(CH $_3$) $_2$], 21.9 [CH(CH $_3$) $_2$], 18.5 [CH of CH(CH $_3$) $_2$]. ^{31}P NMR (126 MHz, DMSO- d_6): δ -34.3. Anal. Calcd for C $_{62}$ H $_{63}$ BFeN $_5$ OPRu: C, 68.14; H, 5.81; N, 6.41. Found: C, 68.80; H, 5.80; N, 6.47. ESI-MS (+ve mode) : [Ru(η^6 -*p*-cymene)(L 7)(PTA)] $^+$: 774.1 (m/z).

5.2.1.5 Synthesis of [Ru(η^6 -*p*-cymene)(L 8)Cl] [23]

Complex **23** was prepared following the same procedure as complex **21** using ligand **HL** 8 . ^1H NMR (400.13 MHz, CDCl $_3$): 8.79 [s, 1H, NC $_{10}$ H $_6$], 7.70 [m, 5H, NC $_{10}$ H $_6$], 7.37 [br.s, 2H, C $_6$ H $_4$], 6.72 [br.s, 2H, C $_6$ H $_4$], 5.08-4.79 [m, 13H, 4H from C $_6$ H $_4$ and 9H from C $_{10}$ H $_9$], 2.54 [m, 1H, CH(CH $_3$) $_2$], 2.12 [s, 3H, C $_6$ H $_4$ CH $_3$], 0.97 [br.s, 6H, CH(CH $_3$) $_2$]. ^{13}C NMR (100.61 MHz, DMSO- d_6): 165.0 [C of CONH], 159.2 [C of C $_9$ H $_6$ N], 139.5 [C of C $_6$ H $_4$], 134.5 [CH of C $_9$ H $_6$ N], 131.8 [C of C $_9$ H $_6$ N], 130.4 [CH of C $_9$ H $_6$ N], 129.1 [C of C $_6$ H $_4$], 126.3 [2 \times CH of C $_6$ H $_4$], 125.6 [CH of C $_9$ H $_6$ N], 124.4 [CH of C $_9$ H $_6$ N], 123.6 [CH of C $_9$ H $_6$ N], 123.1 [C of C $_9$ H $_6$ N], 122.6

[CH of C_9H_6N], 115.7 [2×CH of C_6H_4], 102.4 [C of C_6H_4], 93.0 [C of C_6H_4], 87.7 [2×CH of C_6H_4], 85.0 [C of C_5H_4], 80.6 [2×CH of C_6H_4], 70.6 [5×CH of C_5H_5], 69.0 [2×CH of C_5H_4], 66.0 [2×CH of C_5H_4], 30.7 [$C_6H_4CH_3$], 22.5 [CH(CH₃)₂], 22.0 [CH(CH₃)₂], 18.4 [CH(CH₃)₂]. Anal. Calcd for $C_{36}H_{33}ClFeN_2ORu$: C, 64.77; H, 5.13; N, 4.20. Found: C, 64.49; H, 5.03; N, 4.57. ESI-MS (+ve mode) : $[Ru(\eta^6\text{-}p\text{-cymene})(L^8)]^+$: 667.1 (m/z).

5.2.1.6 Synthesis of $[Ru(\eta^6\text{-}p\text{-cymene})(L^8)PTA]Cl$ [24]

Complex **24** was prepared following the same procedure as complex **22** from Complex **23**. ¹H NMR (400.13 MHz, DMSO-*d*₆): δ 8.84 [d, 1H, $C_{10}H_6NO$], 8.32 [m, 3H, $C_{10}H_6NO$], 8.07 [t, 1H, $C_{10}H_6NO$], 7.94 [t, 1H, $C_{10}H_6NO$], 7.69 [d, 2H, $C_{16}H_{15}FeN$], 7.34 [d, 2H, $C_{16}H_{15}FeN$], 6.53 [d, 1H, CH of C_6H_4], 6.13 [d, 1H, CH of C_6H_4], 5.85 [d, 1H, CH of C_6H_4], 5.43 [d, 1H, CH of C_6H_4], 4.89-3.85 [m, 12H from PTA and 9H from $C_5H_5FeC_5H_4$], 1.30 [s, 3H, $C_6H_4CH_3$], 1.00 [d, 6H, CH(CH₃)₂]. ¹³C NMR (100.61 MHz, DMSO-*d*₆): 167.3 [C of CONH], 160.4 [C of C_9H_6N], 140.0 [C of C_6H_4], 136.9 [C of C_9H_6N], 132.5 [CH of C_9H_6N], 130.5 [C of C_6H_4], 129.1 [2×CH of C_6H_4], 127.2 [CH of C_9H_6N], 125.5 [CH of C_9H_6N], 124.6 [CH of C_9H_6N], 123.8 [C of C_9H_6N], 122.5 [2×CH of C_9H_6N], 115.0 [2×CH of C_6H_4], 103.8 [C of C_6H_4], 95.7 [C of C_6H_4], 88.6 [2×CH of C_6H_4], 85.0 [C of C_5H_4], 81.1 [2×CH of C_6H_4], 72.8 [3×NCH₂N of PTA], 72.5 [5×CH of C_5H_5], 69.0 [2×CH of C_5H_4], 65.5 [2×CH of C_5H_4], 52.1 [3×PCH₂N of PTA], 24.6 [$C_6H_4CH_3$], 22.4 [CH(CH₃)₂], 21.2 [CH(CH₃)₂], 18.4 [CH of CH(CH₃)₂]. ³¹P NMR (126 MHz, DMSO-*d*₆): δ -39.6. Anal. Calcd for $C_{42}H_{45}ClFeN_5OPRu$: C, 58.71; H, 5.28; N, 8.15. Found: C, 58.49; H, 5.80; N, 8.47. ESI-MS (+ve mode): $[Ru(\eta^6\text{-}p\text{-cymene})(L^8)(PTA)]^+$: 824.2 (m/z).

5.2.2 X-ray crystallography

5.2.2.1 X-ray crystallography of ligand **HL**⁷ and **HL**⁸

The description of instrumentation of X-ray crystallography for **HL**⁷ and **HL**⁸ is same as described in Section 2.2.2.2.

5.2.3 Growth inhibition study

The procedure for SRB assay is same as discussed in chapter 2.

5.2.4. Electrochemical study:

Cyclic voltammograms (CVs) were recorded on a CHI620D electrochemical analyzer using a standard three-electrode cell with glassy carbon as a working electrode. The 3 mm diameter glassy carbon working electrode from CH Instruments (CHI 104) was used. The electrode was polished with two different Alpha alumina powders (1.0 and 0.3 micron from CH Instruments) suspended in distilled water on a Microcloth polishing pad. The electrodes were thoroughly rinsed with distilled water throughout the experiment. A platinum wire was used as the counter electrode and saturated calomel as the reference electrode. Scan rates were optimized in an effort to obtain smoother voltammograms. Unless otherwise stated, the scan rate used was 100 mV s^{-1} . A solution of tetrabutylammoniumhexafluorophosphate (Bu_4NPF_6) in CH_2Cl_2 (0.1 M) was employed as the supporting electrolyte. CH_2Cl_2 was distilled from CaH_2 prior to use. Under these conditions the ferrocene/ferrocenium couple, which was used as a reference, had $E_{1/2} = +0.12 \text{ V}$ and $\Delta E_p = 0.10 \text{ V}$. All solutions were purged with argon, and voltammograms were recorded under a blanket of argon.

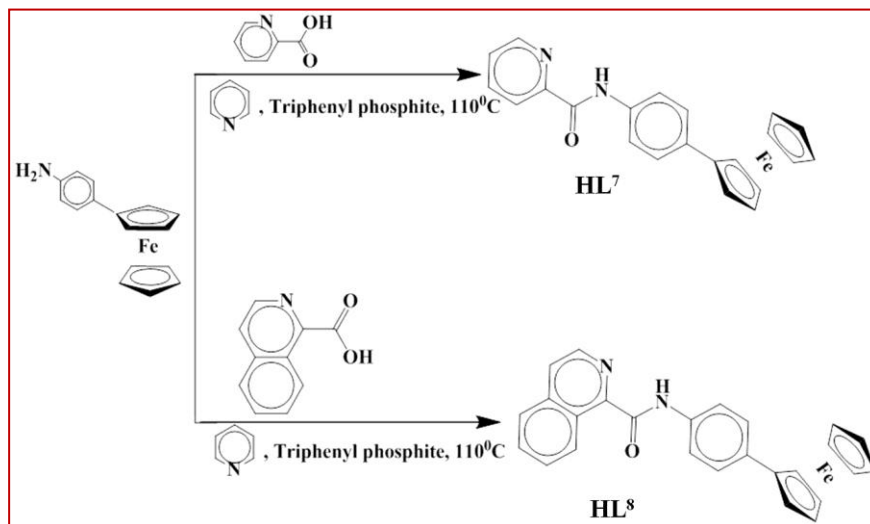
5.2.5. DNA binding experiments

Absorption studies of ligand **HL**⁸ and complex **23** were recorded in PBS buffer, maintaining the pH at 7.4 in the range 200–340 nm. Solutions of ct-DNA sodium salt were prepared freshly before experiment using milli-Q water. Initially UV-vis spectra of free sample was recorded as blank. The titration experiment was carried out by keeping the concentration of sample in buffer constant and adding 10 μL of the ct-DNA solution at a time. After addition of the sample solution, the solution was kept for 5 min and then UV-vis spectra were measured.

5.3 Result and Discussions:

5.3.1 Synthesis of complexes

Two ferrocenamamide ligands **HL**⁷ and **HL**⁸ were prepared from 4-ferrocenyl aniline using picolinic acid or quinoline-1-carboxylic acid in moderate yield (Scheme 5.1).



Scheme 5.1: Synthesis of Ferrocenyl ligands **HL**⁷ and **HL**⁸.

Both the ligands were characterised by NMR, mass, elemental analysis and single crystal XRD. Peak at 9.34-10.27 for amide proton in ¹H NMR confirms the formation of amide bond in both the cases. All the characterisation data corroborated well with the proposed structure (Fig 5.1-Fig 5.6).

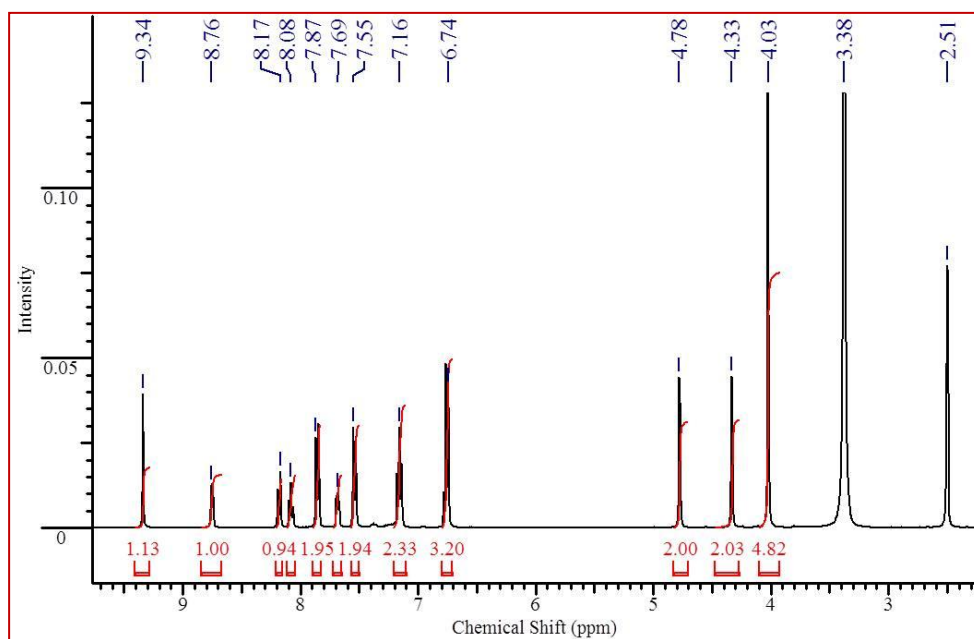


Fig.5.1: ¹H NMR spectra of ligand **HL**⁷.

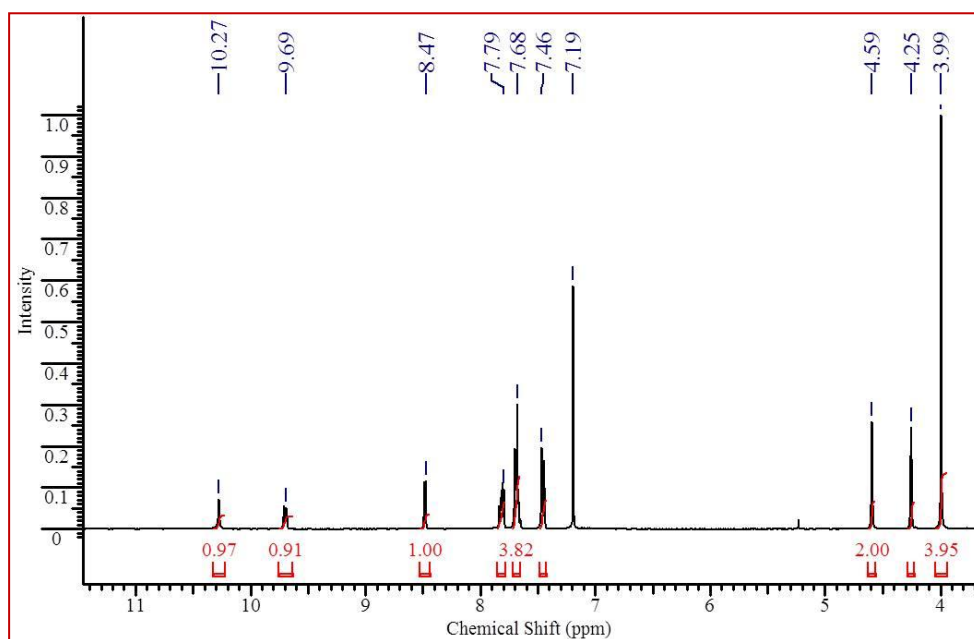


Fig.5.2: ^1H NMR spectra of ligand HL^8 .

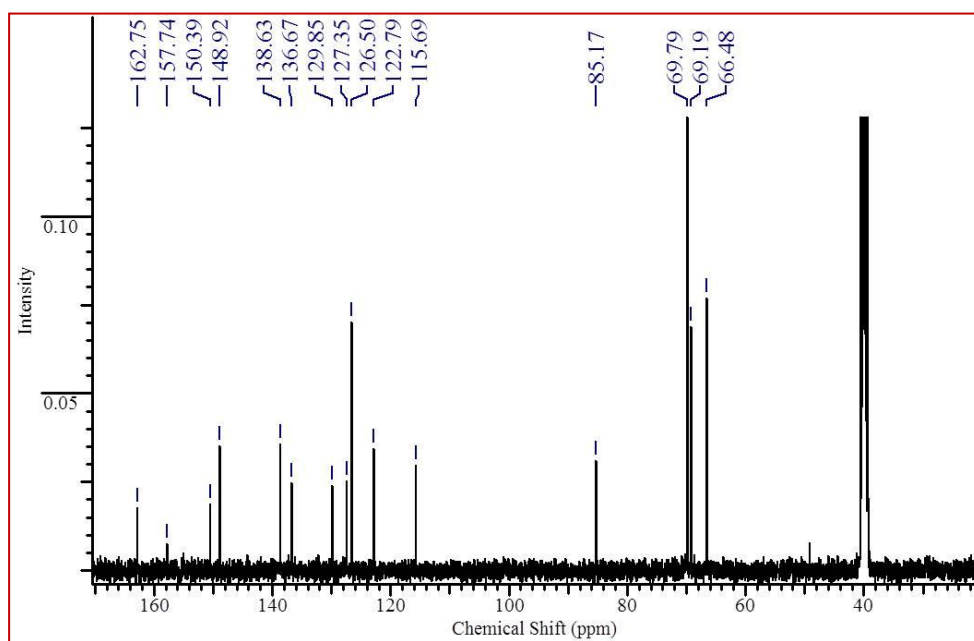


Fig.5.3: ^{13}C NMR spectra of ligand HL^7 .

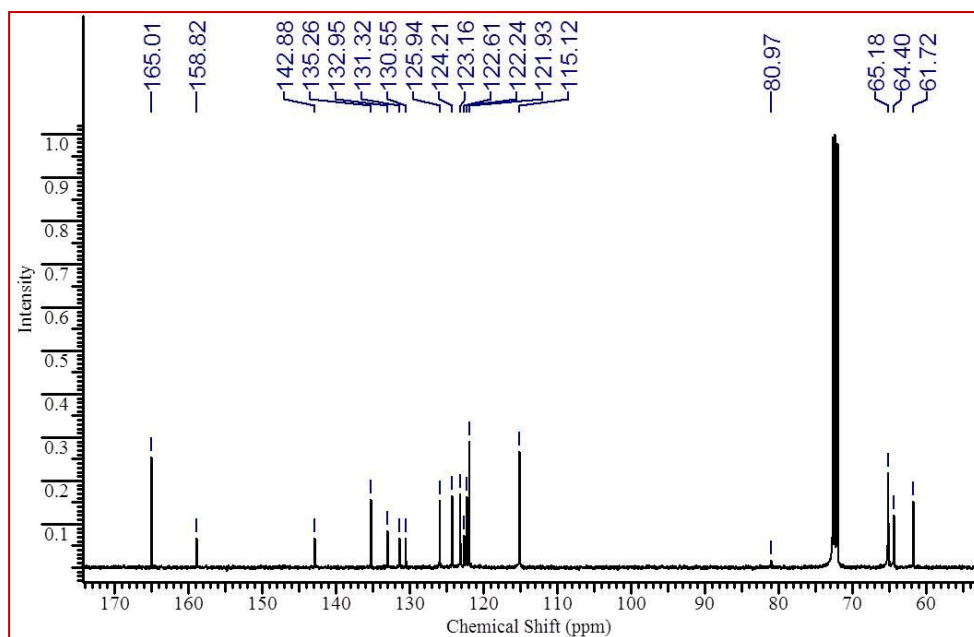


Fig.5.4: ^{13}C NMR spectra of ligand HL^8 .

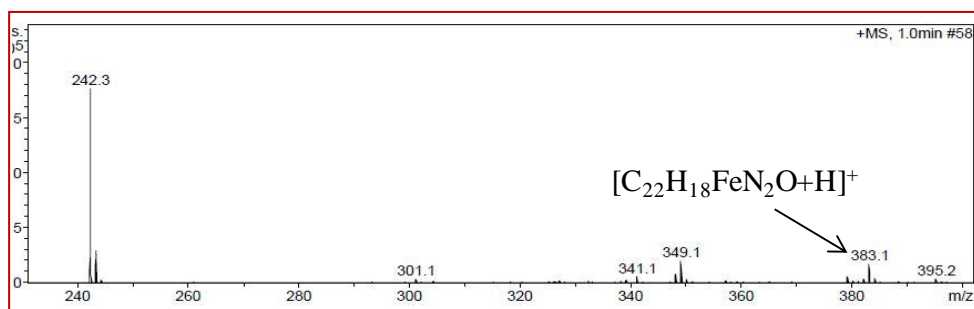


Fig 5.5: ESI-MS of ligand HL^7 .

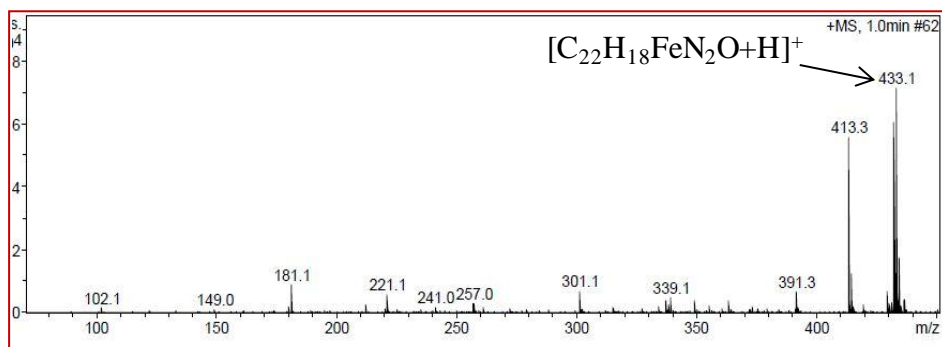


Fig 5.6: ESI-MS of ligand HL^8 .

Both the crystals are dark orange in colour and crystallised in P1 and P21/c space group for HL^7 and HL^8 respectively, where HL^7 crystallises with one molecule of toluene. In both the structures cyclopentadienyl ring adopts eclipsed conformation. Ball and stick diagram of HL^7 and HL^8 are given in Fig.5.7 and Fig.5.8.

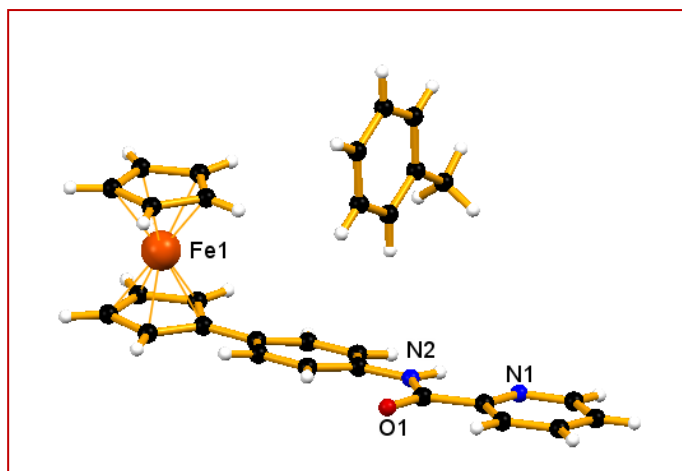


Fig.5.7: The solid state crystal structure of compound **HL**⁷ with partial atomic numbering scheme.

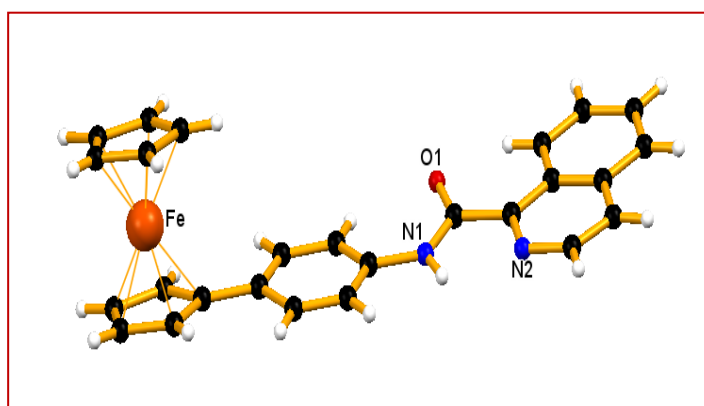
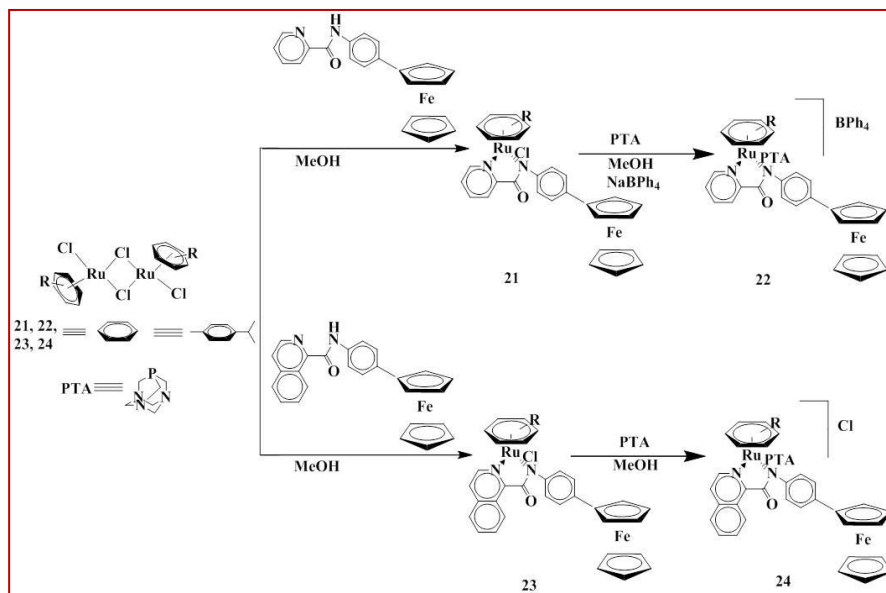


Fig.5.8: The solid state crystal structure of compound **HL**⁸ with partial atomic numbering scheme.

The dichloro ruthenium *p*-cymene complexes **21** and **23** have been prepared when a solution of dimeric $[(\eta^6\text{-}p\text{-cymene})\text{RuCl}_2]_2$ were stirred overnight with the respective ligands [ligand **HL**⁷ for complex **21** and ligand **HL**⁸ for complex **23**] at room temperature (Scheme 5.2). The reaction mixture was evaporated to dryness to get the complexes **21** and **23** as orange solid and the compounds were recrystallized further from suitable solvents. Room temperature substitution of a chloride ligand in ruthenium(II) complexes with the general formula $[\text{Ru}(\eta^6\text{-arene})(\text{L})\text{Cl}]\text{Cl}$ (**L**⁷ = pyridine-2-carboxylic acid(4-ferrocenyl aniline)-amide, $\eta^6\text{-arene}$ = *p*-cymene **22**, and **L**⁸ = quinoline-1-carboxylic acid(4-ferrocenyl aniline)-amide, $\eta^6\text{-arene}$ = *p*-cymene **24**) with 1,3,5-triaza-7-phosphoadamantane (PTA) yielded water soluble complexes $[\text{Ru}(\eta^6\text{-arene})(\text{L})(\text{PTA})]\text{X}$ [**22** and **24**] (Scheme 5.2). Compound **22** was further treated with NaBPh_4 in a

mixture of methanol and dichloromethane mixture to get crystalline $[\text{Ru}(\eta^6\text{-}p\text{-cymene})(\text{L}^7)(\text{PTA})\text{Cl}]\text{BPh}_4$ product as it was difficult to characterize complex **22** with chloride as counter anion.



Scheme 5.2: Synthesis of Complexes **21-24**.

All the complexes are air stable and highly soluble in DMSO and sparingly soluble in DCM, MeOH and other organic solvents. Both the RAPTA compounds are soluble in water, whereas dichloro analogues are weakly soluble in water. All the complexes have been characterized by ^1H and ^{13}C NMR spectroscopy, ESI-MS and elemental analyses. Although complexes **21-24** are sparingly soluble in solvents other than $\text{DMSO-}d_6$, in most of the cases, ^1H NMR was taken in solvents other than $\text{DMSO-}d_6$ as solvent peak of $\text{DMSO-}d_6$ overlaps with the septet peak of $-\text{CH}(\text{CH}_3)_2$. The ^1H NMR spectra of **21-24** show typical bands for *p*-cymene moiety at 5.17-6.53 for ring protons and 2.24-2.54, 1.30-2.12 and 0.65-1.00 ppm for side chain protons as reported earlier (Fig.5.9-Fig.5.12).^[36] In case of complex **22** and **24**, *p*-cymene proton signals shifted little downfield due to coordination of ruthenium centre to PTA and signals for the protons on the PTA ligand overlap with the broad signals assigned to the protons on the ferrocenyl functionality. Furthermore, the signals for the PTA ligand display the typical splitting pattern for an AB spin system and correlate well with splitting patterns observed with other PTA complexes in the literature.^[37]

The lack of an NH signal indicates the deprotonation of the ligand. Coordination of the amide ligand to the ruthenium centre results in a loss of two-fold symmetry of the *p*-cymene moiety, showing two broad multiplets in the range 0.65–1.0 ppm with a broad multiplet observed at ~2.5–3.0 ppm assigned to the single proton on the isopropyl group.

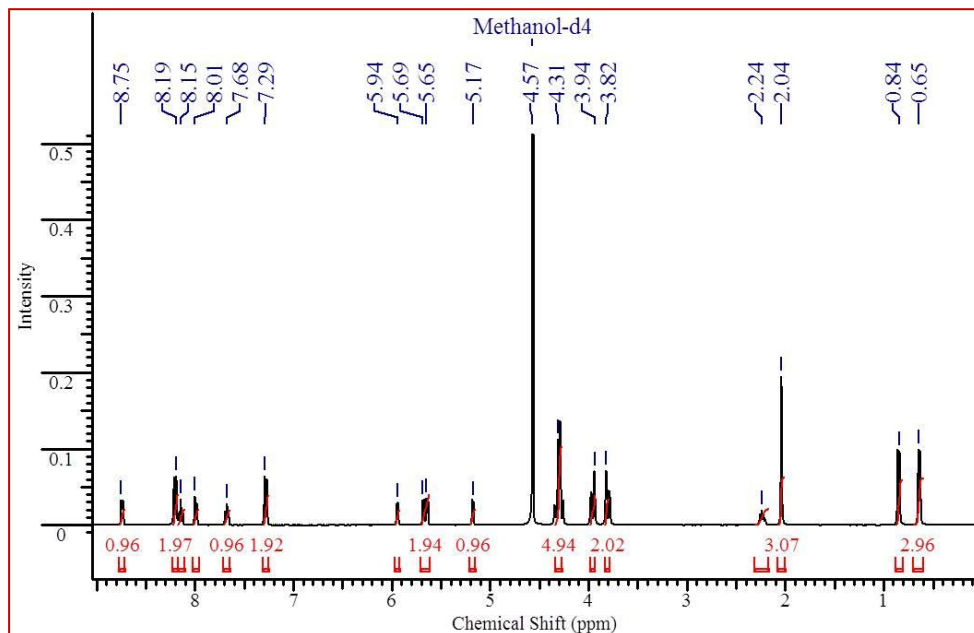


Fig.5.9: ^1H NMR spectra of complex 21.

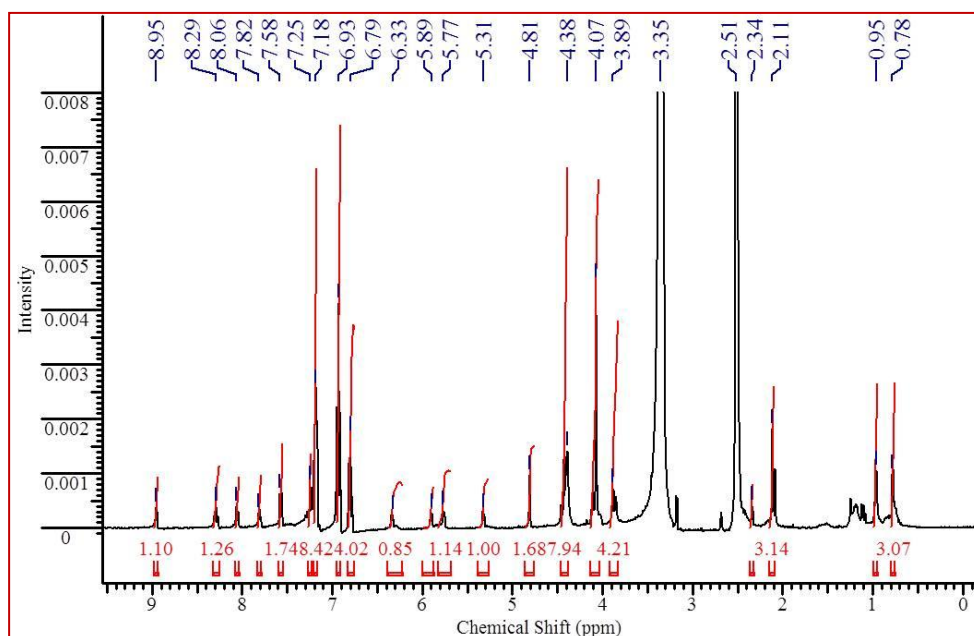


Fig.5.10: ^1H NMR spectra of complex 22.

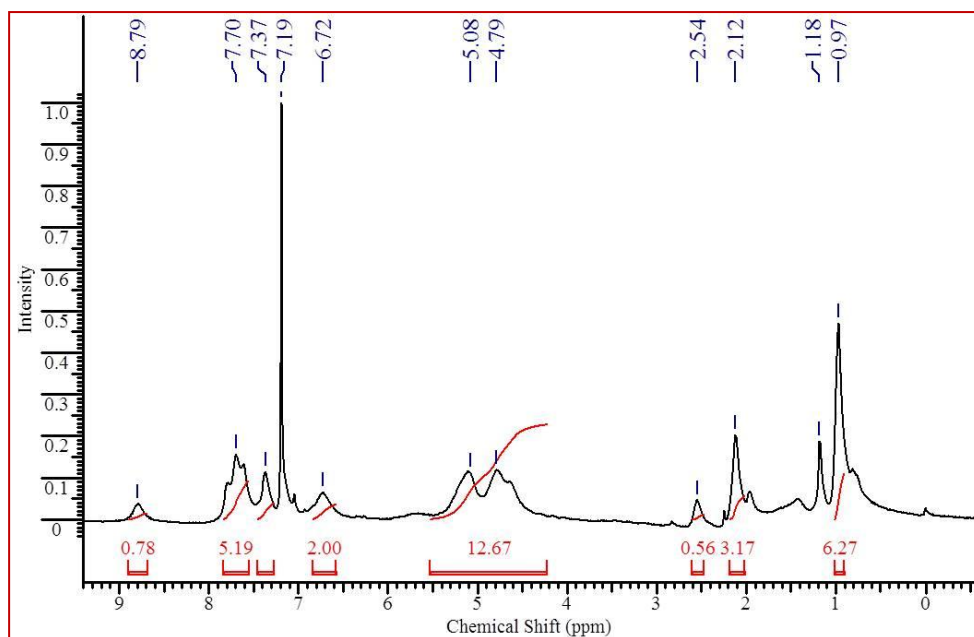


Fig.5.11: ^1H NMR spectra of complex **23**.

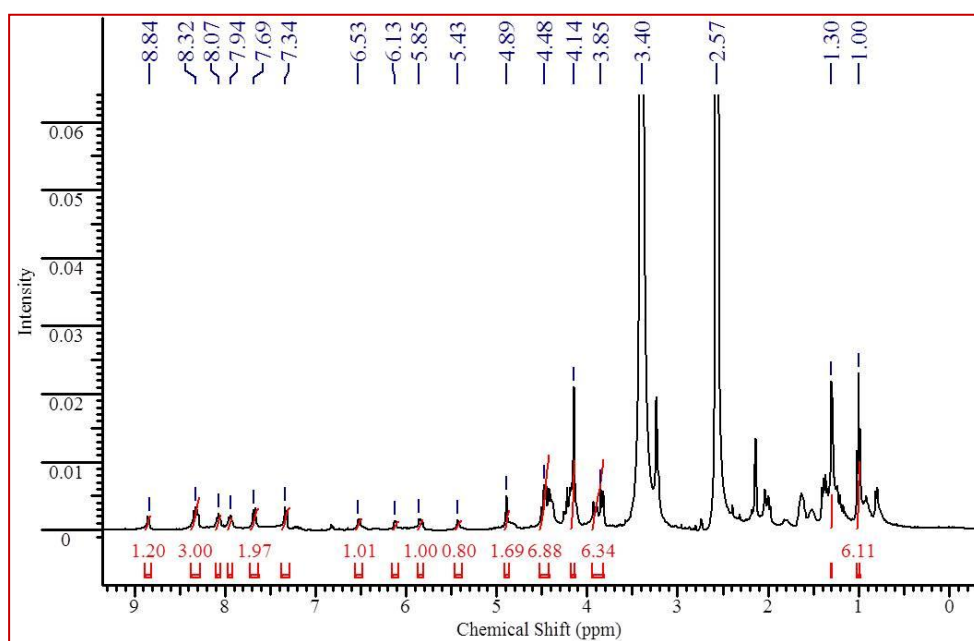


Fig.5.12: ^1H NMR spectra of complex **24**.

The ^{13}C NMR data for **22** and **24** display two singlets for the carbon atoms of the PTA ligand in the range 51–72 ppm, confirming coordination to the ruthenium ion and displacement of the chlorido ligand. The other peaks for compounds **21-24** also corroborate with the proposed structure (Fig.5.13- Fig.5.16).

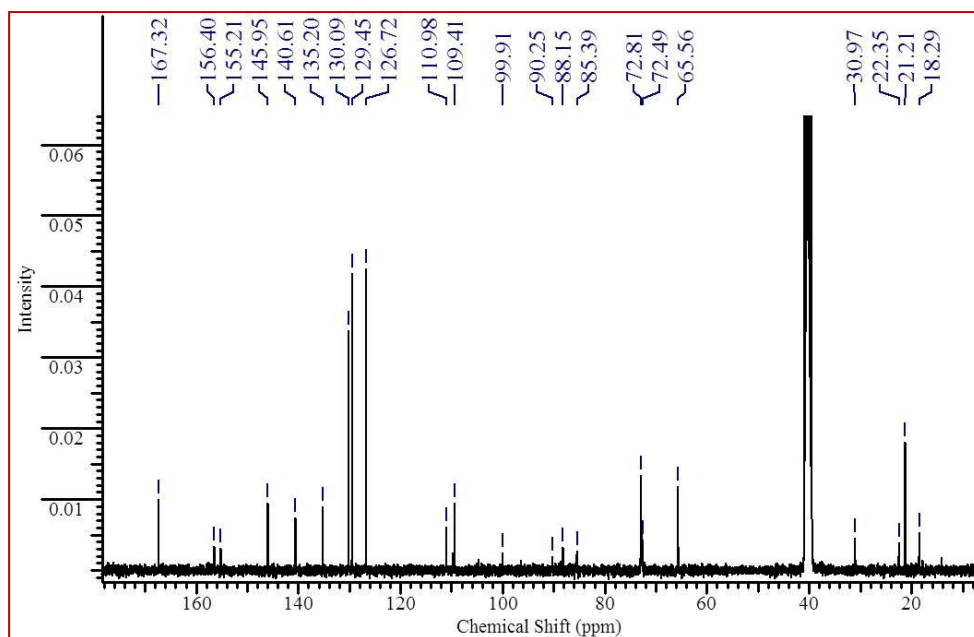


Fig.5.13: ^{13}C NMR spectra of complex 21.

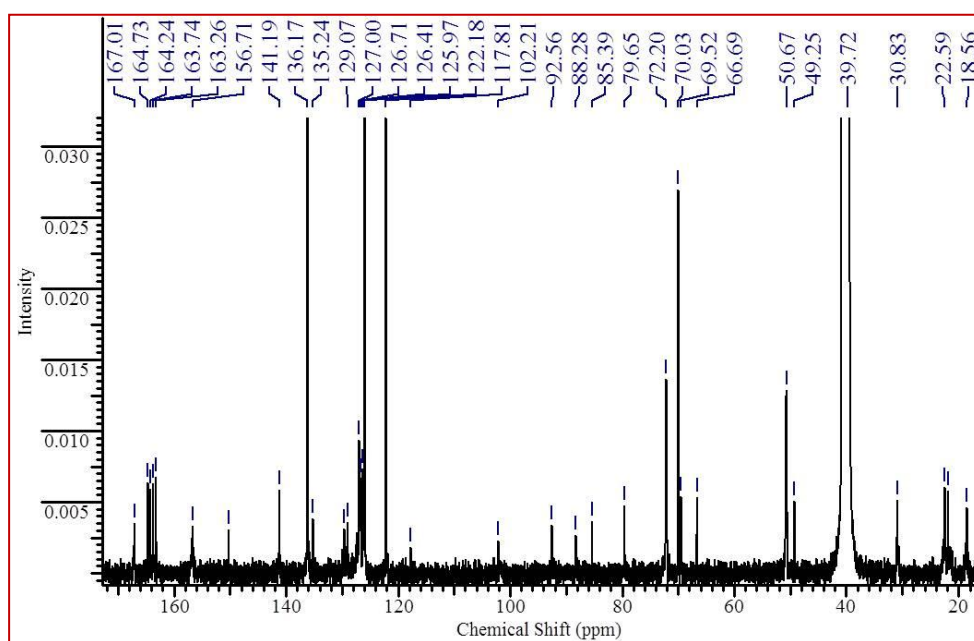


Fig.5.14: ^{13}C NMR spectra of complex 22.

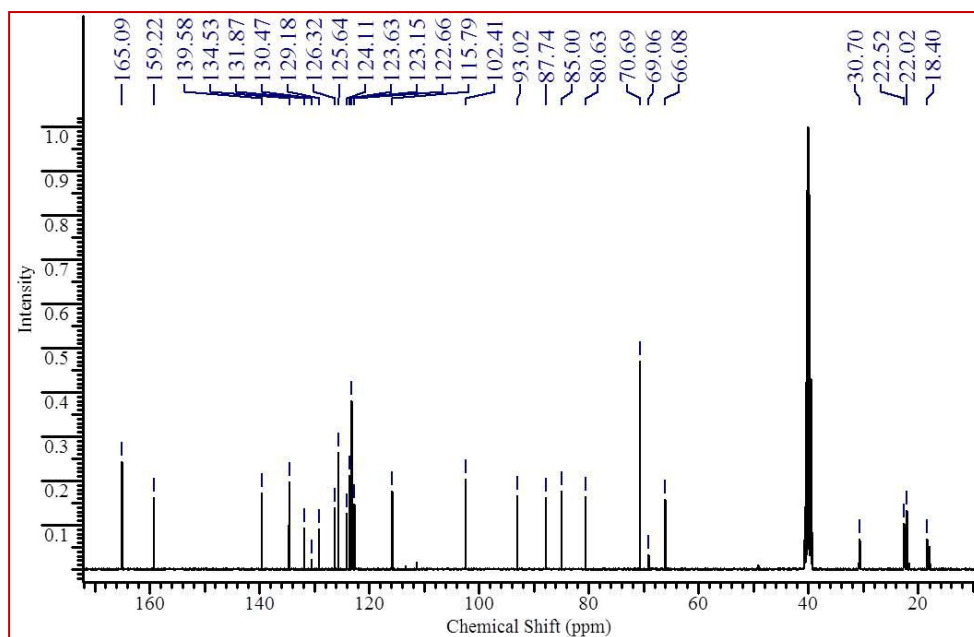


Fig.5.15: ^{13}C NMR spectra of complex **23**.

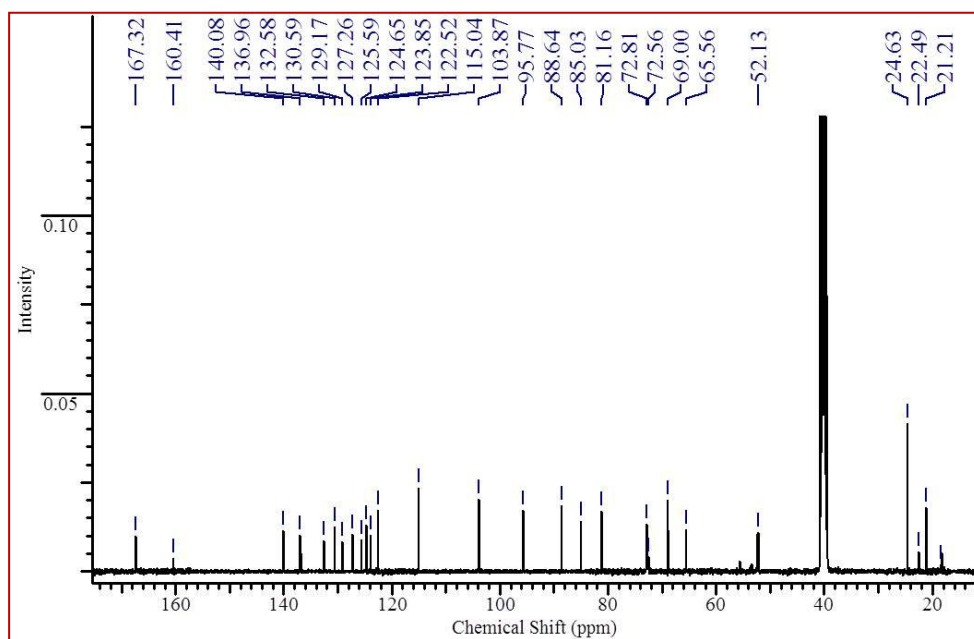


Fig.5.16: ^{13}C NMR spectra of complex **24**.

The ^{31}P NMR spectra of **22** and **24** display a singlet at \sim -34--39 ppm, suggesting a single phosphorous containing moiety and further attesting to the purity of these complexes (Fig.5.17-Fig.5.18).

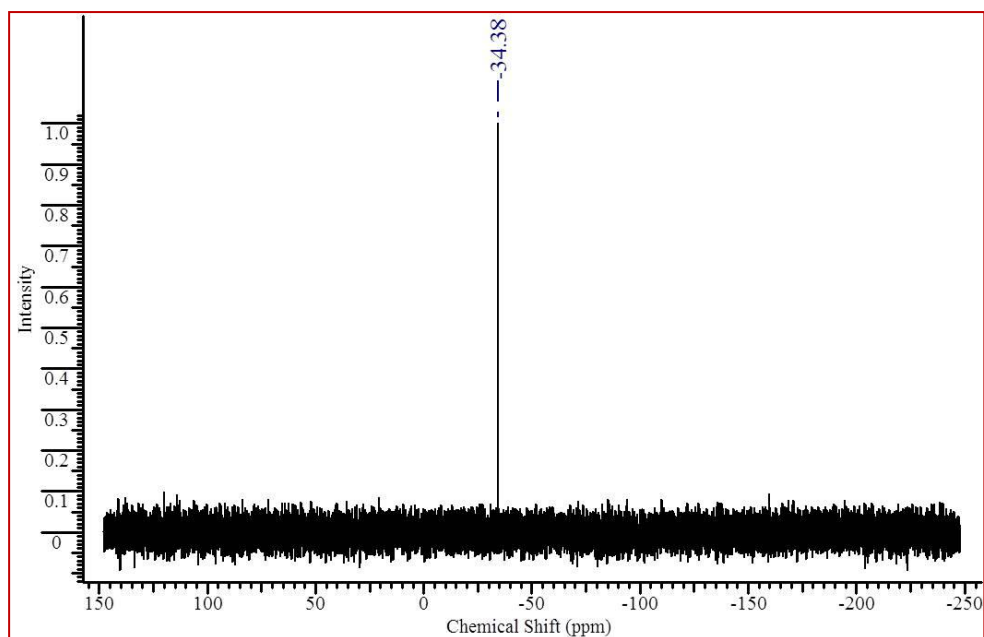


Fig.5.17: ^{31}P NMR spectra of complex 22.

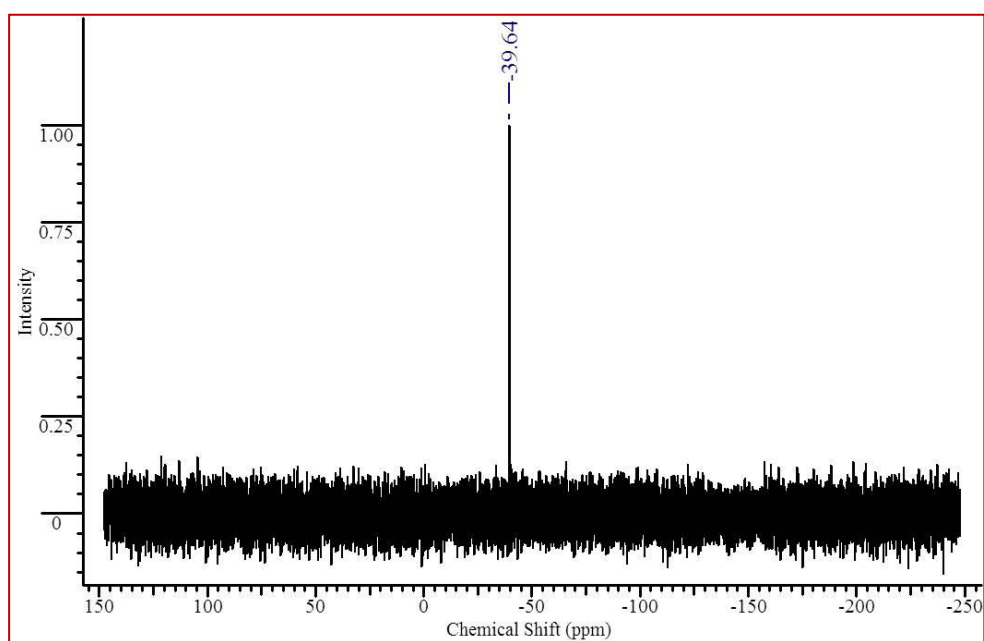


Fig.5.18: ^{31}P NMR spectra of complex 24.

The ESI-MS of **21** and **23** show one main peak envelope corresponding to $[\text{Ru}(\eta^6\text{-}p\text{-cymene})(\text{L})\text{Cl}]^+$ moiety after the dissociation of one labile chloride ligand (Fig.5.19-Fig.5.20),

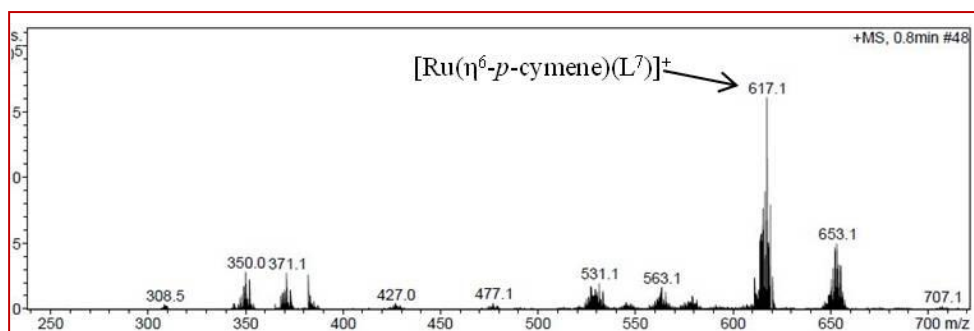


Fig.5.19: ESI-MS spectra of complex 21.

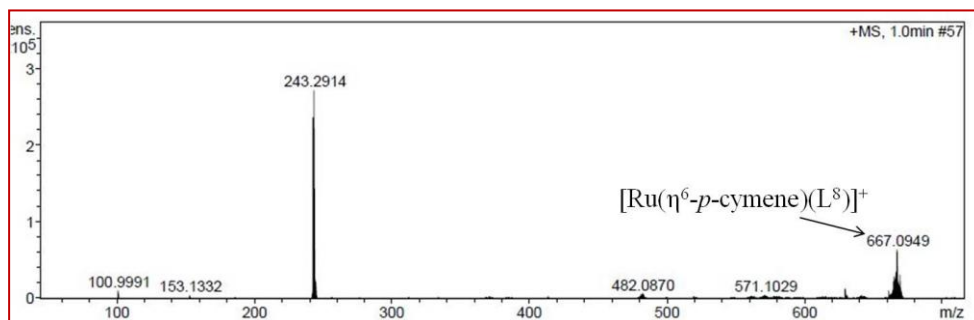


Fig.5.20: ESI-MS spectra of complex 23.

whereas complex 22 and 24 reveal single peak envelope analogous to $[\text{Ru}(\eta^6\text{-}p\text{-cymene})(\text{PTA})(\text{L})]^+$ cationic complex moiety (Fig.5.21-Fig.5.22).

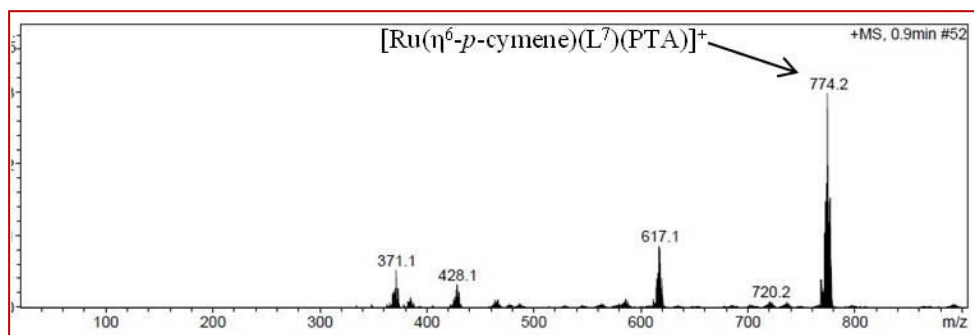


Fig 5.21: ESI-MS spectra of complex 22.

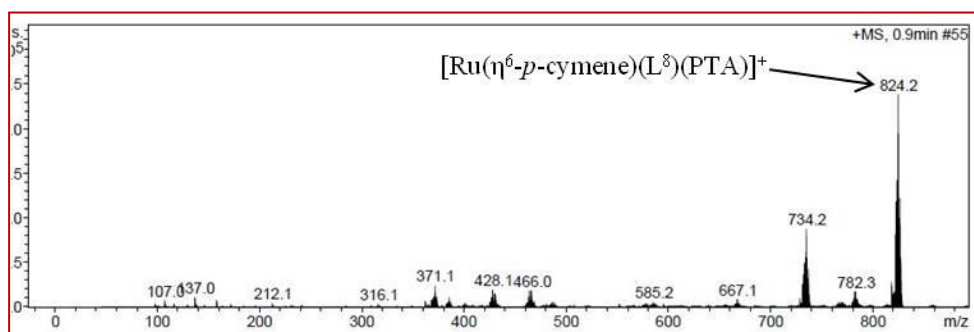


Fig 5.22: ESI-MS spectra of complex 24.

5.3.2 Growth inhibition study of prepared complexes:

The antiproliferative activity of the ligands **HL**⁷ and **HL**⁸ as well as the four Fc-Ru complexes have been evaluated against three different cancer cell lines *viz.*, lung cancer cell line A549, breast cancer cell line MCF7 and cervix cancer cell line HeLa. The results were obtained in terms of GI₅₀ (concentration of the drug that produces 50% inhibition of the cells), TGI (concentration of the drug that produces total inhibition of the cells) and LC₅₀ (concentration of the drug that kills 50% of the cells) using the sulforhodamine B (SRB) assay. All cancer cells were exposed for 24 h to increasing concentrations of the complexes as well as free ligands and their proliferations are reported in terms of GI₅₀ values as values for LC₅₀ and TGIs against all the three cell lines were >80 nm. Adriamycin, a chemotherapeutic drug, was used as a positive control. It is surprising to note that, although **HL**⁷ is highly cytotoxic against all the cell lines, complex **21** is cytotoxic against MCF7, whereas **22** is cytotoxic against A549 cell line only. But in case of **HL**⁸, the ligand has not shown any significant antiproliferative activity against any of the three cell lines, but complex **23** has shown promising antiproliferative activity against all the cell lines in nanomolar concentration. However, complex **24** *i.e.* PTA analogue of complex **23**, is inactive in all three cell lines again. Although it is difficult to find any structure-activity relationships among all the complexes from GI₅₀ values, further studies on the plausible mechanism for the active complexes will be investigated at later stage.

Table 5.1: GI₅₀ value (nM/mL) of the prepared complexes in human cancer cell lines.

Complex	A549	MCF7	HeLa
Ligand HL ⁷	<0.1	<0.1	<0.1
Complex 21	>80	<0.1	>80
Complex 22	<0.1	>80	>80
Ligand HL ⁸	>80	>80	>80
Complex 23	<0.1	<0.1	<0.1
Complex 24	>80	>80	>80
Adriamycin	<0.1	<0.1	<0.1

5.3.3 DNA binding studies:

As DNA is a potential target in cancer therapy, possible interactions of the ligand **HL**⁸ as well as complex **23** with ct-DNA were investigated in order to correlate if DNA binding has any role in antiproliferative activity. DNA can bind to metal complex through three distinct binding sites: major or minor groove binding outside the DNA, electrostatic binding to phosphate group of DNA and intercalation.^[38] The mode of binding of the metal complexes to DNA can be studied using UV-visible spectroscopy as observed changes in the spectra may give evidence of the existing interaction mode. Groove binding generally does not lead to well-defined changes in the energy of the absorption band, the intensity of the absorption band also does not show any marked change. Intercalative binding, on the other hand, generally gives rise to hypochromism with a red shift in the absorption bands of the molecule.^[39,40]

The UV-vis spectra of for both **HL**⁸ and complex **23** show hyperchromic shift upon addition of increasing concentration of ct-DNA, rationalizing the possibility of groove binding owing to the degradation of DNA double helix structure (Fig.5.23). None of the electronic spectra show any clear isosbestic points during the successive addition of DNA. The DNA binding affinities of the complexes were compared by calculating the intrinsic binding constant K_b by the following equation.

$$\frac{[\text{DNA}]}{(\epsilon_a - \epsilon_f)} = \frac{[\text{DNA}]}{(\epsilon_b - \epsilon_f)} + \frac{[\text{DNA}]}{K_b(\epsilon_b - \epsilon_f)}$$

where [DNA] is the concentration of DNA in base-pairs, ϵ_a is the apparent extinction coefficient calculated by absorbance/[complex], ϵ_f is the extinction coefficient of the complex in its free form, and ϵ_b is the extinction coefficient of the complex in the bound form. In both the cases, when data was fitted in the above equation, it gave a straight line with a slope of $1/(\epsilon_b - \epsilon_f)$ and an intercept of $1/K_b(\epsilon_b - \epsilon_f)$. The intrinsic DNA

binding constants, K_b , of **HL**⁷ and **23** have been obtained by monitoring the changes in absorbance at 290 nm with increasing concentrations of DNA. The DNA binding constants for **HL**⁷ and **23** have been found comparable values of 1.38×10^3 and 1.36×10^3 respectively.

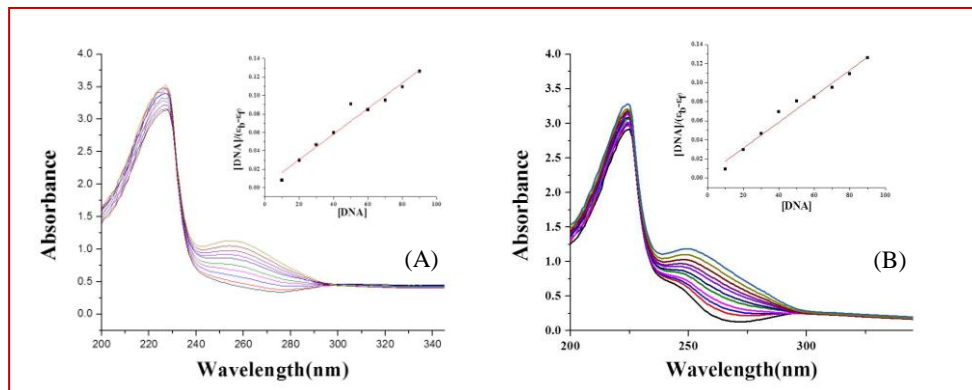


Fig.5.23: Absorption spectral titration of **HL**⁸(A) and **23**(B) with DNA in PBS buffer.

5.3.4 Electrochemical studies:

Cyclic voltametry studies reveal the significant differences for ligands with respect to their Ru-Fc complexes, which are summarised in Table 5.2. Electron withdrawing property of ferrocenamide ligands **HL**⁷ and **HL**⁸ affect the oxidation potentials of the Ru(II) centre upon complexation and these potential data insight into the fundamental character of the ligands in the complexes. Literature studies reveal that ligands which favour oxidation of the ferrocenyl moiety can produce reactive oxygen species, which in turn have the ability to disrupt lipid membranes and influence the antiproliferative activity of the complexes. Thus in order to find the correlation between the prepared ligands as well as complexes and their antitumour activities, all the ligands and complexes were studied by cyclic voltammetry at a glassy carbon working electrode using 5×10^{-4} M dichloromethane solutions containing 0.1 M tetrabutylammonium hexafluorophosphate as the supporting electrolyte, a platinum-wire counter electrode, and a SCE reference electrode. A comparison of the relevant electrochemical data is given in Table 5.2.

HL⁷ and **HL**⁸ are the ferrocene containing simplest compounds in the series and undergo one-electron reversible oxidation within the whole potential range. Although oxidation

of ferrocene occurs at 0.17 V, in presence of electron withdrawing $>C=O$ group of amide linkage, oxidation of ferrocene/ferrocenium redox couple shifts towards a more positive value at 0.33V and 0.32V in case of **HL**⁷ and **HL**⁸ respectively (Fig.5.24).^[41] Due to the coordination with Ru(II), the N-atom of picolinic acid moiety contribute negligible effect on the redox potential of ferrocene/ferrocenium couple, indicating no significant electronic coupling between the ferrocene and the picolinic acid unit. However the presence of the Ru(II) centre in **21-24** is reflected by an additional wave due to the Ru(II)/Ru(III) couple at a higher range (Fig.5.25).

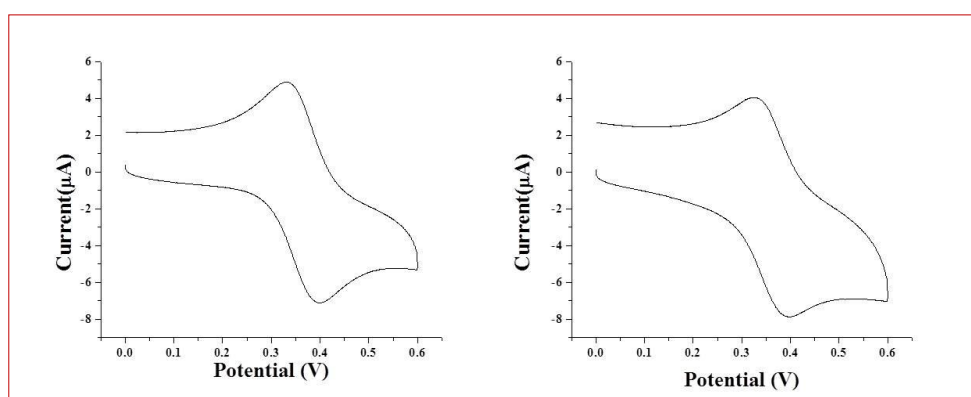


Fig.5.24: Cyclic voltammogram of **HL**⁷ and **HL**⁸ showing a full scan as recorded in DCM (scan rate 100 mVs^{-1}). The potential scale is referenced to SCE.

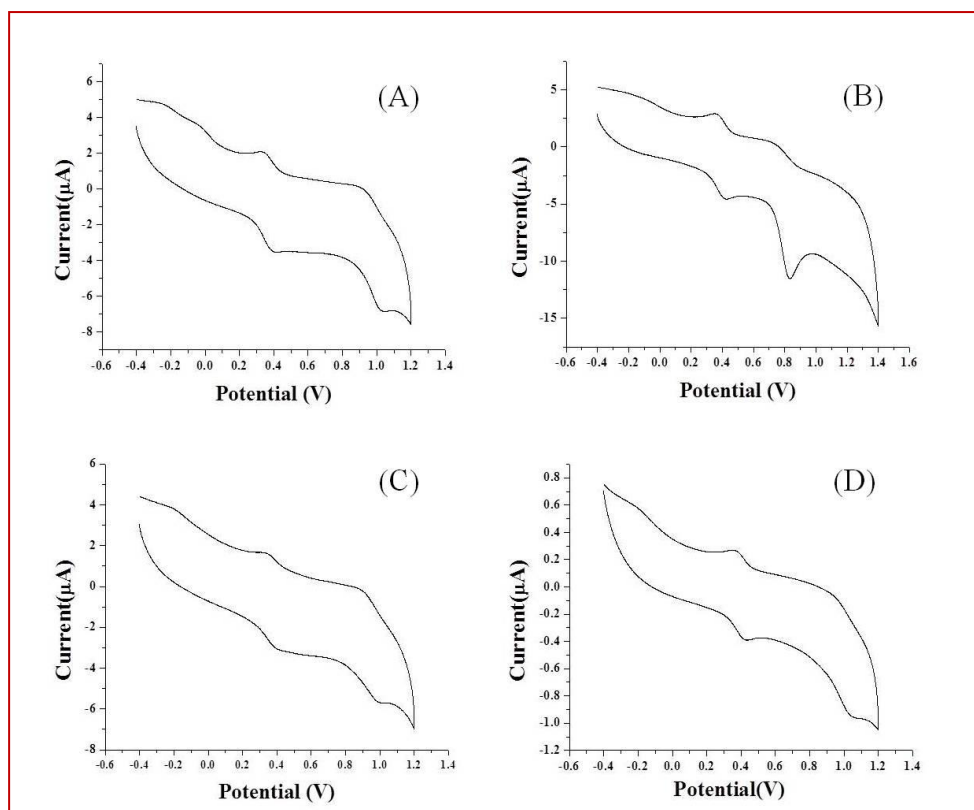


Fig.5.25: Cyclic voltammogram of **21-24** [clockwise (A) to (D)] showing a full scan as recorded in DCM (scan rate 100 mVs^{-1}). The potential scale is referenced to SCE.

Table 5.2: Redox potential of prepared complexes.

	E_{pa}	E_{pc}	ΔE_p	$E_{1/2}^c$	i_{pa}/i_{pc}	Ru(II)/Ru(III)	Ru(II)/Ru(III)
						E_{pa}	E_{pc}
Ligand HL⁷	0.33	0.40	0.07	0.36	0.68	-	-
Complex 21	0.32	0.38	0.06	0.35	0.58	0.92	1.04
Complex 22	0.35	0.42	0.07	0.38	0.63	0.72	0.83
Ligand HL⁸	0.32	0.39	0.07	0.35	0.53	-	-
Complex 23	0.32	0.41	0.08	0.36	0.55	0.88	1.00
Complex 24	0.36	0.41	0.05	0.38	0.65	0.90	1.05

The redox response of the Ru(η^6 -arene) unit is strongly influenced by the number of arene ring attached to

the ligand. As expected, increasing the number of electron-donating phenyl group at the amide ring makes the Ru(II)/Ru(III) oxidation more facile. Although, Ru(II)/Ru(III) redox potential is not so prominent in case of complex **22**, But anodic peak potential decreases in case of **23** and **24** than **21** because of the presence of one extra phenyl ring in **L**⁸.

5.4 Conclusion

Heterometallic ferrocenyl-derived ruthenium arene complexes have been successfully synthesized from Ru-Fc amide ligands. All complexes were characterized using an array of spectroscopic and analytical techniques, which confirmed formation of the desired compounds. Electrochemical studies were performed, revealing that the *N,O-p*-cymene-Ru(II)-PTA complexes result in two irreversible redox processes (oxidation of the Fe(II) and Ru(II) centres). Antiproliferative activity and interactions with bio molecules have also been investigated for all the reported complexes.

5.5 References

- [1] Donzello, M. P., Viola, E., Ercolani, C., Fu, Z., Futur, D., Kadish, K. M. (2012), Tetra-2,3-pyrazinoporphyrazines with externally appended pyridine rings. 12. New heteropentanuclear complexes carrying four exocyclic cis-platin-like functionalities as potential bimodal (PDT/cis-platin) anticancer agents, *Inorg. Chem.*, 51, 12548-12559. (DOI: 10.1021/ic301989a)
- [2] González-Pantoja, J. F., Stern, M., Jarzecki, A. A., Royo, E., Robles-Escajeda, E., Varela-Ramirez, A., Aguilera, R. J., Contel, M. (2011), Titanocene–phosphine derivatives as precursors to cytotoxic heterometallic TiAu₂ and TiM (M = Pd, Pt) compounds. studies of their interactions with DNA, *Inorg. Chem.*, 50(21), 11099-11110. (DOI: 10.1021/ic201647h)
- [3] Wenzel, M., Bertrand, B., Eymin, M-J., Comte, V., Harvey, J. A., Richard, P., Groessl, M., Zava, O., Amrouche, H., Harvey, P. D., Le Gendre, P., Picquet, M., Casini, A. (2011), Multinuclear cytotoxic metallodrugs: physicochemical characterization and biological

- properties of novel heteronuclear gold–titanium complexes, *Inorg. Chem.*, 50(19), 9472-9480. (DOI: 10.1021/ic201155y)
- [4] Pelletier, F., Comte, V., Massard, A., Wenzel, M., Toulot, S., Richard, P., Picquet, M., Le Gendre, P., Zava, O., Edafe, F., Casini, A., Dyson, P. J. (2010), Development of bimetallic titanocene-ruthenium-arene complexes as anticancer agents: relationships between structural and biological properties, *J. Med. Chem.*, 53(19), 6923-6933. (DOI: 10.1021/jm1004804)
- [5] Nieto, D., González-Vadillo, A. M., Brūna, S., Pastor, C. J., Ríos-Luci, C., León, L. G., Padrón, J. M., Navarro-Ranningerand, C., Cuadrado, I. (2012), Heterometallic platinum(II) compounds with β -aminoethylferrocenes: synthesis, electrochemical behaviour and anticancer activity, *Dalton Trans.*, 41, 432-441. (DOI: 10.1039/c1dt11358e)
- [6] Lease, N., Vasilevski, V., Carreira, M., de Almeida, A., Sanaú, M., Hirva, P., Casini, A., Contel, M. (2013), Potential anticancer heterometallic Fe-Au and Fe-Pd agents: initial mechanistic insights, *J. Med. Chem.*, 56, 5806-5818. (DOI: 10.1021/jm4007615)
- [7] Nieto, D., Bruña, S., González-Vadillo, A. M., Perles, J., Carrillo-Hermosilla, F., Antiñolo, A., Padrón, J. M., Plata, G. B., Cuadrado, I. (2015), Catalytically generated ferrocene-containing guanidines as efficient precursors for new redox-active heterometallic platinum(II) complexes with anticancer activity, *Organometallics*, 34, 5407-5417. (DOI: 10.1021/acs.organomet.5b00751)
- [8] Fouda, M. F. R., Abd-Elzaher, M. M., Abdelsamaia, R. A., Labib, A. A., (2007), On the medicinal chemistry of ferrocene, *Appl. Organomet. Chem.*, 21(8), 613-625. (DOI: 10.1002/aoc.1202)
- [9] Deka, B., Bhattacharyya, A., Mukherjee, S., Sarkar, T., Soni, K., Banerjee, S., Saikia, K. K., Deka, S., Hussain, A. (2017), Ferrocene conjugated copper(II) complexes of terpyridine and traditional Chinese medicine (TCM) anticancer ligands showing selective toxicity towards cancer cells, *Appl. Organomet. Chem.*, 32(4), e4287. (DOI: 10.1002/aoc.4287)

- [10] Patra, M., Gasser, G. (2017), The medicinal chemistry of ferrocene and its derivatives, *Nat. Rev. Chem.*1(66), 1-12. (DOI: 10.1038/s41570-017-0066)
- [11] Top, S., Dauer, B., Vaissermann, J., Jaouen, G. (1997), Facile route to ferrocifen, 1-[4-(2-dimethylaminoethoxy)]-1-(phenyl-2-ferrocenyl-but-1-ene), first organometallic analogue of tamoxifen, by the McMurry reaction, *J. Organomet. Chem.*, 541, 355-361. (DOI: 10.1016/S0022-328X(97)00086-7)
- [12] Top, S., Tang, J., Vessières, A., Carrez, D., Provot, C., Jaouen, G. (1996), Ferrocenyl hydroxytamoxifen: a prototype for a new range of oestradiol receptor site-directed cytotoxics, *Chem. Commun.*, 955-956. (DOI: 10.1039/CC9960000955)
- [13] Top, S., Vessières, A., Cabestaing, C., Laios, I., Leclercq, G., Provot, C., Jaouen, G. (2001), Studies on organometallic selective estrogen receptor modulators. (SERMs) Dual activity in the hydroxy-ferrocifen series, *J. Organomet. Chem.*, 637-639, 500-506. (DOI: 10.1016/S0022-328X(01)00953-6)
- [14] Hillard, E., Vessières, A., Le Bideau, F., Plazúk, D., Spera, D., Huché, M., Jaouen, G. (2006), A series of unconjugated ferrocenyl phenols: prospects as anticancer agents, *Chem. Med. Chem.* 1, 551-559. (DOI: 10.1002/cmdc.200500035)
- [15] Dive, D., Biot, C. (2008), Ferrocene conjugates of chloroquine and other antimalarials: the development of ferroquine, a new antimalarial, *Chem. Med. Chem.*, 3(3), 383-391. (DOI: 10.1002/cmdc.200700127)
- [16] Fourie, E., Erasmus, E., Swarts, C. J., Jakob, A., Lang, H., Joone, G. K., Rensburg, C. E. J. (2011), Cytotoxicity of ferrocenyl-ethynylphosphine metal complexes of gold and platinum, *Anticancer Res.*, 31(3), 825-829. (DOI: 0250-7005/2011)
- [17] Muenzner, J. K., Biersack, B., Albrecht, A., Rehm, T., Iacher, U., Milius, W., Casini, A., Zhang, J., Ott, I., Brabek, V., Stuchlikova, O., Andronache, I. C., Kaps, L., Schuppan, D., Schobert, R. (2016), Ferrocenyl-coupled N-heterocyclic carbene complexes of gold(I): a

- successful approach to multinuclear anticancer drugs, *Chem.-A Eur. J.*, 22(52), 18953-18962. (DOI: 10.1002/chem.201604246)
- [18] Mitra, K., Basu, U., Khan, I., Maity, B., Kondaiah, P., Chakravarty, A. K. (2014), Remarkable anticancer activity of ferrocenyl-terpyridine platinum(II) complexes in visible light with low dark toxicity, *Dalton Trans.*, 43, 751-763. (DOI: 10.1039/C3DT51922H)
- [19] Mitra, K., Shettar, A., Kondaiah, P., Chakravarty, A. R. (2016), Biotinylated platinum(II) ferrocenylterpyridine complexes for targeted photoinduced cytotoxicity, *Inorg. Chem.*, 55(11), 5612-5622. (DOI: 10.1021/acs.inorgchem.6b00680)
- [20] Kapdi, A. R., Fairlamb, I. J. S. (2014), Anti-cancer palladium complexes: a focus on PdX₂L₂, palladacycles and related complexes, *Chem. Soc. Rev.*, 43, 4751-4777. (DOI: 10.1039/C4CS00063C)
- [21] Tabrizi, L., Chiniforoshan, H. (2017), The cytotoxicity and mechanism of action of new multinuclear scaffold Au^{III}, Pd^{II} pincer complexes containing a bis(diphenylphosphino) ferrocene/non-ferrocene ligand, *Dalton Trans.*, 46, 14164-14173. (DOI: 10.1039/C7DT02887C)
- [22] Ma, D-L., Wang, M., Mao, Z., Yang, C., Ng, C-T., Leung, C-H. (2016), Rhodium complexes as therapeutic agents, *Dalton Trans.*, 45, 2762-2771. (DOI: 10.1039/C5DT04338G)
- [23] Tabrizi, L., Chiniforoshan, H. (2017), Designing new iridium(III) arene complexes of naphthoquinone derivatives as anticancer agents: a structure-activity relationship study, *Dalton Trans.*, 46, 2339-2349. (DOI: 10.1039/C6DT04339A)
- [24] Govender, P., Riedel, T., dyson, P. J., Smith, G. S. (2016), Regulating the anticancer properties of organometallic dendrimers using pyridylferrocene entities: synthesis, cytotoxicity and DNA binding studies, *Dalton Trans.*, 45, 9529-9539. (DOI: 10.1039/C6DT00849F)
- [25] Mu, C., Chang, S. W., Prosser, K. E., Leung, A. W. Y., Santacruz, S., Jang, T., Thompson, J. R., Yapp, D. T. T., Warren, J. J., Bally, M. B., Timothy, V. (2016), Induction of cytotoxicity in pyridine

- analogues of the anti-metastatic Ru(III) complex NAMI-A by ferrocene functionalization, *Inorg. Chem.*, 55(1), 177-190. (DOI: 10.1021/acs.inorgchem.5b02109)
- [26] Adams, M., de Kock, C., Smith, P. J., Land, K. M., Liu, N., Hopper, M., Hsiao, A., Burgoyne, A. R., Stringer, T., Meyer, M., Wiesner, L., Chibale, K., Smith, G. S. (2015), Improved antiparasitic activity by incorporation of organosilane entities into half-sandwich ruthenium(II) and rhodium(III) thiosemicarbazone complexes, *Dalton Trans.*, 44, 2456-2468. (DOI: 10.1039/C4DT03234A)
- [27] Auzias, M., Gueniat, J., Therrien, B., Süß-Fink, G., Renfrew, A. K., Dyson, P. J. (2009), Arene-ruthenium complexes with ferrocene-derived ligands: Synthesis and characterization of complexes of the type $[\text{Ru}(\eta^6\text{-arene})(\text{NC}_5\text{H}_4\text{CH}_2\text{NHOC-C}_5\text{H}_4\text{FeC}_5\text{H}_5)\text{Cl}_2]$ and $[\text{Ru}(\eta^6\text{-arene})(\text{NC}_3\text{H}_3\text{N}(\text{CH}_2)_2\text{O}_2\text{C-C}_5\text{H}_4\text{FeC}_5\text{H}_5)\text{Cl}_2]$, *J. Organomet. Chem.*, 694(6), 855-861. (DOI: 10.1016/j.jorganchem.2008.08.012)
- [28] Tauchman, J., Süß-Fink, G., Štěpnička, P., Zava, O., dyson, P. J. (2013), Arene ruthenium complexes with phosphinoferrocene amino acid conjugates: Synthesis, characterization and cytotoxicity, *J. Organomet. Chem.*, 723(1), 233-238. (DOI: 10.1016/j.jorganchem.2012.10.009)
- [29] Auzias, M., Therrien, B., Süß-Fink, G. (2012), Heteronuclear complexes containing the *N,N'*-di(2-pyridyl)amidocarboxylferrocene ligand, *Inorganica Chim. Acta*, 387, 446-449. (DOI: 10.1016/j.ica.2012.01.016)
- [30] Auzias, M., Therrien, B., Süß-Fink, G., Štěpnička, P., Ang, W. H., Dyson, P. J. (2008), Ferrocenoyl pyridine arene ruthenium complexes with anticancer properties: synthesis, structure, electrochemistry, and cytotoxicity, *Inorg. Chem.*, 47(2), 578-583. (DOI: 10.1021/ic7018742)
- [31] Govender, P., Lemmerhirt, H., Hutton, A. T., Therrien, B., Bednarski, Smith, G. S. (2014), First- and second-generation heterometallic dendrimers containing ferrocenyl-ruthenium(II)-arene motifs: synthesis, structure, electrochemistry, and preliminary

- cell proliferation studies, *Organometallics*, 33(19), 5535-5545. (DOI: 10.1021/om500809g)
- [32] Barragán, F., Carrison-Salip, D., Gómez-Pinto, I., González-Cantó, A., Sadler, P. J., de Llorens, R., Moreno, Virtudes, González, C., Massaguer, A., Marchán, V. (2012), Somatostatin subtype-2 receptor-targeted metal-based anticancer complexes, *Bioconjug Chem.*, 23(9), 1838-1855. (DOI: 10.1021/bc300173h)
- [33] Albada, B., Metzler-Nolte, N. (2016), Organometallic-peptide bioconjugates: synthetic strategies and medicinal applications, *Chem. Rev.*, 116, 11797-11839. (DOI: 10.1021/acs.chemrev.6b00166)
- [34] Mandal, P., Malviya, N., Guedes da Silva, M. F. C., Dhankhar, S. S., Nagaraja, C. M., Mobin, S. M., Mukhopadhyay, S. (2016), Fine tuning through valence bond tautomerization of ancillary ligands in ruthenium(II) arene complexes for better anticancer activity and enzyme inhibition properties, *Dalton Trans.*, 45, 19277-19289. (DOI: 10.1039/C6DT02969H)
- [35] Almodares, Z., Lucas, S. J., Crossley, B. D., Basri, A. M., Pask, C. M., Hebden, A. J., Phillips, R. M., McGowan, P. C. (2014), Rhodium, iridium, and ruthenium half-sandwich picolinamide complexes as anticancer agents, *Inorg. Chem.*, 53(2), 727-736. (DOI: 10.1021/ic401529u)
- [36] Mandal, P., Kundu, B. K., Vyas, K., Sabu, V., Helen, A., Dhankhar, S. S., Nagaraja, C. M., Bhattacharjee, D., Bhabak, K. P., Mukhopadhyay, S. (2018), Ruthenium(II) arene NSAID complexes: inhibition of cyclooxygenase and antiproliferative activity against cancer cell lines, 47, 517-527. (DOI: 10.1039/C7DT03637J)
- [37] Mandal, P., Malviya, N., Kundu, B. K., Dhankhar, S. S., Nagaraja, C. M., Mukhopadhyay, S. (2018), RAPTA complexes containing N-substituted tetrazole scaffolds: synthesis, characterization and antiproliferative activity, *Appl. Organometal. Chem.*, 32, e4179. (DOI: 10.1002/aoc.4179)

- [38] Liu, H-K., Sadler, P. J. (2011), Metal complexes as DNA intercalators, *Acc. Chem. Res.*, 44 (5), 349–359. (DOI: 10.1021/ar100140e)
- [39] Sathyaraj, G., Kiruthika, M., Weyhermüller, T., Unni Nair, B. (2012), Oxidative cleavage of DNA by ruthenium(II) complexes containing a ferrocene/non-ferrocene conjugated imidazole phenol ligand, *Organometallics*, 31(19), 6980-6987. (DOI: 10.1021/om3007882)
- [40] Selbo, P. K., Sandvig, K., Kirveliene, V., Berg, K. (2000), Release of gelonin from endosomes and lysosomes to cytosol by photochemical internalization, *Biochem. Biophys. Acta.*, 1475, 307-313. (DOI: 10.1016/S0304-4165(00)00082-9)
- [41] Auzias, M., Therrien, B., Süß-Fink, G., Štěpnička, P., Ang, W. H., Dyson, P. J. (2008), Ferrocenoyl pyridine arene ruthenium complexes with anticancer properties: synthesis, structure, electrochemistry, and cytotoxicity, *Inorg. Chem.*, Vol. 47(2), 578-583. (DOI: 10.1021/ic7018742).

Chapter 6

RAPTA Type of Complexes Containing Different Phosphine Ligands: Synthesis, Characterisation and Antiproliferative Activity

6.1 Introduction

Ruthenium has turned out to be the most promising metal for replacing platinum in a future cancer therapy. Many of the ruthenium compounds show low toxicity, and ruthenium(II) complexes exhibit slow ligand exchange kinetics, similar to those of platinum(II) complexes, which seems to be essential for anticancer activity.^[1] Recently, the development of organometallic ruthenium(II)-arene compounds, stabilized in the +2 oxidation state by the η^6 -coordinated arene ligand, have introduced a different metallodrug scaffold as alternative to that of the coordination compounds of ruthenium (II) that have entered into clinical studies so far (KP1019 and NAMI-A).^[2-5] A prominent example of an organometallic ruthenium-based compound is [Ru(*p*-cymene)Cl₂(PTA)], termed RAPTA-C (PTA = 1,3,5-triaza-7-phosphaadamantane)^[6,7], which exhibits generally low cytotoxicity *in vitro*^[8] but relevant antimetastatic^[9,10] and antiangiogenic^[11] properties *in vivo*. Moreover, it has recently been observed that RAPTA-C reduces the growth of primary tumours in preclinical models for ovarian and colorectal carcinomas *via* antiangiogenic mechanism^[12,13] with low general toxicity and tolerance to low pH.^[14,15] RAPTA compounds, characterised by its pseudo-octahedral environment, consists of a ruthenium center, an η^6 -coordinated arene ring, typically *p*-cymene (RAPTA-C) or toluene (RAPTA-T), 1,3,5-triaza-7-phosphaadamantane (PTA) ligand and two chloride ligand. Because of their structural similarity with piano-stools, these types of complexes are also known as half-sandwich piano-stool complexes (Fig.6.1).^[16] RAPTA compounds have been found to show promising antiproliferative activity with their water solubility being imparted by the cage-like 1,3,5-triaza-7-phosphaadamantane (PTA) ligand, binding the metal in a κ^1 -P fashion.^[17] These compounds interact strongly with proteins, with the ability to discriminate binding to different proteins, but show a relatively low propensity to bind DNA, which is considered to be the main target of many metal-based drugs.^[18-20]

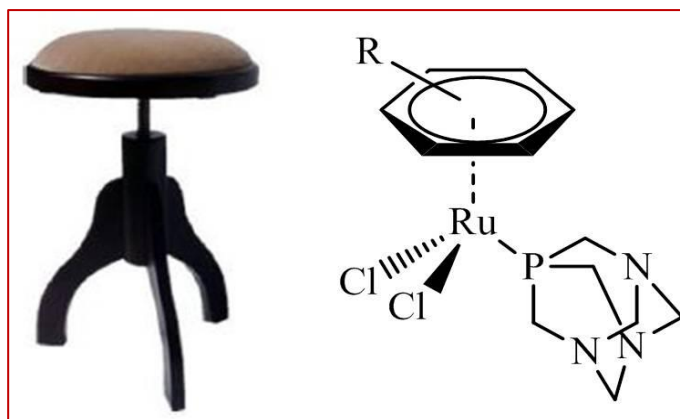


Fig 6.1: (Left) Piano-stool and (right) model of RAPTA complex.

There are various reports where different phosphine ligands have been coordinated to Ru(II) centre in order to develop RAPTA complexes with better anticancer activity. For example, 1,4,7-triaza-9-phosphatricyclo [5.3.2.1] tridecane (CAP) has been used in place of PTA to produce RAPTA type of complexes, which has shown enhanced cytotoxic activity against cancer cell lines than the corresponding PTA analogue with reasonable degree of cancer cell selectivity.^[21] Phosphine ligands, functionalized with perfluorinated chains, show thermomorphic properties *i.e.* significant increase in solubility with increase in temperature.^[22,23] Dyson *et al* developed thermomorphic RAPTA compounds incorporating fluorophosphine ligands, which have shown improved cytotoxicity at elevated temperature.^[24] Ethacryonic acid, a biologically active molecule, has the ability to inhibit the activity of glutathione transferases (GSTs), which is overexpressed in pancreatic cancer cell lines.^[25,26] A series of Ru(II)-arene complexes containing triphenylphosphane ligands, functionalised with ethacryonic acid, have been reported with marked antiproliferative activity against pancreatic cancer cell line BxPC3.^[27] Again, macromolecular RAPTA-C analogue has been prepared by conjugating degradable polymeric micelles with enhanced chemotherapeutic property.^[28] A series of compounds of the general formula $[M(\eta^6\text{-arene})(PTN)Cl]X$ (PTN=3,7-dimethyl-7-phosphatridecane) have been prepared in order to compare the influence of structural variation on the anticancer activity of RAPTA type complexes.^[29]

In this chapter, four new RAPTA type of complexes have been reported utilizing different phosphine ligands. Antiproliferative activity and solution stability study have also been carried out with the prepared complexes.

6.2 Experimental section

6.2.1 Materials and methods

All the required chemicals were purchased from Sigma and used without further purification. The specifications of all the instruments used for analysis purpose were same as described in the section 2.2.1 of the chapter 2.

6.2.1.1 Synthesis of $[\text{Ru}(\eta^6\text{-}p\text{-cymene})(\text{TFP})\text{Cl}_2]$ [25]

To a solution of $[\text{Ru}(\eta^6\text{-}p\text{-cymene})\text{Cl}_2]_2$ (0.1 g, 0.16 mol) in CH_2Cl_2 (50 mL), a methanolic solution (10 mL) of tris(2-furyl) phosphine (0.04g, 0.16 mmol) (TFP) was added dropwise and stirred overnight at room temperature. The resulting orange coloured solution was evaporated to dryness to obtain orange solid as the product. The crude product was dissolved in MeOH and kept in refrigerator overnight, from which single crystals of **25** suitable for X-ray analysis were obtained. Yield: 67%. ^1H NMR (400.13MHz, 298K, CDCl_3) δ : 8.01 [d, 3H, 3 \times CH of $\text{C}_{12}\text{H}_9\text{O}_3\text{P}$], 6.95 [d, 3H, 3 \times CH of $\text{C}_{12}\text{H}_9\text{O}_3\text{P}$], 6.62 [d, 3H, 3 \times CH of $\text{C}_{12}\text{H}_9\text{O}_3\text{P}$], 5.83-5.66 [m, 4H, 4 \times CH of C_6H_4], 1.88 [s, 3H, $\text{C}_6\text{H}_4\text{CH}_3$], 1.02 [d, 6H, $\text{CH}(\text{CH}_3)_2$]. ^{13}C NMR (100.61MHz, CDCl_3) δ : 148.8 [3 \times C of $\text{C}_{12}\text{H}_9\text{O}_3\text{P}$], 144.2 [3 \times CH of $\text{C}_{12}\text{H}_9\text{O}_3\text{P}$], 123.9 [3 \times CH of $\text{C}_{12}\text{H}_9\text{O}_3\text{P}$], 111.7 [3 \times CH of $\text{C}_{12}\text{H}_9\text{O}_3\text{P}$], 108.5 [C of C_6H_4], 97.8 [C of C_6H_4], 90.2 [2 \times CH of C_6H_4], 86.8 [2 \times CH of C_6H_4], 30.2 [$\text{CH}(\text{CH}_3)_2$], 21.7 [2 \times $\text{CH}(\text{CH}_3)_2$], 17.6 [$\text{C}_6\text{H}_4\text{CH}_3$]. ^{31}P NMR (CDCl_3 , 126 MHz): δ -14.3. ESI-MS (+ve mode): $[\text{Ru}(\eta^6\text{-}p\text{-cymene})(\text{TFP})\text{Cl}]^+$: 503.0 (m/z). Anal. Calcd for $\text{C}_{22}\text{H}_{23}\text{Cl}_2\text{O}_3\text{PRu}$ (%): C, 49.08; H, 4.31. Found: C, 49.36; H, 4.53.

6.2.1.2 Synthesis of $[\text{Ru}(\eta^6\text{-}p\text{-cymene})(\text{TFP})_2\text{Cl}]\text{BF}_4$ [26]

$[\text{Ru}(\eta^6\text{-}p\text{-cymene})(\text{TFP})\text{Cl}_2]$ **25** (0.1 g, 0.18 mmol) was dissolved in dry CH_2Cl_2 (50 mL). A methanolic solution of TFP (0.04 g, 0.18 mmol) and NaBF_4 (0.02g, 0.18 mmol) was added with stirring. The mixture was allowed to stir overnight to afford a yellow coloured solution. The mixture was concentrated *in vacuo* to ca. 5 mL and kept overnight at 4°C, from which single crystal of **26** was obtained. ^1H NMR (400.13MHz, 298K, $\text{DMSO-}d_6$) δ : 7.98 [br.s, 6H, 6 \times CH of $\text{C}_{24}\text{H}_{18}\text{O}_6\text{P}_2$], 6.71 [d, 6H, 6 \times CH of $\text{C}_{24}\text{H}_{18}\text{O}_6\text{P}_2$], 6.61 [br.s, 6H, 6 \times CH of $\text{C}_{24}\text{H}_{18}\text{O}_6\text{P}_2$], 6.25 [d, 2H, 2 \times CH of C_6H_4], 5.79 [d, 2H, 2 \times CH of C_6H_4], 2.65 [m, 1H, $\text{CH}(\text{CH}_3)_2$], 1.26 [s, 3H, $\text{C}_6\text{H}_4\text{CH}_3$], 1.14 [d, 6H, $\text{CH}(\text{CH}_3)_2$]. ^{13}C NMR (100.61MHz, CDCl_3) δ : 148.8 [3 \times C of $\text{C}_{12}\text{H}_9\text{O}_3\text{P}$], 144.2 [3 \times CH of $\text{C}_{12}\text{H}_9\text{O}_3\text{P}$], 123.9 [3 \times CH of $\text{C}_{12}\text{H}_9\text{O}_3\text{P}$], 111.7 [3 \times CH of $\text{C}_{12}\text{H}_9\text{O}_3\text{P}$], 108.5 [C of C_6H_4], 97.8 [C of C_6H_4], 90.2 [2 \times CH of C_6H_4], 86.8 [2 \times CH of C_6H_4], 30.2 [$\text{CH}(\text{CH}_3)_2$], 21.7 [2 \times CH(CH_3) $_2$], 17.6 [$\text{C}_6\text{H}_4\text{CH}_3$]. ^{31}P NMR ($\text{DMSO-}d_6$, 126 MHz): δ -13.4. ESI-MS (+ve mode): $[\text{Ru}(\eta^6\text{-}p\text{-cymene})(\text{TFP})_2\text{Cl}]^+$: 735.1 (m/z). Anal. Calcd for $\text{C}_{34}\text{H}_{32}\text{BClF}_4\text{O}_6\text{P}_2\text{Ru}$ (%): C, 49.69; H, 3.92. Found: C, 49.43; H, 3.43.

6.2.1.3 Synthesis of $[\text{Ru}(\eta^6\text{-}p\text{-cymene})(\text{TFP})(\text{PPh}_3)\text{Cl}]\text{Cl}$ [27]

0.1 g of $[\text{Ru}(\eta^6\text{-}p\text{-cymene})(\text{TFP})\text{Cl}_2]$ **25** (0.18 mmol) was dissolved in 30 mL of MeOH and Triphenylphosphine (0.04g, 0.18 mmol), dissolved in MeOH (10 mL) was added dropwise to the solution of it. The mixture was stirred overnight at room temperature. The resulting orange coloured solution was kept overnight at room temperature from which crystalline compound of **27** was obtained. Yield: 71%. ^1H NMR (400.13MHz, 298K, $\text{DMSO-}d_6$) δ : 7.75 [m, 9H, 9 \times CH of $\text{C}_{12}\text{H}_9\text{O}_3\text{P}$], 7.40 [m, 15H, 15 \times CH of $\text{C}_{18}\text{H}_{15}\text{P}$], 5.30 [d, 2H, 2 \times CH of C_6H_4], 5.25 [d, 2H, 2 \times CH of C_6H_4], 1.77 [s, 3H, $\text{C}_6\text{H}_4\text{CH}_3$], 0.93 [d, 6H, $\text{CH}(\text{CH}_3)_2$]. ^{13}C NMR (100.61MHz, $\text{DMSO-}d_6$) δ : 149.5 [3 \times C of $\text{C}_{12}\text{H}_9\text{O}_3\text{P}$], 142.7 [3 \times CH of $\text{C}_{12}\text{H}_9\text{O}_3\text{P}$], 137.0-136.9 [3 \times C of $\text{C}_{18}\text{H}_{15}\text{P}$], 134.4-134.1 [3 \times CH of $\text{C}_{18}\text{H}_{15}\text{P}$], 128.8-128.2 [6 \times CH of $\text{C}_{18}\text{H}_{15}\text{P}$], 123.5 [3 \times CH of $\text{C}_{12}\text{H}_9\text{O}_3\text{P}$], 112.1 [3 \times CH of $\text{C}_{12}\text{H}_9\text{O}_3\text{P}$], 101.1 [C of C_6H_4], 95.7 [C of C_6H_4], 89.9 [2 \times CH of C_6H_4],

87.0 [2×CH of C₆H₄], 30.1 [CH(CH₃)₂], 21.7 [C₆H₄CH₃], 17.5 [CH(CH₃)₂], 15.3 [CH(CH₃)₂]. ³¹P NMR (DMSO-*d*₆, 126 MHz): δ -26.1 to -24.0 [C₁₈H₁₅P], -14.2 to -13.3 [C₁₂H₉O₃P]. ESI-MS (+ve mode): [Ru(η⁶-*p*-cymene)(TFP)(PPh₃)Cl]⁺: 765.1 (m/z). Anal. Calcd for C₄₀H₃₈Cl₂O₃P₂Ru(%): C, 60.00; H, 4.78. Found: C, 60.03; H, 4.43.

6.2.1.4 Synthesis of [Ru(η⁶-*p*-cymene)(TFP)(PTA)Cl]BF₄ [28]

A methanolic solution (10mL) of 1, 3, 5-triaza phosphoadamantane (0.03g, 0.186 mmol) (PTA) was added dropwise to a solution of complex **25** (0.1 g, 0.186 mmol), dissolved in methanol (50 mL). A methanolic solution of NaBF₄ (0.02 g, 0.186 mmol) was added to it and stirred overnight at room temperature. The resulting solution was then filtered and evaporated *in vacuo* to ca. 5 mL and kept at 4°C. Single crystal of complex **28** was obtained after 4-5 days from that concentrated solution. ¹H NMR (400.13MHz, 298K, DMSO-*d*₆) δ: 8.01 [br.s, 3H, 3×CH of C₁₂H₉O₃P], 6.95 [d, 3H, 3×CH of C₁₂H₉O₃P], 6.61 [d, 3H, 3×CH of C₁₂H₉O₃P], 5.81 [d, 2H, 2×CH of C₆H₄], 5.79 [d, 2H, 2×CH of C₆H₄], 4.43 [s, 6H, 3×NCH₂N], 4.17 [s, 6H, 3×NCH₂N], 2.82 [m, 1H, CH(CH₃)₂], 2.09 [s, 3H, C₆H₄CH₃], 0.98 [d, 6H, CH(CH₃)₂]. ¹³C NMR (100.61MHz, DMSO-*d*₆) δ: 149.8 [3×C of C₁₂H₉O₃P], 144.4 [3×CH of C₁₂H₉O₃P], 124.1 [3×CH of C₁₂H₉O₃P], 112.3 [3×CH of C₁₂H₉O₃P], 104.8 [C of C₆H₄], 95.8 [C of C₆H₄], 88.6 [2×CH of C₆H₄], 85.4 [2×CH of C₆H₄], 72.6 [3×NCH₂N of PTA], 51.9 [3×PCH₂N of PTA], 30.7 [CH(CH₃)₂], 23.7 [C₆H₄CH₃], 19.8 [CH(CH₃)₂], 18.5 [CH(CH₃)₂]. ³¹P NMR (CDCl₃, 126 MHz): δ -14.3 [C₁₂H₉O₃P], -34.4 [PTA]. ESI-MS (+ve mode): [Ru(η⁶-*p*-cymene)(TFP)Cl]⁺: 503.0 (m/z), [Ru(η⁶-*p*-cymene)(PTA)Cl]⁺: 428.1 (m/z). Anal. Calcd for C₂₈H₃₅BClF₄N₃O₃P₂Ru(%): C, 45.03; H, 4.72; N, 5.63. Found: C, 45.02; H, 4.71; N, 5.34.

6.2.2 X-ray crystallography

6.2.2.1 X-ray crystallography of complex **25**, **26** and **28**

The description of instrumentation of X-ray crystallography for complexes **25**, **26** and **28** is same as described in Section 2.2.2.3.

6.2.3 Growth inhibition study

The procedure for SRB assay is same as discussed in chapter 2.

6.2.4 Stability studies in DMSO

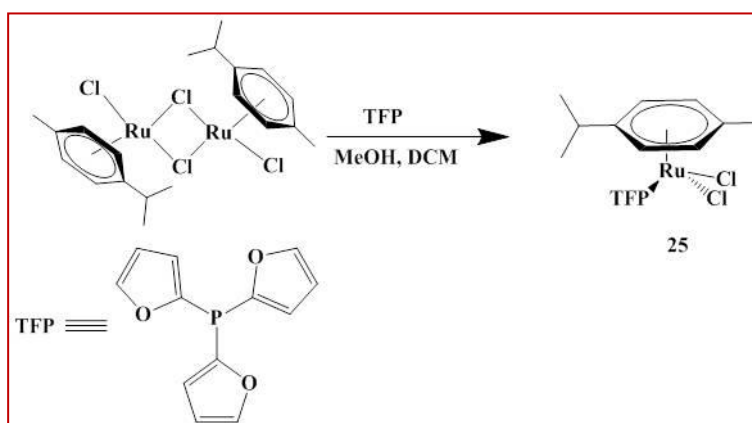
In order to check the stability of the prepared compounds in solution state, 1-2 mg of the sample was dissolved in 1% DMSO and its UV-vis spectra was recorded after 0.5, 24 and 48 h.

6.2.5 Supplementary materials

CCDC 1551675, 1840408, and 1840409 contain the supplementary crystallographic data for **25**, **26** and **28** respectively. These data can be obtained free of charge via <http://www.ccdc.cam.ac.uk/conts/retrieving.html>, or from the Cambridge Crystallographic Data Centre, 12 Union Road, Cambridge CB2 1EZ, UK; fax: (+44) 1223-336-033; or e-mail: deposit@ccdc.cam.ac.uk.

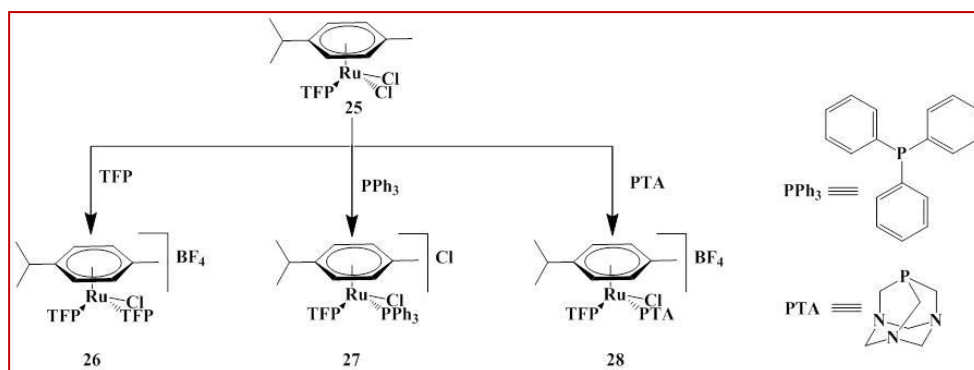
6.3 Result and discussions:

Complex **25** was obtained in moderate yield when tris(2-furyl) phosphine and $[(\eta^6\text{-}p\text{-cymene})\text{RuCl}_2]_2$ was mixed in 1:1 ratio and stirred overnight at room temperature (Scheme 6.1).



Scheme 6.1: Synthesis of compound $[\text{Ru}(\eta^6\text{-}p\text{-cymene})(\text{TFP})\text{Cl}_2]$ **25**.

Whereas, complex **26**, **27** and **28** were prepared by stirring a mixture of complex **25** with appropriate ligands at room temperature (Scheme 6.2).



Scheme 6.2: Synthesis of compounds $[\text{Ru}(\eta^6\text{-}p\text{-cymene})(\text{TFP})_2\text{Cl}]\text{BF}_4$ **26**, $[\text{Ru}(\eta^6\text{-}p\text{-cymene})(\text{TFP})(\text{PPh}_3)\text{Cl}]\text{Cl}$ **27** and $[\text{Ru}(\eta^6\text{-}p\text{-cymene})(\text{TFP})(\text{PTA})\text{Cl}]\text{BF}_4$ **28**.

All the complexes are air stable and soluble in dichloromethane, methanol, DMSO and water. All the complexes have been characterized by ^1H , ^{13}C and ^{31}P NMR spectroscopy, ESI-MS and elemental analyses. Furthermore, complex **25**, **26**, and **28** were additionally characterized in solid state by single crystal X-ray diffraction. The ^1H NMR spectra of complexes **25**, **26**, **27** and **28** show a typical band for the p -cymene moiety in the range of 5.3–6.25 and 5.25–5.79 ppm for ring protons and 2.65–2.82, 1.26–2.09 and 0.93–1.14 ppm for side chain protons (Fig.6.2-Fig.6.5). p -cymene proton signals become little downfield than the $[(\eta^6\text{-}p\text{-cymene})\text{RuCl}_2]_2$ precursor due to coordination to phosphorous containing ligands. For all the complexes, resonance due to the TFP protons is shifted towards the upper field with respect to uncoordinated TFP, confirming the coordination to the metal centre. In case of complex **27**, peaks for TFP protons and peaks for PPh_3 protons appear as two separate multiplets, upfield than the free ligands. In case of complex **28**, two sets of multiplets were observed for two sets of PTA protons as reported earlier.^[30]

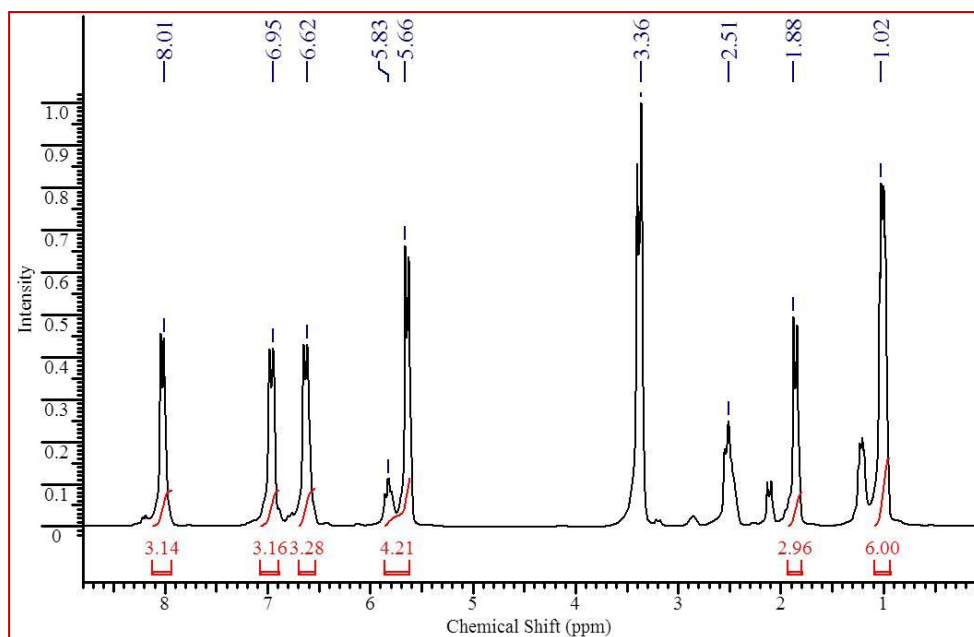


Fig.6.2: ^1H NMR spectra of complex 25.

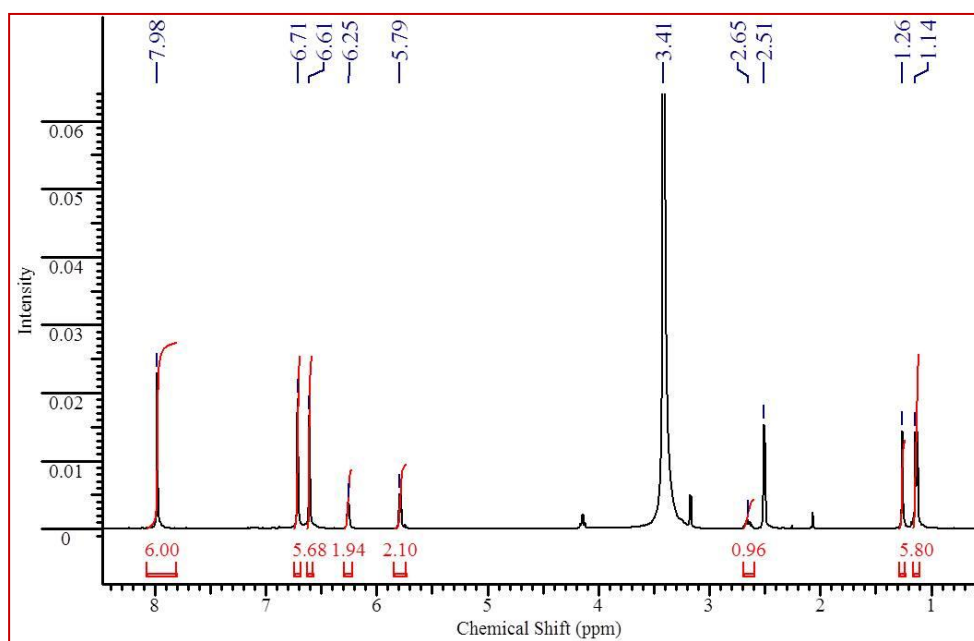


Fig.6.3: ^1H NMR spectra of complex 26.

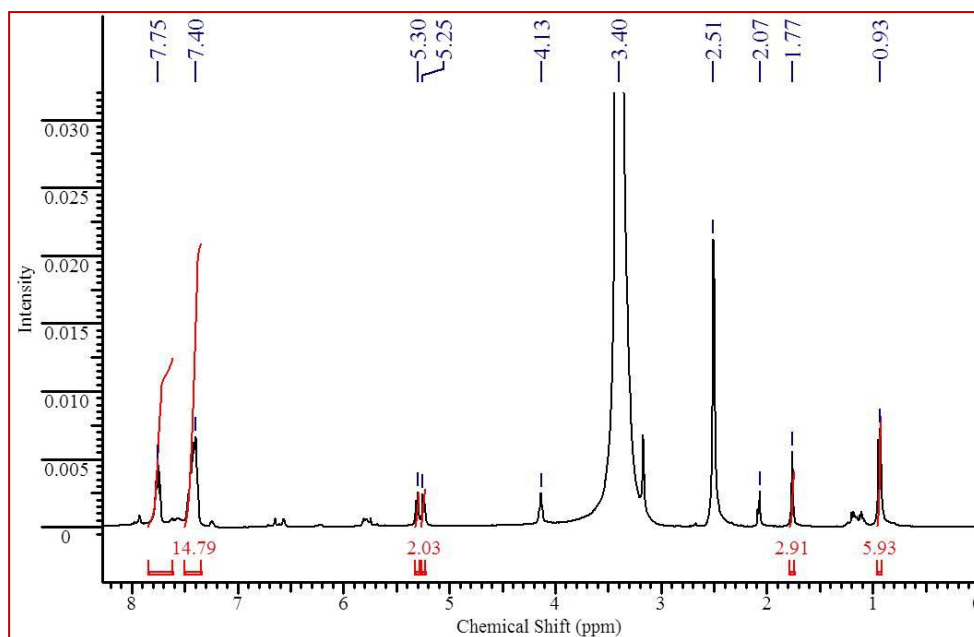


Fig.6.4: ^1H NMR spectra of complex 27.

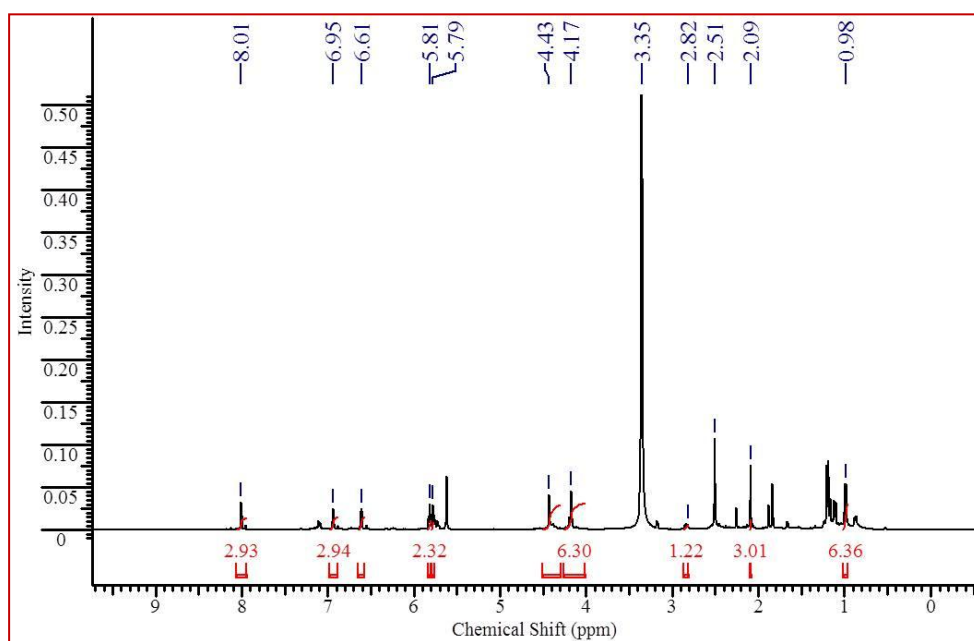


Fig.6.5: ^1H NMR spectra of complex 28.

In case of ^{13}C NMR spectra, peaks for the phosphine ligands (TFP and PPh_3) become downfield than the free ligand owing to their electron donating nature and corroborate well with the proposed structure (Fig.6.6- Fig.6.9).

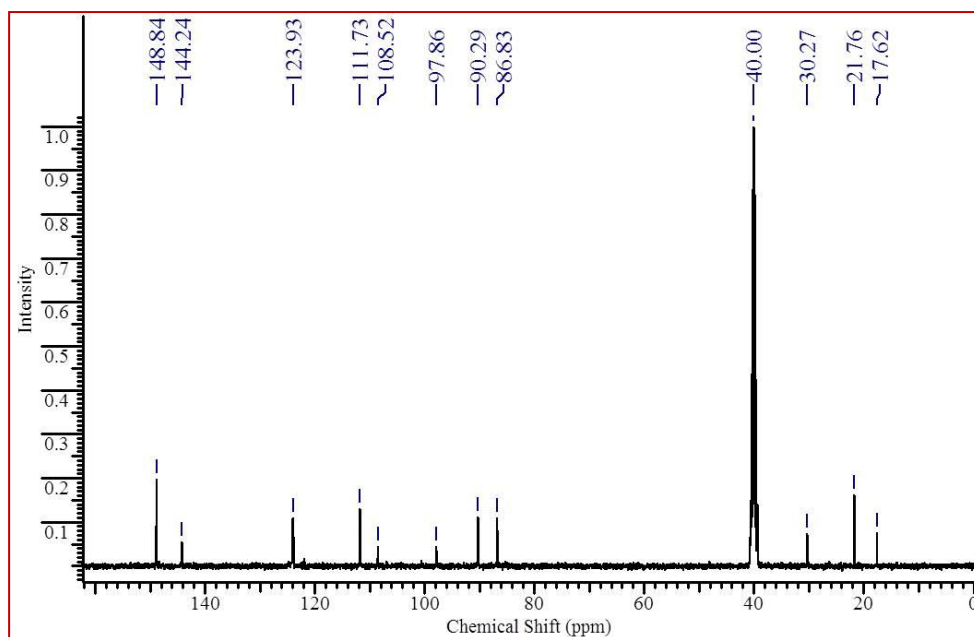


Fig.6.6: ^{13}C NMR spectra of complex 25.

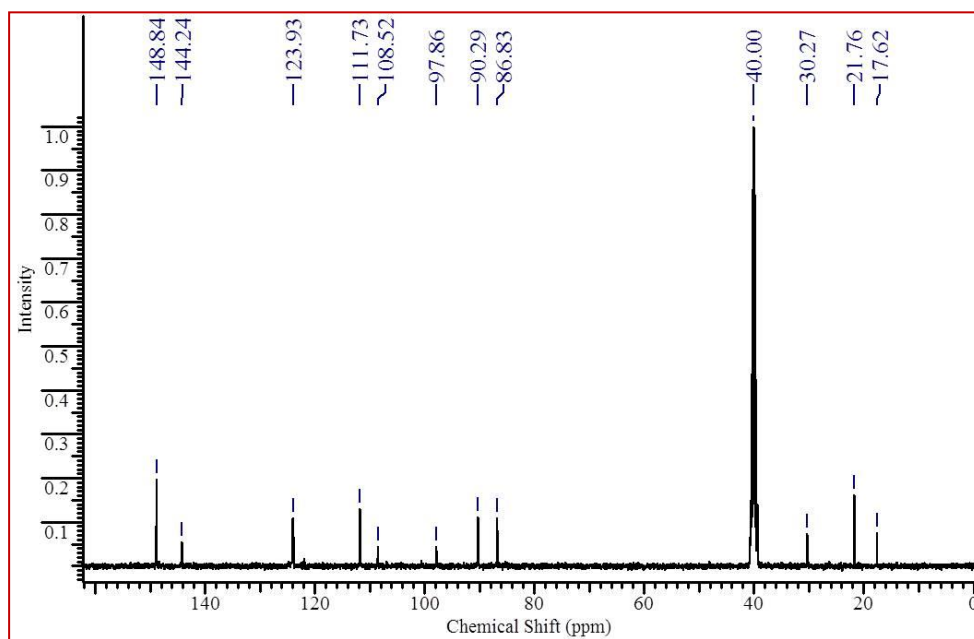


Fig.6.7: ^{13}C NMR spectra of complex 26.

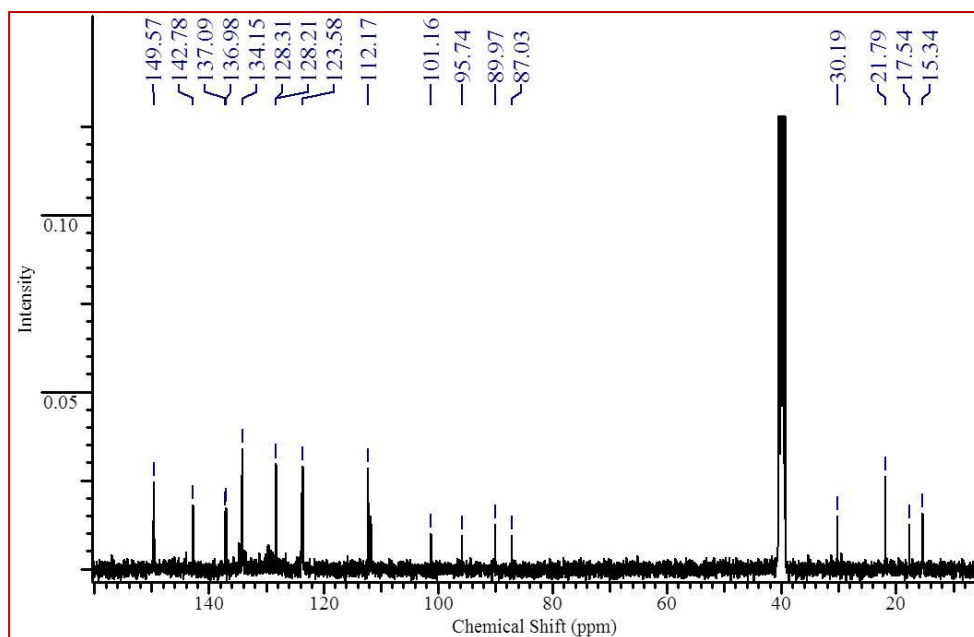


Fig.6.8: ^{13}C NMR spectra of complex 27.

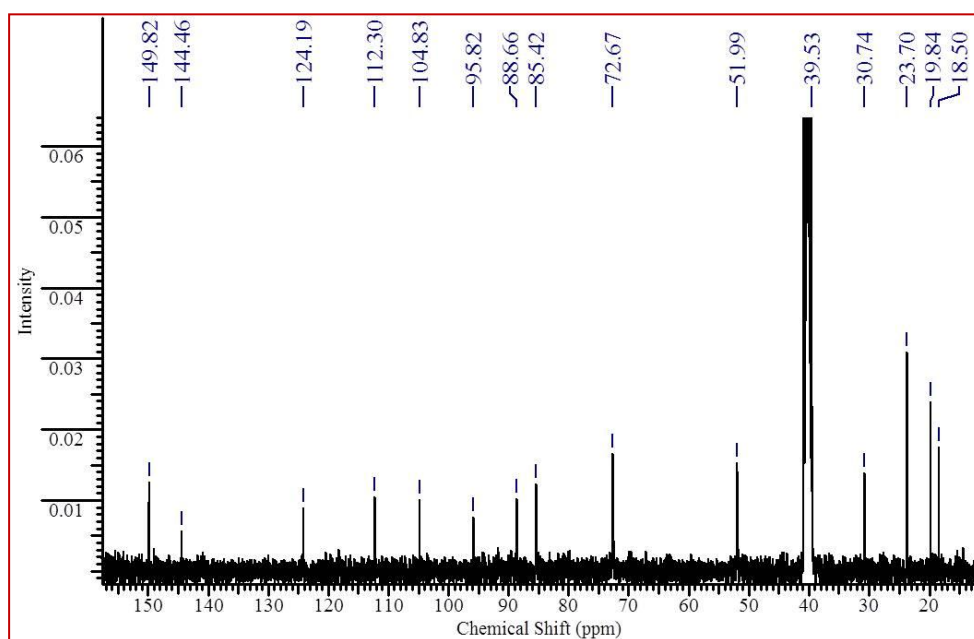


Fig.6.9: ^{13}C NMR spectra of complex 28.

For all the complexes, ^{31}P NMR signals of the phosphine ligands shifted downfield very considerably as compared to the resonance of the free ligand in the range of -34 to -14 ppm (Fig.6.10-Fig.6.13). Shifting of the peaks towards higher δ value confirms the coordination of the ligands to the ruthenium centre.

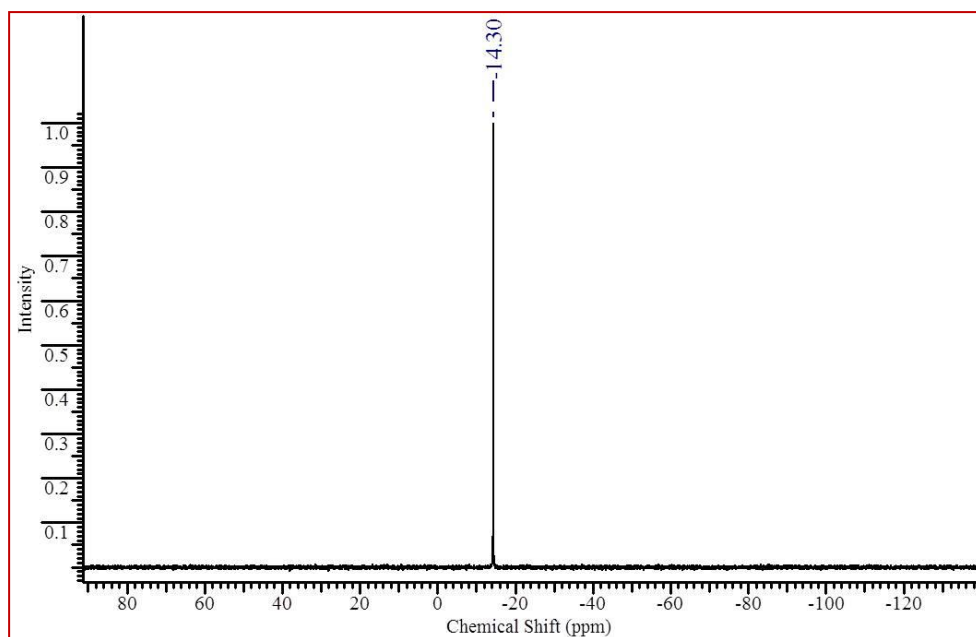


Fig.6.10: ^{31}P NMR spectra of complex 25.

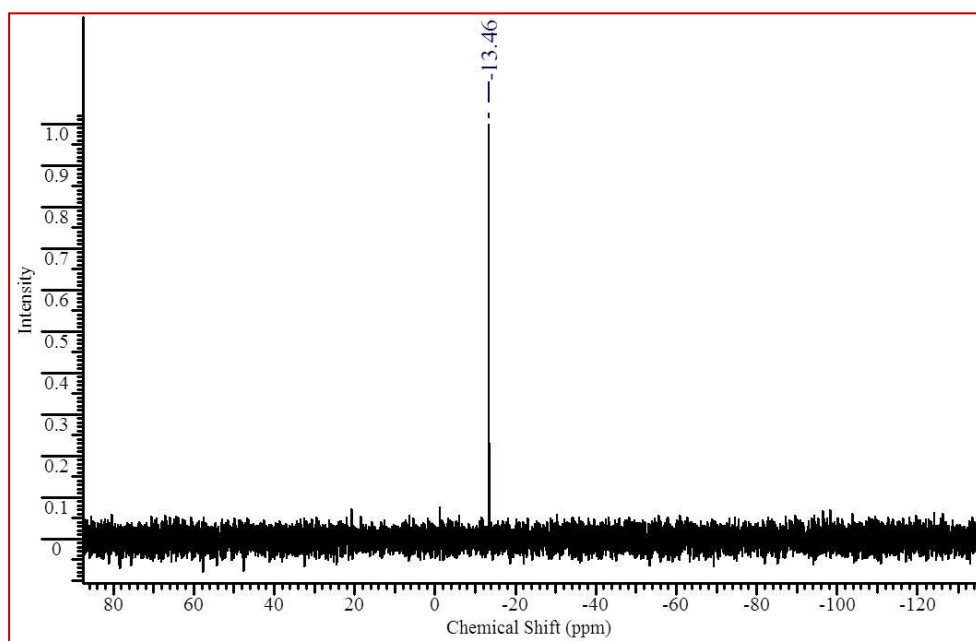


Fig.6.11: ^{31}P NMR spectra of complex 26.

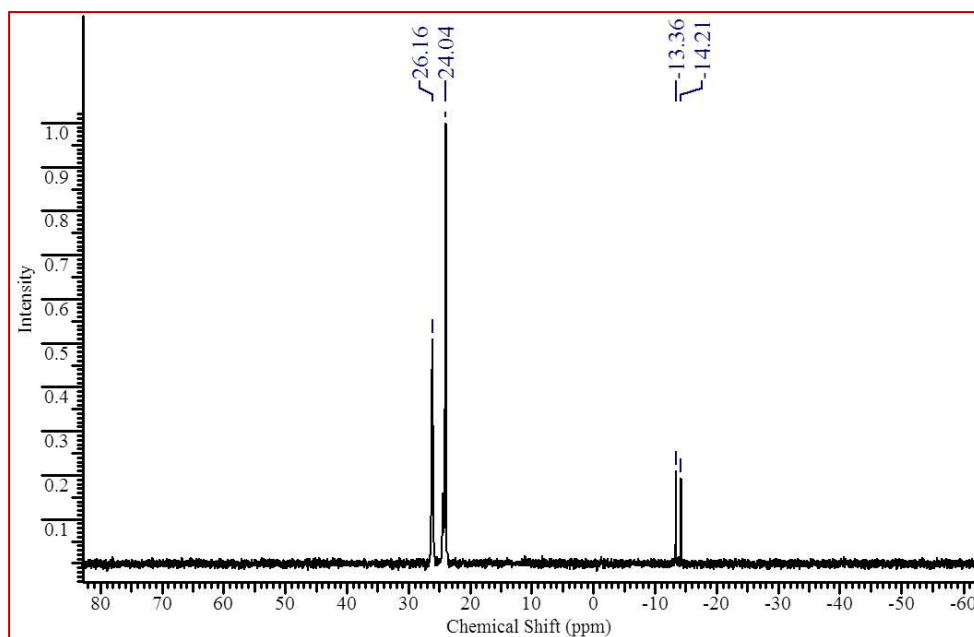


Fig.6.12: ^{31}P NMR spectra of complex **27**.

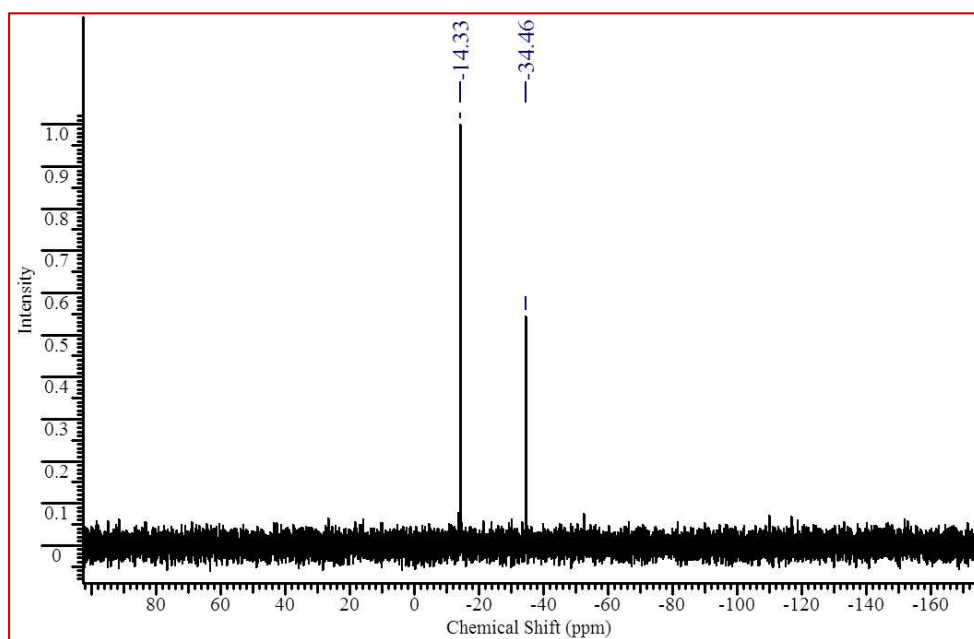


Fig.6.13: ^{31}P NMR spectra of complex **28**.

The ESI mass spectra of **25**, **26**, and **27** revealed one main peak envelope corresponding to $[\text{Ru}(\eta^6\text{-}p\text{-cym})(\text{TFP})\text{Cl}]^+$ (in case of **25**), $[\text{Ru}(p\text{-cym})(\text{TFP})_2\text{Cl}]^+$ (in case of **26**) or $[\text{Ru}(\eta^6\text{-}p\text{-cym})(\text{TFP})(\text{PPh}_3)\text{Cl}]^+$ (in case of **27**), whereas, ESI-MS of **28** shows two peak envelopes, the higher one corresponds to $[\text{Ru}(\eta^6\text{-}p\text{-cym})(\text{TFP})\text{Cl}]^+$ and the other to $[\text{Ru}(\eta^6\text{-}p\text{-cym})(\text{PTA})\text{Cl}]^+$ (Fig.6.14-Fig.6.17).

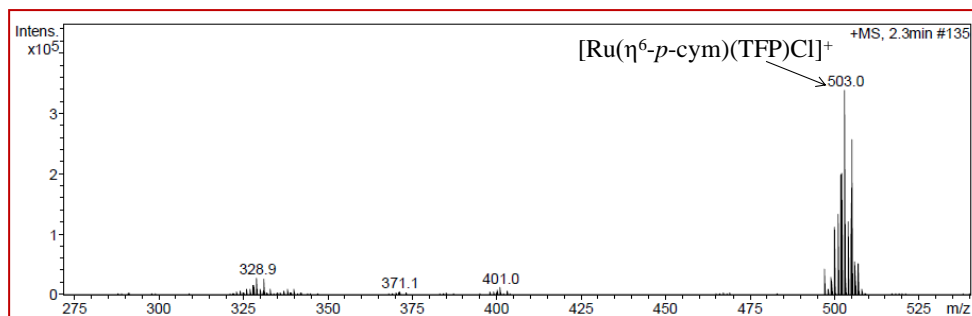


Fig.6.14: ESI-MS of complex **25**.

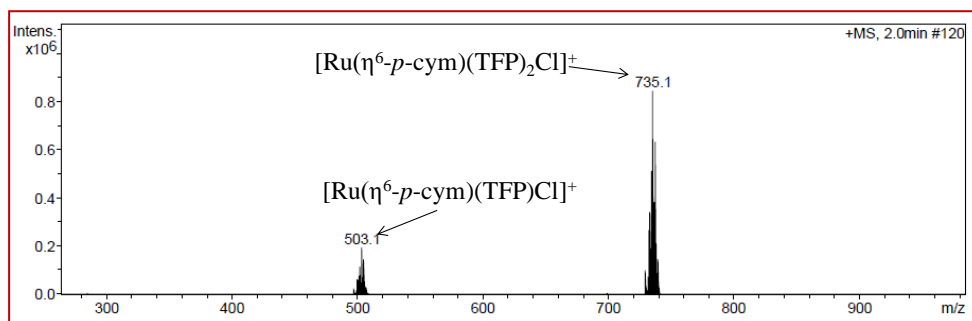


Fig.6.15: ESI-MS of complex **26**.

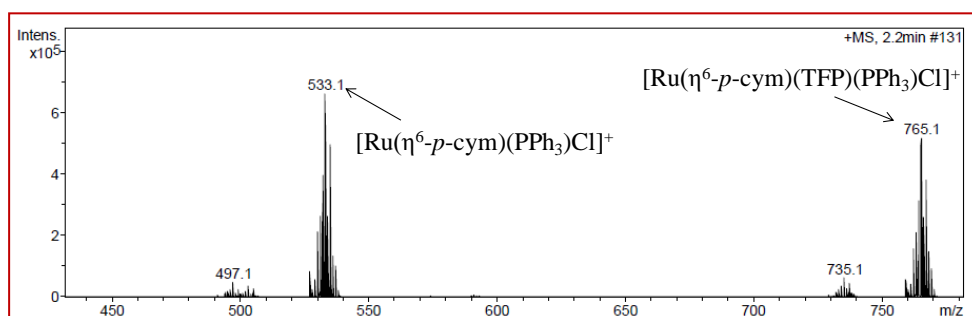


Fig.6.16: ESI-MS of complex **27**.

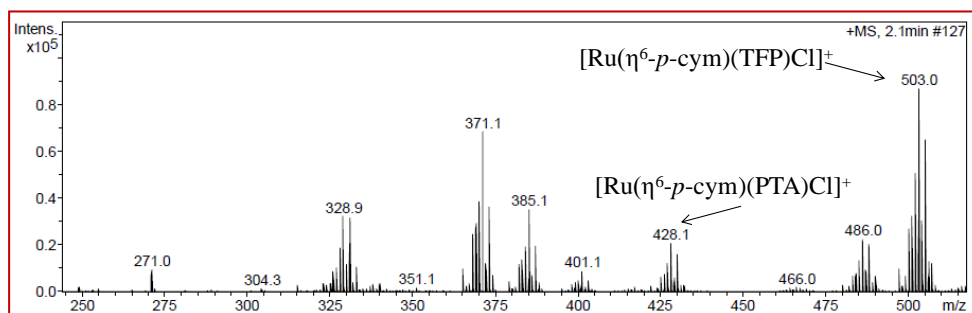


Fig.6.17: ESI-MS of complex **28**.

The solid state structures of complexes **25**, **26** and **28** have been investigated by X-ray crystallography. All the complexes possess a pseudo-octahedral geometry and the η^6 π -bonded arene ring occupies three coordination positions of the octahedron. In case of complex **25**, two coordination sites are occupied by labile chloride ligands, whereas sixth site is coordinated to P-atom of tris(2-furyl) phosphine ligand (Fig.6.18).

In case of complex **26** and **28**, two coordination sites are occupied by phosphine ligands, leaving one coordination centre for chloride ligand. Both the complexes possess BF_4 moiety as counter anion in the crystal lattice (Fig. 6.19 and 6.20).

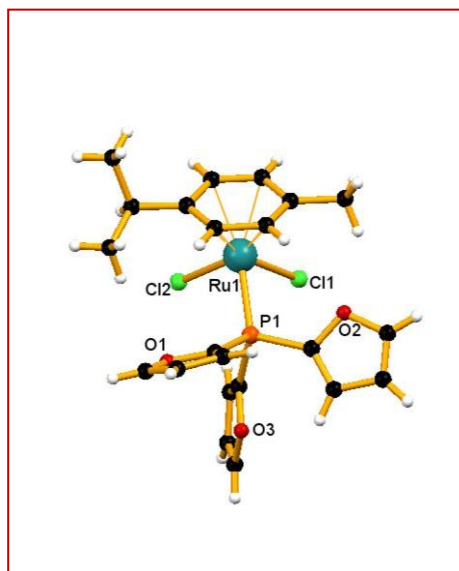


Fig.6.18: The solid state crystal structure of compound **25** partial atomic numbering scheme. Key bond lengths (\AA) and angles ($^\circ$) of complex **25**: $\text{Ru}(1)\text{--P}(1)$: 2.318(1); $\text{Ru}(1)\text{--Cl}(1)$: 2.396(2); $\text{Ru}(1)\text{--Cl}(2)$: 2.407(2); $\text{Ru}(1)\text{--C}_{\text{centroid}}$: 1.465; $\text{Cl}(1)\text{--Ru}(1)\text{--Cl}(2)$: 87.39(2); $\text{Cl}(1)\text{--Ru}(1)\text{--P}(1)$: 82.91(5); $\text{Cl}(2)\text{--Ru}(1)\text{--P}(1)$: 90.23(4).

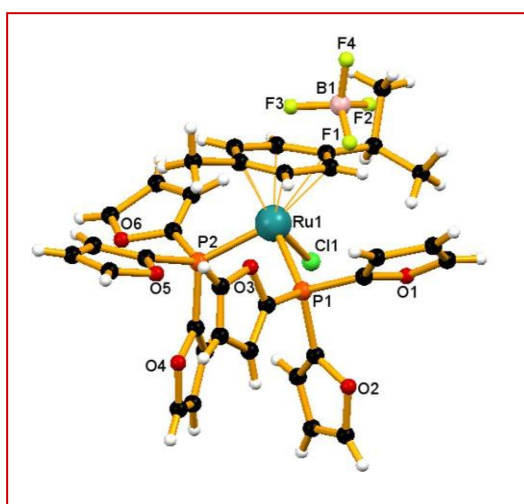


Fig.6.19: The solid state crystal structure of compound **26** partial atomic numbering scheme. Key bond lengths (\AA) and angles ($^\circ$) of complex **26**: $\text{Ru}(1)\text{--Cl}(1)$: 2.372(4); $\text{Ru}(1)\text{--P}(1)$: 2.333(4); $\text{Ru}(1)\text{--P}(2)$: 2.306(5); $\text{Ru}(1)\text{--C}_{\text{centroid}}$: 1.498; $\text{Cl}(1)\text{--Ru}(1)\text{--P}(1)$: 90.0(1); $\text{Cl}(1)\text{--Ru}(1)\text{--P}(2)$: 85.0(2); $\text{P}(1)\text{--Ru}(1)\text{--P}(2)$: 97.1(1).

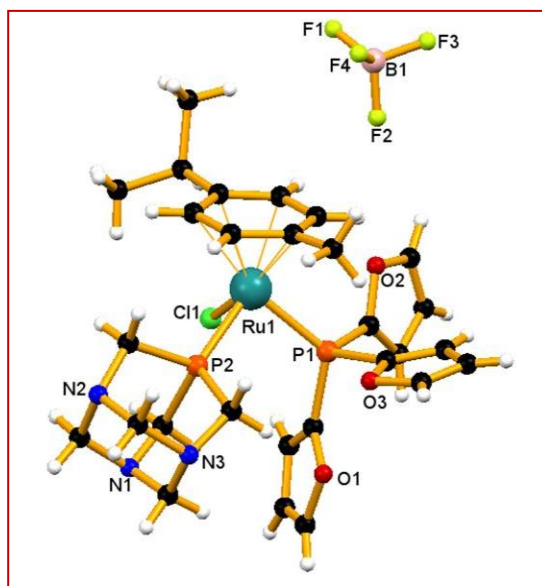


Fig.6.20: The solid state crystal structure of compound **28** partial atomic numbering scheme. Key bond lengths (Å) and angles (°) of complex **28**: Ru(1)–P(1): 2.300(1); Ru(1)–P(2): 2.313(1); Ru(1)–Cl(1): 2.389(1); Ru(1)–C_{centroid}: 1.510; Cl(1)–Ru(1)–P(1): 82.70(4); Cl(1)–Ru(1)–P(2): 87.98(4); P(1)–Ru(1)–P(2): 92.63(4).

6.3.2 Growth inhibition study of prepared complexes

The anticancer activities of the reported complexes have been tested against three different cancer cell lines *viz.*, breast cancer cell line MCF7, lung cancer cell line A549 and cervix cancer cell line HeLa. Results were obtained in terms of GI₅₀ (concentration of drug that produces 50% inhibition of the cells), TGI (concentration of the drug that produces total inhibition of the cells) and LC₅₀ (concentration of the drug that kills 50% of the cells) using sulforhodamine B (SRB) assay. All cancer cells were exposed for 24 h to increasing concentrations of the complexes and their proliferation are reported in terms of GI₅₀ values. Adriamycin, a chemotherapeutic drug was used as a positive control. It is interesting to report that, all the four complexes have shown significant antiproliferative activity against all the cell lines almost to the tune of Adriamycin in terms of nanomolar concentration. The numerical values in terms of GI₅₀ parameter for the reported complexes are within error limit (in nanomolar level), so that deduction of any Structure Activity Relationship (SAR)

among the reported complexes are not possible without further investigation. All the related data are presented in Table 6.1.

Table 6.1: *GI₅₀ value (nM/mL) of the prepared complexes in human cancer cell lines.*

Complex	A549	MCF7	HeLa
Complex 25	<0.1	<0.1	<0.1
Complex 26	<0.1	<0.1	<0.1
Complex 27	<0.1	<0.1	<0.1
Complex 28	<0.1	<0.1	<0.1
Adriamycin	<0.1	<0.1	<0.1

6.3.4. Solution stability study

Activity of a metallodrug depends largely on its stability in the experimental medium. Therefore, it is of great importance to study solution stability of a metallodrug as it can dissociate in the medium before reaching to the target or it can produce the actual reactive species, responsible for its activity, in that particular medium. Complexes **25-28** are unstable in the 1% DMSO-PBS medium and intensity of absorbance band increases with increase in time showing hyperchromism. The strong high energy band at 200-300 nm have been attributed to spin-allowed $\pi\text{-}\pi^*$ transitions. From this observation, it can be inferred that unstability of the complexes in the experimental medium can be the very first step for their promising cytotoxic activity.

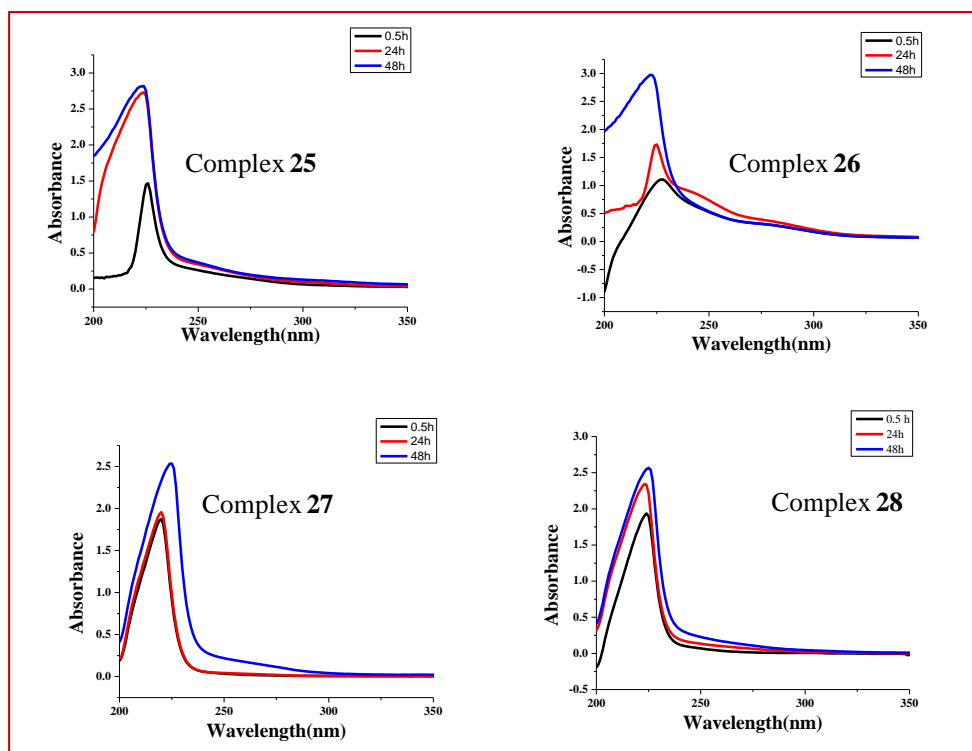


Fig.6.21: Electronic absorption spectra of **25-28** in 1% DMSO-PBS medium.

6.4 Conclusion

In conclusion, through this work four RAPTA type of complexes have been synthesized using different phosphine ligands and characterized using different analytical techniques. The structures of **25**, **26** and **28** have been validated by single crystal X-ray analyses. All the complexes exhibit promising cytotoxicity against different cancer cell lines. This new approach for the lucid design of RAPTA type of complexes may become useful in the future for treating platinum resistant cancers.

6.5 References

- [1] Süß-Fink, G. (2010), Arene ruthenium complexes as anticancer dtugs, Dalton Trans. 39(7), 1673-1688. (DOI: 10.1039/B916860P)
- [2] Sava, G., Zorzet, S., Turrin, C., Vita, F., Soranzo, M., Zabucchi, G., Cocchietto, M., Bergamo, A., DiGiovine, S., Pezzoni, G., Sartor, L., Garbisa, S. (2003), Dual action of NAMI-A in inhibition of solid tumor metastasis: selective targeting of metastatic cells and binding

- to collagen, *Clin. Cancer Res.*, 9, 1898-1905. (DOI: [clicancerres.aacrjournals.org/content/9/5/1898](https://doi.org/10.1158/1078-0432.CCR.010001)),
- [3] Rademaker-Lakhai, J. M., van den Bongard, D., Pluim, D., Beijnen, J. H., Schellens, J. H. M. (2004), A Phase I and pharmacological study with imidazolium-*trans*-DMSO-imidazole-tetrachlororuthenate, a novel ruthenium anticancer agent, *Clin. Cancer Res.*, 10, 3717-3727. (DOI: [clicancerres.aacrjournals.org/content/10/11/3717](https://doi.org/10.1158/1078-0432.CCR.030001))
- [4] Bijelic, A., Theiner, S., Keppler, B. K., Rompel, A. (2016), X-ray structure analysis of indazolium trans-[tetrachlorobis (1*H*-indazole) ruthenate (III)] (KP 1019) bound to human serum albumin reveals two ruthenium binding sites and provides insights into the drug binding mechanism, *J. Med. Chem.*, 59(12), 5894-5903. (DOI: [10.1021/acs.jmedchem.6b00600](https://doi.org/10.1021/acs.jmedchem.6b00600))
- [5] Hartinger, C. G., Jakupec, M. A., Zorbas-Seifried, S., Groessler, M., Egger, A., Berger, W., Zorbas, H., Dyson, P. J., Keppler, B. K. (2008), KP1019, A new redox-active anticancer agent-preclinical development and results of a clinical phase I study in tumor patients, *Chem. Biodiversity*, 5, 2140-2155. (DOI: [10.1002/cbdv.200890195](https://doi.org/10.1002/cbdv.200890195)).
- [6] Ang, W. H., Casini, A., Sava, G., Dyson, P. J. (2011), Organometallic ruthenium-based antitumor compounds with novel modes of action, *J. Organomet Chem.*, 696, 989-998. (DOI: [10.1016/j.jorganchem.2010.11.009](https://doi.org/10.1016/j.jorganchem.2010.11.009))
- [7] Allardyce, C. S., Dyson, P. J., Ellis, D. J., Heath, S. L. (2001), [Ru(η^6 -*p*-cymene)Cl₂(pta)] (pta = 1,3,5-triaza-7-phosphatricyclo-[3.3.1.1]decane): a water soluble compound that exhibits pH dependent DNA binding providing selectivity for diseased cells., *Chem. Commun.*, 1396-1397. (DOI: [10.1039/B104021A](https://doi.org/10.1039/B104021A))
- [8] Ang, W. H., Daldini, E., Scolaro, C., Scopelliti, R., Juillerat-Jeannerat, L., Dyson, P. J. (2006), Development of organometallic ruthenium-arene anticancer drugs that resist hydrolysis, *Inorg. Chem.*, 45, 9006-9013. (DOI: [10.1021/ic061008y](https://doi.org/10.1021/ic061008y))

- [9] Bergamo, A., Gaiddon, C., Schellens, J. H. M., Beijnen, J. H., Sava, G. (2012), Approaching tumour therapy beyond platinum drugs: Status of the art and perspectives of ruthenium drug candidates, *106*(1), 90-99. (DOI: 10.1016/j.jinorgbio.2011.09.030)
- [10] Bergamo, A., Alessla, M., Dyson, P. J., Sava, G. (2008), Modulation of the metastatic progression of breast cancer with an organometallic ruthenium compound, *Int. J. Oncol.*, *33*(6), 1281-1289. (DOI: 10.3892/ijo_00000119)
- [11] Nowak-Sliwinska, P., van Beijnum, J. R., Casini, A., Nazarov, A., A., Wagnières, G., van den Bergh, H., Dyson, P. J., Griffioen, A. W. (2011), Organometallic ruthenium(II) arene compounds with antiangiogenic activity, *J. Med. Chem.*, *54*(11), 3895-3902. (DOI: 10.1021/jm2002074)
- [12] Weiss, A., Berndsen, R. H., Dubois, M., Müller, C., Schibli, R., Griffioen, A. W., Dyson, P. J., Nowak-Sliwinski, P. (2014), *In vivo* anti-tumor activity of the organometallic ruthenium(II)-arene complex $[\text{Ru}(\eta^6\text{-}p\text{-cymene})\text{Cl}_2(\text{pta})]$ (RAPTA-C) in human ovarian and colorectal carcinomas, *Chem. Sci.*, *5*, 4742-4748. (DOI: 10.1039/c4sc01255k)
- [13] Babak, M. V., Meier, S. M., Huber, K. V. M., Reynisson, J., Legin, A. A., Jakupec, M. A., Roller, A., Stukalov, A., Gridling, M., Bernett, K. L., Colinge, J., Berger, W., Dyson, P. J., Superti-Furga, G., Keppler, B. K., Hartinger, C. G. (2015), Target profiling of an antimetastatic RAPTA agent by chemical proteomics: relevance to the mode of action, *Chem. Sci.*, *6*, 2449-2456. (DOI: 10.1039/C4SC03905J)
- [14] Gossens, C., Dorcier, A., Dyson, P. J., Rothlisberger, U. (2007), $\text{p}K_{\text{a}}$ estimation of ruthenium(II)-arene PTA complexes and their hydrolysis products via a DFT/continuum electrostatics approach, *Organometallics*, *26*(16), 3969-3975. (DOI: 10.1021/om700364s).
- [15] Groessl, M., Hartinger, C. G., Dyson, P. J., Keppler, B. K. (2008), CZE-ICP-MS as a tool for studying the hydrolysis of ruthenium anticancer drug candidates and their reactivity towards the DNA

- model compound dGMP, *J. Inorg. Biochem.*, 102, 1060-1065 (DOI: 10.1016/j.jinorgbio.2007.11.018).
- [16] Singh, A. K., Pandey, D. S., Xu, Q., Braunstein, P. (2014), Recent advances in supramolecular and biological aspects of arene ruthenium(II) complexes, *Coord. Chem. Rev.*, 270-271, 31-56.(DOI: 10.1016/j.ccr.2013.09.009).
- [17] Scolaro, C., Hartinger, C. G., Allardyce, C. S., Keppler, B. K., Dyson, P. J. (2008), Hydrolysis study of the bifunctional antitumour compound RAPTA-C, $[\text{Ru}(\eta^6\text{-}p\text{-cymene})\text{Cl}_2(\text{pta})]$, *J. Inorg., Biochem.*, 102, 1743-1748. (DOI: 10.1016/j.jinorgbio.2008.05.004).
- [18] Thota, S., Rodrigues, D. A., Crans, D. C., Barreiro, E. J. (2018), Ru(II) compounds: next-generation anticancer metallotherapeutics?, *J. Med. Chem.*, XXX, XXX-XXX. (DOI: 10.1021/acs.jmedchem.7b01689),
- [19] Riedel, T., Demaria, O., Zava, O., Joncic, A., Gilliet, M., Dyson, P. J. (2018), Drug repurposing approach identifies a synergistic drug combination of an antifungal agent and an experimental organometallic drug for melanoma treatment, *Mol. Pharmaceutics*, 15(1), 116-126. (DOI: 10.1021/acs.molpharmaceut.7b00764)
- [20] Scolaro, C., Bergamo, A., Brescacin, L., Delfino, R., Cocchietto, M., Laurency, G., Geldbach, T. J., Sava, G., Dyson, P. J. (2005), 48(12), 4161-4171. (DOI: 10.1021/jm050015d)
- [21] (Guerriero, A., Oberhauser, W., Riedel, T., Peruzzini, M., Dyson, P. J., Gonsalvi, L. (2017), New class of half-sandwich ruthenium(II) arene complexes bearing the water-soluble CAP ligand as an in vitro anticancer agent, *Inorg. Chem.*, 56, 5514-5518. (DOI: 10.1021/acs.inorgchem.7b00915).
- [22] Soós, T., Bennett, B. L., Rutherford, D., Barthel-Rosa, L. P., Gladysz, J. A. (2001), Synthesis, reactivity, and metal complexes of fluororous triarylphosphines of the formula $\text{P}(p\text{-C}_6\text{H}_4(\text{CH}_2)_3(\text{CF}_2)_n\text{-}_1\text{CF}_3)_3$ ($n = 6, 8, 10$), *Organometallics*, 20, 3079-3086. (DOI: 10.1021/om010193e)
- [23] Wande, M., Gladysz, J. A. (2003), Fluororous catalysis under homogeneous conditions without fluororous solvents: a “greener”

- catalyst recycling protocol based upon temperature-dependent solubilities and liquid/solid phase separation, *J. Am. Chem. Soc.* 19, 5861-5872. (DOI: 10.1021/ja029241s)
- [24] Renfrew, A. K., Scopelliti, R., Dyson, P. J. (2010), Use of perfluorinated phosphines to provide thermomorphic anticancer complexes for heat-based tumor targeting, *Inorg. Chem.*, 49, 2239-2246. (DOI: 10.1021/ic9020433)
- [25] Ang, W. H., Parker, L. J., De Luca, A., Juillerat-Jeanneret, L., Morton, C. J., Lo Bello, M., Parker, M. W., Dyson, P. J. (2009), Rational design of an organometallic glutathione transferase inhibitor, *Angew. Chem. Int. Ed.*, 48(21), 3854-3957. (DOI: 10.1002/anie.200900185)
- [26] Collier, J. D., Bennett, M. K., Hall, A., Cattan, A. R., Lendrum, R., Bassendine, M. F. (1994), Expression of glutathione S-transferases in normal and malignant pancreas: an immunohistochemical study, *Gut*, 35, 266-269 (DOI: 10.1136/gut.35.2.266)
- [27] Biancalana, L., Pratesi, A., Chiellini, F., Zacchini, S., Funaioli, T., Gabbiani, C., Marchetti, F. (2017), Ruthenium arene complexes with triphenylphosphane ligands: cytotoxicity towards pancreatic cancer cells, interaction with model proteins, and effect of ethacrynic acid substitution, *New J. Chem.*, 41, 14574-14588 (DOI:10.1039/C7NJ02300F)
- [28] (Blunden, B. M., Lu, H., Stenzel, M. H. (2013), Enhanced delivery of the RAPTA-C macromolecular chemotherapeutic by conjugation to degradable polymeric micelles, *Biomacromolecules*, 14, 4177-4188 (DOI: 10.1021/bm4013919)
- [29] Renfrew, A. K., Phillips, A. D., Egger, A. E., Hartinger, C. G., Bosquain, S. S., Nazarov, A. A., Keppler, B. K., Gonsalvi, L., Peruzzini, M., Dyson, P. J. (2009), Influence of structural variation on the anticancer activity of RAPTA-type complexes: ptn versus pta, *Organometallics*, 28, 1165–1172 (DOI: 10.1021/om800899e)
- [30] Mandal, P., Malviya, N., Fátima C. Guedes da Silva, M., Dhankhar, S. S., Nagaraja, C. M., Mobin, S. M., Mukhopadhyay, S. (2016), *Dalton Trans*, Fine tuning through valence bond

tautomerization of ancillary ligand in ruthenium(II) arene complex for better anticancer activity and enzyme inhibition property, 45, 19277-19289. (DOI: 10.1039/c6dt02969h)

Chapter 7

General Conclusion and Future Scope

Design and synthesis of new RAPTA type complexes using various chelating ligands of known therapeutic properties, evaluation of their antiproliferative activity and target specificity as well as investigation on their interaction with different biomolecules are the main goals of this work. With this purpose, this thesis includes twenty six new Ru(II)-arene complexes and study of their antiproliferative activity. The stability study and potential target identification has been also taken up in various cases.

RAPTA type complexes (**2**, **4**, **6** and **8**) have been prepared using different picolinamide ligands, when one of them has shown potential antiproliferative activity through valence bond tautomerism as well as significant thioredoxin enzyme inhibition property (Chapter 2). Again, different NSAID ligands with COX inhibition ability have been used as coligand in Ru(II)-arene scaffold (**9-12**) in order to achieve enhanced antiproliferative activity (Chapter 3). In chapter 4, Ru-arene piano-stool complexes have been prepared involving different tetrazoles and some of them have shown high antiproliferative activity against different cancer cell lines and protein molecules (**13-20**). In next chapter, RAPTA type complexes have been prepared (**21-24**) involving ferrocenyl ligands in order to develop heterobimetallic compounds with significant antiproliferative activity (Chapter 5). Finally in chapter 6, RAPTA type complexes have been prepared using different phosphine ligands (**25-28**). Introduction of phosphine ligands have shown very promising antiproliferative activity (Chapter 6).

This project has shown great scope where ruthenium-arene scaffold can act as one of the potential scaffold of next generation metallodrugs for cancer treatment. Functionalization at Ru(II) centre with different chelating ligands with known therapeutic property has shown enhanced biological activity in many cases. Moreover, introduction of

water soluble ligands to the ruthenium-arene moiety, such as replacing the chlorido ligand with a water soluble phosphine ligand (*e.g.* PPh₃ or PTA), increases the water solubility of these complexes which in turn result in lower GI₅₀ values.

Further biological experiments need to be achieved to clearly confirm possible drug targets for these ruthenium(II) arene metallodrugs. Such biological experiments include cell uptake studies, cell fractionation, imaging studies *etc.*, will help further to establish the structure activity relationship. Further development of this area of organometallics based drug is surely to be explored further in near future.